APPLICATION OF ENGINEERED T CELL RECEPTORS TO INVESTIGATE THE FAILURE OF CYTOTOXIC T LYMPHOCYTES TO ELIMINATE THE HIV RESERVOIR

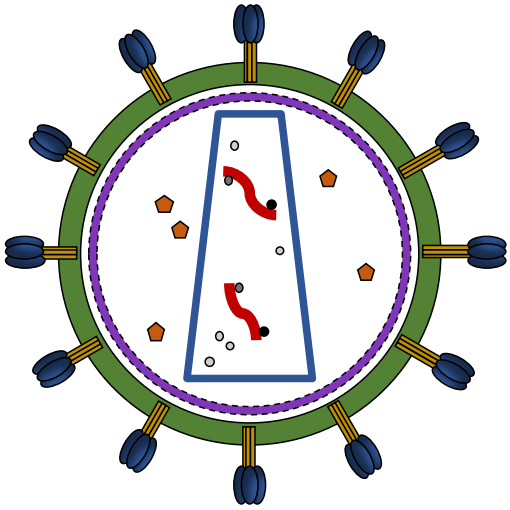

Zoë Ruth Wallace

Thesis submitted in partial fulfilment of the requirement for the degree of Doctor of Philosophy

Keble College

Nuffield Department of Medicine

University of Oxford

Trinity 2017

ABSTRACT

Application of Engineered T Cell Receptors to Investigate the Failure of Cytotoxic T Lymphocytes to Eliminate the HIV Reservoir

Zoë Ruth Wallace
Keble College
Trinity 2017

Thesis submitted in partial fulfilment of the requirement for the degree of Doctor of Philosophy

HIV establishes a reservoir comprising long lived, latently infected CD4+ T cells and monocytic cells early during primary infection. This population represents a major barrier to an HIV cure. This thesis aimed to investigate the role of the immunological synapse in the failure of cytotoxic T lymphocytes (CTLs) to eliminate the HIV reservoir and the potential for engineered bispecific **I**mmune-**m**obilising **m**onoclonal **T** cell receptors **A**gainst **V**iruses (ImmTAV) to overcome this by redirecting fully functional CD8+ T cells against viral targets.

A primary cell model of latency was used to investigate the expression of HIV Gag on latently infected cells and their susceptibility to ImmTAV-mediated elimination. A subset of cells expressed low levels of Gag without spreading infection and ImmTAV-redirected healthy donor CD8+ T cells were able to eliminate up to 40% of infected cells without latency reversal. CD8+ T cells from chronic HIV infected (CHI) donors showed impaired antiviral activity even with ImmTAV redirection.

To investigate this further, confocal microscopy was used to study immunological synapse formation using primary CD8+ T cells from HIV-negative and CHI donors. CD8+ T cells from CHI donors were able to form conjugates with virus-infected cells but exhibited impaired synapse maturation, indicated by reduced Zap70 localisation, delayed microtubule-organising centre polarisation and impaired perforin recruitment to the synapse. ImmTAV redirection partially overcame these defects.

Finally, the impact of antiretroviral agents on T cell mitochondrial function was explored. Exposure to zidovudine increased mitochondrial reactive oxygen species production and susceptibility to apoptosis. However, there was no evidence of impaired mitophagy.

These data show that defects in CD4+/CD8+ T cell synapse maturation contribute to HIV persistence but nevertheless suggest that a subset of HIV reservoir cells may be susceptible to ImmTAV-mediated elimination. The therapeutic potential of ImmTAVs may depend in part on correction of CD8+ T cell exhaustion.

TABLE OF CONTENTS

ACKNOWLEDGEMENTS 7

DPHIL PUBLICATIONS 8

LIST OF ABBREVIATIONS 9

CHAPTER ONE: INTRODUCTION 13

1.1 The Human Immunodeficiency Virus 14
- 1.1.1 Structure of HIV-1 14
- 1.1.2 Viral life cycle 20
- 1.1.3 Transmission of infection 23
- 1.1.4 Clinical course of HIV infection 24
- 1.1.5 The HIV reservoir 25
- 1.1.6 Immune response to HIV infection 32

1.2 Immune retargeting therapies to target the HIV reservoir 36
- 1.2.1 Advent of IRT 36
- 1.2.2 Application of IRT for viral infections 43

1.3 The importance of the immunological synapse 46
- 1.3.1 The immunological synapse 46
- 1.3.2 Cytotoxic synapses 50

1.4 Thesis aims 52

CHAPTER TWO: MATERIALS AND METHODS 53

2.1 Study subjects and cell lines 54
- 2.1.1 HIV seronegative donors 54
- 2.1.2 PBMCs from patients with chronic HIV infection 54
- 2.1.3 PBMCs from SPARTAC trial participants 54
- 2.1.4 PBMCs from RIVER trial participant 55
- 2.1.5 Cell lines 55

2.2 Reagents and buffers 55
- 2.2.1 Buffers 55
- 2.2.2 ImmTAVs 56
- 2.2.3 Antiretroviral agents 56
- 2.2.4 Latency-reversing agents 57
- 2.2.5 Autophagy inhibitors 57

2.3 HIV-1 isolates 57

2.4 HLA typing 58
2.5 Preparation of primary T cells 60
2.5.1 PBMC isolation 60
2.5.2 Thawing cells 60
2.5.3 CD8+ T cell separation 60
2.5.4 Resting cell separation 61
2.6 *In vitro* HIV infection of CD4+ T cells 61
2.6.1 Activated CD4+ T cell infection 61
2.6.2 Resting CD4+ T cell infection 62
2.7 Viral inhibition assay 62
2.8 Latency reversal 63
2.9 Flow cytometry and analysis 63
2.10 Flow cytometry staining 64
2.10.1 p24 intracellular staining 64
2.10.2 Assessment of exhaustion and activation status 64
2.10.3 Mitochondrial reactive oxygen species accumulation 65
2.10.4 Quantification of mitochondrial mass 66
2.10.5 FACS-based autophagic flux assay 66
2.10.6 Intracellular cytokine staining for caspase-3 and IFNγ 67
2.11 Quantification of SL9-specific T cells by staining with HLA-A*0201/SL9 dextramers 68
2.12 Short-term cell line production 68
2.13 Immunofluorescence 68
2.13.1 Antibodies 68
2.13.2 Conjugation of dye to primary antibody for immunofluorescence 69
2.13.3 Preparation of slides for visualisation of cells by confocal microscopy 70
2.13.4 Staining for immunofluorescence 71
2.13.5 Confocal microscopy image acquisition 72
2.13.6 Confocal image analysis: p24 expression 73
2.13.7 Confocal image analysis: immunological synapse molecules 75
2.13.8 Confocal image analysis: conjugate quantification 76
2.13.9 Stimulated emission depletion microscopy image acquisition 77
2.14 Statistical analyses 78

CHAPTER THREE: SUSCEPTIBILITY OF LATENTLY INFECTED CELLS TO IMMTAV-MEDIATED ELIMINATION USING AN *IN VITRO* HIV LATENCY MODEL 79

3.1 Introduction 80

3.2 Results 85

3.2.1 Resting infected CD4+ T cells express low levels of p24 without spreading infection 85

3.2.2 ImmTAV-redirected healthy donor CD8+ T cells can eliminate resting infected CD4+ T cells 88

3.2.3 A high concentration of ImmTAV alone can reactivate HIV within resting infected cells 90

3.2.4 The effect of latency-reversing agents on susceptibility of resting infected CD4+ T cells to HIV ImmTAV-mediated killing 92

3.2.5 CD8+ T cells from CHI patients eliminate p24+ resting infected cells with ImmTAV-redirection 94

3.2.6 Assessment of functional exhaustion in CD8+ T cells 95

3.3 Discussion 99

3.4 Questions addressed in this chapter 109

CHAPTER FOUR: DEVELOPMENT OF A METHOD FOR INVESTIGATING PRIMARY CD8+ T CELL SYNAPSES IN THE CONTEXT OF AN HIV INFECTION 111

4.1 Introduction 112

4.2 Results 116

4.2.1 Comparison of antibodies to detect HIV-1 Gag protein by immunofluorescence 116

4.2.2 Assessment of anti-CD8 antibodies to detect primary effectors in synapses 119

4.2.3 Optimisation of a method to identify Lck in primary T cells 120

4.2.4 Optimisation of method to quantify LFA-1 in T cell synapses 122

4.2.5 Optimisation of method to quantify Zap70 in T cell synapses 127

4.2.6 Optimisation of method to quantify MTOC in T cell synapses 128

4.2.7 Optimisation of method to quantify F-actin in T cell synapses 131

4.2.8 Optimisation of method to quantify perforin in T cell synapses 132

4.2.9 Utility of other microscopy techniques for investigation of immunological synapses 134

4.3 Discussion 139

4.4 Questions addressed in this chapter 147

CHAPTER FIVE: COMPARISON OF PRIMARY CD8+ T CELL IMMUNOLOGICAL SYNAPSES IN THE CONTEXT OF HIV INFECTION.....149

5.1 Introduction.....150

5.2 Results.....153

5.2.1 Kinetics of Gag expression in HIV-infected primary CD4+ T cells 153

5.2.2 LFA-1 localisation at the immunological synapse varies between ImmTAV-redirected CD8+ T cells from different donor groups 153

5.2.3 Early ART during PHI does not fully rescue impaired antiviral activity ...155

5.2.4 Antigen presentation on target cells affects LFA-1 localisation at the immunological synapse.....157

5.2.5 SL9-pulsed T2 cells elicit reproducible immunological synapses with primary CD8+ T cells 160

5.2.6 HIV ImmTAV facilitates formation of fully functional synapses with both activated infected and resting infected primary CD4+ T cells 163

5.2.7 Enrichment of the SL9-specific cytotoxic T lymphocyte population does not alter synapse protein polarisation.....169

5.2.8 IS protein polarisation varies between ImmTAV-redirected CD8+ T cells from HIV-positive and negative donors 171

5.2.9 Live cell imaging of the formation of primary CD8+ T cell synapses 176

5.3 Discussion.....180

5.4 Questions addressed in this chapter.....190

CHAPTER SIX: THE EFFECT OF ZIDOVUDINE ON MITOCHONDRIAL TURNOVER IN PRIMARY T CELLS 193

6.1 Introduction.....194

6.2 Results.....198

6.2.1 Assay optimisation: mitotoxicity 198

6.2.2 ZDV recapitulates the effects of autophagic flux inhibitors.....200

6.2.3 *In vitro* exposure to ZDV, but not tenofovir disoproxil fumarate or darunavir, increases mtROS in T cells.....202

6.2.4 T cells from HIV patients on ZDV-containing ART regimens express more mtROS than those from patients on ZDV-sparing regimens.....204

6.2.5 Assay optimisation: autophagy 206

6.2.6 *In vitro* exposure to ZDV does not affect autophagic flux in T cells 208

6.2.7 No difference in autophagic flux seen in T cells from patients on ZDV-containing or ZDV-sparing ART regimens 209

6.2.8 Assay optimisation: apoptosis.....210

6.2.9 *In vitro* exposure to ZDV increases apoptosis in T cells 212

6.2.10 *Ex vivo* T cells from HIV patients on ZDV-containing ART regimens demonstrate increased apoptosis compared to those from patients on ZDV-sparing regimens 213

6.2.11 Exposure to ZDV *in vivo* does not affect the viral inhibitory activity of CD8+ T cells 214

6.3 Discussion 216

6.4 Questions addressed in this chapter 223

CHAPTER SEVEN: FINAL DISCUSSION 224

7.1 Immunological synapses and the HIV reservoir 225

7.2 CTL exhaustion and metabolism 228

7.3 HIV in perspective 232

REFERENCES 234

APPENDIX 301

Approximate word count: 53,289 (including figure legends)

Acknowledgements

Completing my DPhil felt like an insurmountable task at times but it was made possible and rewarding thanks to the support of those around me including:

My supervisor, Lucy, for her continued help, encouragement and patience from the beginning of my DPhil application through to the end of my thesis writing – a brilliant supervisor through and through. *And my second supervisor*, Jakub, for reassuring me through the ups and downs of microscopy while graciously sharing reagents and running my samples on the advanced microscopes.

The Dorrell lab – Hongbing, Gemma, Kuba, Beth and Sam – for always answering questions, teaching me techniques and coming for lunch (at 12!): a small lab with a huge amount of knowledge and kindness. An extra thanks to Beth, my kindred spirit, for all the tea breaks that kept me sane. *And the rest of the labs*, for all the HIV research camaraderie and the best birthday cake club ever created.

My Oxford friends – Suzanne, Claire, Alejandro, Carlo, James, Hannah, Michaela, Ruth, Aaron, Stephanie, Andrew and Anik – for making me feel at home in Oxford. *And my Colorado friends* – Meredith, Kelly, Sarah and Michael – for never forgetting about me and providing a much-needed link to Colorado.

My parents, for getting me hooked on science as a wee girl and encouraging me to pursue my interests even if it meant moving far far away. *And my sister*, Hannah, for always setting the best (and most stylish) example and for all the care packages that brightened up my week.

Matt, for everything, which made the world of difference to me – the best person to talk to, fake audience to practice on and balance to all the hours of work.

All the donors, who graciously provided blood samples and *Immunocore,* for the ImmTAVs – hopefully this will result in better treatments for all.

DPhil publications

Wallace ZR, Sanderson S, Simon AK, Dorrell L

Exposure to zidovudine adversely affects mitochondrial turnover in primary T cells.

Antiviral Research, September 2016; 133: 178 – 182.

→ **Chapter Six**

Yang H, Buisson S, Bossi G, **Wallace ZR**, Hancock G, So C, Ashfield R, Vuidepot A, Mahon T, Molloy P, Oates J, Paston SJ, Aleksic M, Hassan NJ, Jakobsen BK, Dorrell L

Elimination of latently HIV-infected cells from antiretroviral therapy-suppressed subjects by engineered immune-mobilizing T-cell receptors.

Molecular Therapy, November 2016; 24(11): 1913 – 1925.

→ **Chapter Five**

List of abbreviations

AAF	Autophagy activity factor
AIDS	Acquired immune deficiency syndrome
ANOVA	Analysis of variance
APC	Antigen presenting cell
ARA	Autophagy reagent ‘A’
ARB	Autophagy reagent ‘B’
ART	Antiretroviral therapy
ATG	Autophagy related genes
ATP	Adenosine triphosphate
AZT	Azidothymidine (ZDV)
BDS	Bright detail similarity
BiTE	Bispecific T cell engagers
bNAb	Broadly neutralising antibodies
bsAb	Bispecific antibodies
bsDb	Bispecific diabody
CA	Capsid (HIV); p24
CCR	C-C chemokine receptor
CD	Cluster of differentiation
CHI	Chronic HIV+ infection
CL3	Containment level 3
CMV	Cytomegalovirus
CRF	Circulating recombinant forms
cSMAC	Central supramolecular activation cluster
CTL	Cytotoxic T lymphocyte
CTLA-4	Cytotoxic T-lymphocytes associate protein 4
DART	Dual-affinity retargeting molecule
DC	Dendritic cell
DIC	Differential interference contrast
DMSO	Dimethyl sulfoxide
DNA	Deoxyribonucleic acid
DNV	Darunavir
dSMAC	Distal supramolecular activation cluster
E:T	Effector to target ratio (CD8+ T: CD4+ T)
Env	Envelope (HIV); gp41, gp120
Eomes	Eomedodermin
F-actin	Filamentous actin
FACS	Fluorescence-activated cell sorting
FAO	Fatty acid oxidation
Fc(γ)R	Fc (γ) receptor
FMO	Fluorescence minus one
Gag	Group specific antigen (HIV); p17, p24
GALT	Gut-associated lymphoid tissue

GLUT1	Glucose transporter 1
GPR	Gag+ reservoir cells
HAM/RA	Human anti-mouse/anti-rat antibodies
HAT	Histone acetyltransferase
HBV	Hepatitis B virus
HCV	Hepatitis C virus
HD	Healthy donor
HDAC	Histone deacetylase
HIV	Human immunodeficiency virus
HLA	Human leukocyte antigen
ICAM-1	Intracellular adhesion molecule 1
IFN	Interferon
IgG	Immunoglobulin G
IL	Interleukin
ImmTAC	Immune-mobilising monoclonal TCR against cancer
ImmTAV	Immune-mobilising monoclonal TCR against viruses
IN	Integrase (HIV)
IntDen	Integrated density
IR	Inhibitory receptor
IS	Immunological synapse
ITAM	Immunoreceptor tyrosine-based activation motif
LAG-3	Lymphocyte activation gene 3
LC3	Microtubule associated protein 1 light chain 3
Lck	Lymphocyte-specific protein tyrosine kinase
LCMV	Lymphocytic choriomeningitis virus
LFA-1	Lymphocyte function-associated antigen 1
LPS	Lipopolysaccharide
LRA	Latency-reversing agents
LTR	Long terminal repeat
m121	ImmTAV specific for SL9 with binding anti-CD3
m231	ImmTAV specific for SL9 with non-binding anti-CD3
m232	ImmTAV not specific for HIV with binding anti-CD3
MA	Matrix (HIV); p17
mAb	Monoclonal antibody
MFI	Mean/median fluorescence intensity
miRNA	Micro RNA
MOI	Multiplicity of infection
mRNA	Messenger RNA
mtDNA	Mitochondrial DNA
mtMass	Mitochondrial mass
MTOC	Microtubule-organising centre
mTOR	Mechanistic target of rapamycin
mtROS	Mitochondrial reactive oxygen species
NC	Nucleocapsid (HIV); p7

Nef	Negative regulatory factor (HIV)
NF-κB	Nuclear factor kappa-light-chain-enhanced of activated B cells
NFAT	Nuclear factor of activated T cells
NK	Natural killer cells
NRTI	Nucleotide reverse transcriptase inhibitor
OXPHOS	Oxidative phosphorylation
PBMC	Peripheral blood mononuclear cells
PCR	Polymerase chain reaction
PD-1	Programmed cell death protein 1
PD-L1	Programmed cell death ligand 1
PE	Phycoerythrin
PFA	Paraformaldehyde
PHA	Phytohaemagglutinin
PHI	Primary HIV infection
pHLA	Peptide-HLA complex
PI	Protease inhibitor
PIC	Pre-integration complex (HIV)
PKC (θ)	Protein kinase C (θ)
PLWH	People living with HIV
PM	Plasma membrane
Pol	DNA polymerase (HIV)
Pol-γ	Mitochondrial polymerase γ
PR	Protease (HIV)
pSMAC	Peripheral supramolecular activation cluster
Rev	Regulator of expression of virion proteins (HIV)
RIVER	Research in viral eradication of HIV reservoirs (trial)
RNA	Ribonucleic acid
RRE	Rev response element
RT	Room temperature
RTI	Reverse transcriptase inhibitor
scFv	Single chain variable fragment
SD	Standard deviation
SEB	Staphylococcal enterotoxin B
SIV	Simian immunodeficiency virus
SL9	Gag epitope: SLYNTVATL
SMAC	Supramolecular activation cluster
SP1	Spacer peptide 1 (HIV)
SP2	Spacer peptide 2 (HIV)
SPARTAC	Short Pulsed ART in Primary HIV Infection (trial)
STCL	Short term cell line
STED	Stimulated emission depletion microscopy
STORM	Stochastic optical reconstruction microscopy
SU	Surface protein (HIV); gp120
PALM	Photo-activated localisation microscopy

T-bet	T-box transcription factor
T0	Human T cell line
T2	Human T cell line (TAP deficient)
TaFv	Tandem scFv
TAP	T cell activating protein
TAR	Trans-activation response element
Tat	HIV trans-activator (HIV)
TCCF	Total corrected cellular fluorescence
TCR	T cell receptor
TDF	Tenofovir
T_{ex}	Exhausted T cells
T_{fh}	T follicular helper cells
TIRFM	Total internal reflection microscopy
TM	Transmembrane protein (HIV); gp41
TNF	Tumour necrosis factor
T_{reg}	Regulatory T cell
UTR	Untranslated region (HIV)
VIA	Viral inhibition assay
Vif	Viral infectivity factor (HIV)
Vpr	Viral protein R (HIV)
Vpu	Viral protein U (HIV)
WJR076	B cell line
Yap	Yes-associated protein 1
Zap70	Zeta chain associated protein kinase 70
ZDV	Zidovudine
ZIKV	Zika Virus

CHAPTER ONE: INTRODUCTION

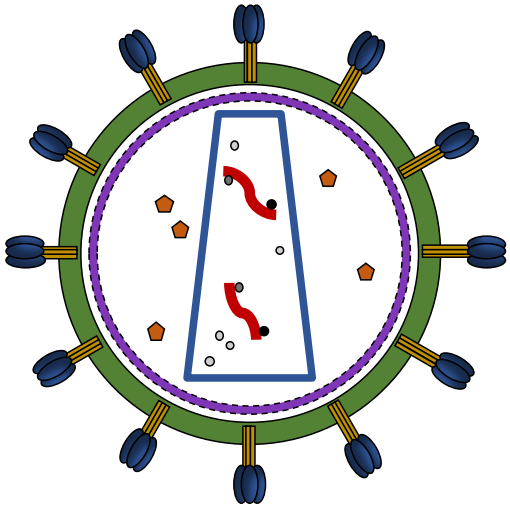

Since the first description of the Acquired Immune Deficiency Syndrome (AIDS) and the subsequent identification of the Human Immunodeficiency Virus (HIV) in the 1980s approximately 70 million people have been infected with HIV and 35 million have died. However, the discovery of antiretroviral therapy (ART) dramatically changed the outcome for people living with HIV (PLWH). PLWH who begin ART can achieve a near normal lifespan and access to ART has reduced the number of transmissions between sexual partners and from HIV-positive mothers to their children. As of 2016, 18.2 million people had access to ART, up from <1 million in 2000. However, there is not only a gap in those with access to ART – especially in Sub Saharan Africa where ~70% of HIV cases worldwide occur – but with those who are aware of their HIV status. Approximately 40% of PLWH worldwide are undiagnosed and therefore not receiving ART, without which the immune system is unable to control viral replication.[1,2] Even on ART the virus is never fully cleared from the body due to the establishment of HIV reservoirs. Because lifelong ART is required to maintain virological suppression and immune competence, there is a strong rational to develop new therapies that can reduce or even eliminate these reservoirs and thus enable patients to discontinue ART. Immune-based therapies are being actively investigated for this strategy and this thesis will assess the role of a new biological therapeutic approach to HIV cure involving engineered bispecific immune-mobilising T cell receptors (ImmTAVs) to mediate clearance of HIV-infected cells.

1.1 The Human Immunodeficiency Virus

1.1.1 Structure of HIV-1

HIV can be divided into two major types – HIV-1 and HIV-2. Originally lentiviruses that naturally infected African primates but were largely non-pathogenic (Simian Immunodeficiency Viruses, SIV), HIV-1 and HIV-2 both entered the human

population independently via multiple zoonotic transmission events, from chimpanzees/gorillas and sooty mangabeys, respectively.[3–5] Despite coding for similar viral proteins the genomes of the two viruses differ (for example, HIV-2 codes for the accessory protein, vpx, but not vpu) and HIV-2 is less pathogenic than HIV-1 plus mainly limited to West Africa.[6–8] For the purposes of this thesis HIV will refer to HIV-1. HIV-1 is a 120 nm wide virus complete with two copies of positive sense single stranded RNA that code for the nine viral genes (figure 1.1).

a

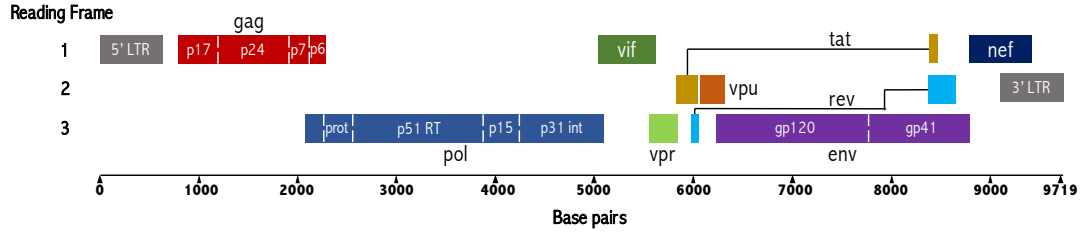

b

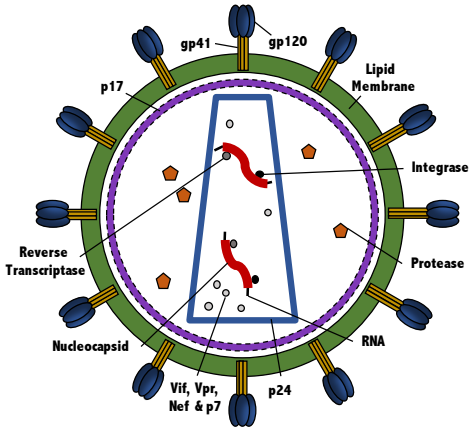

Figure 1.1: The Human Immunodeficiency Virus. (a) The HIV genome encodes all the proteins required for the structure of the virus including the three major genes: *gag*, *pol* and *env*. (b) HIV-1 is comprised of two copies of ssRNA within a conical capsid created by p24 Gag proteins. Included within the capsid are important enzymes (reverse transcriptase, integrase), p7 and accessory proteins (Vif, Vpr and Nef). A matrix of p17 Gag proteins surrounds the capsid and viral proteases. A host-cell derived envelope constitutes the outside of the virus, incorporating viral glycoproteins gp41 and gp120 (appendix 1.1).

Group-specific antigen (Gag)

The Gag polyprotein is comprised of matrix protein (MA; p17), capsid protein (CA; p24), spacer peptide 1 (SP1; p2), nucleocapsid protein (NC; p7), spacer peptide 2 (SP2; p1) and p6 proteins. During viral maturation, the viral protease cleaves the Gag polyprotein in five sites, separating the MA, CA, NC and p6 proteins into individual components. These proteins rearrange to form the mature virion; the NC encloses and

protects the viral RNA, the CA-composed conical core surrounds the NC (and other viral proteins like reverse transcriptase) and the MA proteins associate with the viral membrane to form the matrix and to recruit Env.[9] MA has been implicated in many aspects of virion assembly, including early post entry events, incorporation of Env into the virus and targeting of Gag to the PM.[10] The p6 protein contains late assembly domains that facilitate viral budding and possesses binding sites for inclusion of Vpr into the virus.[9,11] Finally, the two spacer peptides are involved with regulating conformational changes that occur during maturation.[12–14]

Envelope (Env)

The *env* gene encodes the gp160 protein. The host protease, furin, cleaves gp160 into the transmembrane protein gp41 (TM) and the surface protein gp120 (SU) at the endoplasmic reticulum. Assembled into trimers, the heavily glycosylated Env 'spikes' are delivered to the plasma membrane (PM) in vesicles. When the virion buds from the PM the spikes are incorporated into the virion membrane and facilitate re-entry into another target cell.[9,15]

Polymerase (Pol)

The *pol* gene encodes for the necessary viral enzymes found within the virus: reverse transcriptase, integrase (IN), RNase H and protease (PR). Reverse transcriptase has both RNA and DNA-dependent polymerase activities and generates a double stranded DNA from the single stranded RNA template; RNase H eliminates the ssRNA template from the first DNA strand to allow for the second to be synthesised.[16,17] As there is no associated proofreading mechanism replication is error prone, which contributes significantly to the diversity of HIV. IN facilitates the insertion of proviral DNA into the genome of the host cell by trimming the proviral DNA, cleaving the host DNA and ligating the proviral DNA to the free ends.[18] PR cleaves the Gag and Gag-Pol

polyproteins during virion maturation, allowing virion assembly and release to be completed.[9,19]

Regulatory proteins

The proteins Tat (trans-activator of transcription) and Rev (regulator of expression of virus proteins) are important for regulating the life cycle of the virus. Tat is a transcriptional activator that binds the transactivation response element (TAR) on the viral RNA, activating transcription from the HIV long terminal repeat (LTR). The Tat protein is made from the small number of RNA transcripts produced early on and upon binding TAR elicits a positive feedback cycle resulting in a sharp increase in the production of HIV.[20,21] Rev contains both a nuclear import and export signal and is able to shuttle between the cytoplasm and the nucleus. Once inside the nucleus, Rev binds the Rev response element (RRE) within the viral RNA and facilitates export of unspliced or incompletely spliced mRNAs, typically retained in the nucleus, to the cytoplasm.[22–24]

Accessory regulatory proteins

The *nef, vif, vpr* and *vpu* genes encode proteins that are not necessary for replication in *in vitro* systems but are critical virulence factors. Negative factor (Nef) accumulates early in infection and has been implicated with a host of actions that increase the infectivity of the virus and restrict the host's immune response. Nef facilitates downregulation of CD4 and human leukocyte antigen (HLA) class I expression. While downregulating CD4 seems counterintuitive as HIV relies on the receptor for cell entry, reducing its expression produces a controlled infection by preventing superinfection of CD4+ T cells and encouraging release of virions.[25] Downregulation of HLA class I molecules helps protect HIV's host cells from CTL-mediated destruction, as CTLs rely on peptide-HLA presentation for activation, allowing for further production of the virus. In HIV-2 and SIV Nef also mediates downregulation of CD3 which functions to protect

the virus's host cells by preventing activation-induced cell death or any induction of PD-1 that may affect the survival of the T cell. However, *nef* alleles from HIV-1 have lost this ability to suppress T cell activation, resulting in the higher pathogenicity seen in HIV-1 compared to HIV-2 or some strains of SIV in primates.[26–28] Nef can also alter a T cell's programme of activation, inducing transcriptional changes similar to those produced by anti-CD3 T cell activation, by upregulating factors that create an environment favourable to production of the virus.[29] Additionally, Nef is able to retarget Lck, one of the earliest kinases involved in TCR signalling, away from the plasma membrane and into endosomal compartments; this limits TCR signalling at the PM but the compartmentalised Lck is still in the active conformation allowing Nef to generate intracellular signals downstream (discussed further in section 5.1).[30,31] Finally, Nef is able to increase the infectivity of its progeny virions by inhibiting the constitutively expressed host restriction factors, SERINC3 and SERINC5. SERINC5 is normally packaged into budding HIV and can impair the ability of a viral particle to transfer its contents into the cytoplasm of susceptible CD4+ T cells. Nef redirects SERINC5 to endosomal compartments to spatially separate it from the budding virus particles.[32–36]

The viral infectivity factor (Vif) is required for HIV-infection in peripheral blood lymphocytes/macrophages but not in most cells lines; it targets the host enzyme, APOBEC3G, for degradation thereby disrupting its antiviral activity. APOBEC3G deaminates deoxycytidine in viral cDNA replication and must be incorporated into the virus during assembly to assert its antiviral effect; vif prevents this incorporation in new viruses in addition to facilitating its degradation in virus-producing cells.[37–39] The viral protein R (Vpr) enables nuclear localisation of the pre-integration complex (PIC; viral DNA and proteins required for insertion of the viral genome into the host genome) and arrests cells in the G_2 phase of the cell cycle (when the LTR is most active) to increase

virus production.[40,41] The viral protein U (Vpu) facilitates degradation of CD4, which prevents CD4-Env binding in the ER to allow for correct Env assembly and enhances the release of viral particles from the host cell.[42–44] Vpu also facilitates budding of the virion via its antagonism of the cellular host factor, tetherin. Induced by IFN-α, tetherin proteins in Vpu-defective HIV virions are able to bind the viral envelope preventing the release of the virion from the plasma membrane and resulting in the internalisation of the virus in endosomal compartments. Vpu has been shown to both reduce total cellular levels of tetherin and redirect the tethering protein to intracellular compartments within the *trans*-Golgi network.[45,46] All together HIV's virulence factors act to both increase production of the virus and control the host's immune response to achieve favourable survival conditions for the virus.

HIV Clades

Due to the rapid replication and mutation rate of HIV the genomic diversity of the virus has expanded over the course of the HIV pandemic. HIV isolates have been assigned to four groups, based on their zoonotic origins (independent transmission events) and phylogenetic relationships: M group (major, >90% of cases; transmission event from chimpanzees), O group (outlier; from gorillas), N group (non-M, non-O; from chimpanzees) and P group (putative; from gorillas).[3,47,48] Isolates within the M group can be further sub-divided into clades (also known as subtypes) A-K; diversity is also generated by recombination between viruses of different subtypes, resulting in circulating recombinant forms (CRFs; e.g., CRF07_BC). HIV clades are classified according to the nucleotide sequence differences in the *env* region of the genome.[47,49] Between the M and O groups Env proteins may differ by 30 –50% with inter-clade variation at 20 – 30% and intra-clade variation at 10 – 15%.[49] In contrast, the *pol* region of HIV is less divergent because it encodes critical enzymes for the virus, as is the *gag* region, which encodes

inflexible core proteins. Inter- and intra-clade diversity also includes differences in LTR copy number, ability to respond to transcriptional factors, co-receptor usage and syncytium-inducing capacity between clades.[50,51] Global genetic (and consequently antigenic) variability is one of the main challenges for vaccine immunogen design.[47,49,52]

The geographical spread of HIV can be explained in part by the demographic characteristics of PLWH infected with different clades of HIV. For example, clade B is the predominant species in Europe and the Americas and its spread has been largely driven by sexual transmission between men, while the epicentres of the HIV pandemic in Africa and India are dominated by clade C viruses which have spread mainly through heterosexual contact (reviewed in Spira et al.[49]).

1.1.2 Viral life cycle

The viral life cycle of HIV is comprised of seven steps: binding, fusion, reverse transcription, integration, replication, assembly and budding (figure 1.2). HIV infects activated CD4+ T cells, although HIV can also target cells of the monocyte/macrophage lineage, relying on the surface expression of CD4 and the CCR5 or CXCR4 coreceptors. When the viral gp120 binds to the CD4 receptor on the CD4+ T cell conformational changes expose a second binding site for the CCR5 or CXCR4 coreceptor; CCR5 is mainly expressed on memory T cells while CXCR4 is more widespread and found on naïve T cells.[53] Viral isolates in the early stages of HIV infection often use CCR5 (R5 tropic) to enter the cell while later isolates use CXCR4 (X4 tropic); viruses frequently go through an R5X4 stage during the evolution from R5 to X4 tropism.[54] R5 viruses have been associated with transmission of infection; those individuals who are homozygous for the 32 base pair deletion (ΔCCR5) that results in a defective CCR5 that is unable to reach the cell surface are resistant to infection and heterozygotes experience a slower course of disease highlighting the importance of the coreceptor for HIV pathogenesis. X4 viruses

have been associated with a faster decline of CD4+ T cells and disease progression to AIDS especially if acquired early.[53–58]

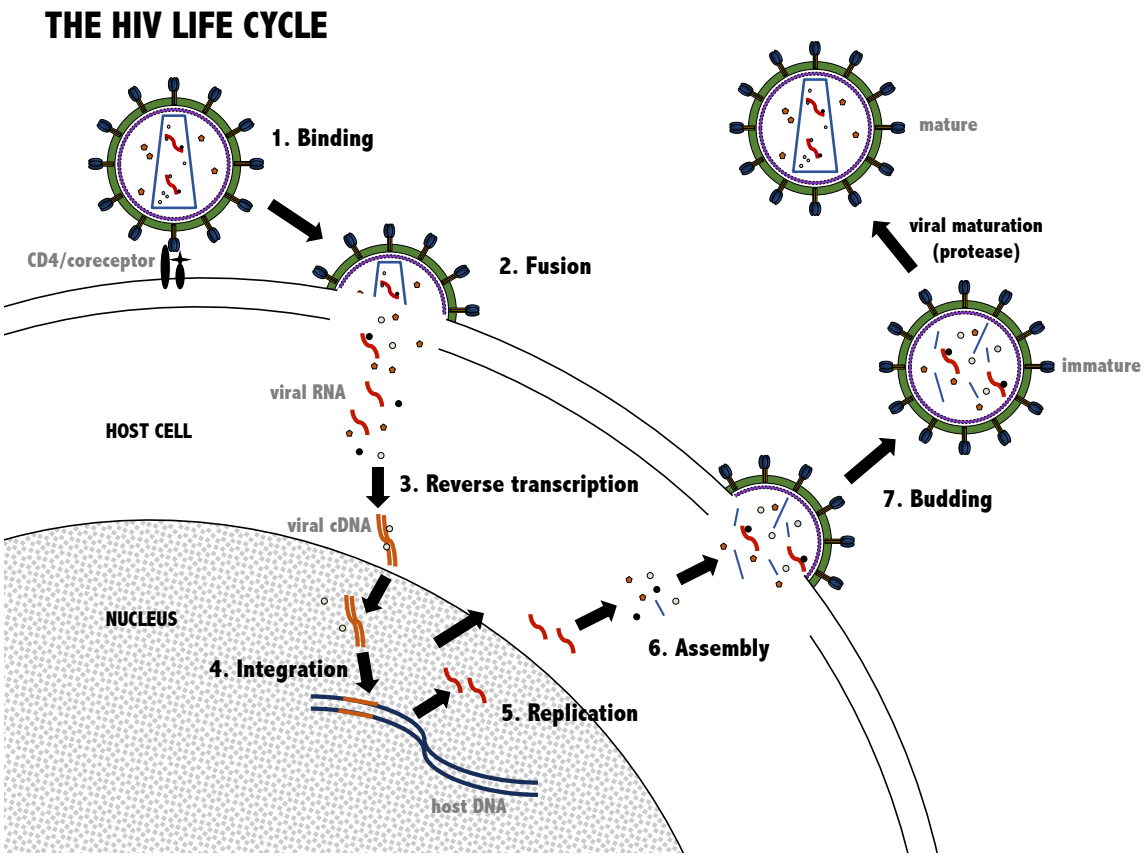

Figure 1.2: Life cycle of the Human Immunodeficiency Virus. The viral life cycle of HIV is comprised of seven steps: 1) binding, 2) fusion, 3) reverse transcription, 4) integration, 5) replication, 6) assembly and 7) budding. Once the immature virus buds the virus's protease cleaves polyproteins to allow for assembly of a mature, infectious virus.

Engagement of both receptors allows gp41 to insert into the PM and another conformational change allows the two membranes to align and fuse. Upon viral entry into the cell, uncoating of the CA occurs, exposing the viral genome. Reverse transcription then follows, using the packaged reverse transcriptase and RNase H enzymes. HIV infects activated CD4+ T cells as this population, in contrast to resting CD4+ T cells, is able to support the reverse transcription process. Resting CD4+ T cells express the restriction factor, SAMHD1, which as a deoxynucleoside triphosphate triphosphohydrolase converts dNTPs into deoxynucleosides and inorganic triphosphates. This enzymatic process reduces the availability of free dNTPs for the virus to use to

create its cDNA, thus blocking viral replication early on. SAMHD1 expression decreases during T cell activation and proliferation such that expression of SAMHD1 is low enough in activated CD4+ T cells that the resultant dNTP concentrations can support viral replication. Interestingly, HIV-2's vpx protein is able to degrade SAMHD1; addition of exogenous dNTPs, silencing of *SAMHD1* or expression of vpx in non-permissive cell lines lessens HIV-1 restriction, although a downstream block still prevents release of virions.[59–62]

The resulting PIC enters the cell's nucleus via nuclear pore complexes. Inside, IN facilitates integration of the viral DNA into the host's DNA. HIV integration is not random – it appears to favour actively expressed genes and the distribution of host factors along the chromatin may impact site usage.[63] It is estimated about 80% of HIV integration events are in genes that comprise 40% of the genome.[64,65] Once integrated, the host's RNA polymerase mediates proviral transcription and multiply spliced viral mRNAs are produced. mRNAs are then exported out of the nucleus (larger mRNAs require Rev-dependent mechanisms) and translated into viral proteins. Together with full length genomic RNA the virus is assembled into immature particles at the PM of the cell and buds, incorporating some of the host's PM within the virion; budding is orchestrated by interactions between the late domain of Gag (p6) and cellular ESCRT machinery, a set of proteins normally involved in membrane remodelling, which are required for virus particle fission from the plasma membrane.[66,67] Concomitant with budding, the viral PR cleaves the Gag and Gag-Pol polyproteins to allow for the assembly of the mature and infectious virus.[68] Antiretroviral classes target different stages of the viral life cycle such as viral entry (co-receptor antagonists and fusion inhibitors), enzyme activity (reverse transcriptase, protease and integrase inhibitors) and production of mature virus (protease inhibitors) thereby inhibiting viral replication and spread of infectious particles.[68,69]

1.1.3 Transmission of infection

Transmission of HIV occurs when blood, semen, vaginal fluids, rectal fluids or breast milk containing infectious virus comes in contact with a mucous membrane or damaged tissue (or is injected into the bloodstream). Horizontal transmission occurs most frequently through sexual intercourse and less commonly through sharing of contaminated needles/syringes, receipt of a contaminated blood product or occupational exposure (needle stick injury). Vertical transmission from a mother to child is most likely to occur during vaginal delivery or through breastfeeding. A systematic review estimated that the per act HIV transmission risk was highest from a blood transfusion (9,250 infections per 10,000) followed by mother-to-child transmission (2,260 per 10,000) then sexual intercourse (varied depending on act, low – 138 per 10,000).[70,71] Viral load is the main determinant of transmission risk; other factors, including co-infection with a sexually transmitted infection, can increase the transmission risk while use of condoms and adherence to ART regimens can drastically reduce the risk.[71–73]

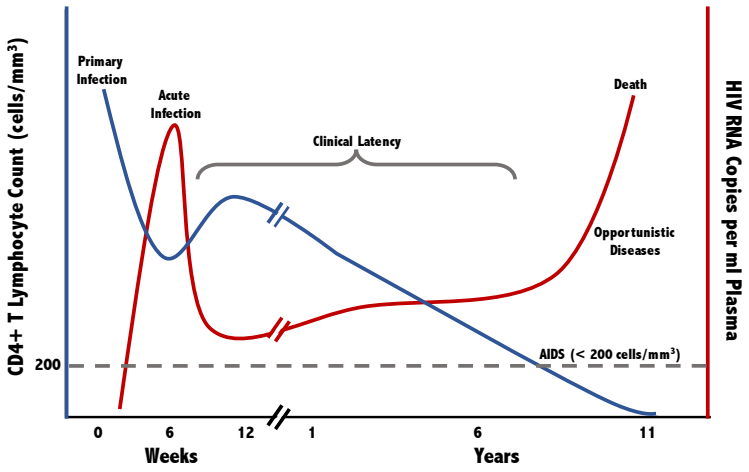

Figure 1.3: Clinical course of HIV infection. During acute HIV infection, the viral load increases and the CD4+ T cell count decreases as the virus infects activated CD4+ T cells and draining lymph nodes. Within these first weeks of infection the latent reservoir is also established. As the immune system begins to mount a response to the virus the viral load decreases, but the CD4+ T cell count does not fully recover. While PLWH on treatment can maintain a normal lifespan, if the virus escapes immunological and treatment control the CD4+ T cell count can drop below 200 cells/mm^3 resulting in clinically defined AIDS, including the acquisition of dangerous opportunistic infections. Figure inspired by McMichael et al.[74]

1.1.4 Clinical course of HIV infection

During acute HIV infection, the interaction between the virus and host immune system dictates the kinetics of both viral replication and CD4+ T cell count (figure 1.3). Viruses first cross the mucosal barrier by transcytosis, capture by or infection of dendritic cells (DCs) or by infecting intraepithelial lymphocytes; damage to the barrier, including inflammation and infection, facilitates this process. Single genome amplification followed by direct sequencing was used to demonstrate that ~80% of mucosally-transmitted HIV infections (clade B and C) started with a single virus.[75,76] After transmission a short period (mean 10 days) before viral RNA is detectable in the plasma marks the 'eclipse phase.'[77] However, during this time virus propagation occurs as it infects CD4+ T cells (as well as monocytes and macrophages) in the submucosa. Virus-infected cells drain to local lymph nodes where the number of available target cells is extremely high. Virus particles are produced at a rate of 10^{10} per day.[78] HIV is able to infect new targets through both cell free and cell-to-cell mechanisms; the cell-cell formation of a virological synapse eliminates the rate-limiting step of viral diffusion for more efficient viral spread although this method of viral propagation is sensitive to viral entry inhibitors.[79–82] Dissemination of the virus occurs as infected cells traffic in and out of lymphoid tissues and free virions are released into the peripheral blood.[83,84] When HIV spreads to the gut-associated lymphoid tissue (GALT), which contains large numbers of CD4+CCR5+ memory T cells, ~80% of the CD4+ T cells in the GALT can be depleted by three weeks post-infection. Additionally, many of the germinal centres in the gut (up to 50%) are lost within the first 80 days.[85–87]

By 21 – 28 days post-infection plasma viraemia reaches its peak and CD4+ T cell numbers in the peripheral blood fall due to the pathogenic effects of HIV preferentially infecting CD4+ T cells; this normally coincides with systemic symptoms such as

headache, fever and malaise. Viraemia then declines towards a steady state, known as the set point, at 12 – 20 weeks. Virus diversification arises as HIV-specific CD8+ T cell responses become detectable and drive the selection of escape mutants (section 1.1.6). The set point is partially determined by host genetics as those who exhibit spontaneous control of viraemia and/or slow progression are more likely to carry certain HLA alleles, such as HLA-B*5701, which are associated with more effective CD8+ T cell responses.[88–90] There has been no recorded case of the immune system naturally resolving an HIV infection as the HIV reservoir is established within the first few days of infection, before adaptive immune responses have developed (discussed further in section 1.1.5). Therefore, chronic infection is inevitable. However, even without treatment, this period may be symptom-free for 10 years; a minority experience extreme outcomes – either very rapid progression or maintenance of a low viral load without treatment for > 10 years.[91,92] In most cases the CD4+ T cell count declines steadily, although in some cases it remains stable then drops steeply, and once the CD4+ T cell count reaches < 200 cells/μl the risk of opportunistic infections and some cancers is greatly increased.[84,93] CD8+ T cell responses may be crucial for maintaining viral suppression even in the presence of ART as depletion of CD8+ T cells in ART-treated SIV-infected rhesus macaques resulted in increased plasma viraemia that was only controlled upon re-establishment of the CD8+ T cell population.[94]

1.1.5 The HIV reservoir

Establishment of the HIV reservoir

During acute HIV infection, viral DNA is inserted into the host cell genome. HIV preferentially infects activated cells as they support efficient viral production. However, proviral DNA may also become integrated in activated CD4+ T cells as they return to a resting state. In this environment HIV is transcriptionally inactive and no viral peptides

are available for display to passing T cells (although this is now debated, discussed in section 3.1). Long-lived central memory and transitional memory T cells contribute to the majority of the CD4+ T cell reservoir.[95] Estimates suggest there is a reservoir of $10^6 – 10^7$ latently infected cells within an individual or about 0.1 – 1 cell per million lymphocytes.[96,97] Despite this low frequency, the latent reservoir persists throughout chronic infection and can support productive infection at any time, as indicated by rapid rebound of viraemia when ART is stopped (reviewed in [98,99]). As HIV does not possess latency genes the virus does not 'choose' latency. The problem of HIV latency is only relevant because of the use of ART, which induces a state of latency by preventing further viral replication and infection of additional CD4+ T cells.

In addition to resting CD4+ T cells, the reservoir is also established in other immune cells and tissues. Monocytes, which can differentiate into macrophages, represent another cellular reservoir of HIV. Viral decay is slower in monocytes and macrophages due to their longer half-life and resistance to viral cytopathic effects.[100–102] These long-term infected cells are more resistant to ART, as only partial inhibition of virus was achieved when monocytes/macrophages were cultured with high concentrations of protease inhibitors, and can even disseminate infection; macrophage cytokine secretion attracts T cells to the vicinity and cell-to-cell spread can occur via a virological synapse.[103–106] The migration of macrophages and T cells out of the peripheral circulation and into tissues of the gastrointestinal tract, central nervous system, spleen and lymph nodes creates anatomical reservoirs.[85,107–110] Lymphoid tissues, especially, contain a high proportion of total body CD4+ T cells and poor drug penetration into the tissues contributes to viral persistence.[111]

The seeding of the reservoir in both peripheral blood mononuclear cells (PBMC) and tissue sites occurs early in primary HIV infection (PHI). Ananworanich et al. reported

that in a study of untreated individuals enrolled in Fiebig I/II stages of the infection, the frequency of PBMCs harbouring HIV DNA peaked at two weeks post-enrolment and reached a set point two weeks later; Fiebig staging categorises the stages of an HIV infection based on the sequential gain in positive HIV clinical diagnostic assays – I/II is defined by viral RNA+ (by PCR) and p24+ (by ELISA) results.[112] Additionally, the size of the established reservoir (as measured by total HIV DNA) has been shown to predict the time to viral load rebound after stopping ART.[113,114] The rapid rate of viral seeding is reflected in the outcome of attempts to eliminate the reservoir with immediate or early ART. In the same study by Ananworanich et al. some individuals were started on ART during PHI but a reservoir of latently infected cells still remained despite reductions in the reservoir size compared with delayed treatment.[112] Similarly, in a study of rhesus macaques that were started on suppressive ART as early as three days post-infection the virus still rebounded after later cessation of ART despite a substantial reduction in the levels of proviral DNA detected in the peripheral blood and mucosa.[115] Even intensification of ART, as in the study by Ramratnam et al., only accelerated the decay of the reservoir but did not fully deplete it.[116,117] Measuring the viral decay over years on ART, and in different treatment groups of PLWH, highlights the kinetics of viral decay and the need for early ART to prevent the establishment of a large reservoir.[118–121]

There is debate about whether ongoing cycles of replication ('re-seeding') or the persistence and proliferation of stable reservoirs of infected cells ('clonal expansion') contribute to the low levels of viraemia that endure in patients on ART; while deemed 'undetectable' by standard clinical tests viraemia is still present in PLWH. If cycles of viral replication were ongoing while on normal ART regimens then intensification of antiretroviral treatment with different drug classes (i.e. addition of (additional) integrase inhibitors or CCR5 antagonists) would prevent the virus from infecting new cells thus

reducing the size of the reservoir. Furthermore, ongoing replication would allow the virus to adapt to selection pressures resulting in a change to the viral sequence. However, multiple studies of PLWH on ART intensification found that there was no decay of the latent reservoir.[122–124] Additionally, longitudinal assessment of viral sequences taken from PLWH over the course of their ART showed no evidence of viral evolution[118–121,125,126]; the DNA sequences from the reservoir were found to be similar to the RNA sequences of the viruses found actively replicating in the plasma before the start of ART.[125] This evidence suggests that clones of cells, infected before treatment began and containing proviruses within, can survive and proliferate maintaining the viral reservoir without active replication.[118,121,122,127]

However, some groups suggest that ongoing replication – at very low levels and possibly in sanctuary sites with limited ART access – maintains the reservoir without evolution of the virus as the ART concentrations are so low that there is no competitive advantage for the virus to evolve. This could explain the absence of resistance mutations described by other groups and the failure of treatment intensification to work.[111,127] Lorenzo-Redondo et al. deep sequenced HIV-1 DNA in cells from the blood and lymph nodes of individuals on treatment and using phylogenies concluded that ongoing replication was occurring based on the divergence of the samples.[111] Lorenzo-Redondo et al.'s description of a model, whereby virus evolution and trafficking between tissue compartments continues in PLWH with undetectable plasma viral loads, has been refuted by other groups who claim that qPCR errors and a small sample size (n = 3) measured over a short time (0, 3 and 6 months on ART) resulted in a limited data set; taking PCR resampling and hypermutations into account another group showed there was no ongoing replication based on the same data set.[126]

Indeed, measuring the size of the viral reservoir presents many difficulties including which samples, method and readout to use. Blood samples are more readily acquired from patients on ART but latently infected cells may also be present in other sites such as lymph nodes or the GALT. To measure the reservoir viral outgrowth assays are thought to underestimate the size of the reservoir as all the proviruses may not be reactivated, while qPCR may overestimate the size, as it does not distinguish whether or not a virus is replication competent.[128] Adding a further layer of complexity the readouts reported by different groups vary including plasma HIV-1 RNA, total HIV-1 DNA, integrated HIV-1 DNA and 2-LTR circles (representative of viral cDNA that fails to integrate and is circularized by host DNA repair enzymes). Analyses of HIV reservoir data must take into account the strengths and weaknesses of the different readouts.

Mechanisms of latency

Maintenance of HIV latency in the reservoir is achieved through a variety of cellular and viral mechanisms that transcriptionally silence the proviral DNA (reviewed in [63,129,130]). As chromatin access affects DNA targeting by the PIC, many proviruses are found at easily accessible sites in highly expressed host genes. However, the competition with adjacent promoters for transcription factors and machinery can inhibit transcription of viral genes, thus helping to establish latency. The 5' LTR serves as the promoter for the viral genome and if it is divergent to a stronger host promoter in the host gene (RNA polymerases travelling away from each other) the RNA polymerase at the LTR may fail to recruit the required elongation complex factors. If the two promoter sites are convergent (RNA polymerases travelling towards each other), the RNA polymerase complexes may collide, halting transcription of both genes. Promoter traffic may be avoided if the proviral DNA is inserted into intergenic regions but as these are enriched

with transcriptional repressor binding sites this may also promote pre-integration latency.[64,131,132]

Post-translational modifications to the chromatin structure near the 5' LTR also influence HIV replication. Viral latency is enhanced by the recruitment of histone deacetylases (HDAC) that remove acetyl groups from histones, further repressing transcription. Hypermethylated CpG islands close to the HIV transcription site can attract the endogenous host protein, MBD2, which recruits HDAC during latency.[133] Similarly, loss or inhibition of Tat lowers the recruitment of transcription-inducing histone acetyltransferases (HAT).[134,135] Host cell transcription factors can also increase latency, for example, overexpression of IκBα, which is normally degraded during cellular activation, prevents NF-κB from entering the nucleus and binding the 5' LTR.[136,137]

Finally, the cellular RNA interference pathway may also maintain viral latency. MicroRNAs (miRNA; ~22 nucleotides in length) are non-coding RNAs that bind mRNA. If the complementarity is correct, the mRNA is cleaved but if the matching is imperfect the translation of the target mRNA is inhibited. Huang et al. investigated the potential miRNA target sites in the 3' untranslated region (UTR) of HIV RNAs and found that five cellular miRNAs that could bind this region were upregulated in resting T cells. After inhibiting these five miRNAs within resting T cells from ART-treated patients, replication-competent virus was recovered.[138] Reversal of latency upon blocking of the miRNAs suggests that cellular miRNAs may play a role in maintaining viral latency. In summary, diverse mechanisms have been implicated in the prevention of transcription and translation of viral proteins at multiple stages, from the exclusion of host transcription factors from the nucleus to host miRNA-mediated destruction of transcribed transcripts.[63,96,99,130]

Eradication strategies

As ART, even started during PHI, does not eliminate the HIV reservoir other eradication strategies have been proposed to target the latently infected cells that contribute the viral reservoir. As latently infected cells can be invisible to the immune system (also see section 3.1) the 'shock and kill' cure strategy aims at selectively reactivating latent viruses with pharmacological agents and then facilitating the killing of these cells, for example, by administering a vaccine to boost the CD8+ T cell response. This approach requires finding latency-reversing agents (LRAs) that can selectively reactivate latently infected cells only, preventing mass reactivation of global populations of T cells (cytokine storms). The latently reactivated cells must be reactivated enough to produce viral proteins which can then be displayed on HLA class I molecules to signal that the cell is infected.[107,139–145] An addendum to the 'shock and kill' strategy is the 'lock-in and apoptosis' strategy. Tateishi et al. synthesized a new compound, L-HIPPO, which is able to capture the HIV-1 protein $Pr55^{Gag}$, preventing $Pr55^{Gag}$ from translocating the virus to the plasma membrane for budding. Without being able to bud, the 'locked-in' viruses induce apoptosis of the cell.[146] Used in conjunction with a 'shock' reagent, this compound could facilitate the 'kill' of the latently infected cells without relying on CD8+ T cell responses. The 'shock and kill' approach, while currently being tested in clinical trials, for example the RIVER trial, requires further work to discover strong yet specific LRAs, dosing strategies and ART requirements (see section 3.1 for further details on 'shock and kill').

In opposition to the 'shock and kill' strategy is an additional strategy aimed not at reactivating virus to remove it, but silencing it forever with the cells. In the 'block and lock' strategy didehydro-cortistatin A (dCA), a Tat inhibitor, is used to block transcription of HIV essentially driving gene expression into a deep latency state. Kessing

et al. reported that dCA prevents viral rebound after interruption of ART or upon stimulation by increasing nucleosomal occupancy at Nucleosome-1.[147] While proviruses would still be hidden within cells this potential functional cure could allow PLWH to stop ART. This strategy would require further studies to determine how long dCA treatment would be required to induce enough transcriptional repression so that reactivation of virus would not occur. Strict monitoring of viral loads would be needed upon removal of ART when testing dCA dosing.

1.1.6 Immune response to HIV infection

Early innate immune responses to acute HIV infection

Studies of plasma donors who acquired HIV suggested that the first detectable innate response was induction of acute-phase protein synthesis; inflammatory cytokines or LPS stimulation (possibly via commensal bacteria that translocated from the damaged gut) may have instigated this initial response (immune response to HIV reviewed in[74,84]). Subsequent waves of cytokines and chemokines, such as IL-18, TNF, IFNγ and IL-22 loosely mirrored the peak in viral load. While some of these cytokines can enhance innate and adaptive immune responses they may also promote viral replication and immunopathology.[148] In addition to soluble factors, innate cellular responses are triggered. During acute HIV infection the population of DCs circulating in the blood decreases as they traffic to the lymphoid organs.[149,150] While some DC functions are impaired, for example, TLR-induced secretion of IL-12, TNFα, and IL-6, DCs can produce IFNα which enhances subsequent adaptive immune responses.[151–153] Natural killer cells (NK) are also activated during acute infection and can produce antiviral cytokines and lyse infected cells. Their role in the control of HIV is supported by evidence that HIV may reduce the expression of activating NK ligands and evades NK

cell-mediated pressure by selecting for sequence polymorphisms in regions of its genome targeted by the NK's killer immunoglobulin-like receptors.[154–156]

Adaptive immune responses to acute HIV infection

While innate responses develop before viral RNA is even detectable, the first CD8+ T cell responses (cytotoxic T lymphocytes, CTLs) are not generally measurable until the peak viraemia occurs. These early responses are specific for Env and Nef and reach their highest frequencies approximately 1 – 2 weeks after peak viraemia.[75,157,158] The lack of sequence divergence from transmitted/founder viruses suggests that these early CD8+ T cell responses do not drive escape mutants.[75,159] However, positive selection of viral mutations within CD8+ T cell epitopes, indicative of immune escape, is evident after the initial CD8+ T cell responses. New waves of T cell populations emerge in response to the viral diversification, targeting epitopes across the entire proteome but particularly in p24 Gag and Pol.[75,157,158,160,161] While previous reports suggested that CD8+ T cell driven escape events happen early and often, recent longitudinal viral sequence data proposed that the time to escape varies widely in patients and occurs slowly during the first three years of infection; 33% of patients studied experienced no escape incident in *gag, pol* or *nef* after two years of observation.[162] Even though HIV infects CD4+ T cells, severely depleting their numbers, HIV-specific CD4+ T cell responses are also primed in acute infection; responses to Gag epitopes are the best characterised, however, they quickly decline due to loss of proliferative capacity and preferential infection by HIV.[163–167]

The first detectable B cell responses, occurring from day eight after RNA detection, are non-neutralising antibodies directed against gp41 and gp120; they may be present as free antibodies or as immune complexes. Although they develop during acute infection, these responses neither control viral replication nor select escape mutants.[168–170]

Neutralising antibodies that drive escape mutants do not occur until at least 12 weeks post-transmission and respond to a narrow range of epitopes.[169,171,172] Broadly neutralising antibodies (bNAb), such as those that recognise conserved epitopes within Env (for example, the CD4 binding site), arise 20 – 30 months post-transmission but only in a small subset of patients; this may reflect both the requirement for extensive hypermutation in B cell receptors and the need for prolonged affinity maturation to elicit such broadly specific antibodies.[168,173,174] In general, the composition of the B cell population is affected directly and indirectly by the presence of HIV; viral replication in mucosal sites severely damages follicular B cells and germinal centres while HIV-induced early class switching results in an increase in memory B cells and plasma cells but a decline in naïve B cells. B cells are further hindered by the lack of help from CD4+ T follicular helper cells (T_{fh}), which normally reside in germinal centres and provide support to B cells necessary for somatic hypermutation of antibodies and maturation of the cells. During HIV infection this T cell population expands however it fails to provide help to B cells as PD-1 triggering on the T_{fh} reduces cell proliferation, activation and IL-21 secretion.[175] These effects may hinder the specificity and speed of the B cell response.[176,177]

The consequences of chronic immune activation

The clinical latency phase of an HIV infection lasts for years in PLWH.[178,179] Persistent HIV replication is associated with chronic immune activation that is not completely resolved even after sustained virological suppression under ART (reviewed in Klatt et al.[180]). An emerging view is that gut mucosal barriers are damaged by viral infection through destruction of CD4+ T cells and subsequent fibrosis, allowing microbial products to breach the tight mucosal barrier. These products recruit inflammatory cells and decrease mucosal regulatory cells, driving cellular activation and establishing a

vicious cycle. However, there is a disparity between this microbial translocation described in macaques (with SIV) compared to the reported lack of microbial translocation of natural hosts, like sooty mangabeys.[180–183] Hyper-activated monocytes and macrophages have impaired phagocytic responses to bacteria, DC subsets are altered and NK production of cytokines, like IFNγ and TNF, is reduced. B cells also appear dysfunctional and do not produce optimal antibody responses.[184–186] T cells from untreated PLWH display an activated phenotype, indicated by expression of CD38 and HLA-DR, together with upregulation of inhibitory receptors (IR) such as PD-1 and CTLA-4. Expression of both negative regulators and activation markers has been associated with disease progression.[187] Deeks et al. suggested that a T cell 'activation set point' can be defined by the level of CD38 expression and that this was predictive of the rate of CD4+ T cell decline and correlated with HIV viral load in untreated individuals.[188–191]

A high proportion of HIV-specific CD8+ T cells, the main contributors to initial control of the virus, may be lost rapidly due to apoptosis during acute infection.[192] Those that survive may become functionally impaired over time due to chronic antigen stimulation. This is manifested by reduced perforin and cytokine production, reduced proliferation and impaired lytic and antiviral inhibitory activity. A loss in the ability to self-renew in addition to deletion of exhausted clones results in a small, dysfunctional anti-HIV T cell response.[189,193–196] Part of the decrease of function of both B cells and CD8+ T cells is due to the loss of CD4+ T cell help, including the release of cytokines needed for isotype class switching and CTL proliferation, as the CD4+ T cell count declines.[175,197] This is in sharp contrast to the CD8+ T cell responses seen in rare individuals (elite controllers or long-term nonprogressors), that generally display intact antiviral functions and the capacity to secrete multiple cytokines

(polyfunctionality).[193,198,199] ART improves immune function, but even in patients with an undetectable viral load for many years an elevated level of activation is evident.[200–202] This persistent immunologic dysfunction and the overall systemic failure to clear HIV from the body suggests a more targeted approach is needed to enhance CD8+ T cell antiviral activity and potency.

1.2 Immune retargeting therapies to target the HIV reservoir

Attempts to eliminate HIV by therapeutic vaccination have been unsuccessful, in part because they generally boost CD8+ T cells that are functionally exhausted or ineffective due to pre-existence of escape mutants. However, novel immune retargeting therapies (IRT) originally developed for cancer immunotherapy may provide a solution. Although the first approaches to immune retargeting involved the adoptive transfer of engineered T cells, this is not within the scope of this literature review (reviewed in [203–205]).

1.2.1 Advent of IRT

Bispecific antibodies

Therapeutic monoclonal antibody (mAb) treatments were developed to induce immune-mediated tumour cell killing through both complement-dependent cytotoxicity and antibody-dependent cytotoxicity (ADCC). For example, the mAb, rituximab, binds CD20 on lymphocytes involved in Hodgkin's lymphoma and recruits effector cells with Fcγ receptors (FcγR) to bind the Fc portion of the mAb.[206] However, mAb therapies are limited by both their large size (~150 kDa) and the propensity for circulating immunoglobulins to compete for FcγR on effector cells. To overcome these limitations, bispecific antibodies (bsAbs) were developed. As tumour-infiltrating lymphocytes are known to mount an effective anti-cancer response, bsAbs were developed in order to

retarget T cells towards tumours as attempts to develop therapeutic T cell-based cancer vaccines failed.[207] Available in many different formats, bsAbs are able to bind two different targets simultaneously and have been engineered to be smaller and more potent as an IRT.[208] bsAbs can also have other non-retargeting functions, such as blocking cytokines, as reviewed in Fan et al.[209]

The first bsAb platform, introduced in 1995, was the trifunctional hybrid antibody (Triomab; figure 1.4). The Triomab was comprised of one half of a tumour-specific mouse IgG2a and one half of a CD3-specific rat IgG2b. This combination allowed for retargeting and activation of T cells towards cancer cells presenting the chosen antigen. This resulted in tumour lysis, cytokine release and ADCC even at picomolar concentrations. Additionally, the mouse/rat Fc-portion was still able to activate FcγR+ cells and immunogenicity caused by human anti-mouse/rat antibodies (HAMA/HARA) was reduced compared to earlier platforms; the induction of HAMA/HARA can shorten the serum half-life of the bispecific and may trigger adverse reactions thus reducing the clinical applicability.[210] Catumaxomab (anti-CD3/anti-EpCAM) was approved for use in cancer patients with EpCAM+ carcinomas with limited or no other treatment options.[211]

However, the Triomab platform was still relatively large. To reduce the size, the minimal binding domains of two different antibodies (the variable heavy and light chains) were associated resulting in a single chain variable fragment (scFv). Tandem scFv (TaFv) bispecifics were made by covalently bonding two scFv with a flexible peptide linker in a tandem orientation (figure 1.4). The flexibility provided by the tandem linker enhanced simultaneous, but targeted, binding and the smaller size facilitated easier tumour penetration.[212] The combination of an anti-CD3 scFv to an anti-tumour associated antigen scFv was given the moniker Bispecific T cell Engagers (BiTE). BiTEs can redirect polyclonal T cells to serially kill tumour cells with a strong cytotoxic response even at

low concentrations and low effector to target ratios.[213,214] However, because of the smaller size BiTEs do not remain in the serum for extended periods and in a clinical trial with blinatumomab (anti-CD19/anti-CD3) it was necessary to use continuous infusions to maintain serum levels.[215]

Achieving a slightly different orientation, bispecific diabodies (bsDb) are a second type of scFv-based platform. These are formed by non-covalently linking two scFvs with a short peptide; the variable domains are oriented against each other creating a small, rigid bispecific molecule. The slight instability resulting from the lack of a covalent bond was improved by adding a disulphide bond resulting in a Dual-Affinity Re-Targeting protein (DART). DARTs have a prolonged storage and serum stability and do not form aggregates.[216] A direct comparison of an anti-CD3/anti-CD19 DART and BiTE proved that DARTs were better at inducing B cell lysis and T cell activation; this was likely due to a higher association rate and target affinity.[217] Clinical trials involving different DARTs and BiTEs are underway to assess *in vivo* efficacy and dosing strategies.[209]

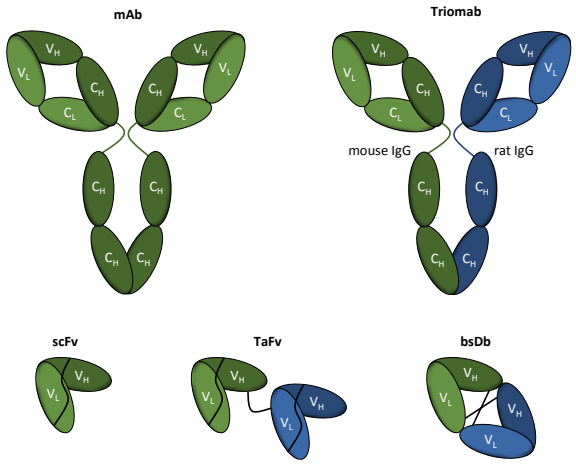

Figure 1.4: Bispecific antibody platforms. Trifunctional hybrid antibodies (Triomab) are comprised of the halves of two different antibodies to form a full-size monoclonal antibody (mAb). Single chain variable fragments (scFv) are comprised of the variable portions of the heavy and light chains and are connected via a peptide linker. Two scFv can be combined in tandem with a flexible peptide linker to create a tandem scFv (TaFv) or in opposition with a short linker to create a bispecific diabody (bsDb). Heavy chains shown in dark colours, light chains shown in light colours and linkages shown by dark lines; colours represent different specificities of the arms.[208,209,218]

Despite the engineering improvements seen over the course of bsAb development there are still limitations with the technology. While possible cancer antigen targets have been determined, any antibody technology is limited to surface presented antigens on tumour tissues.[219] Another issue, a key factor for clinical use, is the immunogenicity of the bsAb. As they are comprised of rat and mouse antibodies, the foreign epitopes induce production of neutralising HAMA/HARA, which can trigger a cytokine release syndrome.[208,220] Additionally, crosslinking of FcγR+ cells and T cells may activate the latter in the absence of target antigen. This risk was reduced by removal of the Fc region in BiTEs and DARTs, although other immune activation effects have been reported in clinical trials with BiTEs.[221]

The lack of an Fc-portion in some bsAb platforms comes at a cost as the Fc-portion enhances the serum half-life through neonatal-Fc receptor (FcR) mediated recycling by endothelial cells.[222] To circumvent this limitation, and to avoid continuous infusions, small bsAbs can be altered with pegylation, N-glycosylation or linkage to anti-CD16 antibody fragments to improve serum retention. However, steric hindrance may impact cytotoxicity.[223] The decrease in size associated with the TaFv technology (50 – 60 kDa) allows for better and more homogeneous tumour penetration. This ability to penetrate the tumour, where the technology is needed the most, may render the serum concentration less important. The bsAb technology can also be difficult to manufacture as mammalian cells are usually needed and this increases time and cost. While scFv can be produced in bacteria TaFv can form insoluble aggregates reducing the production yields.[224] In general, an ideal bsAb technology needs to have a high affinity for target antigens without causing non-specific activation, a high storage and serum stability and ease of manufacture.[208,209]

Bispecific T cell Receptors (TCR)

The bsAbs discussed above are able to redirect T cells via an anti-CD3 antibody or fragment, an important step for the anti-tumour immune response, but the restriction in specificity to cell surface antigens limits their scope. An alternative and possibly complementary option to BiTEs and DARTs is an Immune-Mobilising Monoclonal T cell receptor Against Cancer (ImmTAC). The ImmTAC comprises a humanised anti-CD3 scFv coupled to an engineered high-affinity monoclonal TCR (figure 1.5). The TCR portion is able to target intracellular antigens presented on HLA class I molecules, allowing the ImmTAC to target a much larger pool of tumour antigens. Unlike engineered 'TCR-like' antibodies TCRs are naturally better able to recognise the flat two-dimensional conformation of the peptide-HLA complex (pHLA). As in BiTEs and DARTs, the anti-CD3 scFv is able to activate T cells by binding CD3 and recruiting T cells to form an immunological synapse.[219,225–227]

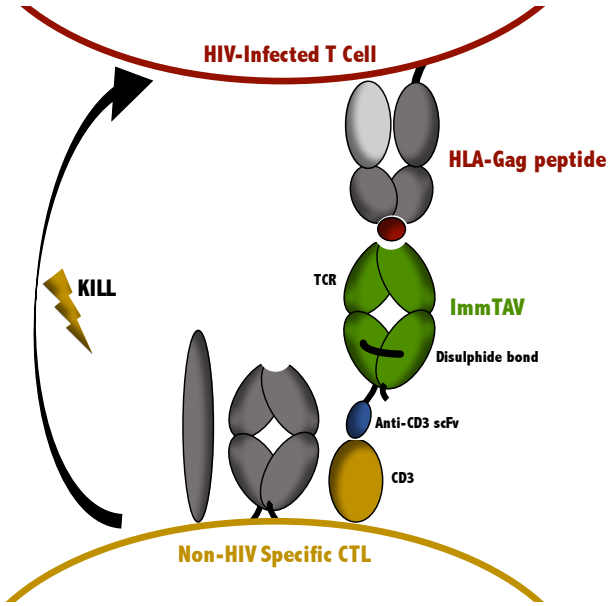

Figure 1.5: Immune-mobilising monoclonal TCR against viruses (ImmTAV). The engineered monoclonal TCR end of the bispecific m121 ImmTAV recognizes the HLA-A2 presented SL9 peptide (from HIV Gag) on HIV-infected CD4+ T cells with picomolar affinity. The anti-CD3 scFv end, by binding CD3 on T cells, can redirect non-HIV specific CD8+ T cells to kill the infected cell. The 'ImmTAC' has the same structure but includes a TCR that recognises cancer antigens.

To achieve a soluble, stable and functional bispecific TCR many engineering challenges had to be overcome. Natural TCRs bound to the cell benefit from the stability of the plasma membrane, which allows them to retain native ligand binding. A disulphide

bond between the alpha and beta constant domains of the soluble ImmTAC allowed the TCR chains to achieve a native-like conformation that is not immunogenic *in vivo*. A phage display technique was also used to select and enhance the affinity of natural TCRs; by targeting mutation(s) in all six complementarity determining regions of the TCR a one million-fold or higher increase in affinity compared to natural TCRs was achieved. The ImmTAC's TCR binds its cognate antigen with a higher affinity than the effector anti-CD3 end, with off-rates of several hours and minutes respectively, ensuring that the ImmTAC function is primarily governed by binding to the correct target yet ensuring that T cell engagement is sufficient to achieve an effector response. The ImmTAC is able to recognise tumour cells expressing as few as 10 HLA-peptide complexes even at picomolar concentrations. The requirements for a successful bispecific molecule also apply to the ImmTACs: small (75 kDa), stable, soluble, easily manufactured in *E. coli* and a low risk of immunogenicity.[219,225,226]

The first ImmTAC to reach the clinic targeted the melanoma antigen, gp100; ImmTACs targeting three other tumour-associated antigens: MAGE-A3 (cancer testis antigen), Melan-A/MART-1 (primary/metastatic melanomas) and NY-ESO-1 (cancer testis antigen) were also developed. The ImmTACs were able to activate unstimulated CD8+ T cells and their potency depended on the ImmTAC-pHLA affinity. The activated CD8+ T cells showed polyfunctional memory responses (IL-2, IFNγ, and TNF production) and a subset of CD4+ T cells also produced TNF and IL-2 and were able to lyse tumour cells. In a mouse tumour model, *in vitro* imaging showed the lysis of tumour cells by ImmTAC-redirected CD8+ T cells even at low concentrations and effector to target ratios.[225,226] Interestingly, the IMCgp100 ImmTAC also elicited cross-presentation of melanoma antigens by DCs. After inducing T cells to lyse tumour cells the resultant antigens activated DCs, which were able to display the tumour antigens on their surface

and activate both melanoma-specific and polyclonal ImmTAC-redirected T cells.[227] Clinical trials of IMCgp100 not only proved safe in uveal melanoma patients but there was tumour shrinkage in those with poor prognosis and immune checkpoint antagonist resistant disease.[228]

Although theoretically there is a larger selection of target antigens for ImmTAC development there are limitations. Ideally, a tumour-specific antigen or mutation found only in tumours represents the cleanest target but these are rare and may not occur at a sufficient frequency even for the high affinity ImmTAC. Overexpressed or aberrant versions of self-proteins are more common for tumours but may be expressed in normal tissues.[219,229] Differences in expression may provide a therapeutic window wherein the location or level of expression in normal tissues is minimal in comparison to the tumour, allowing for safe use of an ImmTAC. However, as the TCR is restricted by a given HLA class I allele, this limits the use of the ImmTAC to individuals carrying this allele. The first ImmTACs are all HLA-A*0201-restricted as this allele is the most frequent across the world. Nevertheless, similar restrictions can also be seen in antibody therapies, which only target certain tumour mutations not present in every cancer case.[219,226,230] As the ImmTAC targets peptides in the context of human HLA alleles, safety testing to assess cross-reactivity in animal models is of limited or no use. Instead, combinations of *in vitro* tests on whole blood and tissues are used to screen for cross-reactivity. Pre-clinical data with the most advanced ImmTAC, IMCgp100, demonstrated the validity of this approach.[219,228] In summary, ImmTACs represent a new therapeutic option that may be used in combination with other bispecific molecules, monoclonal antibodies or conventional cancer treatments to overcome tolerance and clear tumours.

1.2.2 Application of IRT for viral infections

The similarities between the tumour and chronic viral infection environments lend support for exploring the use of bispecific molecules for chronic viral infections (reviewed in Kim et al.[231]). As described previously, during chronic viral infections persistent antigen exposure can exhaust the immune system, similar to the effect seen with cancer antigens.[232,233] Whereas conventional therapeutic HIV vaccines can only mobilise a fraction of the CD8+ T cell repertoire, including those clones in the exhausted immune response which failed to control the virus initially, IRT has the potential to redirect a larger population of CD8+ T cells to target HIV-infected cells potentially mitigating viral escape. The affinity enhancement of the bispecific molecules also allows for targeting of infected cells with low antigen expression, including resting infected cells, and in contrast to tumour antigens the viral antigens targeted by bispecific molecules are immunogenic as they are not expressed in the thymus.[231–233]

One of the early bispecific viral therapeutics was a tetravalent bispecific antibody that targeted hepatitis B virus (HBV) surface antigens. Attempts to produce mAbs against the surface antigens (S protein) for prophylaxis of HBV infection were unsuccessful as many immune escape mutants emerged.[234] To improve the protection against infection, Park et al. developed a multivalent bsAb comprised of two consecutive scFv fused to the Fc region of a human IgG1 that was able to bind the S and preS2 antigens of HBV.[235] For targeting HIV, Duval et al. developed a bispecific antibody comprised of a broadly reactive anti-gp41 antibody (F240) and an anti-IgA receptor (CD89). This bsAb recognised primary isolates from all clades of HIV and recruited neutrophils for destruction of the infected cells; as neutrophils are competent at mediating cell cytotoxicity and are partially resistant to infection the recruitment of neutrophils instead of T cells provided an alternative for destruction of infected cells.[236] The retargeting with

an antibody other than anti-CD3 represents an interesting idea for increasing the specificity of the cells that are recruited. Anti-CD3 recruits both CD8+ and CD4+ T cells, including potentially suppressive regulatory T cells (T_{reg}), which have been found in high numbers in tumours.[237]

With the advancement of bsAb technology, more recently bsAbs targeting HIV Env, fused to an anti-CD3 scFv, have been developed for treatment of chronic HIV infection. Sung et al. reported the development of an HIV x CD3 DART comprising a non-neutralising mAb against Env (A32 or 7B2) and a humanised anti-CD3 mAb. These HIV x CD3 DARTs were able to redirect polyclonal CD8+ T cells from both HIV seronegative and ART-suppressed HIV-seropositive donors to kill HIV-infected CD4+ T cells *ex vivo*. The reduction in virus recovery even without the addition of CD8+ T cells (infected CD4+ T cells and DARTs only) also suggested that the DARTs recruited cytotoxic CD4+ T cells. The DARTs did not induce T cell activation or lysis in the absence of Env.[238] However, the effectiveness of the DARTs could be limited as Env is highly variable and expression is low. Additionally, viral escape from the use of anti-Env DARTs may occur as viral escape from single anti-Env bNAbs has been reported in trials of bNAb infusions during ART followed by ART interruption.[239,240]

Sloan et al. also developed a panel of HIV x CD3 DARTs that utilised bNAbs. The PGT121 and PGT145-based DARTs (in addition to the previously described A32 and 7B2 DARTs) successfully mediated CTL killing of HIV-infected resting primary cells with low Env expression. Using *ex vivo* PBMCs from patients on suppressive ART these DARTs were able to significantly reduce viral RNA in culture supernatants after 14 days suggesting that a portion of the HIV reservoir cells may express enough Env to be targeted.[241] Naturally occurring bNAbs have also been re-engineered to improve their potency as a component of a bispecific molecule. Rudicell et al. used sequencing and

bioinformatics to enhance the neutralisation capacity of the VRC07 anti-Env bNAb; VRC07-523 as part of a bsAb was able to redirect follicular CD8+ T cells to kill HIV-infected cells.[242,243]

Given the limitations of targeting HIV Env as discussed earlier, the ImmTAC platform technology has been applied to target the Gag protein, which is highly conserved and highly abundant in infected cells. The prototype molecule, known as an Immune-mobilising monoclonal T cell Receptor Against Viruses (ImmTAV) was designed to target the HLA-A*0201-restricted Gag p17 epitope, SLYNTVATL (SL9) and known escape mutants.[244] Two candidates that target the same epitope but with different binding half-lives (indicated by batch numbers, m121 and m134) were tested in *in vitro* model systems and *ex vivo* assays with CD4+ T cells from patients. Our laboratory reported that these HIV-specific ImmTAVs were able to elicit elimination of Gag+ cells even at nanomolar concentrations and low effector to target ratios. As with the bsAbs, the ImmTAVs were able to redirect CD8+ T cells from both HIV seronegative and ART-suppressed donors. Epitope counting analysis using a biotinylated mTCR with the same specificity showed that the epitope density on infected cells ranged from 8 to 46 epitopes, highlighting the sensitivity of the engineered TCR.[245] This provided the first evidence that ImmTAVs may have the potential to target HIV reservoir cells *ex vivo*. While encouraging, it is likely that a combination of several ImmTAVs would be needed to achieve clinical benefit. Additionally, the ability to improve killing by retargeting the CD8+ T cells of chronically infected patients or healthy donors, provides scope to investigate the T cell-T cell interaction mediated by the ImmTAV.

1.3 The importance of the immunological synapse

1.3.1 The immunological synapse

The immune retargeting mediated by the bispecific molecules described in section 1.2 brings an effector and target cell together, facilitating the formation of an immunological synapse (IS). The IS refers to the temporal and spatial organisation of structural and signalling molecules between a lymphocyte and an antigen presenting cell (APC; reviewed in [246–248]). The IS serves as a conduit for signals transmitted or received by the T cell.[249,250] Although interactions between APCs and lymphocytes had been described in terms of functional outcomes, the advent of advanced microscopy-based techniques allowed for the description of the structural rearrangements that occur when the two cells communicate.[249–251] A majority of this pioneering work defining the IS has relied on *in vitro* systems such as supported lipid bilayers and mouse models.[252–256] The mature IS is comprised of three supramolecular activation clusters that form a 'bullseye' pattern: the central (cSMAC) region contains the TCR-CD3-pHLA complex and costimulatory molecules like CD28 or inhibitory molecules like CTLA-4; the peripheral (pSMAC) region is comprised of adhesion molecules, like lymphocyte function-associated antigen 1/intracellular adhesion molecule 1 (LFA-1/ICAM-1), and signalling cascade proteins like lymphocyte-specific protein tyrosine kinase (Lck); larger transmembrane cell surface proteins like CD43, CD44, and CD45 plus actin comprise the distal (dSMAC) region (figure 1.6).[249,257]

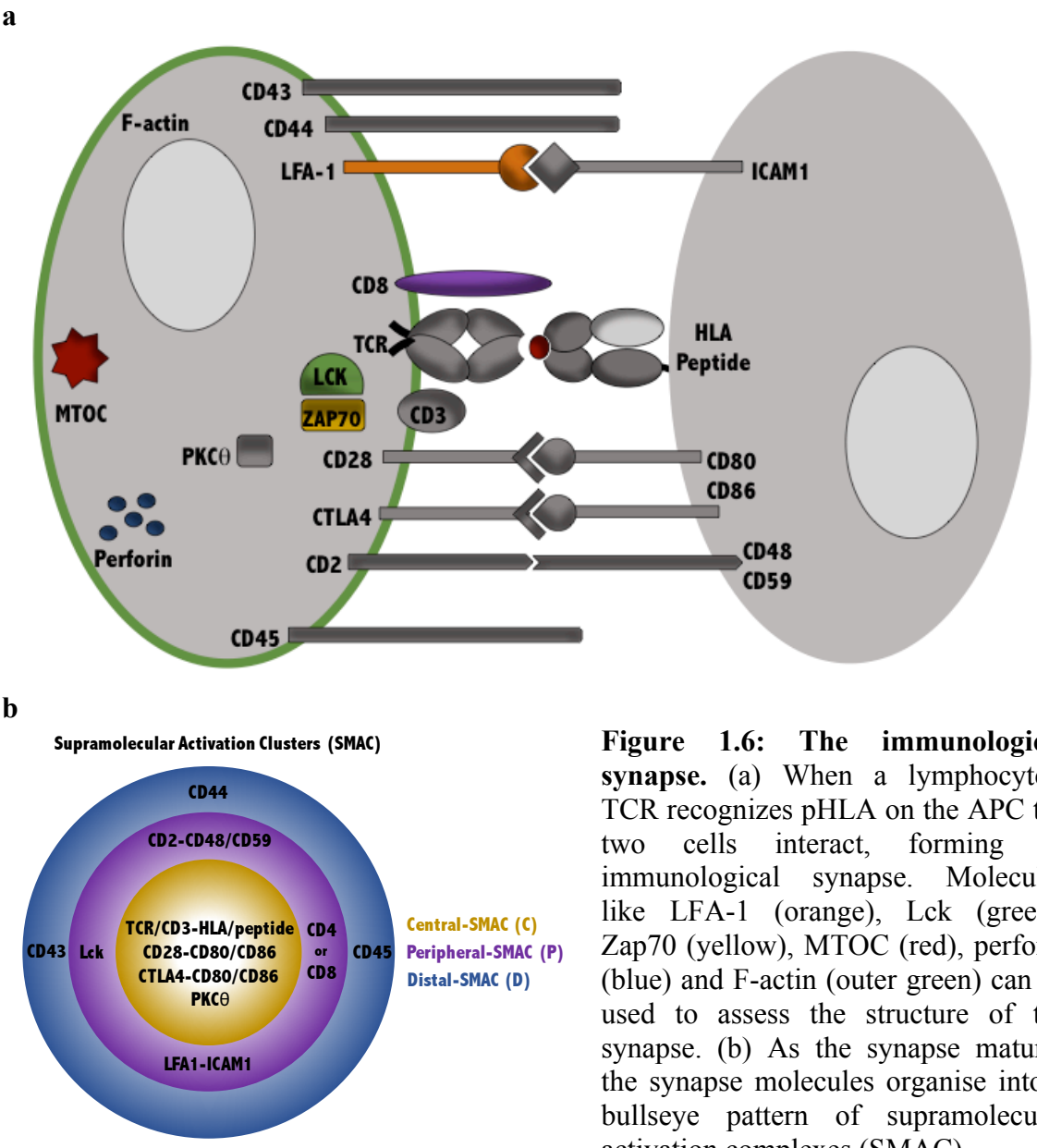

Figure 1.6: The immunological synapse. (a) When a lymphocyte's TCR recognizes pHLA on the APC the two cells interact, forming an immunological synapse. Molecules like LFA-1 (orange), Lck (green), Zap70 (yellow), MTOC (red), perforin (blue) and F-actin (outer green) can be used to assess the structure of the synapse. (b) As the synapse matures the synapse molecules organise into a bullseye pattern of supramolecular activation complexes (SMAC).

The bullseye arrangement indicates a mature synapse but this structure is the endpoint of molecular reorganisation and signalling between the two cells occurs before this point.[258] The first stage in the formation of the IS requires the highly motile lymphocyte to slow down to allow for the TCR-pHLA signalling to occur. LFA-1 expressed on the lymphocyte binds ICAM-1 on the APC creating adhesive interactions to bring the cell to a stop; the time from antigen recognition to arrest is dependent on the quantity of antigen.[259,260] Studies with ICAM-1-deficient mice showed that the LFA-

1/ICAM-1 interaction was crucial for memory responses but not cytokine production or proliferation.[261] Recognition of antigen induces the creation of microclusters of 11 – 17 TCRs plus separate LFA-1 microclusters in the dSMAC.[262] Both types of cluster move through the pSMAC towards the cSMAC by an actin-dependent mechanism but only TCR clusters penetrate the actin-free cSMAC. This exclusion of LFA-1 may be related to the size of the molecule as TCR/pHLA complexes are ~15 nm whereas LFA-1/ICAM-1 complexes are 40 nm.[263] This 'kinetic segregation' model also applies to the exclusion of CD45 to the dSMAC (the smallest variants are ~22 nm) and is supported by thermodynamics; grouping molecules by size allows the correct pairings to interact regardless of the 'height' of their neighbours.[264]

Signalling begins when the TCRs form microclusters in the pSMAC and upon localising to the cSMAC the signalling decreases. In a comparison of antigenic peptide dosing phosphotyrosine staining showed that higher doses of peptide elicited less phosphotyrosine staining in the cSMAC even though the cSMAC formed with greater efficiency.[258,265,266] This seemingly contradictory pattern may be explained by the natural recycling of TCRs. TCRs triggered by agonist ligands become degraded in lysosomal compartments in order to control the level of signalling and consequent T cell activation. If the cSMAC functions as one of these compartments, then in the case of strong agonist signalling (higher dose of peptide) TCRs would become degraded at the easily formed cSMAC resulting in the reduced phosphotyrosine staining; likewise, the weak agonist (lower dose) would not stimulate the degradation process, resulting in more phosphotyrosine detection.[267,268] Because of the consistent inwards flow of microclusters of TCR, and subsequent degradation, continuous formation of TCR microclusters is required at the periphery to maintain signalling.[262]

TCR-mediated tyrosine kinase signalling is the first step in a cascade of signalling molecules that transmit the antigen-derived information to the T cell. Lck and Fyn phosphorylate tyrosine residues in the immunoreceptor tyrosine-based activation motifs (ITAMs) of the CD3 cytoplasmic domain. This leads to the recruitment of zeta chain associated protein kinase 70 (Zap70), which becomes activated and phosphorylates SLP-76 and Lat. These scaffolding sites provide binding positions for the continuation of signalling events to promote cytoskeletal rearrangements, activation of additional signalling paths and recruitment of relevant transcription factors.[269] The recruitment and activation of the kinase, PKC-θ, is particularly important for the activation of the NF-κB, NFAT and AP-1 transcription factors.[270–272] Additionally, the production of inositol triphosphate triggers the release of Ca^{2+} from the endoplasmic reticulum; this in turn instigates a Ca^{2+} influx into the cell through calcium channels and the elevated Ca^{2+} concentration activates Ca^{2+}-dependent enzymes and transcription factors, like NFAT.[273] These transcription factors translocate to the nucleus to regulate expression of genes required for cell survival and effector functions. Signalling can be inhibited and controlled by the binding of inhibitory receptors like CTLA-4, which competes with CD28 for binding of CD80/CD86. Once bound, it recruits the phosphatase SHP2 which dephosphorylates activated CD3 subunits.[274]

The initiation of signalling and the formation of an IS results in changes to the morphology of the cell and polarisation of the molecules within. As lymphocytes migrate integrin-mediated adhesions at the leading edge promote forward mobility, and unlike other cell types, the microtubule-organising centre (MTOC) is positioned towards the rear of the cell.[275] However, once a stable contact is formed the MTOC begins to migrate towards the synapse directed by the minus end protein, dynein, which may pull the

microtubules and thus the MTOC towards the IS. The distance of the MTOC from the IS is crucial in CTLs for the release of cytotoxic granules at the cytotoxic synapse.[276]

1.3.2 Cytotoxic synapses

The effector functions of cytotoxic CD8+ T cells and NK cells require the directed release of granules towards the correct target cell without bystander destruction. This specificity is achieved by the formation of a cytotoxic synapse, a specialised form of an IS (reviewed in[277–281]). While the synapse formed with a naïve CD8+ T cell may last for hours, and priming of the cell to divide and differentiate takes days, the already primed CTL's effector functions are triggered within minutes of forming a cytotoxic synapse.[256,276,277] Additionally, while the antigen sensitivity of a CTL is similar to that of a helper T cell, CTLs are able to kill after forming only three pHLA complexes and without complete signaling.[282]

Upon TCR microcluster signalling, within the first 20 seconds of contact between the two cells, filamentous actin (F-actin) begins to accumulate at the synapse but then rapidly clears. The subsequent reorganisation of membranes to form tight contacts provide an ideal interface for the release of cytotoxic granules into the junction between the two cells and thus ensure that only the target cell is killed. Two minutes post-contact the TCR clusters appear at the cSMAC, as described earlier, and the MTOC migrates towards the synapse bringing the cytotoxic granules, which have polarised towards it, with it. Within six minutes these granules are released into the synaptic cleft and the perforation of the target cell's membrane (by perforin) and cleavage of proteins (by granzymes) results in blebbing and destruction of the cell. According to the bullseye model of the SMACs, the region of cytotoxic granule release lies within the cSMAC, dividing the central region into a TCR-based and granule-based region. In a comparison of CD8+ and CD4+ cytotoxic T cell clones both types of cell used the perforin/granzyme

pathway to kill but CD8+ CTLs formed more stable synapses and were 100-fold more efficient.[283,284] While CTLs are also able to kill via the CTL's Fas ligand binding CD95 on target cells perforin-mediated killing is faster.[285] CTLs are known to kill multiple targets in rapid succession and this serial killing is facilitated by the quick retraction of the MTOC from the plasma membrane before the target cell even starts to die.[256,276] As the centrosome retracts the microtubules reorganise and any transiting granules, which have not yet docked, retract back into the cell with the MTOC. This process prevents any further access of granules to the IS and allows the cell to repolarise to another target cell immediately.[286]

NK cells also form cytotoxic synapses to achieve efficient killing. NK cell-mediated killing is triggered by antibody recognition of the Fc receptor CD16. However, this binding alone does not initiate polarisation of the granules as other NK activating receptors are required to elicit a synergistic cytotoxic response. Signalling, including the recruitment of Fyn, leads to the formation of cSMAC and pSMAC regions. However, unlike CTLs not all synapses formed by an NK cell result in killing; the ratio of activating tyrosine kinases to the inhibitory phosphatase, SHP-1, determines the fate of the synapse with a higher ratio resulting in a cytotoxic synapse.[287,288] As a result, in studies of NK cell synapses the NK cells sustained the IS for a longer period of time compared to T cells.[251] The formation of a mature bullseye pattern acts as a checkpoint to assess the balance of activating and inhibitory signals, unlike in a CTL which once triggered exerts its effector function rapidly.[280,289] Despite the differences between the two cell types, the shared process of SMAC formation and degranulation highlights the importance of coordinated structural rearrangements to achieve the most efficient killing. The number of molecules and steps that are required suggest that failure at any step along the pathway could result in a CTL that is unable to clear target cells. As CTLs from PLWH fail to clear the

infection, the failure may be a result of an inability to form a mature and functional synapse.

1.4 Thesis aims

This thesis aims to address questions concerning the failure of cytotoxic T cells to eliminate HIV in chronically infected patients including:

- **Are latently infected CD4+ T cells susceptible to elimination via ImmTAV-mediated killing?**
- **Can an HIV-specific ImmTAV be used to study the development of immunological synapses between primary CD4+ and CD8+ T cells?**
- **Can studying the immunological synapse between CD8+ T cells and HIV-infected CD4+ T cells shed light on the failure of CTLs to kill HIV-infected CD4+ T cells during chronic HIV infection?**
- **To what extent do antiviral therapies impact T cell fitness and function?**

CHAPTER TWO: MATERIALS AND METHODS

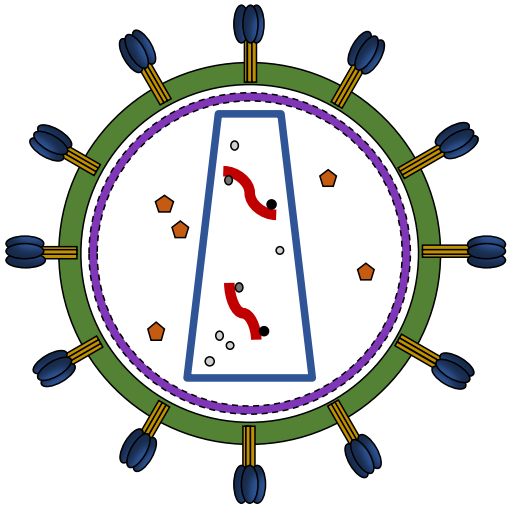

2.1 Study subjects and cell lines

2.1.1 HIV seronegative donors

For healthy controls, peripheral blood mononuclear cells (PBMCs) were isolated from the peripheral blood of healthy adult volunteers (covered by the Human Tissue Authority licence no. 12217) or from HIV seronegative buffy coats acquired from the NHS Blood Transfusion Service (Bristol, England). All donor samples were processed within one day of collection and were either used fresh or were cryopreserved in foetal calf serum (FCS; Sigma-Aldrich, UK) with 10% dimethyl sulfoxide (DMSO; Sigma-Aldrich).

2.1.2 PBMCs from patients with chronic HIV infection

PBMC samples from patients with chronic HIV infection were acquired from three different studies.[290–292] Initial blood samples were obtained with written informed consent from all participants and approval from UK Research Ethics Committees (Dorrell et al. 2006 – Gene Therapy Advisory Committee, Medicines and Health Products Regulatory Agency, local Research Ethics Committee; Holloway et al. 2013 – Oxfordshire Research Ethics Committee (No. 10/H0604/95); Hancock et al. 2017 – Gene Therapy Advisory Committee, Medicines and Health Products Regulatory Agency (No. 2009-012662-31), Oxford University Hospitals NHS Trust). Isolated PBMCs were cryopreserved in the NDM Research Building (covered by the Human Tissue Authority licence no. 12217). All subjects had received combination ART for at least one year and were virologically suppressed at the time of sampling.

2.1.3 PBMCs from SPARTAC trial participants

PBMC samples from HIV positive subjects who had initiated ART during primary HIV infection (SPARTAC trial) were obtained through the CHERUB collaboration including Prof John Frater and Prof Sarah Fidler. The cohort included 10 HLA-A*0201

participants from arm C of the trial (assigned to receive 48 weeks of ART) who were virologically suppressed and had started ART within six months of seroconversion.[293]

2.1.4 PBMCs from RIVER trial participant

Blood samples from HIV positive subjects who had initiated ART during primary HIV infection (RIVER trial) were obtained with written informed consent and ethics approval (REC reference 14/SC/1372). The blood samples were collected as described in Fun et al. and the PBMCs were depleted of resting CD4+ T cells.[294] The remaining fraction of one patient's PBMCs (CD8+ and CD25+CD69+HLA-DR+CD4+ cells) was used in this thesis (cell separation by Axel Fun, University of Cambridge).

2.1.5 Cell lines

T2 cells were obtained from the American Type Culture Collection. T2 cells (HLA-A*02/B*51) were derived from T0 cells and carry just one chromosome 6; they are TAP-deficient and present only peptides derived from leader sequences or exogenous peptides as used in this thesis. Immunocore Ltd. provided the T0 cells; these cells were derived from a B cell line (721.174) and a T cell line (CEM) and are triploid (class 1 HLA-A*01/A*02/A*31 and HLA-B*08/B*40/B*51). The WJR076 B cell line (HLA-A*02/B*57) was a gift from Dr Gerry Gillespie (University of Oxford). Cryopreserved cell lines were thawed and cultured in R10 for at least one week before use to allow them to resume their normal cell cycle. Cells were counted and resuspended in fresh R10 every 3 – 4 days to maintain a productive cell density (0.5 – 1 million cells/ml) and to limit exhaustion of nutrients.

2.2 Reagents and buffers

2.2.1 Buffers

R0: RPMI-1640 (Sigma-Aldrich) with 1% penicillin/streptomycin (Sigma-Aldrich) and 1% L-glutamine (Sigma-Aldrich)

R10: RPMI-1640 with 10% FCS, 1% penicillin/streptomycin and 1% L-glutamine

R10 with IL-2: R10 with 20 IU/ml IL-2 (PeproTech)

H10: R0 with 10% human AB serum (Sigma-Aldrich), filtered

MACS buffer: 2 mM EDTA (Life Technologies Ltd.) and 0.5% BSA (Sigma-Aldrich) in PBS (Life Technologies Ltd.)

Paraformaldehyde (PFA): 2 – 4 % PFA (Insight Biotechnology Ltd.) in PBS

Lysolecithin PFA: 4% PFA (in PBS; Insight Biotechnology Ltd.) with L-α-lysophosphatidylcholine (20 μg/ml; Sigma-Aldrich)

NP-40: 0.1% Nonidet P-40 (Sigma-Aldrich) in PBS

Saponin buffer: 0.1% saponin (MP Biomedicals UK) and 0.5% BSA in PBS

2.2.2 ImmTAVs

Immune-mobilising monoclonal TCRs against viruses (ImmTAV) were provided by Immunocore Ltd. mTNF121 (used at 10^{-11} to 10^{-8} M) comprised a disulphide linked TCR, recognising the HIV-1 p17 epitope SLYNTVATL (SL9) with picomolar affinity (and escape variants – SLYNT**I**ATL, SLYNT**I**A**V**L, SLYNTVA**V**L, SL**F**NT**I**ATL, SL**F**NT**I**A**V**L, SL**F**NTVATL and SL**F**NTVA**V**L) fused to an anti-CD3 scFv.[226,245] mTNF231 (used at 10^{-9} to 10^{-8} M) comprised the same SL9 TCR fused to a non-binding anti-CD3 scFv. mTNF232 (used at 10^{-9} to 10^{-8} M) and irrelevant ImmTAC (used at 10^{-9} to 10^{-8} M) were comprised of non-SL9 specific TCRs fused to the binding anti-CD3 scFv portion.

2.2.3 Antiretroviral agents

Antiretroviral agents were used *in vitro* at concentrations equivalent to the therapeutic C_{max} measured in patients where possible. Zidovudine (ZDV; 5 μM) was obtained from Oxford University Hospitals NHS Trust Pharmacy. Tenofovir disoproxil

fumarate (TDF; 10 μM) and darunavir (DAR; 10 μM) were obtained through the NIH AIDS Reagent Program.

2.2.4 Latency-reversing agents

To reactivate HIV in resting cell infections the latency-reversing agents (LRA) bryostatin (10 nM, stock at 5 μM in PBS; Sigma-Aldrich), romidepsin (40 nM, stock at 4 μM in PBS; Sigma-Aldrich), acitretin (5 μM, stock at 10 mM in DMSO; Sigma-Aldrich) and vorinostat (350 nM, stock at 2 mM in DMSO; Sigma-Aldrich) were added, alone or in combination, to resting infected cells.

2.2.5 Autophagy inhibitors

Autophagic flux inhibitors were included in autophagy assays to manipulate autophagic flux in PBMCs including chloroquine (15 μM in water; Sigma-Aldrich), bafilomycin (0.1 μM in ethanol; Sigma-Aldrich) and the proprietary autophagy reagent A (ARA; inhibitor of autophagic flux, 1:1000 in water; Merck Millipore). Equal volumes of ethanol or water were used as diluent controls.

2.3 HIV-1 isolates

HIV-1_{IIIB} is a clade B, CXCR4 tropic isolate and was obtained from the Centre for AIDS Reagents, NIBSC, Health Protection Agency, UK. The preparation and titration of the stock of HIV-1_{IIIB} used in this thesis was completed by another member of the research group as previously described.[295,296] In short, for propagation of virus, PBMCs from HIV-seronegative donors (2 x 10^6 cells/ml) were stimulated with phytohaemagglutinin (PHA; 5 μg/ml) in R10 for three days, after which the cells were washed and spinoculated with HIV-1_{IIIB} (2000 rpm) for two hours at 25°C. After spinoculation 80% of the supernatant was removed and the remaining cells and virus were resuspended in R10 with IL-2 (1 x 10^6 cells/ml) in a tissue culture flask. The cells were incubated at 37°C /5% CO_2 for seven days and aliquots were taken at two, three,

five, and seven days post-spinoculation for analysis of the rate of infection (section 2.10.1). The supernatant containing the viral particles was collected on days three and five and stored at -80°C in 2 ml freezer vials; R10 with IL-2 culture medium was replaced as necessary.

To titrate the HIV-1_{IIIB}, stimulated PBMCs were infected with ten-fold serial dilutions of virus in replicates (four/titration). After six days, flow cytometry was used to assess the %p24+ cells in each of the wells; wells with %p24+ cells > 1% were scored as 'infected.' The Reed-Muench method was then used to calculate the 50% tissue culture infective dose ($TCID_{50}$) based on the number of infected and uninfected wells for each dilution of virus; this included calculating the proportionate distance (PD) based on the two dilutions achieving >50% infected wells and <50% infected cells (appendix 2.1).[297] The $TCID_{50}$ was then used to calculate the number of plaque-forming units (PFU). To determine the volume of virus required for a specific multiplicity of infection (MOI; ex: MOI of 0.01 = 10,000 virus particles/1,000,000 cells) the number of cells to be infected (ex: 1 x 10^6) and the PFU of the virus available was used (appendix 2.1).[298]

2.4 HLA typing

In order to identify HLA-A2+ donors PBMCs were initially screened by staining with an HLA-A2-specific antibody (BioLegend) and analysed using flow cytometry. 200,000 cells/donor were plated in a 96-well plate (1800 rpm, 3 minutes) then washed in PBS. They were then stained with LIVE/DEAD™ fixable aqua dead cell stain (0.5 µl/sample; Invitrogen) and HLA-A2-PE (1.5 µl/sample) in PBS for 20 minutes at room temperature (RT). Cells were then washed twice in PBS and resuspended in 200 µl of 2% PFA. Samples were acquired on a CyAn flow cytometer (Beckman Coulter) and data analysed using FlowJo software (version 9 or above; FlowJo, LLC). The mean

fluorescence intensity (MFI) of HLA-A2-PE of the alive (LIVE/DEAD$^{neg.}$) population was compared to known HLA-A2-positive or negative PBMC controls (figure 2.1).

In order to confirm the HLA-A2 status, DNA was extracted from donor PBMCs and sent to the DNA Sequencing/HLA Typing Laboratory (WIMM, John Radcliffe Hospital) for typing by ARMS-PCR with probe-specific primers. In brief, 1 x 10^6 cells were added to 1 ml RBC lysis buffer (Qiagen), then centrifuged at 1500 rpm for 5 minutes. Supernatant was discarded and 200 µl cell lysis solution (Qiagen) was added to the cell pellet followed by gentle mixing. 200 µl protein precipitation solution (Qiagen) was added and the solution was gently inverted for three minutes. The sample was centrifuged again and the supernatant was transferred into a new tube. 600 µl isopropanol was added and mixed gently to precipitate the DNA. The sample was centrifuged again and the pellet was washed in 70% ethanol. After a final spin the supernatant was discarded and the lid was left off to allow the alcohol to evaporate. The pellet was resuspended in 30 ml sterile distilled water.

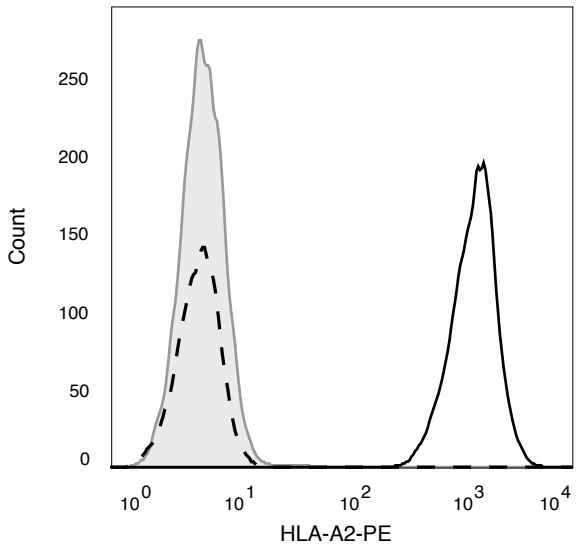

Figure 2.1: Identification of HLA-A2+ donors. To screen for HLA-A2+ donors PBMCs were stained using an anti-HLA-A2-PE antibody. A histogram of the MFI of the PE fluorescence was compared to those from previously HLA typed HLA-A2-positive (solid black line) and HLA-A2-negative donors (grey shaded line); HLA-A2-PE isotype control shown for comparison (dashed black line).

2.5 Preparation of primary T cells

2.5.1 PBMC isolation

To separate PBMCs from fresh blood or buffy coats (diluted in 150 ml R0) blood was added to Lymphoprep^{TM} (STEMCELL Technologies) in 50 ml tubes to isolate the PBMCs via density gradient centrifugation (2000 rpm, 20 minutes; no brake). The lymphocyte layer (located between the Lymphoprep and the plasma) was removed and washed twice in R0 (2000 rpm, 10 minutes). Cells were resuspended in R10 for counting. If using fresh, PBMCs were rested in R10 (1 x 10^6 cells/ml) at 37°C/5% CO_2 for at least two hours before use; otherwise the freezing protocol was followed. Pelleted cells were resuspended in chilled FCS and combined with a 20% DMSO in FCS mix to make a 10% DMSO solution in CS (5 – 30 x10^6 cells/ml). The solution was quickly aliquoted intocryovials (1 ml cell suspension/vial) and stored overnight at -80°C in an isopropanol cooling box. Cells were transferred to vapour phase liquid nitrogen the next day for long-term storage.

2.5.2 Thawing cells

To thaw frozen cells the vials were agitated in a 37°C water bath until only a small pellet remained. Cells were added dropwise to warmed R10 with DNase I (6 µg in 10 ml R10; Sigma-Aldrich) then washed twice in R10 (1500 rpm, 5 minutes). Cells were resuspended in R10 and rested for at least two hours at 37°C. Before use cells were counted using a Z Series Coulter Counter (20 µl cell suspension in 10 ml buffer; 1:500 dilution factor; Beckman Coulter) and viewed under a microscope using the Trypan Blue stain (Sigma-Aldrich) to assess cell viability.

2.5.3 CD8+ T cell separation

Magnetic bead separation was used to isolate CD8+ T cells from PBMCs. Cells were centrifuged at 1500 rpm for 10 minutes then resuspended in 80 µl MACS buffer and

20 µl anti-CD8 microbeads per 15 x 10^6 cells (Miltenyi Biotec). After 15 minutes at 4°C cells were washed in MACS buffer and resuspended in 500 µl MACS buffer per 15 x 10^6 cells. 500 µl cell suspension was added to each MS column (Miltenyi Biotec) in the MACS magnetic separator (pre-eluted with 500µl MACS buffer). The column was washed three times with 500 µl MACS buffer and the eluent was collected in a tube ($CD8^{neg.}$ fraction). The column was removed and 1 ml buffer was pushed through the column into a second tube using the plunger (CD8+ fraction). Cells were washed in R10, counted and resuspended at 1 x 10^6 cells/ml in R10. $CD8^{neg.}$ cells were used for infections (as CD4+) while CD8+ cells were used as effectors.

2.5.4 Resting cell separation

To isolate resting cells, $CD8^{neg.}$ cells (from section 2.5.3) were rested for 2 – 24 hours at 37°C then centrifuged at 1500 rpm for five minutes. Cells were resuspended in 100 µl PBS and stained with CD25-PE, CD69-PE and HLA-DR-PE (4 µl each per 10 x 10^6 cells; BD Biosciences) for 15 minutes at RT. Cells were washed with PBS (1500 rpm, 10 minutes). The pellet was then resuspended in 80 µl MACS buffer and 20 µl anti-PE microbeads (Miltenyi Biotec) per 10 x 10^6 cells for 15 minutes at 4°C. Cells were washed and run through MS columns as described in section 2.5.3 The first eluted fraction contained the resting cell population as confirmed by flow cytometry ($CD25^{neg.}$/$CD69^{neg.}$/$HLA\text{-}DR^{neg.}$).

2.6 *In vitro* HIV infection of CD4+ T cells

2.6.1 Activated CD4+ T cell infection

Freshly separated $CD8^{neg.}$ cells (1 x 10^6 cells/ml R10) were activated with PHA (5 µg/ml) for three days at 37°C. Cells were transferred to 14 ml round bottomed capped tubes, then washed twice in R10 and counted; a portion of cells were resuspended in R10 with IL-2 and returned to 37°C as uninfected controls. HIV-1_{IIIB} was added to the

remaining cells at 100 µl/10^6 cells (multiplicity of infection, MOI = 0.01) and cells were spinoculated at 2000 rpm for two hours at 27°C. Cells were washed twice in R10, counted and resuspended at 1 x 10^6 cells/ml in R10 with IL-2. Infected cells were cultured at 37°C for 5 – 7 days.

2.6.2 Resting CD4+ T cell infection

The method of generating resting infected CD4+ T cells was described by Pace et al.[239] In short, $CD8^{neg.}$/$CD25^{neg.}$/$CD69^{neg.}$/HLA-$DR^{neg.}$ cells were rested for 2 – 3 days post-purification. Cells were infected with HIV-1_{IIIB} by spinoculation (as described in section 2.6.1) but with 500 µl to 1 ml virus/10^6 cells (MOI = 0.05 to 0.1). After spinoculation cells were washed first in R10 with DNase I then an additional two times in R10 alone. An aliquot of cells was cultured with darunavir (10 µM) to confirm the absence of a spread of infectious virus in resting cells. Infected cells were cultured at 37°C for 5 – 6 days.

2.7 Viral inhibition assay

To assess the viral inhibitory capacity of CD8+ T cells a viral inhibition assay (VIA) was used as described previously.[295] On day zero $CD8^{neg.}$ T cells were isolated from a vial of thawed PBMCs (sections 2.5.2 – 2.5.3) and activated with PHA (section 2.6.1). On day three activated cells were infected with HIV-1_{IIIB} at an MOI of 0.01 (section 2.6.1); meanwhile, a new vial of cells was thawed and the CD8+ T cells isolated and rested. After infected cells were washed and counted, these infected targets and CD8+ T effectors were co-cultured in replicates at various effector to target ratios (E:T) in wells of a 96-well plate (200 µl R10 with 1 x 10^5 targets/well). Target cells cultured alone (1 x 10^5 cells) and uninfected cells were always plated as controls. For experiments in which ImmTAVs (m121 and controls) were used to redirect CD8+ T cells, the final ImmTAV concentration was 10^{-9} M unless otherwise stated. Cells were co-cultured at

37°C for 5 – 7 days, after which the frequency of p24+ cells was determined by p24 intracellular staining (section 2.10.1). CD8+ T cell antiviral inhibitory activity was calculated using the following equation:

$$\% \text{ Elimination} = \left[\frac{\%p24 +_{\text{CD4 alone}} - \%p24 +_{\text{coculture with CD8+}}}{\%p24 +_{\text{CD4 alone}}}\right] * 100$$

For the resting cell infection VIA a few changes were made to the VIA protocol. On day zero resting $CD8^{neg.}$ T cells (sections 2.5.3 – 2.5.4) were cultured in R10 alone for three days, after which they were infected with HIV-1_{IIIB} (MOI = 0.05 – 0.1), thoroughly washed with R10/DNase, then cultured for an additional five days. On day eight resting infected CD4+ T cells were combined with purified CD8+ T cells, with or without ImmTAVs, and cultured for two days followed by p24 intracellular staining.

2.8 Latency reversal

To reactivate latent virus LRAs (section 2.2.4) were added to resting infected CD4+ cells plated into 96-well plates (1 – 2 x 10^5 cells/well; section 2.6.2). After six hours' culture at 37°C cells were washed in R10 twice, then resuspended in R10 for an additional 42 hours followed by p24 intracellular staining. For VIAs, CD8+ T cells and ImmTAVs were added after the six hour wash for an additional 42 hours followed by staining.

2.9 Flow cytometry and analysis

For all flow cytometry experiments single stain (compensation beads stained with each antibody individually; BD Biosciences) and fluorescence minus one controls (FMO – cell samples stained with all fluorochromes in a panel but one) were run alongside samples during each acquisition period on the flow cytometer (CyAn, Beckman Coulter; LSRFortessa X-20, BD Biosciences). FlowJo software was used for analysis of acquired samples. First, single stain controls were used to create a compensation matrix to correct for fluorescence spillover emissions; this compensation matrix was then applied to all

samples. Next, a gating strategy was applied to all samples to identify lymphocyte (forward scatter vs. side scatter), single cell (forward scatter vs. pulse width), alive (LIVE/DEAD$^{neg.}$) and CD8+ T cell (CD3+CD8+) or CD4+ T cell (CD3+CD8$^{neg.}$ populations. For gating of further cell subpopulations (for example, PD-1+ populations) gates were set using the appropriate FMO control and applied to the other samples.

2.10 Flow cytometry staining

2.10.1 p24 intracellular staining

Cell cultures containing infected cells were analysed as described previously.[295] Briefly, cells were harvested, pelleted (1800 rpm, three minutes in 96-well plates) and washed in PBS. Samples were stained with LIVE/DEAD (0.5 µl/sample in 100 µl PBS) for 20 minutes at RT, washed with PBS and fixed with lysolecithin PFA for two minutes at RT. Cells were then permeabilised with 50% cold methanol for 15 minutes at 4°C then 0.1% NP-40 for five minutes at 4°C. Cells were stained with cell surface antibodies (CD3-APC-Cy7 and CD8-APC, BioLegend; CD4-PerCP, BD Biosciences) and p24 (KC-57-FITC; Beckman Coulter) for 15 minutes; for resting cell infections CD25/CD69/HLA-DR antibodies (all conjugated to PE; BD Biosciences) were added to confirm purity. Cells were washed twice in PBS and resuspended in 200 µl PBS. Samples were acquired on a CyAn flow cytometer. Uninfected controls were used to set the p24+ gate.

2.10.2 Assessment of exhaustion and activation status

To assess PD-1 expression, cells were washed in PBS, pelleted (1800 rpm, three minutes), and stained with LIVE/DEAD (as in section 2.10.1). After washing, cells were stained with cell surface markers (as in section 2.10.1) and PD-1-PE (1.5 µl/sample; BioLegend) in 100µl PBS for 20 minutes at RT. After washing, cells were resuspended in 2% PFA and run on a CyAn flow cytometer.

For the activation staining panel, PBMCs were washed in PBS, pelleted and stained with LIVE/DEAD followed by staining with cell surface markers (0.15 – 1 µl/sample of CD3-APC Fire 750, CD4-PE Dazzle CF594, CD8-PerCP in 100 µl PBS for 15 minutes at RT. Cells were then fixed in CytoFix (BD Biosciences) for 20 minutes at 4°C followed by staining for intracellular markers (p24-FITC; CD154-BV421 and CD69-APC, BioLegend; 0.1 – 1.25µl/sample in 100 µl CytoPerm) for 20 minutes at RT. After washing, cells were resuspended in PBS and run on an LSRFortessa X-20. An uninfected control was used to gate on p24+ populations.

For the second exhaustion staining panel, PBMCs were stained and fixed according to the PD-1 staining protocol (no permeabilisation required) but using a surface marker panel comprised of CD3-APC-Cy7, CD4-PE Texas Red, CD8-PerCP/Cy5.5, CD45RA-PE/Cy7, CD27-APC, PD-1-PE, CD39-BB515, and CCR7-BV421 (BioLegend). Samples were run on an LSRFortessa X-20.

2.10.3 Mitochondrial reactive oxygen species accumulation

PBMCs were pelleted into a 96-well plate (< 10^6/well, 1500 rpm, four minutes) and washed with PBS followed by staining with LIVE/DEAD for 20 minutes at RT. After washing the cells, they were stained with 100 µl of MitoSOX^{TM} Red (5µM in PBS; Invitrogen) for 15 minutes at 37°C. Cells were washed twice in FACS buffer (0.5% BSA in PBS) then stained with cell surface antibodies (CD3-APC-Cy7, CD4-Pacific Blue; BioLegend) for 20 minutes at 4°C. After all staining was complete samples were washed and resuspended in 200 µl FACS buffer for acquiring on a CyAn flow cytometer. MitoSox+ populations (cells producing mitochondrial reactive oxygen species, mtROS) were analysed within the alive CD3+CD4+ or CD3+CD4$^{neg.}$ (CD8+) populations.[299]

2.10.4 Quantification of mitochondrial mass

To measure mitochondrial mass (mtMass) cells were stained following the MitoSox protocol (section 2.10.3) but instead of MitoSox cells were incubated with 100 µl MitoTracker Green™ (150 nM in FACS buffer; Invitrogen) after the cell surface staining step. Histograms of the MitoTracker fluorescence signal (FITC channel) were used to calculate the change in mitochondrial mass according to the following equation:

$$\%\ \text{change mitochondrial mass} = \left(\frac{\text{MFI}_{\text{treated}} - \text{MFI}_{\text{control}}}{\text{MFI}_{\text{control}}}\right) * 100$$

2.10.5 FACS-based autophagic flux assay

A FACS-based assay that detects LC3 II was used to measured autophagic flux in primary T cells (FlowCellect™ Autophagy LC3 Antibody-Based Assay Kit, Merck Millipore). Cells were treated for two hours with zidovudine (section 2.2.3), autophagy inhibitors (section 2.2.5) or controls in a 96-well plate. The plate was then washed with PBS (1800 rpm, three minutes). Cells were stained with LIVE/DEAD followed by surface markers as in section 2.10.1. After staining, cells were washed with 100 µl 1x assay buffer per well and then 100 µl 1 x autophagy reagent B (ARB) was added. Plates were immediately centrifuged, the supernatant was discarded and the anti-LC3-FITC antibody (1:20 in 1 x assay buffer, 100 µl/sample) was added for 30 minutes at 4°C. After washing if fixation was required 100 µl of 2% PFA was added for 15 minutes at 4°C, then washed out with assay buffer. Samples were resuspended in 200 µl assay buffer and acquired on a CyAn flow cytometer. The MFI(LC3) of the treatment sample (cultured with autophagy inhibitor) and the basal sample (untreated) was then used to calculate the Autophagy Activity Factor (AAF):

$$\text{AAF} = \frac{(\text{MFILC3}_{\text{treatment}} - \text{MFILC3}_{\text{basal}})}{\text{MFILC3}_{\text{basal}}}$$

2.10.6 Intracellular cytokine staining for caspase-3 and IFNγ

To determine T cell responses to HIV, cells were stimulated with HIV-1 consensus B Gag peptides (NIH AIDS Reagent Program) and stained for intracellular IFNγ and caspase-3. To begin with, thawed PBMCs were rested overnight then plated into 96-well plates at 1 x 10^5 cells/well. Cells were stimulated with 2 μg/ml of one of two peptide pools (HIV-1 consensus B Gag 15-mer peptides with 11 amino acid overlaps totalling 123 peptides; originally pooled as part of a matrix plate but pooled again into two final pools 'A' and 'B' – see appendix 2.2), Staphylococcal enterotoxin B (SEB; 1 μg/ml as positive control; Sigma-Aldrich), or PBS (negative control). Co-stimulatory antibody cocktail CD28/CD49d (1 μg/ml) was added to each well and cells were incubated for 30 minutes at 37°C. Protein transport inhibitors, brefeldin (1/1000; BD Biosciences) and monensin (1/1000; BD Biosciences) were added and the cells were incubated for an additional 5 ½ hours. The plate was then placed at 4°C overnight until ready for staining.

Cells were washed with PBS (1500 rpm, five minutes), stained with LIVE/DEAD, washed with FACS buffer, stained with cell surface markers (CD3-APC-Cy7, CD8-APC, CD4-PerCP), and washed again in FACS buffer (section 2.10.1). CytoFix was then added for 20 minutes at RT. Cells were then washed with CytoPerm (1800 rpm, five minutes). IFNγ-FITC (BioLegend) and activated caspase-3-PE antibodies (2 μl each; BD Biosciences) in 100 μl CytoPerm were then added for 20 minutes at RT. Cells were washed with CytoPerm twice then resuspended in 2% PFA. Samples were acquired on a CyAn flow cytometer. The percentage caspase-3+ populations of total T cells (CD4+ or CD8+) and HIV-specific T cells (CD4+IFNγ+ or CD8+IFNγ+) were determined.

2.11 Quantification of SL9-specific T cells by staining with HLA-A*0201/SL9 dextramers

To screen for SL9-specific responses, PBMCs (5 x 10^5 cells) were pelleted in a round bottom tube and 10 µl dextramer (Immudex, Copenhagen) was added to the residual R10. After 10 minutes at RT in the dark cell surface antibodies (CD3-APC-Cy7, CD8-APC, CD4-PerCP) were added for an additional 15 minutes. Samples were washed in 2 ml PBS (1500 rpm, five minutes) after which LIVE/DEAD in PBS was added. After 20 minutes the samples were washed in PBS and resuspended in 2% PFA prior to acquisition on a CyAn flow cytometer.

2.12 Short-term cell line production

To generate SL9-specific short term CD8+ T cell lines (STCL), PBMCs from chronic ART-treated patients were screened for SL9-specific responses by staining with an HLA-A*0201/SL9 dextramer (section 2.11). PBMCs from reactive donors were then resuspended at 2 x 10^6 cells/ml in H10 with 25 ng/ml IL-7 (Bio-Techne). 1 ml of cell suspension was added to each well of a 12-well plate with PBS in the empty wells. 4 µg/ml SL9 peptide (1 mM stock; Sigma-Aldrich) was added to each well and cells were cultured at 37°C. On day three, IL-2 was added at 1.8 x 10^3 units/ml and cells were returned to 37°C. On day seven, 1 ml fresh H10 and IL-2 was added; this was

repeatedon days eight and nine if the medium turned yellow. On day 10, cells were washed in PBS twice then rested in R10 (1 x 10^6 cells/ml) before use; 2 x 10^5 cells were used to determine the percentage of SL9+ CD8+ T cells by dextramer staining.

2.13 Immunofluorescence

2.13.1 Antibodies

Immunofluorescence staining of HIV-infected cells used the following primary antibodies: mouse monoclonal to HIV-1 p18 (1:500; NIBSC), human monoclonal to

HIV-1 gp120-A488 (1:75; 2G12 clone, a gift from Dr Jakub Chojnacki, WIMM) and human monoclonal to HIV-1 p24 (1:75; 37G12 clone, NIBSC and Polymun). The 37G12 primary could not be used with an anti-human secondary due to non-specific binding. It was conjugated to the Abberior STAR 635P dye (section 2.14.2; Abberior) or KK114 dye (a gift from Dr Jakub Chojnacki, WIMM).

CD8+ T cells were identified using either a mouse monoclonal to CD8α (1:50; clone 37006, R&D Systems) or rabbit polyclonal to CD8α (1:200; Abcam). For immunological synapse imaging, primary antibodies included a mouse monoclonal to Lck (1:50; clone 3A5, Santa Cruz Biotechnology), mouse monoclonal to phospho$_{394}$-Lck (1:100; clone 755103, R&D Systems), rabbit polyclonal to active-caspase-3 (1:300; Abcam), mouse monoclonal to CD11/CD18 (for LFA-1, 1:100 pre-permeabilisation; Abcam), rabbit polyclonal to α-tubulin (for MTOC, 1:50; Abcam); rabbit polyclonal to Zap70 (1:100; Abcam), Alexa Fluor 488 phalloidin (for F-actin, 1.25 µl ethanol solution/50 µl total volume; Invitrogen) and mouse monoclonal to human perforin (1:100; clone dG9, BioLegend). All primaries (except those already conjugated to a dye) were used with a goat secondary antibody (anti-mouse or anti-rabbit) coupled to Alexa Fluor 488, 568 or 647 (1:1000; Life Technologies Ltd.).

2.13.2 Conjugation of dye to primary antibody for immunofluorescence

To overcome the non-specific binding of the goat anti-human secondary antibody used with the human anti-p24 antibody (37G12) a fluorescent dye was conjugated to the primary antibody. Primary 37G12 antibody was concentrated to 2 – 4 mg/ml using spin columns (Spin-X UF 500µl 50k MWCO; Corning) and centrifugation at 3700 x g for five minutes rounds. The concentration was confirmed using the 'protein A280' module of a NanoDrop^{TM} (ThermoFisher Scientific); placing 1.3 µl of antibody on the probe of the NanoDrop provided the concentration and purity of the IgG. Next, the conjugation mix

(150 µl total volume) was prepared: 100 µl IgG solution, 20 µl 0.2 M $NaHCO_3$ (pH 8.3), Aberrior STAR 635P dye (3:1 molar dye to antibody ratio; dye at 1254 M, IgG at 150,000 M) and PBS. The mix was incubated for one hour at RT with constant shaking. The unbound dye was removed via filtration through a new spin column and washes with 4 ml of PBS. The mixture was then further concentrated to 200 µl by repeated rounds of centrifugation in the same spin column. Antibody concentration and degree of labelling (DOL) was calculated using measurements from the NanoDrop – the protein A280 module followed by the 'UV-VIS' module was used to determine Abs (280 nm) and Abs (max absorption wavelength of the dye). The antibody concentration (M) and DOL (moles dye/moles protein) was calculated using the following equation:

$$\text{Ab conc (M)} = \left(\frac{\text{Abs}_{280\text{nm}} - (\text{Abs}_{\text{max}} * \text{CF}_{280\text{nm dye}})}{\text{Ext coef}_{\text{antibody}}}\right)$$

$$\text{DOL} = \frac{\text{Abs}_{\text{max}}}{(\text{Ext coef}_{\text{dye}} * \text{Ab conc})}$$

For Abberior STAR 635P and IgG:

- $CF_{280nm\ dye} = 0.47$
- $\text{Ext coef}_{\text{antibody}} = 210{,}000$
- $\text{Ext coef}_{\text{dye}} = 75{,}000$

Once the desired DOL was achieved (further rounds of conjugation and concentration were sometimes needed) 2.5 mg/ml BSA and 2 mM sodium azide were added to stabilise the antibody for freezing in aliquots.

2.13.3 Preparation of slides for visualisation of cells by confocal microscopy

To make slides for confocal microscopy 13 mm glass coverslips (VWR) were placed into 24-well plates and coated with 5 µg/ml fibronectin (Sigma-Aldrich) in PBS. The plate was incubated at 37°C for at least one hour, after which the fibronectin was removed and cells were immediately added. Alternatively, slides were soaked in poly-L-

lysine (1:10 in water; Sigma Aldrich) for 30 minutes, blotted dry on a paper towel, then placed in 24-well plates followed by addition of cells. After settling for 5 – 30 minutes cells were fixed for 15 minutes with 2% PFA or 10 minutes with 4% PFA depending on the antibody. After removal of PFA wells were covered in PBS until ready for staining.

For visualisation of T2-T cell conjugates T2 cells (5 x 10^5/slide) were pelleted in a 14 ml round bottomed tube, washed in R0, then pulsed with 12.5 μM SL9 peptide in R0 for 5 ½ hours at 37°C. After pulsing, cells were washed and mixed with CD8+ T cells (E:T of 1) and 10^{-9} M m121 ImmTAV (or control ImmTAVs) in 300 μl R10/well. HLA-A2+ CD8+ T cell donors were used to prevent any HLA-mismatched alloreactivity.[245,300] After quickly mixing, the cell mixture was added to the prepared coverslips in the 24-well plate. Co-cultures were left for 5 – 30 minutes at 37°C followed by fixation. For the formation of primary T cell-T cell conjugates, infected CD4+ T cells (either resting or activated, see sections 2.6.1 – 2.6.2) or CD4+ T cells from ART-treated patients (PHA-stimulated to reactivate autologous virus) replaced SL9-pulsed T2 cells as targets; E:T ratios varied depending on experiment.

2.13.4 Staining for immunofluorescence

The general staining method for immunofluorescence was as follows. After cells were settled and fixed on coverslips in the wells of the plate (section 2.13.3) they were permeabilised with 0.1% Triton-X100 (Sigma-Aldrich) for 10 minutes. To wash cells, PBS was added dropwise to the well, left for five minutes, then carefully removed. After two washes, cells were blocked with blocking buffer (2.5% goat serum and 0.5% BSA in PBS; Life Technologies Ltd.) for 45 minutes at RT. Cells were stained either by adding the primary antibody to the coverslip in the well (200 μl total volume 0.5% BSA in PBS) or the coverslip was removed with tweezers then inverted on a 50 μl bubble of antibody/buffer on Parafilm® (Sigma-Aldrich); the former method was preferred for

delicate samples or experiments with short settling time periods. After primary antibody staining for one hour cells were washed three times followed by the secondary antibody (1:1000) for one hour at RT. Cells were then washed twice in PBS and once in distilled water. For optimisation experiments with saponin buffer, the cells were blocked/permeabilised for 30 minutes with saponin buffer (with added 2.5% goat serum and 2.5% human serum) and the saponin buffer was also used for washes plus primary and secondary antibody steps.

The coverslip was then inverted onto a 2 µl droplet of Vectashield® mounting medium (Vector Laboratories) on a glass slide. The coverslip was sealed with clear nail polish and after drying was stored at 4°C until microscope acquisition (< 1 month). For the LFA-1 primary antibody the primary and secondary staining was performed before permeabilisation: cells were fixed, blocked, stained with anti-LFA antibody followed by secondary antibody, permeabilised and then stained with CD8 and p24 antibodies. For all experiments, a control slide with cells stained with secondary antibodies only was prepared to check for non-specific staining.

2.13.5 Confocal microscopy image acquisition

Immunofluorescence samples were acquired using either an LSM 510 or 880 inverted confocal microscope (Zeiss), both with Zen software (v. 2.1; Zeiss). A 63x plan-apochromat objective (1.4 NA oil) was used for all immunological synapse analyses and a 40x plan-apochromat objective (1.3 NA oil) was used for conjugate quantification. The following dyes – A488 (used for all immunological synapse markers), A568 (used for CD8) and Abberior STAR 635P (used for p24) – were excited using the 458/488/514 nm (Argon), 561 nm (HeNe) and 633 nm (HeNe) lasers respectively. A differential interference contrast (DIC) image was acquired for assessment of cell morphology. Laser settings were optimised to prevent over- or under-saturation of the stains and were kept

the same between comparable experiments. Pixel size was adjusted in accordance with the resolution to prevent over- or under-sampling.

To identify conjugates the slide was scanned using the eyepiece of the microscope alternating between red fluorescence (to visualise CD8+ T cells) and DIC (to see morphology) until a possible conjugate was found. To confirm the correct pairing (CD8+ T cell and T2 or infected CD4+ T cell) the 'live' imaging program was run; if a correct pairing was identified (CD8+ cell touching a T2 cell, as defined by large morphology, or p24+ cell) a final image was acquired of the conjugate. For immunological synapse imaging, one image in all colours (synapse marker in 488 nm, CD8 in 568 nm, p24 in 647 nm (if required) and DIC) was taken at the widest section of the cells ('the equator') to identify the correct conjugates. Then, a Z-stack of the synapse marker (26 images, 0.37 μm apart) was taken to maximise data acquisition. Images of at least 10 conjugates per condition were acquired.

To quantify the number of T2-T cell conjugates, the slide was moved around without direct visualisation under the microscope to minimise bias. Upon random stopping, the eyepiece was only used to confirm that there were in focus T2 cells (targets) in the field of view; using the 40x objective an overview image of the slide (DIC and CD8 only) was then acquired for counting. This was repeated until at least 50 target cells were found per condition per donor, depending on the cell density on the slide (see section 2.13.8 for analysis).

2.13.6 Confocal image analysis: p24 expression

All analysis of .lsm and .czi images was done using ImageJ (NIH) with the Bio-Formats plugin; individual macros were written using the macro editor to streamline analysis of large numbers of images. To analyse p24 expression in target cells the total corrected cellular fluorescence (TCCF) of each CD4+ T cell was calculated. An outline of

the cell, looking at the DIC channel, was drawn using the 'freehand sections' tool. Switching to the p24 channel, but maintaining the outline, a measurement of the area, integrated density (IntDen), mean, min and max was taken using the 'measure' tool. This was repeated with an area of the background near the cell. The measurements were then used to calculate the TCCF (figure 2.2):

$$\mathrm{TCCF} = \mathrm{IntDen}_{\mathrm{cell}} - (\mathrm{Area}_{\mathrm{cell}} * \mathrm{MFI}_{\mathrm{background}})$$

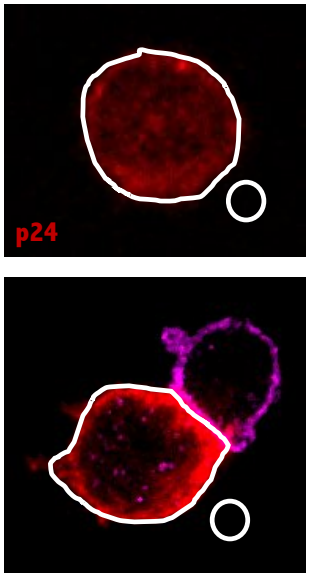

Figure 2.2: Total corrected cellular fluorescence (TCCF) of p24+ cells. In ImageJ the p24 channel of an image of a possibly infected cell either alone (top) or in conjugate with a CD8+ T cell (bottom) was used to measure the integrated density (IntDen) and area of the cell as well as the MFI of a background region. The product of the area of the cell and the MFI of the background region was subtracted from the IntDen of the cell to calculate the TCCF.

For each experiment, a slide of uninfected CD4+ T cells was also stained for p24 and the TCCF of approximately 50 cells was also calculated. The mean TCCF(p24) of the uninfected cells was then used as a cut-off for detection of p24 in the target cells (either on their own or in a conjugate); values below the mean were excluded from further analyses. The TCCF was used to determine whether the $CD8^{neg.}$ cell in a T cell-T cell pair expressed p24 and if the p24 signal was below the cut-off the T cell-T cell pair was excluded from further synapse analysis. For T2-T cell conjugates the target T2 cell was pulsed with peptide not virus and was easily identified without a cell marker as T2 cells are larger (~ 12 μm) than CD8+ T cells (~7 μm).

2.13.7 Confocal image analysis: immunological synapse molecules

Once an appropriate conjugate was determined (section 2.13.6) the synapse molecules were analysed (figure 2.3). For LFA-1 the A488 channel Z-stack was combined into one image using the 'SumStacks' module on ImageJ. From this image, the LFA-1 at the contact (% of total) was measured by drawing an outline around the synapse (on the CD8+ T cell where it touched the target cell), measuring the IntDen for the LFA-1 channel and then doing the same for an outline of the entire CD8+ T cell. The LFA-1 localised was compared between conditions.

$$\text{LFA1 at contact (\% of total)} = \left(\frac{\text{IntDenLFA1}_{\text{synapse}}}{\text{IntDenLFA1}_{\text{whole cell}}}\right) * 100$$

In single, unstimulated cells Zap70 resides in the cytoplasm whereas upon signalling via the T cell receptor/CD3 complex it localises to the plasma membrane. To quantify Zap70 polarisation the same method used for LFA-1 quantification was applied (Zap70 at contact (% of total)). Alternatively, the percentage of conjugates with Zap70 localised to the periphery vs. the centre of the CD8+ T cell was calculated for each condition.

To analyse the MTOC the Z-stack of the α-tubulin channel was used to identify where the MTOC was located within the CD8+ T cell (defined as the point where microtubules converge into a visible point of maximal brightness). A line was drawn from this point to the centre of the synapse and measured. The lengths (μm) were compared between conditions.

F-actin typically accumulates at the synapse then clears to the dSMAC. To analyse F-actin distribution the equator image of F-actin was used to determine the F-actin at the contact (% of total) in the CD8+ T cell (same method as LFA-1).

Finally, to measure perforin at the synapse the Z-stack of perforin in the CD8+ T cell was used to categorise perforin distribution into one of three categories: distal

(located at the far side of the CD8+ T cell away from the synapse), dispersed (located throughout the CD8+ T cell) or docked (polarised to the synapse). The percentage of distal, dispersed and docked perforin was compared between conditions.

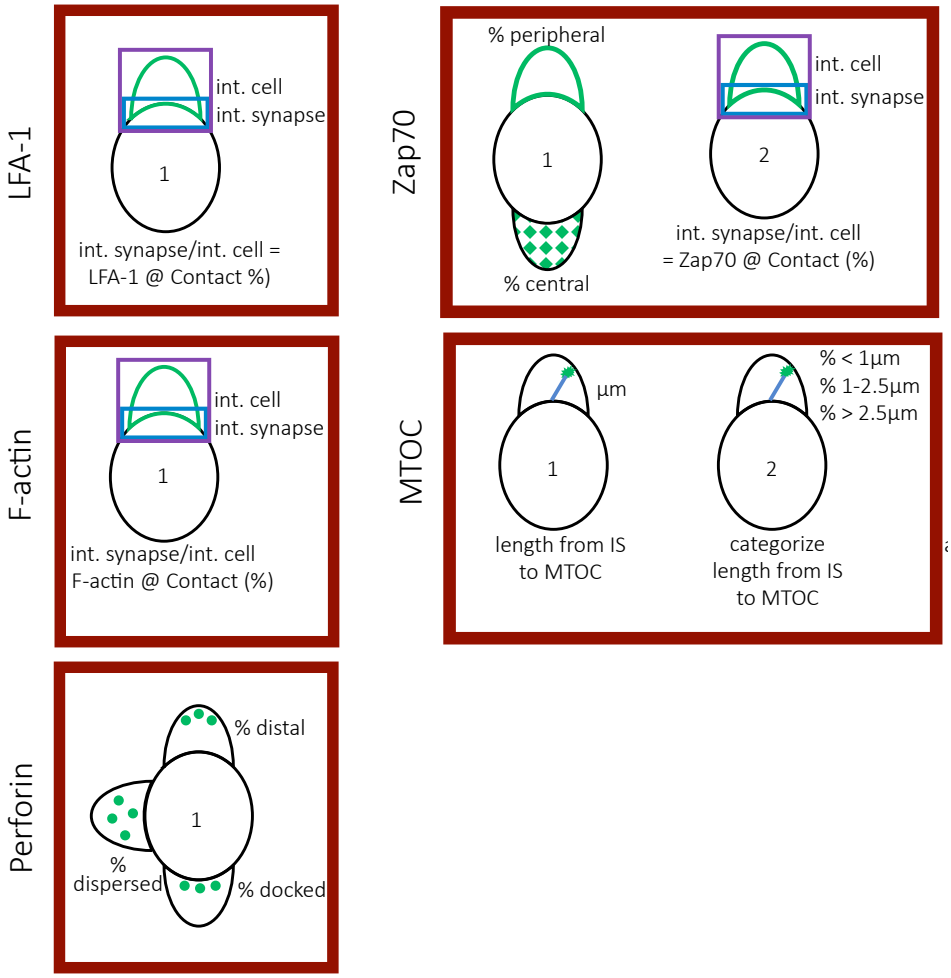

Figure 2.3: Final methods for synapse analysis. Schematics show the chosen methods for analysis of LFA-1, Zap70, F-actin, MTOC and perforin polarisation in the CD8+ T cell of a T cell-T cell or T2-T cell conjugate.

2.13.8 Confocal image analysis: conjugate quantification

To quantify the number of T2-T cell conjugates that formed the low power images (section 2.13.5) were used to count the total number of T2 cells and the number of T2 cells in conjugates with CD8+ T cells (figure 2.4); if a T2 cell formed a conjugate with multiple CD8+ T cells each synapse counted as one conjugate. The percentage of T2 cells in conjugates was calculated from these counts and compared between conditions.

Because T cell-T cell conjugate formation was rare the random method used for T2-T cell conjugates did not always find conjugates. Instead, slides of T cell-T cell conjugates under different ImmTAV conditions (m121, m231, etc.) were coded so that the observer was blinded to the experimental conditions. The observer marked as many synapses as possible searching through the eyepiece for 15 minutes and the final synapse count was based on the number of correctly paired cells after image acquisition and analysis.

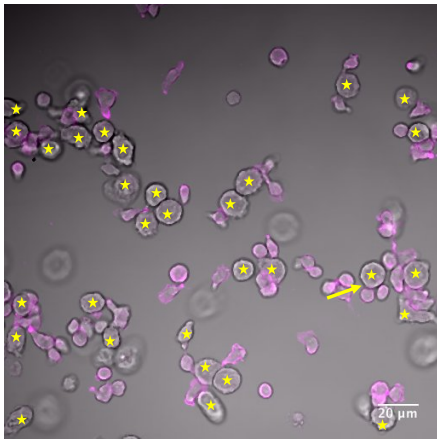

Figure 2.4: Quantifying numbers of T2-T cell conjugates. To quantify the number of T cell conjugates formed several random, blind images were acquired on the microscope at low power (DIC and CD8 channel shown overlaid). The number of target cells counted are shown marked with yellow stars and an example target cell in conjugate with an effector is marked with the yellow arrow. Scale bar represents 20 µm.

2.13.9 Stimulated emission depletion microscopy image acquisition

Stimulated emission depletion microscopy (STED) was used to improve the resolution for p24 and synapse marker distribution. A custom RESOLFT STED or Leica SP8 Gated STED microscope was used (in collaboration with Dr Jakub Chojnacki, WIMM) to analyse prepared slides. The STED laser channel was used for p24 (KK114 or Abberior STAR 635P) and/or synapse markers (Alexa Fluor 488) while CD8 (Alexa Fluor 568) was included in the non-STED channel to identify cell pairs. XY and Z-stack confocal images were acquired for all channels first, followed by acquisition with the STED laser to allow for a comparison of the resolution gain when using STED. Images were analysed using ImageJ software.

2.14 Statistical analyses

GraphPad Prism (v.7.0a) and Microsoft Excel was used to perform all statistical analyses. Any technical replicates for each donor were averaged and multiple donors were combined by determining the pooled mean, pooled standard deviation (SD) and standard error of the mean (SEM). Where a normal distribution was assumed, data were analysed with parametric tests ((RM) one-way ANOVA (with or without Dunnett's, Tukey's or Sidak's multiple comparisons tests – adjusted P values shown), (un)paired t tests or multiple t tests); apparently skewed data were analysed with non-parametric tests (Mann-Whitney tests or Kruskal-Wallis tests).[301,302]

CHAPTER THREE: SUSCEPTIBILITY OF LATENTLY INFECTED CELLS TO IMMTAV-MEDIATED ELIMINATION USING AN *IN VITRO* HIV LATENCY MODEL

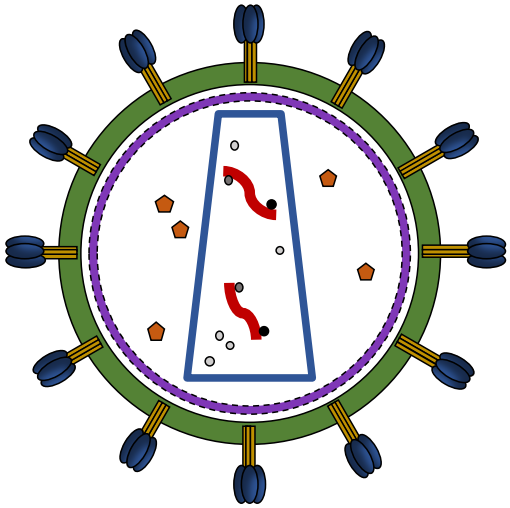

3.1 Introduction

A reservoir of latently infected memory CD4+ T cells is established early in the course of an HIV infection, allowing the virus to persist even during treatment with suppressive ART regimens (reviewed in [98,303]). Latently infected cells can be defined as infected cells that contain integrated but transcriptionally silent proviral HIV DNA (but upon activation are capable of generating infectious viral particles).[304,305] This classical definition implies that latently infected cells cannot be targeted by the host immune response. However, new evidence suggests that this binary depiction of reservoir cells may be too simplistic.[304] Low levels of HIV RNA have been detected in resting CD4+ T cells from patients on ART suggesting that the provirus within the cells was not fully transcriptionally silent.[306–308] However, compared to activated CD4+ T cells there was less HIV RNA in resting CD4+ T cells and the transcripts were often abortive or unspliced.[306,307,309] While these differences in the composition of the RNA transcripts may not have resulted in protein expression it is also possible that non-productive infection in these cells reflects partial blocks at multiple stages of viral gene transcription, supporting the concept of a 'spectrum' of latency. At one end are the classically defined latently infected cells with provirus that is completely transcriptionally silent. Resting CD4+ T cells that transcribe integrated HIV DNA but do not produce HIV proteins, as described in these ART patients, are intermediate on the spectrum. Finally, there are resting CD4+ T cells that can express HIV proteins but still do not spread infection. This latter population was generated in an *in vitro* model of HIV latency, wherein resting CD4+ T cells were directly infected with HIV and produced p24 but did not support a spreading infection ('Gag+ reservoir cells', GPR cells).[239,304] GPR cells may also exist *in vivo* as Gag+ resting CD4+ T cells from chronic HIV infected (CHI) donors on ART contained more copies of HIV DNA per cell than $Gag^{neg.}$ resting CD4+ T cells did,

although further investigation of this rare population of cells is needed.[310] However, some groups would debate whether this final category of cells are truly latent, as protein production may result in elimination of the cells by immune effector mechanisms.[311,312]

If a proportion of the viral reservoir were comprised of GPR cells then these could be targeted by immune-based therapies without the need for viral reactivation. However, because of the low antigen expression, T cells may not be able to recognise the infected cells as TCRs typically have low affinity for pHLA complexes (micromolar range) and fast dissociation rates (seconds).[310] To overcome this, 'shock and kill' strategies have been proposed. Latency-reversing agents (LRAs) are applied to selectively reactivate latent proviruses (the 'shock'; reviewed in[313,314]). Infected cells that resume virion production are rendered potentially susceptible to HIV-mediated cytopathic effects or immune clearance, mediated by immunomodulatory enhancement strategies such as vaccines or bispecific molecules (the 'kill'; reviewed in [98,313,315]). Effective LRAs target host cell-mediated molecular mechanisms that regulate expression of genes, into which HIV has integrated, within the resting CD4+ T cells. For example, histone deacetylases remove acetyl groups from the amino acids on a histone; this allows the histones to tightly wrap the DNA creating a repressive chromatin environment (i.e. at the HIV promoter). HDAC inhibitors reverse this process by inducing HIV chromatin acetylation, promoting virus production without full cellular activation. Protein kinase C (PKC) agonists target signalling pathways within the host cell that lead to transcription complex formation, transcript initiation and processing of the transcription complex. Combinations of different classes of LRAs have been shown to enhance viral reactivation *in vitro*.[144,316] The key challenge for latency reversal *in vivo* is to selectively reactivate proviruses within latently infected cells without causing global activation as this could increase spread of infectious virus or cause a cytokine storm.

Because of the requirement to carefully reverse latency in infected cells, LRAs may not be adequate for inducing cell death from viral cytopathic effects alone. In clinical trials where LRAs, including vorinostat, romidepsin and panobinostat, were administered *in vivo* to CHI patients on suppressive ART there was a measurable increase in cell-associated HIV-1 RNA production (indicative of transcription) and/or plasma viraemia but no reduction in the frequency of latently infected cells.[143,317–319] This failure to clear the latently infected cells indicates that a functional immune response is needed for the 'kill.' This can be seen with CTLs from elite controllers which contribute to the control of HIV replication and limit seeding of the reservoir.[199,320] *In vitro* studies have also shown that *ex vivo* CD8+ T cells from elite controllers can kill both non-productively infected cells and GPR cells which both represent populations that may contribute to the HIV reservoir.[92,310] However, in the majority of CHI patients their CD8+ T cells have a limited impact on virological control and reservoir size. This is in part due to mutational escape by HIV and the resultant functional exhaustion of the cells but also a reduction in their frequency during ART.[189,193,321–324]

To combat this dysfunction therapeutic vaccines were designed that might enhance CD8+ T cell responses to clear HIV-infected cells. However, therapeutic vaccines have been tested in ART-treated patients, but without LRAs, generally without success.[290,325–328] Even though to date no vaccine has permitted sustained ART interruption, in the context of 'shock and kill' therapy a LRA and ART would be used in parallel, helping prevent viral replication and escape. In the few therapeutic vaccine trials that have investigated the impact of a vaccine on the reservoir size none have had a significant effect, likely due to the lack of viral protein expression in latently infected cells.[292,329,330] To address this, several clinical trials investigating 'shock and kill' have been conducted or are ongoing.[139,314,331,332]

An alternative to vaccine-induced immunomodulation is the application of bispecific molecules to retarget non-HIV-specific CD8+ T cells towards the latently infected targets. As discussed in section 1.2.1, DARTs are antibody-based molecules that can simultaneously bind two different cell surface molecules; for example one arm, derived from an anti-HIV antibody, binds HIV's Env while the other arm binds CD3 on CD8+ and CD4+ T cells.[238] DARTs are thus able to bind infected CD4+ T cells and redirect polyclonal populations of CD8+ T cells to kill them, eliminating the need for recruitment of pre-existing HIV-specific T cells. However, in directly infected resting T cells Env was barely detectable compared to Gag, suggesting that few latently infected cells may be detected by a DART.[239] Additionally, the variability of HIV's Env protein may restrict the DARTs use in cells infected with a strain of the virus with a mutation at the epitope the DART recognises.

Engineered bispecific T cell receptors against viruses, or ImmTAVs, represent a different class of bispecific molecules that may overcome these limitations. Like DARTs, ImmTAVs are able to simultaneously recognise an infected target and redirect non-HIV-specific CD8+ T cells via an anti-CD3 single chain variable fragment (scFv). However, as ImmTAVs recognise HIV epitopes via a TCR when presented by HLA molecules this expands the potential targets to include intracellular proteins. There is the potential to develop ImmTAVs against a wide range of epitopes by selection and engineering of diverse TCRs (albeit with the limitation that their use is limited to subjects with the relevant HLA allele(s)). A crucial step in the development of both DARTs and ImmTAVs is affinity enhancement through site-directed mutagenesis of the Fab and TCR domains. In the case of ImmTAVs, picomolar affinities for pHLA can be achieved, which significantly increases the likelihood of engagement with a virus-infected cell compared with a natural CD8+ T cell; in comparison DARTs and BiTEs exhibit nanomolar

affinities for their peptide targets.[217,226,238,245] An HIV-specific ImmTAV was shown to redirect CD8+ T cell killing of HIV-infected primary CD4+ T cells *ex vivo* including activated infected CD4+ T cells from healthy donors (HD) and reactivated latently infected CD4+ T cells from ART-treated patients. However, as the latter are rare *in vivo* these experiments are challenging to reproduce.[245]

The aim of this chapter was to use a latency model to examine whether latently infected cells are susceptible to elimination via an ImmTAV-mediated 'shock and kill' strategy. Antiviral activity of both ImmTAV-redirected healthy donor and CHI donor CD8+ T cells was compared by using directly infected resting CD4+ T cells, as described by Pace et al. (O'Doherty model), and a previously developed viral inhibition assay.[239,295] The mechanisms underlying any differences in antiviral activity between the two groups were then investigated.

3.2 Results

3.2.1 Resting infected CD4+ T cells express low levels of p24 without spreading infection

The O'Doherty model of HIV latency relies on directly infecting resting CD4+ T cells with HIV to develop a population of Gag-expressing cells that do not spread infection.[239,310] To replicate this model magnetic bead separation was applied to CD4+ T cells to remove the activated (CD25+/CD69+/HLA-DR+) fraction. The resting ($CD25^{neg.}$/$CD69^{neg.}$/$HLA\text{-}DR^{neg.}$) fraction was stained with the same three activation markers to assess purity. The samples were 98% pure immediately after separation but after three days' rest were >99% resting. Resting CD4+ T cells were spinoculated with HIV-1_{IIIB} (MOI = 0.01) then cultured alone, with a protease inhibitor (PI; darunavir, 10 μM) or a reverse transcriptase inhibitor (RTI; tenofovir, 10μM). After four days, the p24 expression was measured by FACS for all three conditions (figure 3.1a). There was no difference in the percentage of p24+ cells between the +/- PI samples (1% vs. 1.02%) indicative of a non-spreading infection. The $PI^{neg.}$ sample was then stimulated with PHA to reactivate latent virus, after which it was cultured with and without PI again. After two days, the p24+ population was higher in the $PI^{neg.}$ sample (3.04%) compared to the PI+ sample (1.33%) indicating that the infected cells contained replication-competent virus. The resting status of resting infected CD4+ T cells was also confirmed by comparing the PD-1 expression between activated infected and resting infected cells (figure 3.1b).[333,334] The size of the PD-1+ population and MFI(PD-1) was higher in the activated population compared to the resting (activated vs. resting % p24+, mean (SEM): 34.4% (3.2) vs. 3.3% (1.01); MFI, mean (SEM): 21.4 (0.7) vs. 8.7 (1.2)).

To compare the p24 expression between resting and activated infected samples, CD4+ T cell infections using the same MOI of HIV-1_{IIIB} (0.01) were set up and stained

for p24. By FACS the percentage p24+ population and MFI(p24) of the activated CD4+ T cells (25.4% p24+; MFI of CD4+ T cells = 255; MFI of p24+ T cells = 690) was higher than the resting CD4+ T cells (4.25% p24+; MFI of CD4+ T cells = 41.1; MFI of p24+ T cells = 302).

a

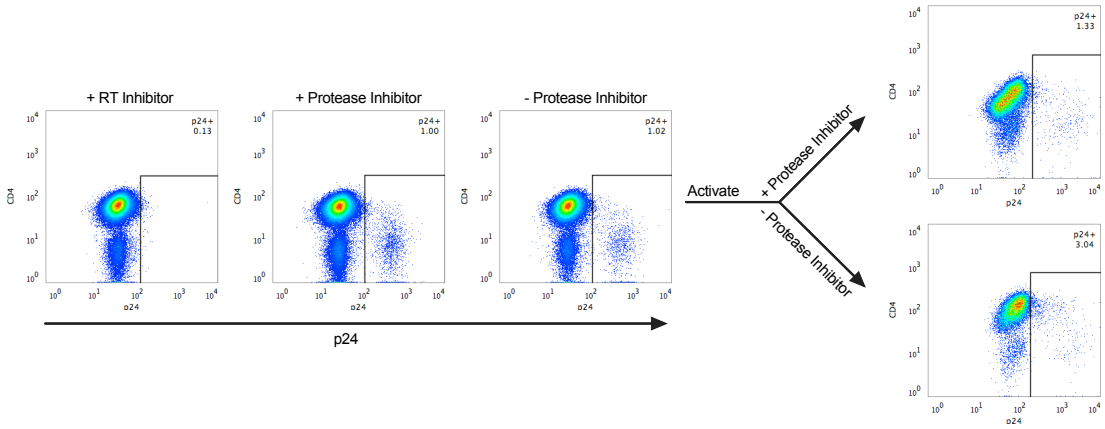

b

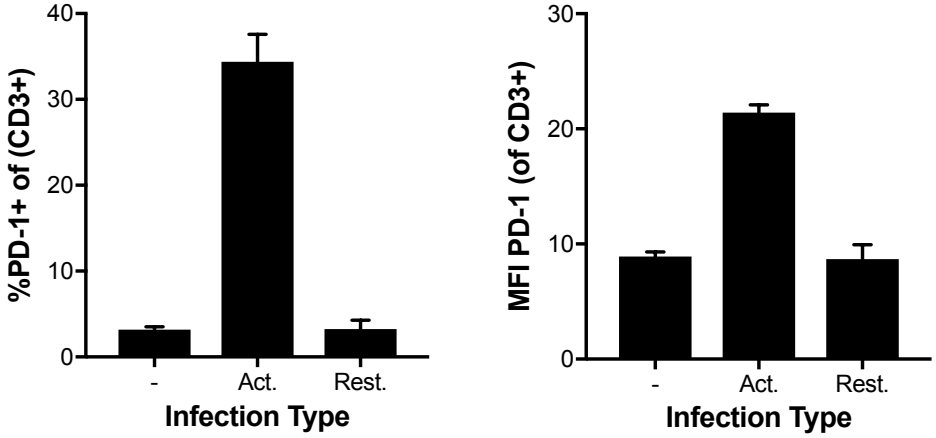

Figure 3.1: Directly infected resting CD4+ T cells express p24 without spreading infection. (a) $CD25^{neg.}/CD69^{neg.}/HLADR^{-neg.}/CD4+$ T cells were spinoculated with HIV-1_{IIIB} (MOI = 0.01) and cultured alone or with a protease inhibitor (darunavir, 10μM) or a RTI (tenofovir, 10μM) for four days before measuring intracellular p24. The resting cells cultured alone (-PI) were then activated with PHA and cultured with and without the protease inhibitor for an additional 48 hours. X-axis = p24, Y-axis = CD4. (b) The PD-1 expression (%PD-1+ of CD3+ T cells, left; MFI(PD-1) of CD3+ T cells, right) was also compared between uninfected, activated infected and resting infected T cells (n = 2). Mean with SEM shown.

To determine whether the p24+ population could be enlarged, while still maintaining the resting phenotype, different MOIs of virus were tested. The p24+ population expanded with the higher MOI and remained non-spreading (figure 3.2, left).

After two days of PHA stimulation, the p24+ population increased, confirming the presence of replication-competent virus (figure 3.2, right). An MOI of 0.05 or 0.1 was chosen for further study. To confirm the kinetics of infection in resting cells, recently spinoculated cells (MOI = 0.1) were cultured for 4 – 7 days. Peak frequency of infected cells was observed at six days but as the cells appeared most viable and resting at five days this time point was chosen for future use (figure 3.3).

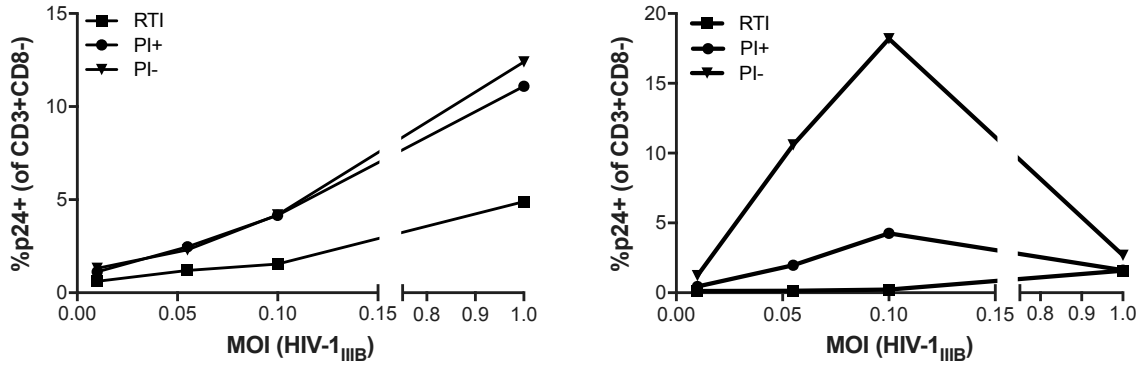

Figure 3.2: Titration of virus for directly infecting resting CD4+ T cells. Resting CD4+ T cells were spinoculated with HIV-1_{IIIB} using an MOI from 0.01 to 1 then cultured with tenofovir (RTI, 10μM), darunavir (PI, 10μM) or alone for four days before measuring intracellular p24 (left). On day four resting cells were activated with PHA for an additional 48 hours before measuring p24 expression (day six post-infection, right).

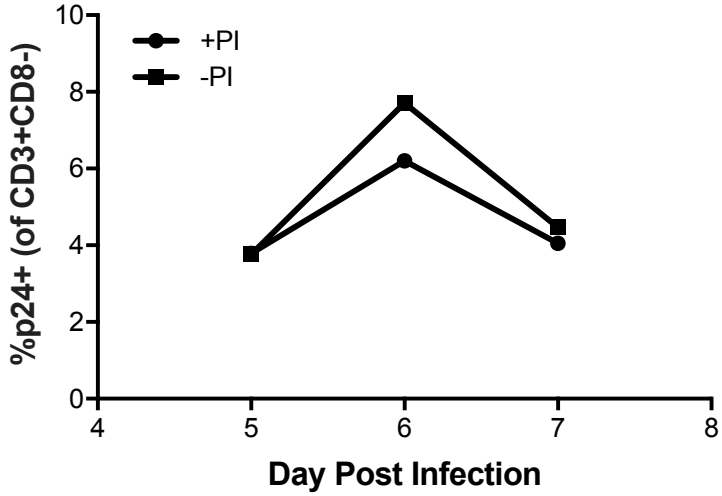

Figure 3.3: p24 kinetics of resting infected CD4+ T cells. Resting CD4+ T cells were spinoculated with HIV-1_{IIIB} (MOI = 0.1) then cultured with and without darunavir (PI, 10μM). Intracellular p24 expression was measured on days 5 – 7 post-infection.

3.2.2 ImmTAV-redirected healthy donor CD8+ T cells can eliminate resting infected CD4+ T cells

HIV-specific ImmTAVs were able to redirect HD CD8+ T cells to eliminate activated infected CD4+ T cells from HD and *ex vivo* reactivated CD4+ T cells from ART-treated CHI patients.[245] To assess whether the reduced p24 expression in resting infected cells would impact ImmTAV-redirected clearance they were used as targets in a viral inhibition assay. Resting infected HD cells (five days post-infection) were co-cultured with autologous HD CD8+ T cells (E:T of 1) with and without ImmTAV (irrelevant TCR or HIV-specific m121 ImmTAV at 10^{-8} or 10^{-9} M) for 48 hours. A co-culture time of seven days, to match the previously published results, was not feasible as cell survival was poor under the IL-2-free culture conditions used to avoid any activation of cells (not shown).[245] Without ImmTAV redirection there was no spontaneous elimination of target cells. However, infected cell elimination was detected with the addition of 10^{-9} M of m121 ImmTAV (no ImmTAV vs. 10^{-9} M m121 % elimination mean, (SEM): 1.48% (7.9) vs. 20.4% (8.3), P = 0.0015 for all groups). The higher concentration of 10^{-8} M for both the irrelevant TCR and m121 ImmTAV appeared to increase the infection resulting in a negative elimination (10^{-8} M irrelevant vs. 10^{-8} M m121 % elimination, mean (SEM): -26.2% (8.2) vs. -13.3% (9.2); figure 3.4). The irrelevant ImmTAV was not tested at the 10^{-9} M concentration due to the acquisition of new ImmTAV controls (m231, m232 – see figure 3.5b).

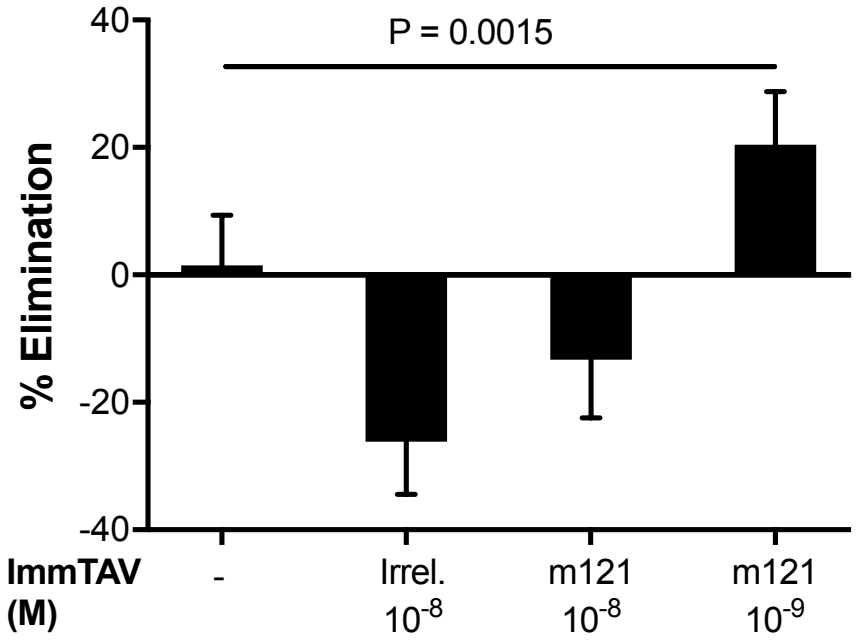

Figure 3.4: Elimination of resting infected cells by ImmTAV-redirected healthy donor CD8+ T cells. Resting infected CD4+ T cells (1 x 10^5) from healthy donors (n = 2 from four independent experiments) were co-cultured with autologous CD8+ T cells (E:T of 1) and ImmTAV (10^{-8} M irrelevant TCR ImmTAV or 10^{-8} – 10^{-9} M m121 ImmTAV) for 48 hours before assessment of intracellular p24. % Elimination was calculated by comparing the %p24+ cells in CD4/CD8/ImmTAV samples to the %p24+ cells in infected CD4+ T cells cultured alone. Mean and SEM shown. Groups were analysed by one-way ANOVA. Note: 'negative elimination' apparent in both donors.

An E:T of 1 was used in figure 3.4 but to test the efficacy of HIV ImmTAV redirection further, various E:T ratios (0.1 – 5) were compared using 10^{-9} M m121 ImmTAV. Peak percentage elimination was observed at an E:T of 2 (E:T of 1 (no ImmTAV) vs. 0.1 vs. 0.2 vs. 1 vs. 2 vs. 5 % elimination, mean (SEM): -3.5% (8.1) vs. 10.6% (12.5) vs. 9.3% (2.6) vs. 20.5% (4.9) vs. 39.9% (4.3) vs. 28.1% (3.5), P = 0.0008; figure 3.5a). To confirm that the elimination was specific to the m121 ImmTAV, additional controls were made available for use in a subsequent VIA; these were m231, which was identical to m121 but with a non-binding anti-CD3 scFv, and m232, which had another non-HIV specific TCR (WT-1) fused to a functional anti-CD3 scFv. No elimination was detected with either of these ImmTAV controls at both 1 and 2 E:T ratios (figure 3.5b).

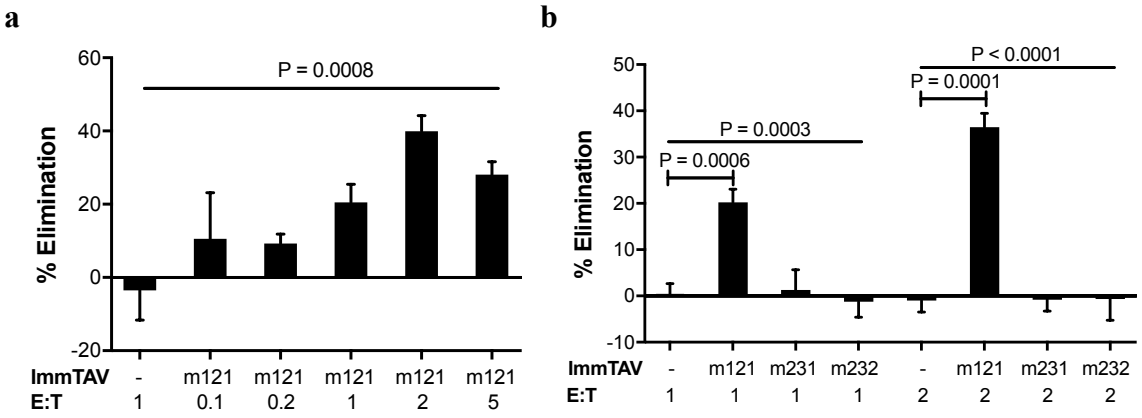

Figure 3.5: Range of ImmTAV-redirected elimination of resting infected cells. Resting infected CD4+ T cells (1 x 10^5) from healthy donors (n = 2) were co-cultured with autologous CD8+ T cells at varying E:T ratios and (a) 10^{-9} M m121 ImmTAV or (b) 10^{-9} M m121, m231 (non-binding anti-CD3) or m232 (non-HIV-specific TCR) ImmTAV for 48 hours before assessment of intracellular p24. % Elimination was calculated by comparing the %p24+ cells in CD4/CD8/ImmTAV samples to the %p24+ cells in infected CD4+ T cells cultured alone. Mean and SEM shown. Groups were analysed by one-way ANOVA with Dunnett's multiple comparisons test (for (a) multiple comparisons with 'no ImmTAV' control: n.s, n.s., n.s., P = 0.0002, P = 0.009).

3.2.3 A high concentration of ImmTAV alone can reactivate HIV within resting infected cells

In the VIA in figure 3.4 the higher concentration of the m121 and irrelevant TCR ImmTAV resulted in apparent negative elimination. To assess whether this increase was due to reactivation of latent virus and spread of infection, resting infected CD4+ T cells were cultured with the m121, m231 and m232 ImmTAVs at a range of concentrations and in the absence of CD8+ T cells for 48 hours before staining for p24 and activation markers (CD69 and CD154; acquisition and analysis completed in collaboration with Dr Jakub Kopycinski, in our laboratory). The p24+ population only increased in samples cultured with the m121 or m232 ImmTAVs at the 10^{-8} M concentration (figure 3.6a). CD154 expression was low in all the samples (appendix 3.1) but CD69 expression also increased after exposure to the highest ImmTAV concentration. This effect was most pronounced in uninfected cells, indicating a non-specific effect (figure 3.6b).

Furthermore, it was not seen in cells exposed to m231, indicating that the effect was mediated by the anti-CD3 scFv.

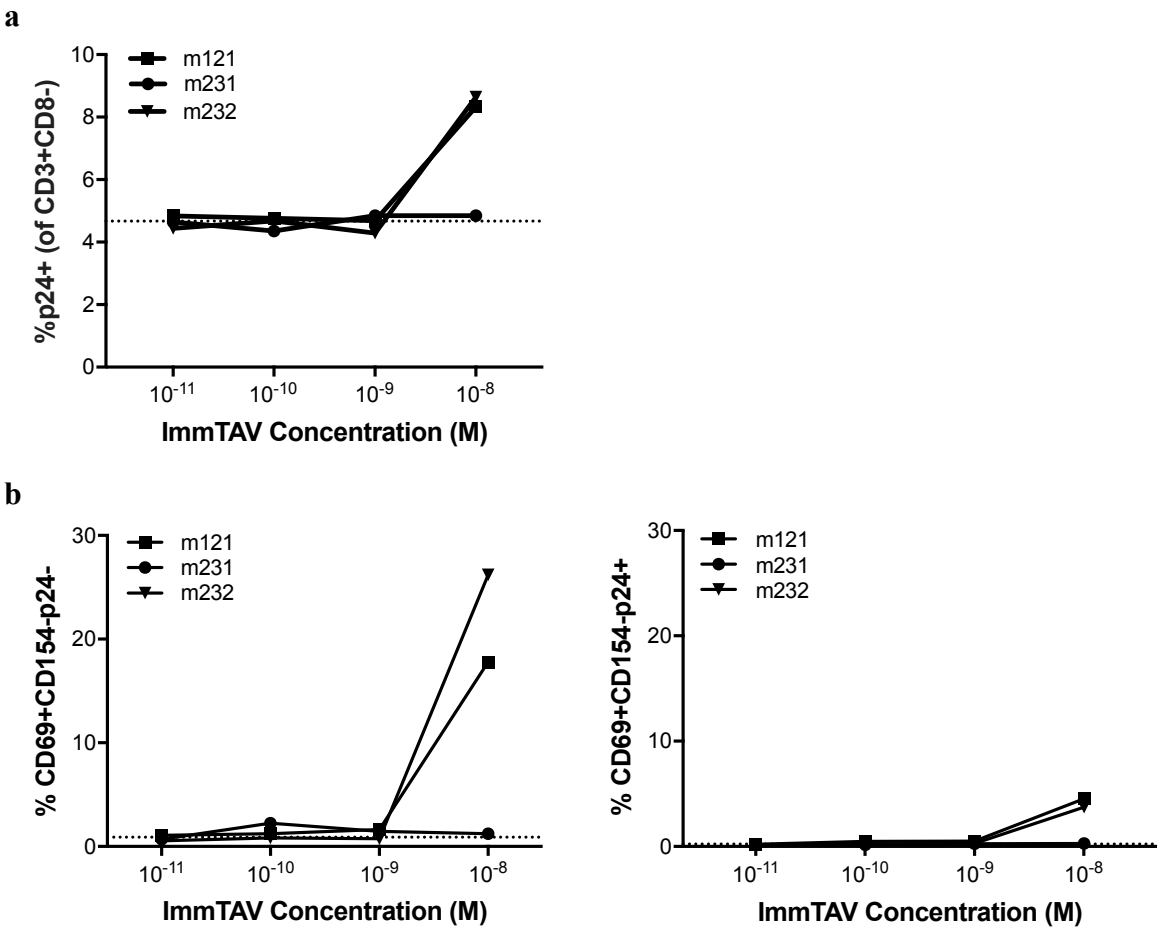

Figure 3.6: High concentrations of ImmTAV reactivate cells and latent virus. Resting infected CD4+ T cells were cultured with m121, m231 or m232 ImmTAV at varying concentrations (10^{-11} – 10^{-8} M) for 48 hours before assessment of (a) intracellular p24 or (b) CD69 and CD154 expression (CD154 expression was low under all conditions, CD69+CD154$^{neg.}$p24$^{neg.}$ and CD69+CD154$^{neg.}$p24+ populations shown). Dotted line represents the p24 or activation marker expression of resting infected cells cultured without ImmTAV.

To assess whether the reactivation effect of the 10^{-8} M ImmTAV concentrations would elicit a negative elimination, all four ImmTAVs ('irrelevant' TCR, m121, m231 and m232) were compared in a VIA with resting cell targets. The irrelevant, m121 and m232 ImmTAVs caused negative elimination at the 10^{-8} M concentration but not at the lower 10^{-9} M concentration; neither concentration of m231 had any effect on the

elimination of target cells (10^{-8} M m121 vs. irrel. vs. m231 vs. m232 % elimination, mean (SD): -13.7% (3.7) vs. -14.7% (5.4) vs. 4% (6.6) vs. -16.5% (14.4); figure 3.7).

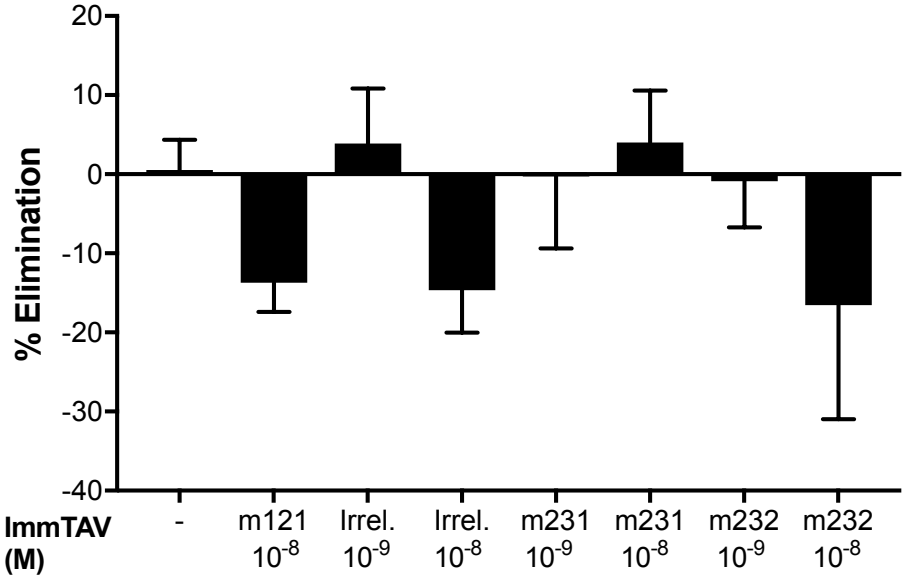

Figure 3.7: High concentrations of ImmTAV induce 'negative elimination' of resting infected CD4+ T cells. Healthy donor (n = 1) resting infected CD4+ T cells (1 x 10^5) were co-cultured with autologous CD8+ T cells (E:T of 1) and m121, m231, m232 or irrelevant ImmTAV at 10^{-8} or 10^{-9} M for 48 hours before assessment of intracellular p24. % Elimination was calculated by comparing the %p24+ cells in CD4/CD8/ImmTAV samples to the %p24+ cells in infected CD4+ T cells cultured alone. Mean and SD shown.

3.2.4 The effect of latency-reversing agents on susceptibility of resting infected CD4+ T cells to HIV ImmTAV-mediated killing

As part of a proposed 'shock and kill' strategy LRAs are used to reactivate latent virus before the application of an immunotherapeutic to enhance elimination of the infected cells.[142,335] A panel of LRAs comprising bryostatin (10 nM, PKC agonist), romidepsin (40 nM, HDAC inhibitor), acitretin (5 μM, retinoic acid derivative) and vorinostat (350 nM, HDAC inhibitor) were cultured with resting infected cells to assess which LRA(s) would reactivate virus with the most efficiently in this latency model; PHA, as a mitogen, was used as a positive control as it reactivated virus better than PMA/ionomycin in previous tests (not shown). LRAs were washed out after six hours as longer co-culture times were found to be toxic to the cells (not shown). 48 hours after

this, the cells were stained for p24 and the percentage change in frequency of p24+ cells to the untreated sample was calculated. Romidepsin or romidepsin in combination with bryostatin significantly increased the p24+ population (romidepsin vs. bryostatin/romidepsin % change to control, mean (SEM): 83.7% (7.4) vs. 101.6% (14.2); P = 0.0009, P = 0.0001 compared to DMSO control; figure 3.8).

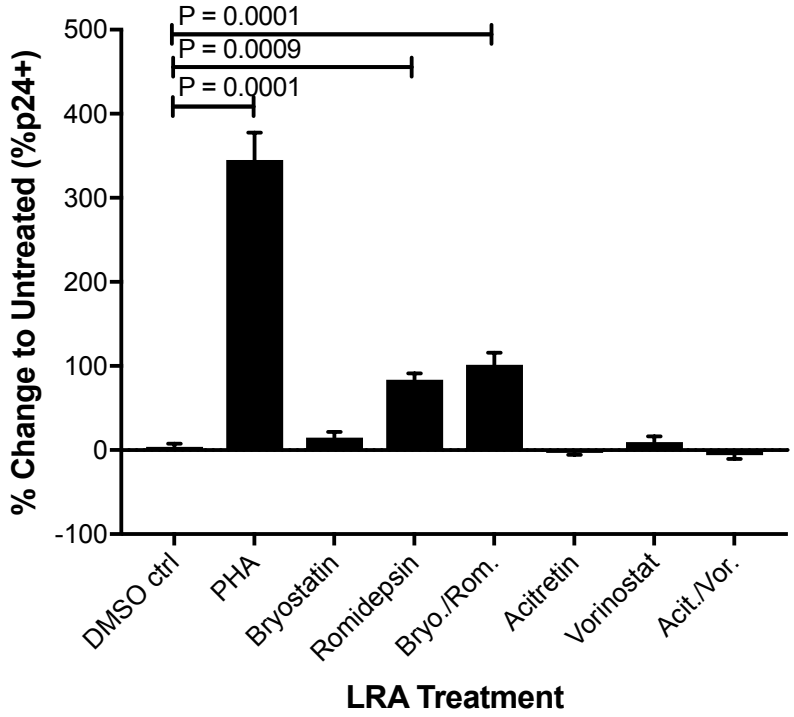

Figure 3.8: Comparison of latency-reversing agents in resting cell infection latency model. Resting infected CD4+ T cells from healthy donors (n = 2) were cultured with latency-reversing agents bryostatin (10 nM), romidepsin (40 nM), bryostatin/ romidepsin, acitretin (5 μM), vorinostat (350 nM) or acitretin/ vorinostat; DMSO was used as a diluent control and PHA as a positive control. Intracellular p24 was assessed 48 hours after washing out LRAs. % Change of the p24+ population to the untreated resting infected cells is shown. Mean and SEM shown. Groups were analysed by one-way ANOVA with Dunnett's multiple comparisons test (P < 0.0001 for all groups).

Bryostatin/romidepsin were then used in combination with the m121 ImmTAV in a VIA. HD resting infected CD4+ T cells were cultured with bryostatin/romidepsin or PHA for six hours, washed, then cultured with m121 ImmTAV (10^{-9} M) and autologous CD8+ T cells at an E:T of 2 for two days. For this experiment, percentage elimination was calculated by comparing the percentage p24+ cells of the LRA-treated CD4/CD8/ImmTAV culture to the LRA-treated CD4/CD8 culture. A mean (SEM) 41.6%

(3.8) of infected cells were eliminated after PHA stimulation compared to 25.9% (4.1) after bryostatin/romidepsin stimulation (figure 3.9a). The remaining p24+ population after PHA stimulation and ImmTAV-redirected CD8+ T cell killing was still higher than the original p24+ population of unstimulated resting infected CD4+ T cells alone (figure 3.9b).

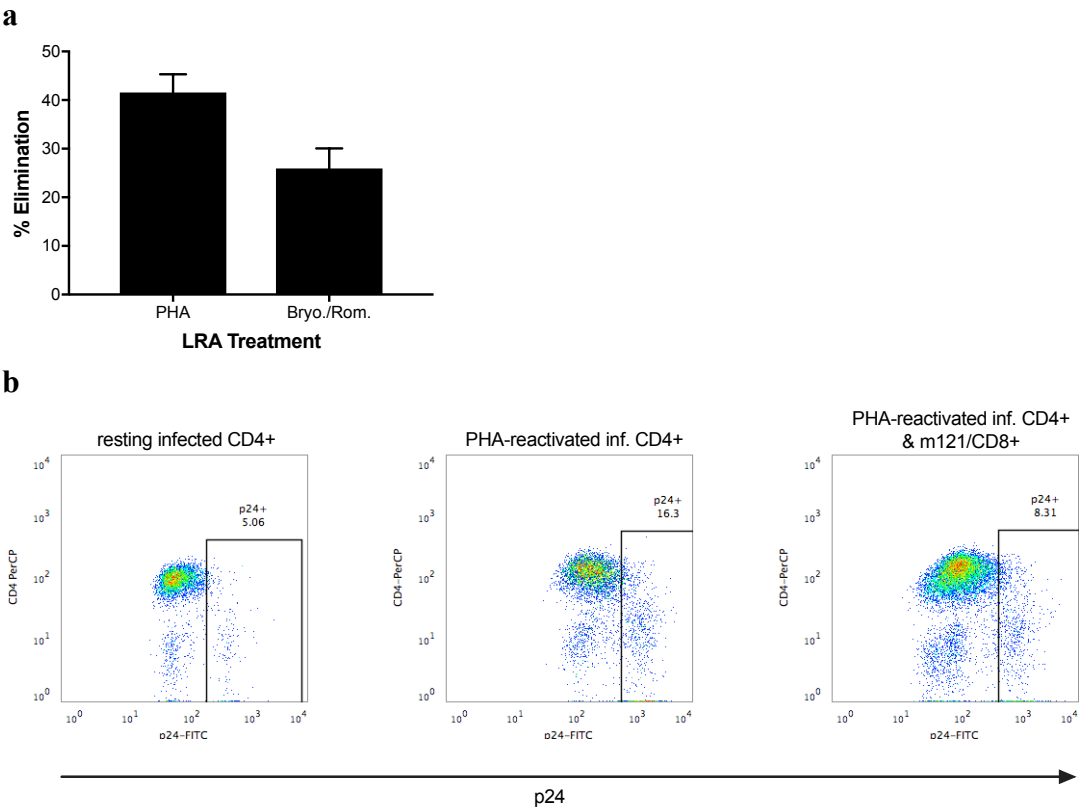

Figure 3.9: Latency-reversing agents do not improve ImmTAV-directed elimination of resting infected CD4+ T cells. Healthy donor CD8+ T cells (2 x 10^5; n = 2) were co-cultured with resting infected cells (1 x 10^5) that had been treated for six hours with PHA or bryostatin/romidepsin (10 nM/40 nM). (a) Intracellular p24 expression was measured after two days co-culture. % Elimination was calculated by comparing the %p24+ cells in the LRA-treated CD4/CD8/ImmTAV sample to the %p24+ cells in LRA-treated CD4/CD8 sample. (b) Example of p24+ expression in resting infected cells (left) and PHA-reactivated infected cells before (middle) and after (right) ImmTAV-redirected CD8+ T cell killing. Mean and SEM shown.

3.2.5 CD8+ T cells from CHI patients eliminate p24+ resting infected cells with ImmTAV-redirection

It was previously shown that CD8+ T cells from ART-treated CHI patients were inferior to HD CD8+ T cells in ImmTAV-redirected killing assays.[245] To assess whether

ImmTAV-redirected CHI CD8+ T cells could eliminate resting infected cells CHI donors with pre-existing responses to SL9, the cognate epitope for the m121 ImmTAV, were chosen for analysis in the VIA. Without ImmTAV-redirection the natural CTL responses eliminated only 5.6% (4.8) of the resting infected cells whereas the m121 ImmTAV (10^{-9} M) increased the elimination to 13.7% (4.1) and 26.8% (6.8) at E:T ratios of 1 and 2 respectively (figure 3.10).

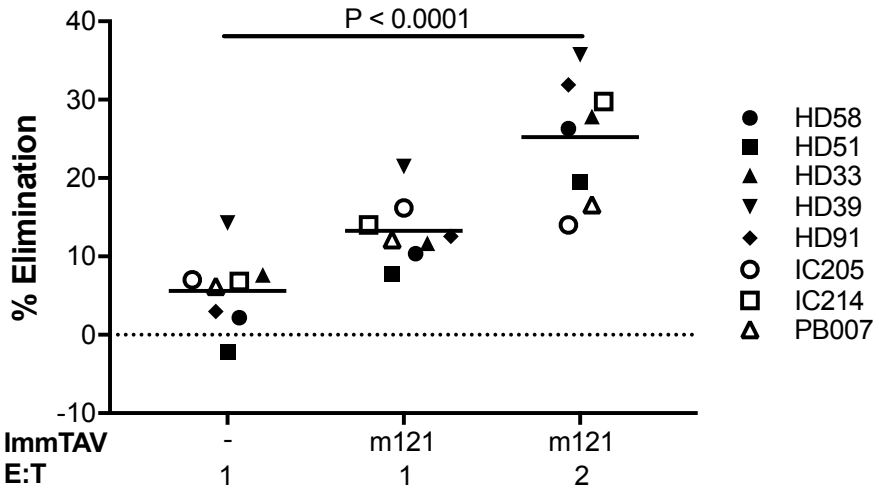

Figure 3.10: Impaired elimination of resting infected CD4+ T cells by CHI patient CD8+ T cells. CD8+ T cells from chronic HIV patients (n = 9) on ART were co-cultured with resting infected healthy donor CD4+ T cells (1 x 10^5) alone (E:T of 1) or with m121 ImmTAV (10^{-9} M, E:T of 1 or 2) for 48 hours before measuring intracellular p24. % Elimination was calculated by comparing the %p24+ cells in CD4/CD8/(ImmTAV) samples to the %p24+ cells in infected CD4+ T cells cultured alone. Mean shown. Groups were analysed by one-way ANOVA.

3.2.6 Assessment of functional exhaustion in CD8+ T cells

As CHI patient CD8+ T cells were less effective than HD CD8+ T cells at eliminating resting infected targets in the latency model, I investigated whether this was due to functional exhaustion (acquisition and analysis completed in collaboration with Dr Jakub Kopycinski, in our laboratory). CD8+ T cells from ten healthy and ten ART-treated CHI donors were assessed for PD-1 and CD39 expression on CD8+ T cells, using anti-CD45RA, CCR7 and CD27 antibodies to define the T cell memory subsets within the CD8+ T cell population (appendix 3.2).[336] There was no significant difference in the

composition (proportions of naïve, central, effector or terminally differentiated cells) of the CD8+ T cell populations between the CHI and healthy donors (figure 3.11).

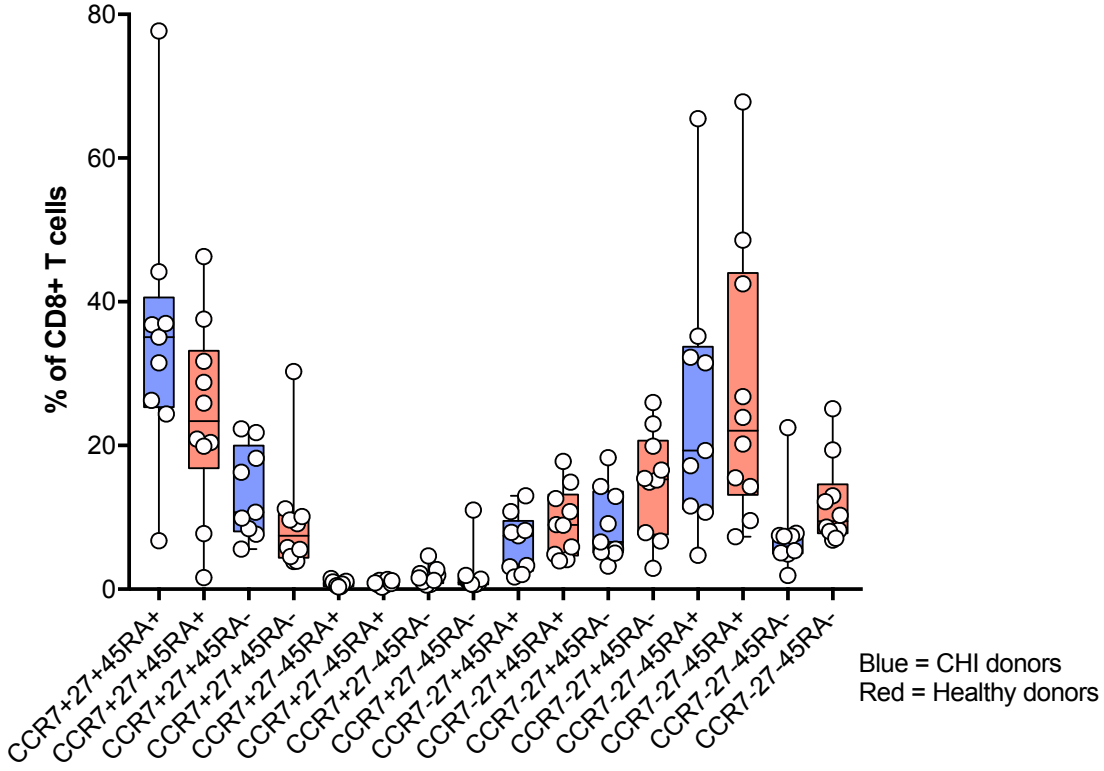

Figure 3.11: Comparison of CD8+ T cell subpopulations. CD8+ T cells from CHI donors (n = 9, blue) and healthy donors (n = 10, red) were stained for CCR7, CD27 ('27') and CD45RA ('45RA') expression to define CD8+ T subpopulations. There was no significant difference between the two donor groups for any of the subpopulations. Groups were analysed by one-way ANOVA ($P < 0.0001$) with Sidak's multiple comparisons test.

There was a significantly higher proportion of CD39+ CD8+ T cells in the CHI donors compared to the healthy donors in the effector memory subset (CHI vs. HD, mean (SD): 3.8% (2.4) vs. 1.4% (1.1), $P = 0.0002$) but not within the other subsets, although there was a trend toward a higher proportion of CD39+ CD8+ T cells in the CHI donors' central memory subset (figure 3.12a). Although not significant, there was also a trend towards a higher population of CD39+PD1+ CD8+ T cells in the CHI donors compared to the healthy donors for the central memory (CHI vs. HD, mean (SD): 3.6% (1.8) vs. 2.1% (1.1)) and effector memory (CHI vs. HD, mean (SD): 3.61% (2.5) vs. 2.2% (1.3))

subsets (figure 3.12a). PD-1 expression was also higher in the central and effector memory subsets compared to the naïve subset but there was no significant difference in expression between the two donor groups (figure 3.12a). As CD39 is polymorphic CD39 expression in the total CD8+ T cells from all the donors was compared. Only 15% of donors expressed <1% CD39+ CD8+ T cells (figure 3.12b).[187]

CD39 expression was also assessed on CD4+ T cells from the HIV-positive and HIV-negative subjects as it was reported to be upregulated on CD4+ T_{reg} from PLWH and correlated with immune activation.[337] There was a significantly larger population of CD39+ CD4+ T cells in the CHI donors compared to the healthy donors (CHI vs. HD, mean (SD): 7.7% (2.5) vs. 4.6% (2.4), P = 0.02; figure 3.12c).

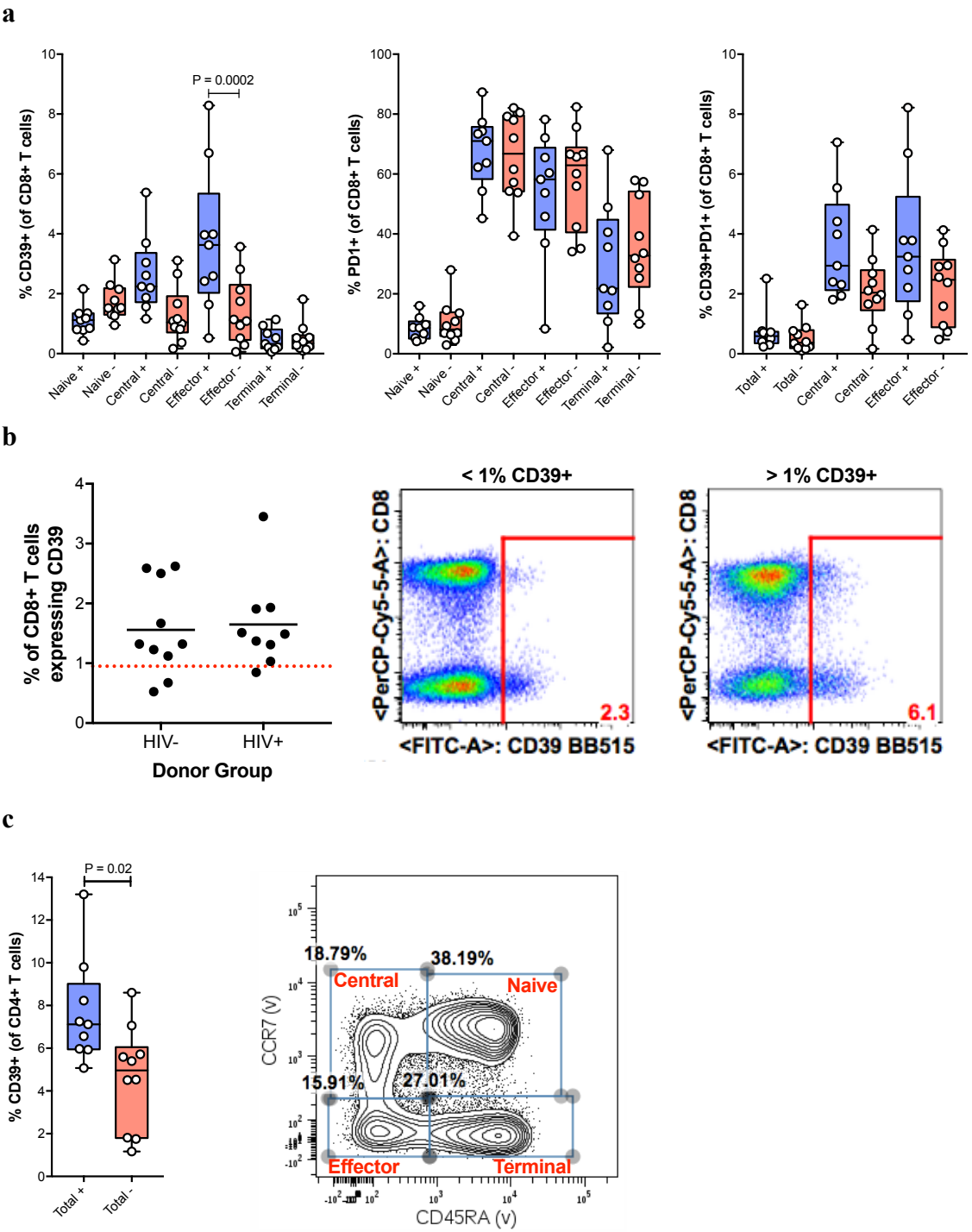

Figure 3.12: Analysis of exhaustion markers in T cell subsets. PBMCs from CHI donors (n = 9; +) and healthy, seronegative donors (n = 10; -) were stained for CD39 and PD-1 expression. (a) Box and whisker plots are shown for the CD39+, PD1+ and CD39+/PD1+ populations of the naïve, central memory, effector memory and terminally differentiated CD8+ T cell subsets (see gating strategy) for each donor group. (b) Plot showing % of CD8+ T cells expressing CD39 with cut-off for donors with < 1% CD39 expression (red line) and example FACS plots of CD39 expression. (c) A box and whisker plot for CD39+ expression on the CD4+ T cells of each donor group is shown. Groups in (a) were analysed by one-way ANOVA ($P < 0.0001$ for all groups) with Sidak's multiple comparisons test and groups in (c) by unpaired t test. CHI donors are shown in blue and healthy donors in red.

3.3 Discussion

The work in this chapter investigated the susceptibility of GPR cells to elimination by ImmTAV-redirected CD8+ T cells. Resting CD4+ T cells directly infected with HIV expressed less p24 than activated infected cells but were still susceptible to clearance by ImmTAV-redirected healthy and CHI donor CD8+ T cells.

The O'Doherty model of HIV latency is based on direct infection of resting CD4+ T cells without altering the cellular phenotypes (table 3.1).[239,310] Infection rates reported in the original description of the model using an NL4-3 virus ranged from < 1% to 13% p24+ populations.[304] HIV-1_{IIIB} was chosen for this investigation as it produced consistently high rates of infection in previous work involving activated cells.[295] Achieving a reproducible infection while maintaining the resting state of the cells was difficult as sensitivity to reactivation during infection varied amongst donors. While an MOI of 0.1 resulted in the highest frequency of infected cells (up to 8% p24+ CD4+ T cells) this was often associated with reactivation, therefore, an MOI of 0.05 was chosen despite the slight decrease in infection (figure 3.2). Compared to other latency models the O'Doherty model provided certain advantages (table 3.1). The use of primary cells and direct infection of resting cells matches physiological conditions *in vivo* more closely. A similar model described by Lewin also relied on directly infecting resting CD4+ T cells but with slight alterations to the chemokine environment, which may have affected their phenotype as CCR7 expression was downregulated and CCR5 expression increased.[338] To achieve higher frequencies of resting infected CD4+ T cells others have activated the cells before infection and then cultured them for long periods (up to four weeks) with cytokines or feeder cells prior to isolation of resting cells (Romerio, Siliciano, Planelles and Cloyd models).[339–342] However, long-term culture may alter the composition of the cell population, for example transitional memory cells may be lost.[95,343]

Table 3.1: Latency models for studying the HIV reservoir

Model*	Description
Lewin[338]	Isolation of resting CD4+ T cells, incubation with CCL19/21, direct infection
O'Doherty[239,304,310]	Isolation of resting CD4+ T cells, direct infection
Greene[344]	Isolation of CD4+ T cells, infection with reporter virus, short culture
Romerio[339]	DC-activation of CD4+ T cells, infection, culture with IL-7
Siliciano[342]	CD4+ T cells transduced with Bcl-2, infection with GFP-virus, culture without cytokines, isolate $GFP^{neg.}$ cells
Planelles[340]	Prime naïve cells, infection with defective HIV, culture with IL-2
Cloyd[341]	Long term culture of activated infected cells with feeder cells and IL-2
Verdin[345]	Transfection of Jurkat cells with retroviral vector, infection with GFP virus, isolation of $GFP^{neg.}$ cells
Zack[346]	Infection of CD4+CD8+ thymocytes with reporter virus, culture with IL-2/IL-4
Siliciano[97,128]	Viral outgrowth assay: isolate resting CD4+ T cells from patients, reactivate, culture with MOLT-4/CCR5 cells, measure outgrowth
Garcia[347]	Infect BLT mice (treated with ART) → harbour resting infected CD4+ T cells

*Model named after senior investigator

The most significant finding from the work described in this chapter is that despite low Gag expression, the HIV ImmTAV was able to recognise resting infected CD4+ T cells without the need for an LRA-induced 'shock' (figure 3.4). As expected, HD CD8+ T cells alone were unable to recognise resting infected cells except when redirected by the ImmTAV; use of a non-HIV specific ImmTAV (m232) or HIV-specific ImmTAV with a non-binding anti-CD3 (m231) did not successfully redirect cells, confirming the specificity of the m121 ImmTAV (figure 3.5). A comparison of these results with historical data showed that maximal ImmTAV effects were lower with resting than activated infected CD4+ T cells. This is likely due to differences in epitope density.[245]

Interestingly, a high concentration of ImmTAV did not improve clearance, but increased the spread of infection (figures 3.4, 3.6 and 3.7). As this was observed with

both the m121 and m232 ImmTAVs, this suggested that the effect was mediated by the anti-CD3 scFv. Indeed, the m231 ImmTAV, which lacked a binding anti-CD3 chain, did not cause activation of the cells and reactivation of virus at any concentration (figure 3.6). As CD4+ T cells also express CD3, they could also be activated by the anti-CD3 scFv. It is possible that serial triggering occurred at the 10^{-8} M concentration, thus delivering a signal that was sufficient to drive transcription of latent proviruses.[348,349] However, previous work in our laboratory confirmed that the ImmTAV, when added alone to activated infected CD4+ T cells, did not increase infection by recruiting uninfected CD4+ T cells (Dr Hongbing Yang, unpublished). The reactivation effect was highest with the m232 ImmTAV which suggests an additional explanation for the enhanced infection at 10^{-8} M ImmTAV concentrations: this may be a result of HLA-restricted cross-reactivity which has been seen with some candidate immune-mobilising TCRs at concentrations greater than 10^{-9} M.[225,226,350]

While it is expected that therapeutic dosing would be achieved with ImmTAV concentrations less than or equal to 10^{-9} M, a non-specific activating effect could be harnessed to provide both the 'shock and kill' with one molecule. Pegu et al. reported applying a dual specificity antibody, recognising the CD4-binding site of Env and the CD3 antigen, to both reactivate latent virus and redirect CD8+ T cells. While the combination of the bispecific molecule and CD8+ T cells eliminated latently infected cells in an *in vitro* model of latency the success of the anti-CD3 arm at stimulating *env* gene expression in latently infected CD4+ T cells from ART-treated patients *ex vivo* varied widely.[348]

As the ImmTAV-redirected HD CD8+ T cells eliminated only 40% of resting infected cells in the absence of any LRAs, different LRAs were compared to see whether LRA treatment could enhance killing. Only romidepsin or a combination of

bryostatin/romidepsin had any significant effect on the frequency of Gag+ cells (figure 3.8). Stimulation with the mitogen, PHA, confirmed that the cells carried replication-competent virus that was not inducible by most LRAs on their own. Acitretin enhances RIG-I signalling *ex vivo* (RIG-I, a cytosolic pathogen recognition receptor, senses HIV RNA and activates innate antiviral signalling) and in combination with vorinostat has been shown to induce apoptosis specifically in HIV-infected cells.[351] In the latency model the combination of acitretin/vorinostat slightly decreased the p24+ population suggesting that this combination may have provided both the 'shock and kill' without the ImmTAV (figure 3.8).

Limitations of the latency model may have accounted for the partial effect of LRAs on viral reactivation in resting infected cells. For all the LRAs, reactivation efficiency varied between donors and infections. The LRAs also proved toxic to the CD4+ T cells, even after six hours, and this limited the duration of time the cells could be exposed to the treatment and how long they could be cultured before p24 expression was measured. A study of HDAC inhibitors and PKC agonists reported assorted impacts of LRAs on cell viability and function. Exposure to romidepsin reduced cell viability after 48 hours co-culture and reduced antigen-specific proliferation over five days. Bryostatin also proved toxic to PBMCs and limited the number of proliferative cycles of antigen stimulated T cells.[352] Walker-Sperling et al. also reported that the LRAs used in this thesis, romidepsin and bryostatin, also had an impact on CD8+ T cell function. Following the failure of peptide stimulated CD8+ T cells to reduce HIV RNA in LRA-reactivated CD4+ T cells from ART-treated patients, CD8+ T cells from elite suppressors were cultured directly with bryostatin and romidepsin. This direct exposure significantly inhibited the ability of elite suppressor CD8+ T cells to suppress infection in a mechanism linked to increased cell death.[142] In this thesis LRAs were washed out of the

culture before addition of the CD8+ T cells but this study has implications for the use of LRAs *in vivo*.

Despite reactivating virus in resting infected cells alone LRA exposure did not have an impact on viral clearance by ImmTAV-redirected effectors (figure 3.9a). This result may have been due to the inter-assay variation in reactivation as defined by the proportion of the p24+ population – the percentage change of p24+ cells to the untreated sample (mean 41%) was lower than in the initial tests of the LRA (figure 3.8). The specific infected cell elimination may have also been masked by the concomitant viral spread induced by the effect of the LRAs. For example, PHA treatment activated more of the resting infected cells than bryostatin/romidepsin but after co-culture with the ImmTAV and effectors the remaining p24+ population was still higher than the unstimulated resting infected cells suggesting there were newly infected cells still to be eliminated (figure 3.9b). A longer co-culture time may be required to detect elimination under these conditions but this was not attempted as resting cell viability after separation, infection, reactivation and prolonged culture was a limiting factor. Another possibility is that reactivation by LRAs did not increase the SL9 epitope density on the cell surface.[245] In summary, the data obtained with LRAs are inconclusive due to their weak and variable effects and narrow window of toxicity in primary cells. Other latency models were considered but LRA effects in these models are poorly predictive of their effects *in vivo*.[97,128,144,353]

CD8+ T cells from CHI patients were not as effective at killing resting cell targets as HD CD8+ T cells (figures 3.4 and 3.10). This is consistent with published data showing the same phenomenon with autologous reactivated cells.[245] It could reflect persistent functional exhaustion despite effective ART, which is the consequence of an altered programme of memory T cell differentiation that results in the hierarchical loss of

effector functions, upregulation of inhibitory receptors (IR) and altered expression of key transcription factors.[195,354] Previous studies reported that CD8+ T cells from CHI donors (virologically suppressed on ART) expressed more PD-1 and activation markers, like CD38, but had smaller populations of perforin-expressing cells compared to HD or long-term nonprogressors; this pattern of expression correlated with exhausted function including lower proliferative capacity.[190,193,354,355] Incorporation of multiple markers of IR and activation are crucial to assess the exhaustion status of cells as PD-1 alone may not necessarily be indicative of exhaustion; PD-1 is also a T cell activation marker and can be induced via CD3 signalling.[356–358] Duraiswamy et al. reported that PD-1 was expressed on memory CD8+ T cells in healthy donors and the presence of PD-1 did not affect their ability to secrete cytokines.[356] Additionally, as ART has been shown to reduce the surface expression of inhibitory molecules effective virological suppression may have contributed to reduced PD-1 expression in the CHI patients.[359]

To investigate the exhaustion status of the CHI donor CD8+ T cells a flow cytometry panel comprising PD-1 and CD39 was developed. CD39, an ectonucleotidase, hydrolyses extracellular adenosine triphosphate (ATP) into adenosine monophosphate, which is then catalysed to adenosine by CD73. Adenosine regulates immune responses including inhibiting T cell proliferation and secretion of cytokines.[337] Gupta et al. reported that CD39 expression on antigen specific CD8+ T cells specific for hepatitis C virus (HCV) or HIV – chronic viral infections – was higher than on those cells specific for EBV or CMV (or total CD8+ T cells from healthy donors). Additionally, the co-expression of CD39 with PD-1 marked cells with transcriptional signatures of T cell exhaustion.[336] CD39 has also been implicated in the suppressive tumour environment, as tumour-infiltrating lymphocytes (found in tumours but not lymph nodes) were marked by

high expression of CD39 and exhibited an exhausted phenotype – expression of IR (Tim-3, Lag-3 and PD-1) and reduced production of TNF and IL-2.[360]

While Gupta et al. analysed CD39 expression in both antigen-specific and total CD8+ T cells, only the total CD8+ T cell populations were investigated in this thesis. However, additional cellular markers were included to define the naïve (CCR7+CD45RA+), central memory (CCR7+CD45RA$^{neg.}$), effector memory (CCR7$^{neg.}$CD45RA$^{neg.}$), and terminally differentiated effector (CCR7$^{neg.}$CD45RA+) subsets. There was a significantly larger proportion of CD39+ cells, and a trend towards a larger proportion of CD39+PD1+ CD8+ T cells, in the effector memory CD8+ T cell subset of the CHI donors compared to the healthy donors (figure 3.12a). PD-1 expression was high in both groups and this may have masked any difference in the CD39+PD1+ double positive populations. The exhaustion phenotype in the effector memory subset is important because healthy donor effector memory T cells showed the strongest capacity to clear HIV infected cells when redirected by an ImmTAV.[245] The increased expression of CD39 in the CHI donor CD8+ T cells, especially the effector memory subset crucial for ImmTAV-redirected killing, suggests that the impaired killing seen in section 3.2.5 could be related to the CD39/adenosine pathway. However, it is important to take into consideration the polymorphism of the CD39 molecule. Roederer et al., using an immunophenotyping approach, investigated 78,000 immune traits in a large cohort of twins and found that CD39 expression per cell was associated with an 'on/off' control; those homozygous for the rs7096317A SNP express the most CD39 on their surface while heterozygotes express half as much (although still enough to remain CD39+) and those homozygous for the rs7096317G SNP expressed no CD39.[361] Thus in the analysis of CD39 expression between the CHI donor and healthy donor groups the difference in the frequency of CD39+ CD8+ T cells between the two groups may be due to HD with

the rs7096317G SNP, resulting in lack of CD39 expression regardless of their exhaustion phenotype. While SNP data was not available for the CHI donors and healthy donors studied, only 15% of the donors expressed <1% CD39 (figure 3.12b), compared to the 50% reported by Hoffman et al.[187]

Further work is required to support the potential link to exhaustion provided by the higher frequency of CD39+ CD8+ T cells in CHI donors. Hoffman et al.'s investigation of exhaustion in SPARTAC trail participants included assessment of CD39 and other IR, like Tim-3, in addition to the expression of the T-bet and Eomes transcription factors. The percentage of CD8+ T cells expressing CD39 was higher within the T-bet^{dim}Eomes^{hi} than the T-bet^{hi}Eomes^{dim} populations.[187] This confirms the work of Buggert et al. who found that IR were elevated in chronically infected individuals and highly associated with the T-bet^{dim}Eomes^{hi} transcriptional profile; the virus specific CD8+ T cells belonging to this phenotype exhibited poor polyfunctional effector characteristics.[362]

An assessment of the T-bet and Eomes expression of the CD8+ T cells from the CHI and healthy donors used in this thesis would help provide a link between the surface expression of exhaustion markers and the transcriptional pathway to effector dysfunction. Addition of further activation and inhibitory markers would also allow for a more definitive classification of exhaustion especially by measuring the degree of co-expression.[356,359,363] IRs, including CTLA-4, LAG-3, 2B4, CD160 and TIM3, regulate the cell in multiple ways. IR competition for ligands affects microcluster formation and modulates intracellular mediators, leading to attenuation of positive signals from activating receptors and induction of inhibitory genes.[187,364,365] Functional exhaustion in CD8+ T cells could also be further explored using immune checkpoint receptor antagonists. In previous studies, anti-PD-1 or anti-PD-L1 blocking antibodies improved

cell proliferation, cytokine production, cell survival and overall effector function in CD8+ T cells from CHI patients.[190,193,359,366,367]

Interestingly, there was also a larger proportion of CD39+ CD4+ T cells in the CHI donors compared to the healthy donors which corroborates the findings of Nikolova et al. who reported that more T_{reg} from PLWH expressed CD39 compared to seronegative donors.[337] While no additional T cell markers were included to define the regulatory T cell population in this thesis, the presence of CD39 on total CD4+ T cells suggests a possible role for T_{reg} suppressive activity in the observed CD8+ T cell functional impairment that merits further investigation. CD39 expression on CD8+ T cells may also define a population of CD8+ T_{reg} as recent evidence suggests that HIV-infected patients have increased levels of CD8+CD28-CD127^{lo}CD39+ T_{reg} cells, a population previously only described in the tumour microenvironment. The frequency of this population correlated with clinical disease as well as chronic immune activation.[368] This population was not assessed in this thesis but defining this subset of CD8+ T_{reg} could provide further understanding of the exhaustion status of CHI patients' cell.

In summary, the HIV-specific ImmTAV was able to detect resting infected CD4+ T cells without LRAs despite their low Gag expression. This supports the theory that the latent reservoir may be comprised of cell populations on a spectrum according to the level of viral gene transcription and suggests that at least a portion of latently infected cells could be targeted with optimised 'shock and kill' strategies. Recent modelling of HIV dynamics under integrase inhibitor therapy in individuals suggested that the dynamics of cell subpopulations, including long-lived, resting infected cells with slow integration, may contribute to the overall observed viral kinetics; the variations of integration and survival in these subpopulations may make them differentially affected by treatments.[369] Further work is needed to clarify the effects of LRAs in this model and to understand why

CD8+ T cells from CHI patients fail to match the antiviral activity of healthy donors, even with ImmTAV redirection, to grasp the full redirection potential of the ImmTAV. Chapters five and six investigate whether impaired antiviral activity is caused by defects in the ability of CHI donor CD8+ T cells to form immunological synapses with target cells.

3.4 Questions addressed in this chapter

- *Can latently infected cells express Gag?*

  Yes. After directly infecting resting CD4+ T cells low levels of p24, compared to activated infected cells were detected by FACS in a population of cells that did not spread infection (figures 3.1; section 3.2.1).

- *Can resting infected cells be cleared by ImmTAV-redirected CD8+ T cells?*

  Yes. ImmTAV-redirected HD CD8+ T cells eliminated up to 40% (mean) of resting infected CD4+ T cells at an E:T of 2 (figures 3.4 – 3.5). This effect was only achieved with the HIV-specific ImmTAV with the active anti-CD3 scFv at the recommended 10^{-9} M concentration as higher concentrations of ImmTAVs with the anti-CD3 scFv reactivated CD4+ T cells (figures 3.6 – 3.7; sections 3.2.2 – 3.2.3).

- *Does reactivation of latently infected cells with an LRA improve ImmTAV-redirected killing?*

  No. Bryostatin/romidepsin were able to reactivate latent virus in resting infected cells but this did not improve the clearance of infected cells by ImmTAV-redirected CD8+ T cells. This suggests that presentation of the cognate epitope was not enhanced following LRA treatment, despite an increase in Gag expression (figures 3.8 – 3.9; section 3.2.4).

- *Can CD8+ T cells from CHI donors eliminate resting infected cells?*

  Yes, but poorly. Pre-existing virus-specific CD8+ T cells from CHI donors were only able to eliminate 5.6% of the resting infected cells. ImmTAV redirection modestly improved killing to 13.7% and 26.8% at an E:T of 1 and 2 respectively, which was less than that seen with ImmTAV-redirected HD CD8+ T cells (figure 3.10). This impairment suggests global dysfunction in CHI donor CD8+ T cells,

as seen by the presence of a significantly larger CD39+ CD8+ T cell population in CHI donors compared to healthy donors (figures 3.12; sections 3.2.5 – 3.2.6).

CHAPTER FOUR: DEVELOPMENT OF A METHOD FOR INVESTIGATING PRIMARY CD8+ T CELL SYNAPSES IN THE CONTEXT OF AN HIV INFECTION

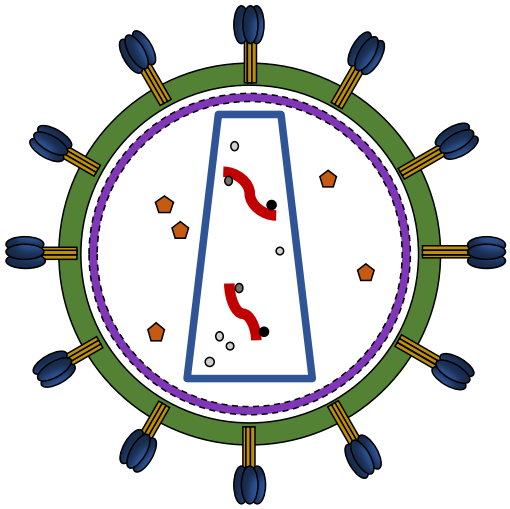

4.1 Introduction

The availability of new microscopy techniques has greatly enhanced the understanding of the immunological synapse (IS) as each technique offers the opportunity to obtain increasingly higher resolution images. When Monks et al. first described the three-dimensional segregation of molecules at the IS they acquired images of the interacting cells along the X-Y and Z-axes before using deconvolution software to merge the slices into a 3D structure.[249,250] This method produced an image of the cell-cell interface without requiring the APC to be positioned directly on top of or below the effector cell. However, resolution and information were lost through the Z-stack and deconvolution process.

The limitations of this method have been addressed by many studies that have made use of anti-CD3-coated glass coverslips in place of an APC. By coating coverslips with specifically designed pHLA complexes of interest, co-stimulatory molecules, or adhesion receptors the T cell can settle on the coverslip and interact as it would with an APC. This interaction can be captured from below the coverslip with total internal reflection fluorescence microscopy (TIRFM): a laser beam is reflected off the interface at a critical angle and the resulting evanescent light wave penetrates the sample less than 200 nm deep in the Z-direction thus generating an image of the surface of the cell interacting with the pseudo-APC. However, as cells respond to surfaces, the glass coverslip may cause activation of the cell and artificial reorganisation of surface molecules. To overcome this lipid bilayer surfaces can be applied to the coverslip, mimicking the fluid surface of an APC.[246,247,250,280,370–374] As outlined in section 1.3.1 this model has been used to understand TCR segregation kinetics on the microdomain level, describing a further aspect of segregation of molecules before the mature SMAC formation.[253,375] The supported bilayer method may recapitulate the synapse by

incorporating a plasma membrane-like structure into the synapse but the stiff glass and limited diversity of proteins incorporated into the bilayer can still limit the formation of a physiologically relevant synapse.[370,371] Additionally, it restricts the study of the cell to the basal membrane, restricting study of the molecules and signalling occurring within the cell.

Light microscopy has limited resolution, which restricts the ability to identify small structures or differentiate between altered patterns of clustering. Super resolution techniques have been developed that improve the resolution from ~200 nm down to below 50 nm in the X-Y direction. STED, PALM/STORM (Photo-Activated Localisation Microscopy/Stochastic Optical Reconstruction Microscopy) and SIM (Structured Illumination Microscopy) all manipulate light through the use of differentially calibrated lasers, grids and fluorophores, which enable acquisition of images at a higher resolution than the diffraction limit of light. For example, STED uses two lasers to shrink the effective excitation area of the laser beam (figure 4.1). The first laser excites the fluorophore to a higher state while a second laser, with a doughnut shape, de-excites the fluorophore in all areas except the hole in the middle. This suppresses fluorescence emission except at the centre of the STED beam which is smaller than the original excitation beam. This microscopy technique was used to redefine the kinetics of F-actin clearing at the NK immunological synapse; super resolution images showed a pervasive network of actin with small hypodense regions that allowed granules to pass through, thus challenging the original theory of total F-actin clearance at the centre of the IS.[376,377]

Despite the clear benefits of super resolution microscopy there are still unresolved challenges with this type of imaging, such as labelling of the proteins of interest, controlling the timing of signalling or interactions and achieving meaningful statistical significance. With typical light microscopy the size of the antibody labelling the protein

of interest does not impact the image greatly because of the limited resolution. However, when trying to resolve two molecules 50 nm apart the size of the label suddenly becomes an important concern. Additionally, with the amount of laser power required to manipulate the fluorophores, such as the double lasers used in STED, the degree of photo-bleaching increases as well. When multiple colours are required this issue increases and synchronisation of the beams becomes more complicated. Finally, the cell type used for any super resolution microscopy experiment is important as using cells transfected to overexpress protein, to increase signal size, may lead to artificial associations and artefacts.

Figure 4.1: Schematic of lasers for STED microscopy. The effective excitation volume is reduced by adding a doughnut-shaped STED laser to de-excite the fluorophores, except those in the centre. This improves the resolution beyond the diffraction limit of light to ~50 nm. From left to right: conventional microscopy excitation volume, STED laser, effective excitation volume in STED mode.

For the aforementioned reasons special dyes, fluorophores, chemical tags and antibody fragments (Fab) are required to accurately label the molecules while remaining biocompatible. Once an appropriate labelling method has been selected further choices must be made to make the best use of available resources. There is a tight balance between achieving adequate signal without phototoxicity, quickly capturing synapse dynamics while keeping maximum resolution and striving for statistical power with the time investment of super resolution imaging. Despite the inherent complexities the steady development of hardware, software and protocols that combine different microscopy

techniques is paving the way for super resolution microscopy that is easier to use and can be applied to live-cell and 3D-imaging. Other microscopy techniques have also been developed to tackle model specific requirements such as two-photon microscopy, which is able to penetrate tissues to image cell-cell interactions *in vivo*, or atomic force microscopy to measure the adhesions force kinetics between interacting cells.[370,378–383]

There is currently a gap in the literature regarding the study of physiologically relevant synapses between primary CD8+ T cells and APCs in the context of an HIV infection.[31,256,384–387] This reflects the scarcity of data on the IS in primary human CD8+ T cells generally, the specific challenges of working with HIV-infected material and the lack of super resolution microscopy or TIRFM in containment level 3 facilities. The focus of the work in this chapter was to design a stable and repeatable protocol to identify both CD8+ T cells and HIV-infected targets involved in the conjugate; SL9-pulsed T2 cells were also tested as an alternative non-primary target cell. For HIV-infected or SL9-pulsed targets the m121 ImmTAV was also applied to mediate synapse formation when using HIV-naïve HD CD8+ T cells. The use of primary cells imposed limitations on the type of synapse molecules that accurately described the IS but a panel of markers spanning distinct stages of synapse formation was eventually developed. Confocal microscopy was chosen as this relies on a pinhole to remove out-of-focus light, eliminating the need for deconvolution, but is flexible enough to allow imaging of multiple markers throughout a cell pair. Alternative target cells and microscopes were also evaluated for their potential to provide different perspectives on synapse formation. This chapter covers the optimisation work required for the immunological synapse investigation described in chapter five.

4.2 Results

The optimisation process for each antibody was dependent on the manufacturer's instructions and protocols previously reported in the literature; for example, several fixation methods were tested for the anti-Zap70 antibody as reported fixation methods varied. Optimisation is only shown if method was in question. If not mentioned or optimised the 'basic protocol' refers to 4% PFA fixation, 0.1% TX100 permeabilisation, 2.5% goat serum blocking and primary/secondary antibodies at the end.

4.2.1 Comparison of antibodies to detect HIV-1 Gag protein by immunofluorescence

To identify HIV-infected target cells under the microscope primary antibodies against different HIV proteins were assessed by confocal microscopy. HIV-infected primary CD4+ T cells were detectable by anti-p24, p17 or gp120 antibodies at optimised titrations (figure 4.2a). Since the gp120 expression was not as well defined as the two Gag antibodies, no further testing with this antibody was performed. The TCCF of the p24 stain was higher than the p17 stain with a larger range of expression (p24 vs. p17, median (range): 2032 (224.3 – 14261) vs. 943 (-492.6 – 6110); figure 4.2b) and was able to detect both mature and immature forms of Gag making it a valuable tool for detecting Gag in GPR cells.

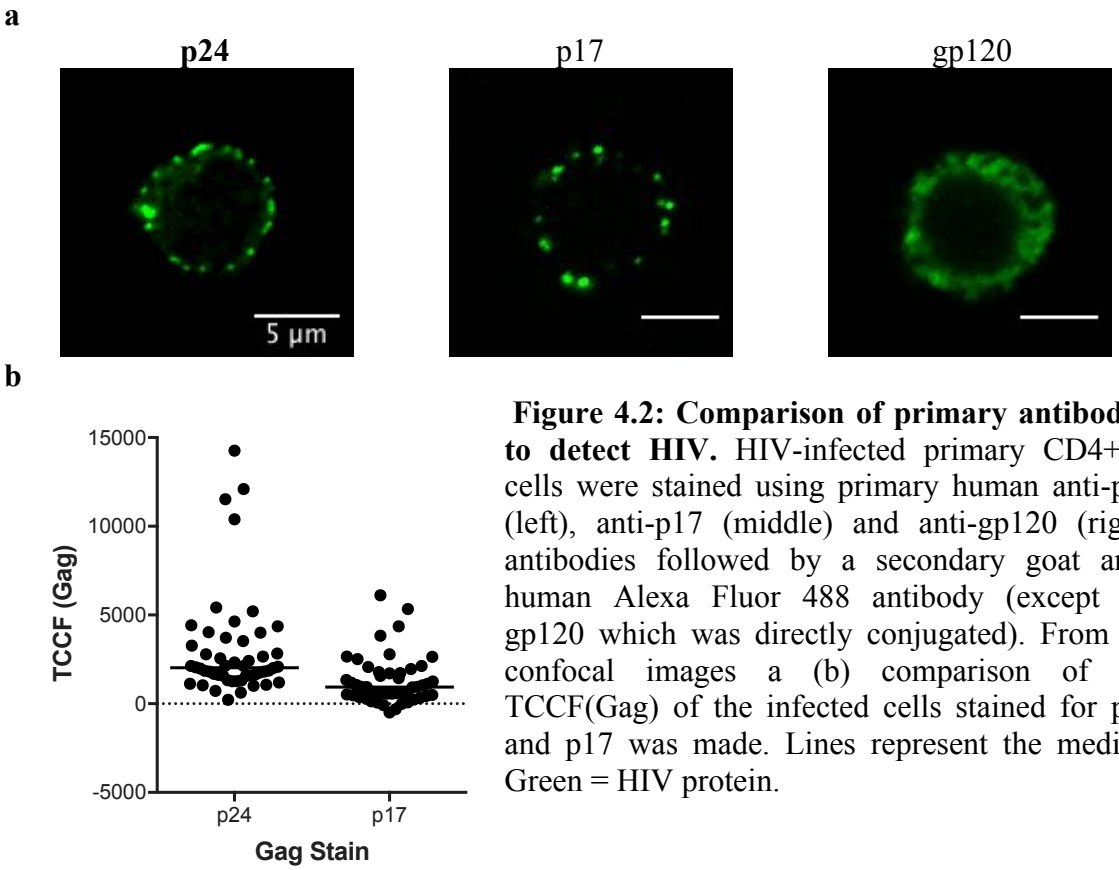

Figure 4.2: Comparison of primary antibodies to detect HIV. HIV-infected primary CD4+ T cells were stained using primary human anti-p24 (left), anti-p17 (middle) and anti-gp120 (right) antibodies followed by a secondary goat anti-human Alexa Fluor 488 antibody (except for gp120 which was directly conjugated). From (a) confocal images a (b) comparison of the TCCF(Gag) of the infected cells stained for p24 and p17 was made. Lines represent the median. Green = HIV protein.

Uninfected control slides also stained positive for HIV proteins but upon further staining of uninfected cells with the secondary antibody only this was determined to be because of non-specific binding by the latter (figure 4.3, left). Alterations to the blocking buffer, blocking time, wash steps and secondary antibody concentration did not eliminate the non-specific binding, so the p24 antibody (37G12) was then conjugated to a far-red dye (Abberior STAR 635P) to remove the need for a secondary antibody. In a comparison of the conjugated p24 antibody to the original primary/secondary combination the TCCF(p24) difference between the uninfected and infected cells was significant for both (conjugated infected vs. uninfected, median: 864 vs. 377, $P < 0.0001$; primary/secondary infected vs. uninfected, median: 1755 vs. 502, $P < 0.0001$) but as there were no TCCF(p24)^{high} uninfected cells with the conjugated p24 antibody, as seen with the primary/secondary combination, this staining method was chosen (figure 4.3, right).

To determine how best to measure p24 expression in the target cells the TCCF(p24) of a summed Z-stack taken of the entire cell and a single image taken at the widest part or 'equator' of the cell were compared. In 16 cells with differing p24 expression there was a strong correlation in TCCF(p24) values obtained by the two methods of image acquisition ($r^2 = 0.96$; figure 4.4). The 'equator' method was chosen to limit acquisition times and risk of photo bleaching.

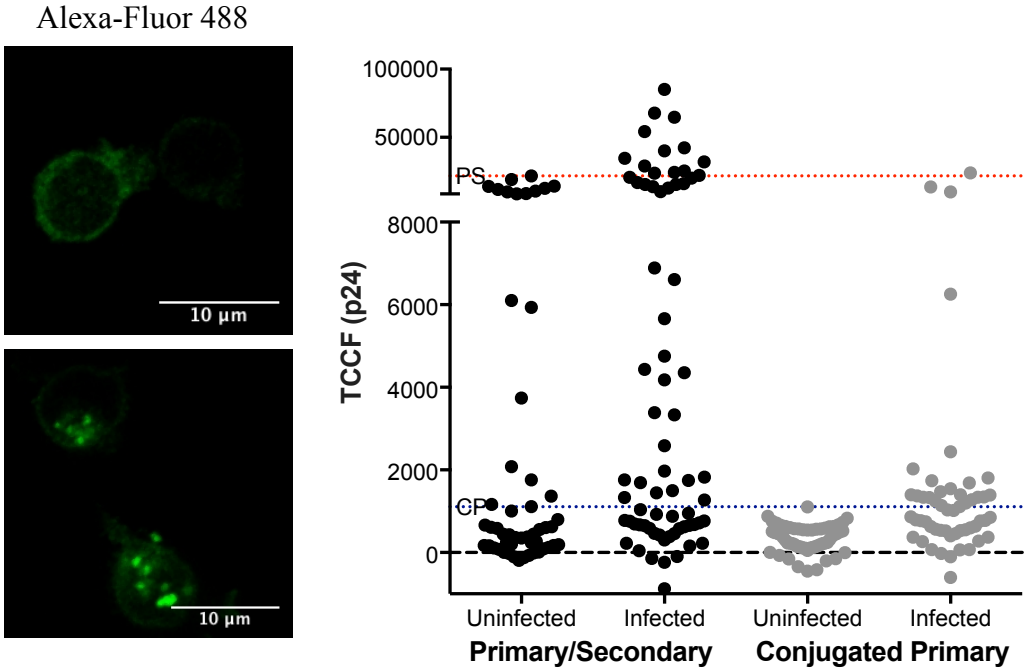

Figure 4.3: Non-specific staining following use of anti-human secondary antibody. (Left) Uninfected primary cells stained with anti-human secondary antibodies alone appear infected under the microscope due to non-specific binding of the antibody. Green = Alexa Fluor 488. (Right) Uninfected and HIV-infected CD4+ T cells were stained with either a primary p24/secondary anti-human antibody (black) or with a primary p24 antibody directly conjugated to a secondary dye (grey) for immunofluorescence. Immunofluorescence images of the p24 stain were used to calculate the total corrected cellular fluorescence (TCCF(p24)) for all groups and the uninfected sample was used to set a cut-off for p24-positivity for the infected sample (red = primary/secondary cut-off; blue = conjugated primary cut-off); each dot represents a cell.

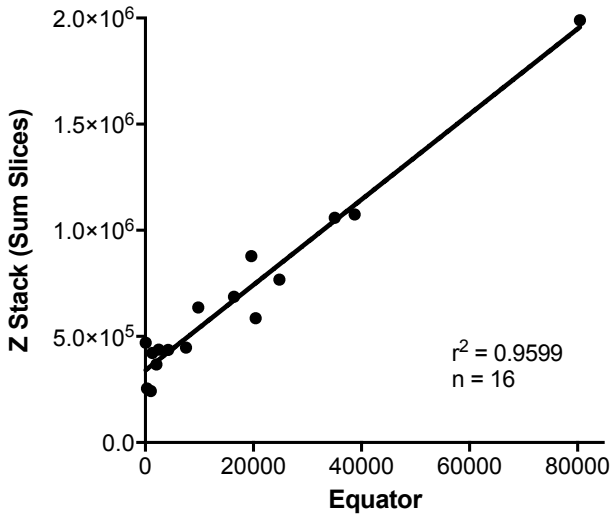

Figure 4.4: TCCF(p24) comparison at the 'equator' versus a summed Z-stack. Confocal images (n = 16) of the p24 channel taken at the widest part of the infected cell ('equator') and throughout the cell via Z-stacks that were summed together ('Sum Slices') were used to compare the TCCF(p24). Linear regression shown ($r^2 = 0.9599$).

4.2.2 Assessment of anti-CD8 antibodies to detect primary effectors in synapses

A mouse anti-CD8α chain antibody clearly detected effector cells by immunofluorescence (figure 4.5, left). However, for panels involving mouse primary antibodies against the synapse proteins, like Lck, a primary antibody from another species was required. A rabbit anti-CD8α antibody from SCBT tested did not stain the CD8 molecules clearly, resulting in patchy CD8 expression even with the different fixation times (10 – 30 minutes; double fixation before and after CD8 stain) and antibody titrations tested (figure 4.5, middle image). A rabbit anti-CD8α antibody from Abcam against a different epitope did stain the CD8+ cells clearly as long as the cells were permeabilised (figure 4.5, right). The mouse anti-CD8α and Abcam rabbit anti-CD8α antibodies were used for future work.

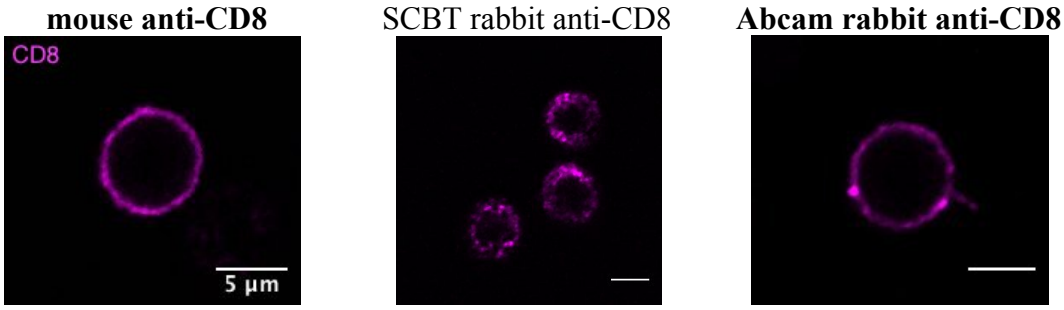

Figure 4.5: Identification of a rabbit anti-CD8 antibody for immunofluorescence. Confocal microscopy images of primary CD8+ T cells stained with mouse anti-CD8α antibody (left), SCBT rabbit anti-CD8α antibody with suboptimal staining (middle), and Abcam anti-CD8α antibody (right). Magenta = CD8α.

4.2.3 Optimisation of a method to identify Lck in primary T cells

Lck is one of the first tyrosine kinases involved in signalling via the TCR complex during the formation of an IS.[388–391] As reported fixation methods to identify Lck varied, CD8+ T cells were fixed with 4% PFA or 50% methanol (in PBS) for 5, 10 or 30 minutes before staining with the mouse anti-Lck primary antibody (Santa Cruz). Sparse Lck patterning was visible under all conditions but 30 minutes of PFA fixation achieved the clearest Lck staining (figure 4.6).

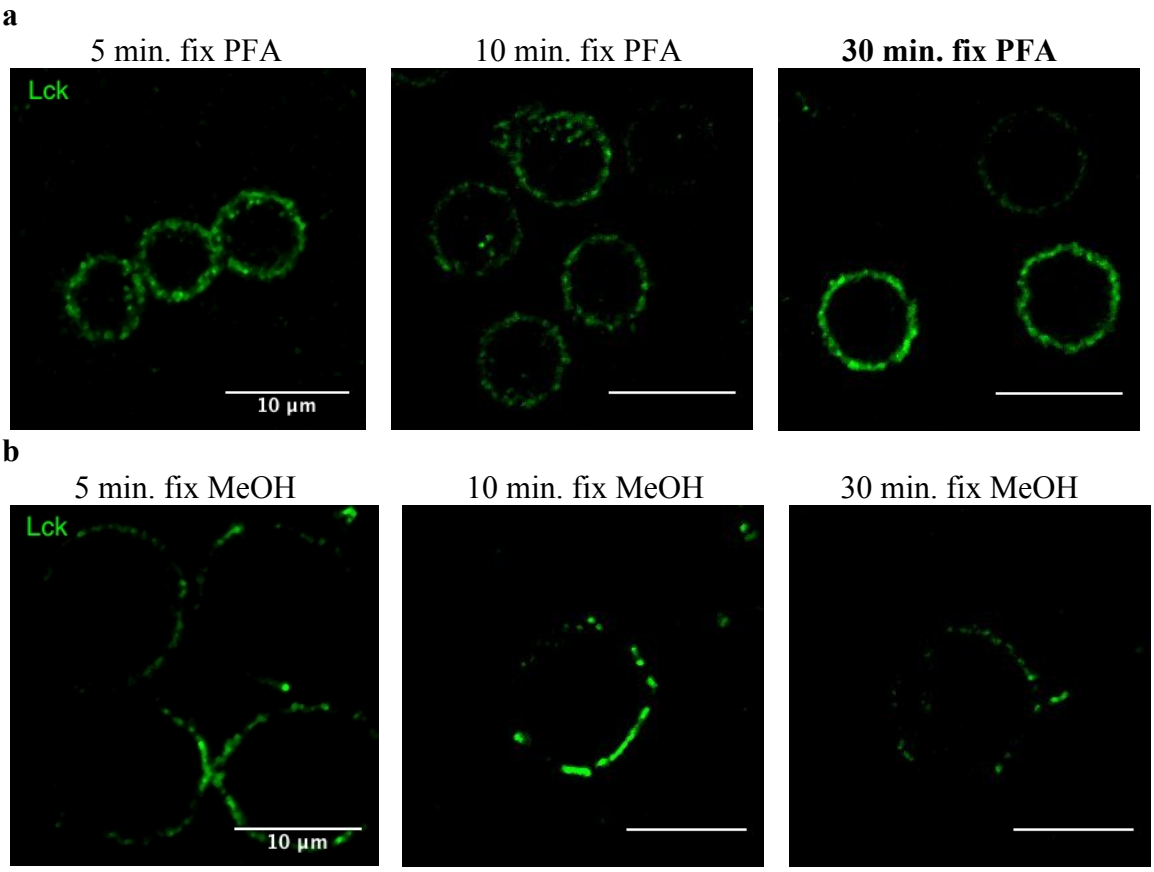

Figure 4.6: Different fixation methods for use with anti-Lck antibody. PBMCs were fixed for 5, 10 or 30 minutes (left to right) with (a) 4% PFA or (b) 50% methanol before staining with an anti-Lck primary antibody. Green = Lck.

The active form of Lck, phosphorylated at the Y394 (tyrosine) position, is present in resting T cells but accumulates at the IS after APC-T cell interaction.[31,390,392] To investigate this pattern of expression PBMCs were stimulated with PHA or left unstimulated before staining with the anti-Lck antibody or an anti-Lck^{Y394} antibody (active form). The ring-like expression remained similar under all four conditions except in the stimulated cells stained with anti-Lck^{Y394} where the Lck expression was patchy throughout the cell (figure 4.7a). To determine whether Lck expression would be more distinct at the site of an IS primary CD8+ T cells were co-cultured with SEB-pulsed WJR076 B cell line cells, a 'model APC', for 1 or 30 minutes then stained with both Lck antibodies. Again, Lck expression was either patchy throughout the CD8+ T cell or ring-like around the edge (figure 4.7b). As Lck expression was weak and inconsistent with

published data, despite all attempts at optimisation, this protein was not used for further synapse analysis.[31,258]

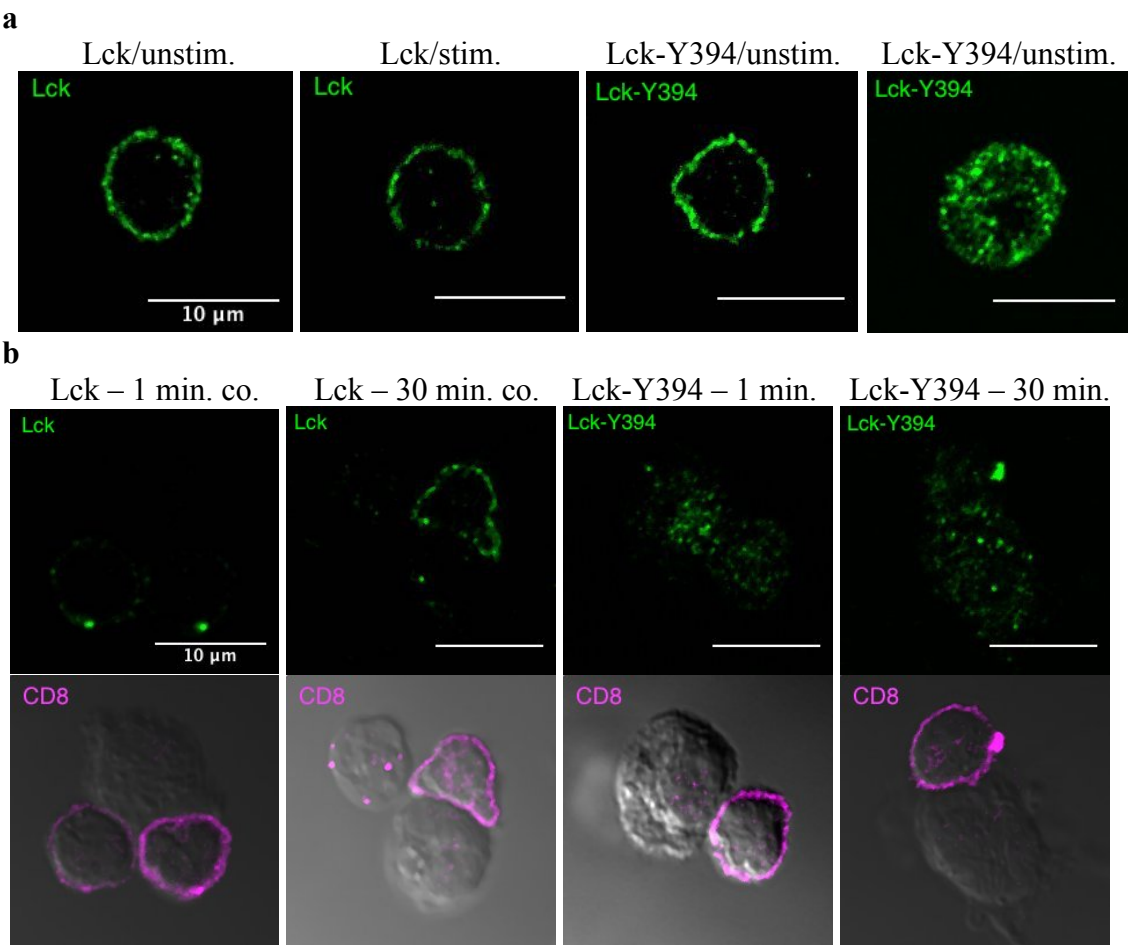

Figure 4.7: Comparison of anti-Lck and anti-Lck^{Y394} antibodies. (a) PBMCs were left unstimulated or stimulated with PHA before staining with an anti-Lck or anti-Lck^{Y394} primary antibody. From left to right: Lck + unstim., Lck + PHA, Lck^{Y394} + unstim., Lck^{Y394} + PHA. (b) CD8+ T cells were cultured with an SEB-stimulated B cell line for 1 or 30 minutes before staining for Lck. From left to right (top = Lck, bottom = CD8 on DIC of same pair): 1 min. Lck, 30 min. Lck, 1 min. Lck^{Y394}, 30 min. Lck^{Y394}. Green = Lck, magenta = CD8 on DIC image.

4.2.4 Optimisation of method to quantify LFA-1 in T cell synapses

LFA-1 is the main T cell adhesion molecule that initiates IS formation by binding to ICAM-1 on the APC and stabilising contact.[384,393,394] To assess LFA-1 staining at the synapse CD8+ T cells were co-cultured with SEB-pulsed B cells before staining for LFA-1 using the basic protocol. However, no LFA-1 was visible anywhere on the CD8+ T cell

(figure 4.8a). As alterations to antibody concentration and fixation did not affect this staining (not shown) different permeabilisation methods were tested. LFA-1 expression was visible with the use of a saponin buffer, however, the buffer affected the clarity of the CD8 stain (figure 4.8b). LFA-1 staining was improved by both omission of permeabilisation and permeabilisation with 0.1% TX100 after the LFA-1 primary antibody step (figure 4.8c, d). As permeabilisation was required for staining with p24 and CD8 antibodies the latter method was chosen for the synapse panel.

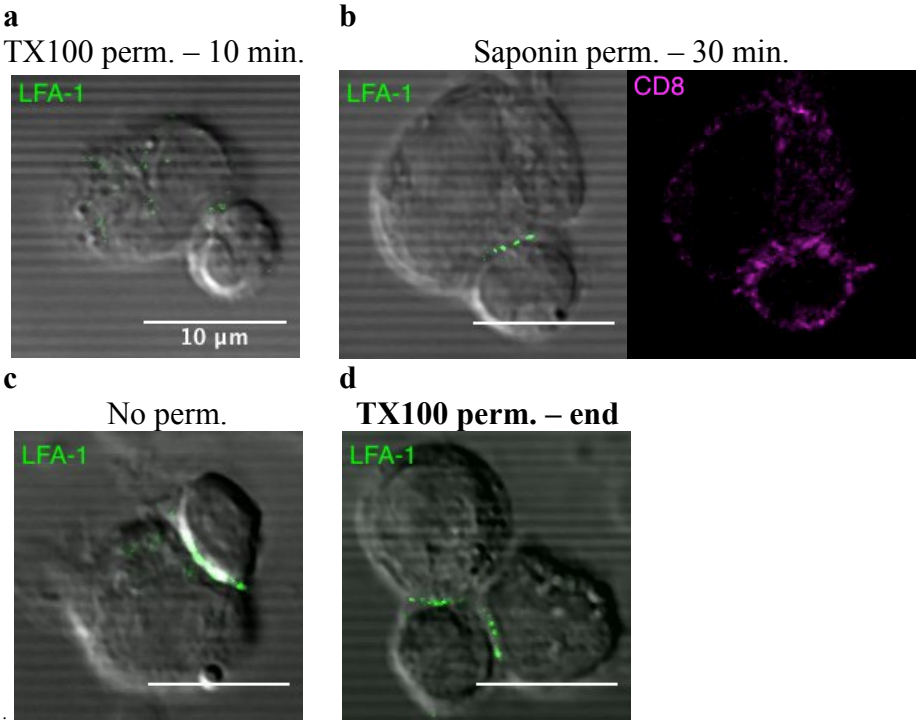

Figure 4.8: Comparison of permeabilisation methods for LFA-1 staining. CD8+ T cells were cultured with SEB-pulsed B cells for 30 minutes then stained for LFA-1 under different permeabilisation conditions. Cells were permeabilised with (a) 0.1% TX100 for 10 minutes (normal perm. protocol), (b) saponin buffer for 30 minutes, (c) no permeabilisation or (d) 0.1% TX100 for 10 minutes after the LFA-1 staining. Green = LFA-1 (on DIC image – smaller cell = CD8+ T cell), magenta = CD8.

As stated earlier, SEB-pulsed B cells are useful as a model APC but are less physiologically relevant to the research question than primary CD4+ T cells. To ensure that LFA-1 expression was detectable when different APCs were used ImmTAV redirected CD8+ T cells (10^{-9} M m121) were co-cultured with SL9-pulsed T2 cells or

HIV-infected primary CD4+ T cells. LFA-1 expression was visible at the synapse for all three target cells (figure 4.9a), however, it was not consistent in every synapse (figure 4.9b).

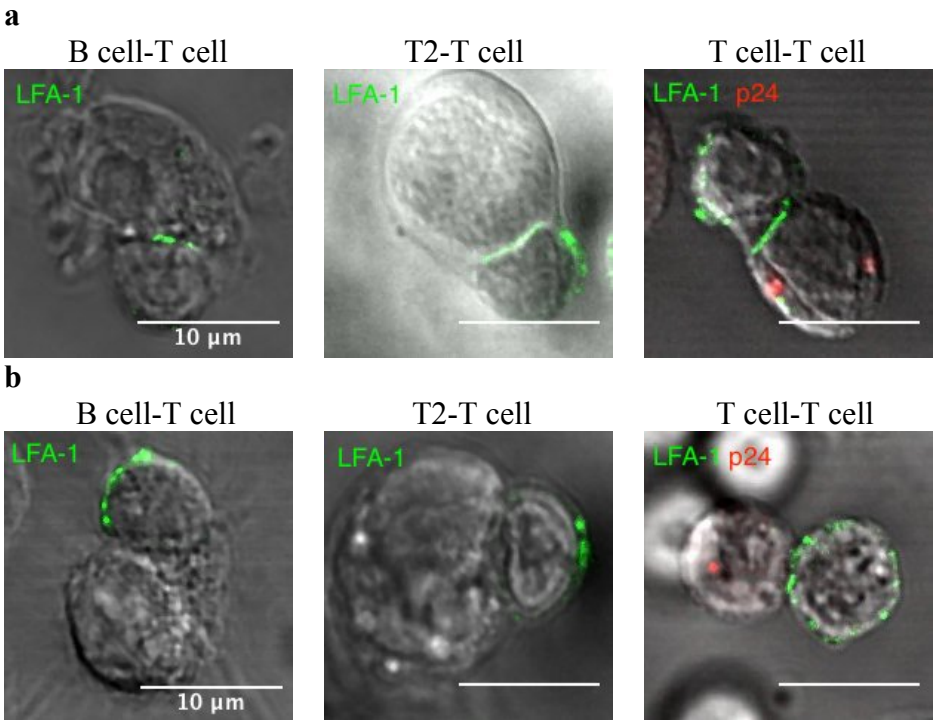

Figure 4.9: LFA-1 polarisation in B cell-T cell, T2-T cell and T cell-T cell immunological synapses. Comparison of LFA-1 polarisation in CD8+ T cell conjugates with SEB-pulsed B cells, SL9-pulsed T2 cells (+ m121 ImmTAV) and HIV-1_{IIIB} infected CD4+ T cells (+ m121 ImmTAV; from left to right). Examples shown of (a) complete polarisation of LFA-1 to the synapse in the CD8+ T cells and (b) incomplete polarisation of LFA-1 to the synapse. Green = LFA-1, red = p24 on DIC images.

LFA-1 expression at the IS has been quantified using various methods including measuring the percentage of cells with LFA-1 polarisation (L2), the percentage of LFA-1 expression in the proximal/medial/distal portions of a cell (L3) or the amount of LFA-1 at the synapse in comparison to the whole cell (percentage localisation – L1, figure 4.10).[385,395–399] This final method was chosen as the first method was not compatible with low conjugate numbers and it was difficult to divide the cell into three areas for the second method. Of note, while a few pairs of cells did show obvious LFA-1 polarisation at the contact this was not always the case, especially with HIV-infected CD4+ T cell

targets; LFA-1 polarisation appears more obvious with more artificial targets as shown by other groups.[79,384,398] Attributing a binary 'polarised' or 'non polarised' status for LFA-1 was difficult as the LFA-1 polarisation could vary depending on the slice of a Z-stack. As so few cells were easily categorised as 'polarised', to avoid losing conjugates to analyse, all cells with the correct cell pairing were assessed for LFA-1 at the contact (% of total). Analysis was completed using a single image taken at the 'equator' or widest part of the cell (figure 4.11, left), a composite image based on the maximum value at a particular pixel over all the slices of a Z-stack (figure 4.11, middle) or a summed Z-stack of all the pixels in all the slices (figure 4.11, right; Sum Stack). All three methods measured the LFA-1 intensity at the synapse but the Sum Stack method was chosen, as no signal was lost during analysis.

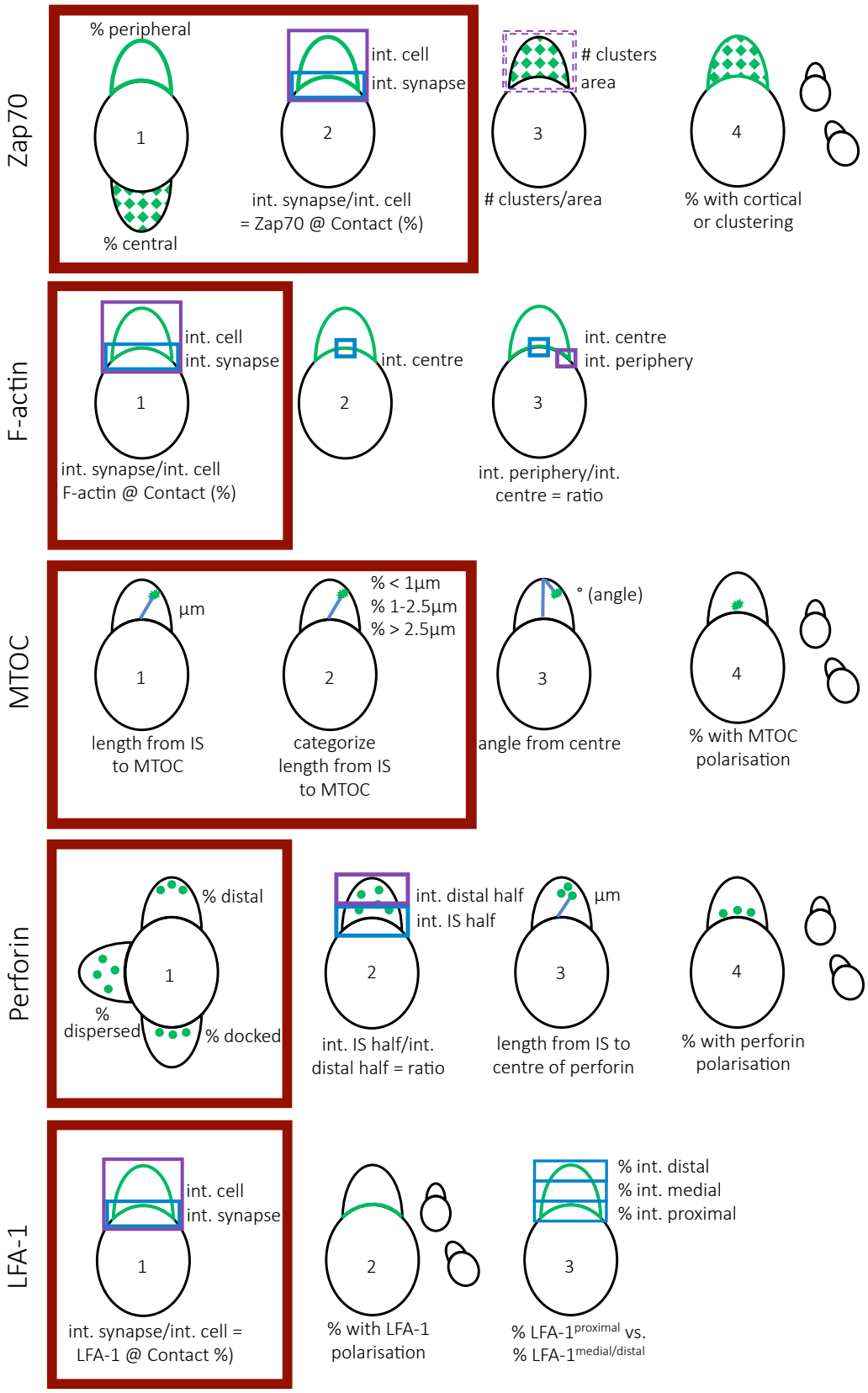

Figure 4.10: Methods for synapse analysis. Graphical representations of the different methods cited in the literature for analysing Zap70 (Z1-4), F-actin (F1-3), MTOC (M1-4), perforin (P1-4) and LFA-1 (L1-3) expression. Chosen methods boxed in red.

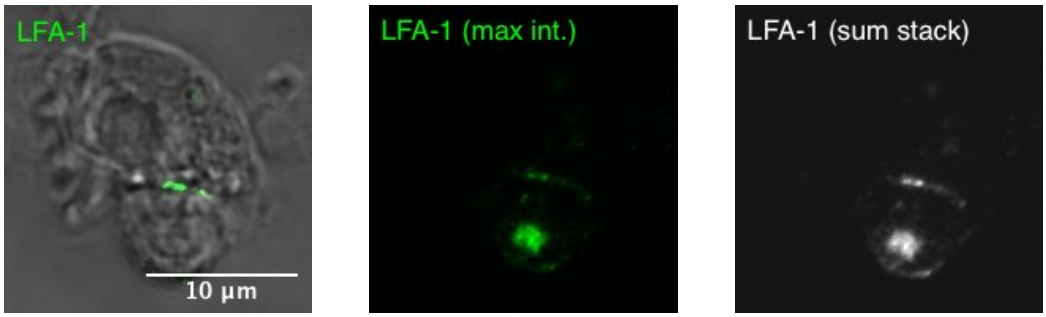

Figure 4.11: Comparison of analysis methods for quantifying LFA-1 localisation. LFA-1 expression can be measured using the 'equator' slice of LFA-1 (left), the 'Max Intensity' of a Z-stack of LFA-1 (middle) or the 'Sum Stack' summation of a Z-stack of LFA-1 (right). Green = LFA-1, white = LFA-1 in Sum Stack.

4.2.5 Optimisation of method to quantify Zap70 in T cell synapses

Upon TCR-pHLA contact and subsequent phosphorylation of the CD3 and TCR-ζ cytoplasmic domains Zap70 is recruited from the cytoplasm to the plasma membrane to facilitate the signalling cascade required for the formation of a mature synapse.[386] To optimise staining for Zap70 various fixation methods were compared. Zap70 expression was not visible when the cells were fixed with 50% methanol (not shown) but staining improved when PFA was used; Zap70 was more visible after fixation with 4% PFA for 10 minutes than it was with 2% PFA for 15 minutes (figure 4.12).

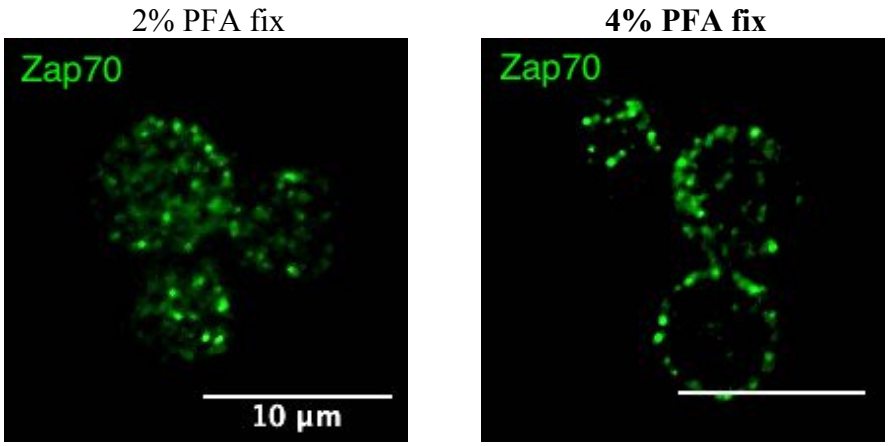

Figure 4.12: Comparison of fixative methods for Zap70 staining. CD8+ T cells were fixed with 2% PFA for 15 minutes (left) or 4% PFA for 10 minutes (right) before staining for Zap70. Green = Zap70.

Other groups have analysed Zap70 expression either by measuring the percentage of cells with Zap70 clustering (Z4), counting the number of Zap70 clusters (Z3), calculating the percentage of Zap70 at the synapse (Z2) or comparing the percentage of cells with either peripheral or central localised Zap70 (Z1 'binning', figure 4.10).[258,400–402] The first two methods required better resolution than was achievable with the available confocal microscope or a different type of microscopic technique to count individual Zap70 clusters. When ImmTAV-redirected CD8+ T cells (10^{-9} M m121) were conjugated to SL9-pulsed T2 cells Zap70 expression was easily categorised into either a peripheral or a central location in the CD8+ T cell (Z1, figure 4.13) and localisation at the synapse could be assessed in the Sum Stack image, as with the LFA-1 (Z2). As both methods provided comparable data they were both used for Zap70 expression studies.

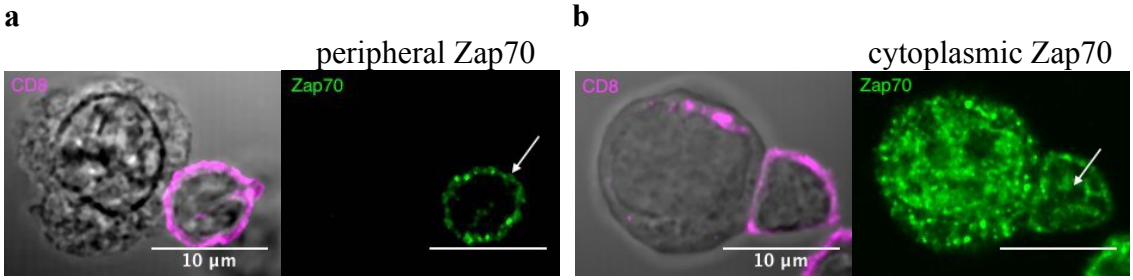

Figure 4.13: Zap70 localisation at the immunological synapse. CD8+ T cells were co-cultured with m121 ImmTAV and SL9-pulsed T2 cells then stained for Zap70. Localisation of Zap70 (a) at the periphery (arrow) vs. (b) in the cytoplasm (arrow) of the CD8+ T cell is shown. Green = Zap70, magenta = CD8 on DIC image.

4.2.6 Optimisation of method to quantify MTOC in T cell synapses

After intracellular signalling occurs the MTOC migrates towards the immunological synapse.[247,256,276] Using an anti-α-tubulin antibody to stain for the MTOC (region of brightness where microtubules converge), different fixation/permeabilisation methods reported in the literature were compared. Both fixation with 4% PFA for 10 minutes (followed by 0.1% TX100 for 10 minutes) or 100% methanol for 10 minutes resulted in a clearly defined MTOC (figure 4.14); however, the 100% methanol affected the visibility of the CD8 stain so this condition was not used.

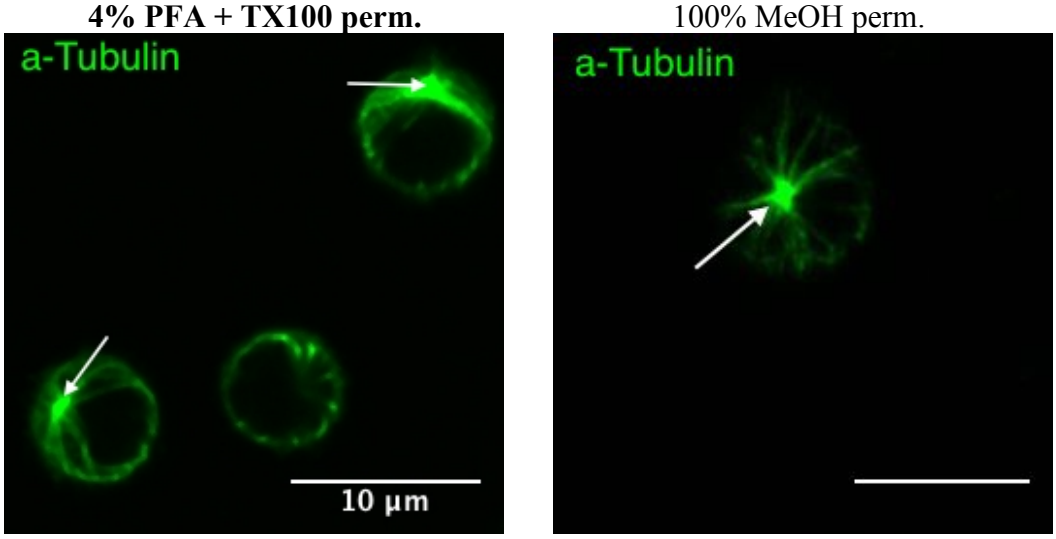

Figure 4.14: Fixation of cells for α-tubulin staining. CD8+ T cells were fixed with 4% PFA for 10 minutes, followed by 0.1% TX100 for 10 minutes (left) or 100% methanol for 10 minutes (right), before staining for α-tubulin. Green = α-tubulin (arrow = MTOC).

Other groups have analysed MTOC location by determining the angle of the MTOC from the centre (M3) or measuring the distance from the MTOC to the centre of the IS (M1, figure 4.10).[384,399,403,404] A comparison of these two methods using ImmTAV-redirected CD8+ T cells (10^{-9} M) in conjugates with SL9-pulsed T2 cells showed that the variation of angles was greater than the variation of lengths (angle vs. length, mean (SD): 5° (6.5) vs. 1.3 µm (0.6)); additionally, it was difficult to measure the angle from the centre due to the varying orientations of the cells (figure 4.16). The chosen method for analysis was the distance from the MTOC to the IS (M1) which could also be binned into categories of distance (< 1 µm, 1-2.5 µm, >2.5 µm) (M2, figure 4.10). A Z-stack of each cell was acquired and 3D rendered to confirm that the MTOC was not further from the IS than a single slice measurement could suggest (figure 4.15).

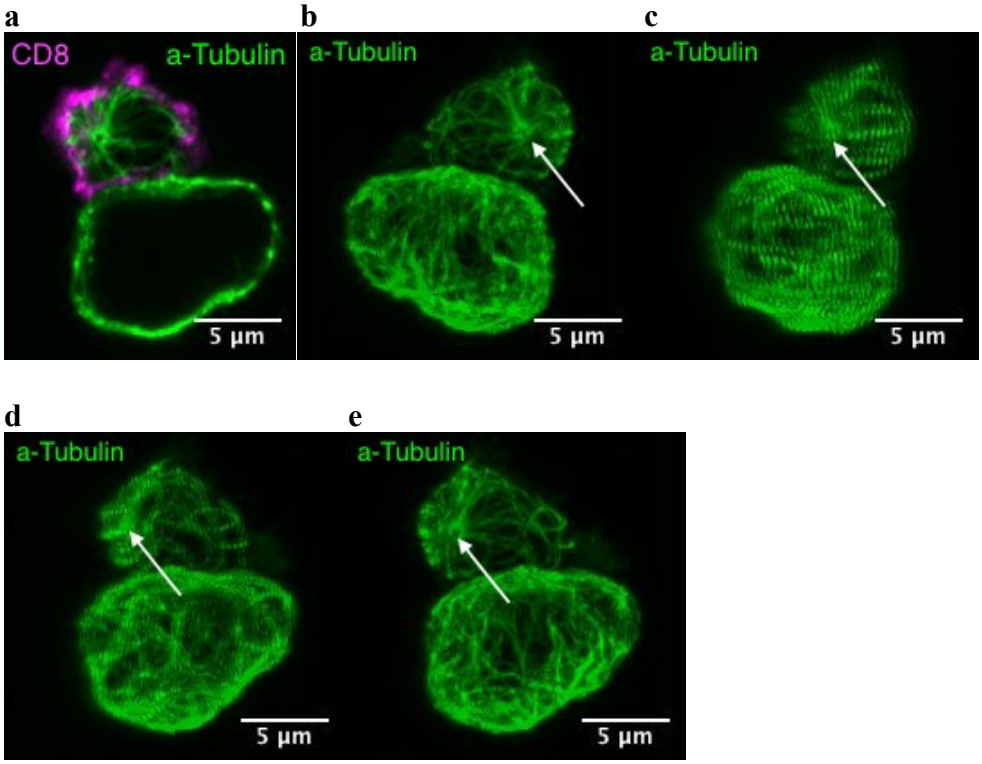

Figure 4.15: 3D rendering of α-tubulin stain. A (a) cross-sectional image of α-tubulin and (b – e) Z-stack slices rendered into a 3D projection (rotated clockwise around the y-axis) were used to assess MTOC position (arrow). Green = α-tubulin, magenta = CD8.

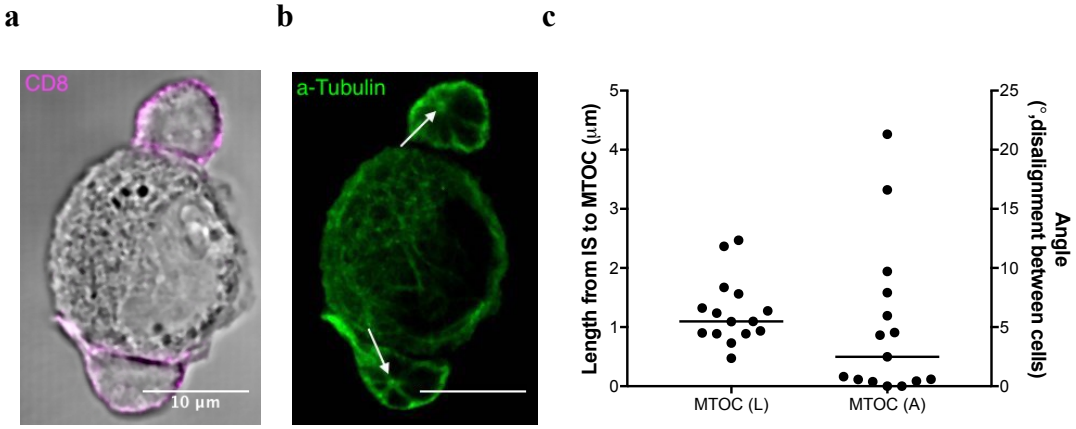

Figure 4.16: Comparison of analysis methods for measuring MTOC polarisation. CD8+ T cells were co-cultured with m121 ImmTAV and SL9-pulsed T2 cells then stained for α-tubulin. The (a) DIC image with CD8 overlay was used to identify conjugates and the (b) α-tubulin image was used to measure the MTOC location. (c) The length from the IS to the MTOC versus the angle of misalignment is compared in T2-T cell synapses (n = 15); each dot represents a conjugate imaged by microscopy. Horizontal lines represent the mean. Green = α-tubulin (MTOC = arrow), magenta = CD8 (on DIC image background).

4.2.7 Optimisation of method to quantify F-actin in T cell synapses

F-actin localises to the IS at the start of IS formation but quickly clears from the centre to allow for granules to be deposited.[373,405,406] Under the basic protocol the signal from the phalloidin stain used to identify F-actin was very strong in CD8+ T cells (10^{-9} M m121) conjugated with SL9-pulsed T2 cells (figure 4.17, top left). F-actin expression at the synapse has been analysed previously by calculating the percentage of F-actin at the synapse (percentage localisation – F1), measuring the intensity of F-actin at the centre of the IS (F2) or determining the ratio of F-actin at the periphery of the synapse compared to the centre (F3, figure 4.10).[384] Due to the density of F-actin within the cell, summation of a Z-stack for analysis purposes made it difficult to identify the position of the synapse relative to the rest of the cell (figure 4.17, bottom left); F-actin localisation was more easily defined in an image taken at the equator of the cell (figure 4.17, top left). For the F2 and F3 methods it was difficult to identify positions to measure the centre vs. the periphery of the synapse as each conjugate formed with different touching surface areas and F-actin density. However, F-actin localisation at the synapse (F1) using the equator image was easy to define and yielded similar results in comparison to using the Z-stack image (figure 4.17).

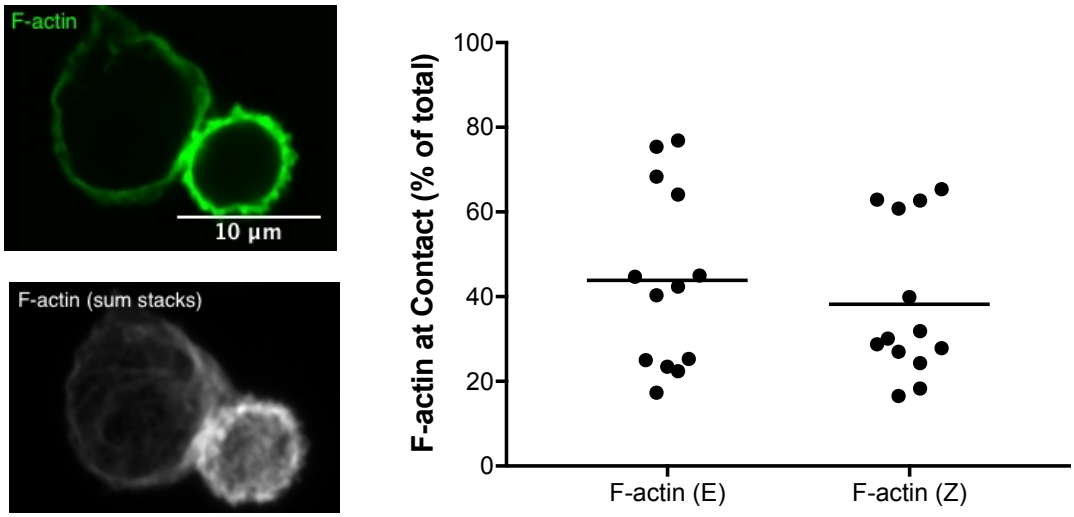

Figure 4.17: Comparison of analysis methods for measuring F-actin polarisation. CD8+ T cells were co-cultured with m121 ImmTAV and SL9-pulsed T2 cells then stained for F-actin. F-actin images were (left) acquired at the equator (top image) and throughout the cell in a Z-stack (bottom, summed to form a Sum Stack). (Right) Comparison of F-actin polarisation at the synapse using the equator (E) or Sum Stack images (Z); each dot represents a conjugate imaged by microscopy. Horizontal lines represent the mean. Green = F-actin, black and white = Sum Stack of F-actin.

4.2.8 Optimisation of method to quantify perforin in T cell synapses

Perforin polarises to the MTOC and is delivered to the synapse to facilitate killing of the target cell.[276,278] Cellular permeabilisation with either saponin buffer or 0.1% TX100 resulted in clear perforin expression but as saponin buffer affects the intensity of the CD8 stain 0.1% TX100 was chosen as the main permeabilisation method (figure 4.18). Perforin expression has been analysed by determining the percentage of cells with perforin polarisation at the synapse (P4), measuring the length from the IS to the middle of the perforin expression (P3), comparing the expression of perforin in two halves of the cell (P2) and categorising perforin expression as docked, dispersed or distal to the IS (P1, figure 4.10).[407–412] As with the other molecules, determining the percentage of cells with fully polarised perforin (P4) was limited when conjugate numbers were low, whereas binning the perforin expression into the three categories (P1) was easier and provided information about the distribution of perforin in the cells where perforin was not polarised

to the IS (figure 4.19). Perforin granules were too spread out to be able to measure the distance between the centre of the distribution and the synapse (P3, figure 4.19a). Likewise, it was difficult to perform a comparison of perforin expression in each half of the cell (P2, distal side vs. synapse side) because of the heterogeneity in cell shapes and positions (figure 4.19c). The binning method, using Sum Stack images, to visualise expression throughout the cell was chosen as the clearest way to analyse perforin expression.

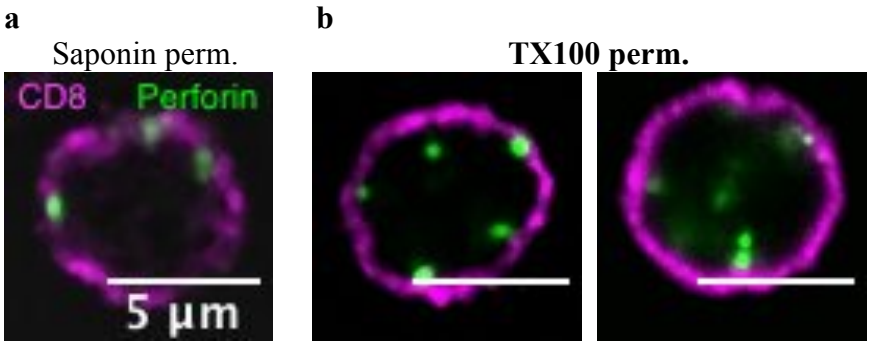

Figure 4.18: Permeabilisation of cells for perforin staining. CD8+ T cells were stained for CD8 and perforin after permeabilisation with (a) saponin or (b) 0.1% TX100. Green = perforin, magenta = CD8.

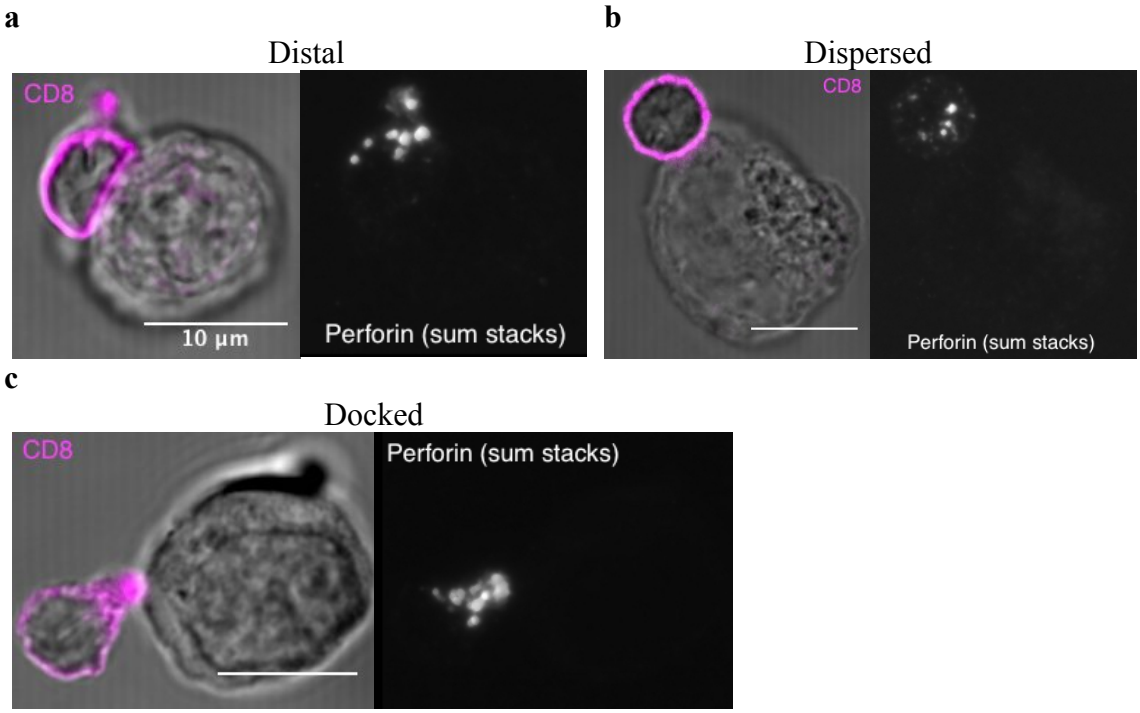

Figure 4.19: Comparison of analysis methods for measuring perforin localisation. CD8+ T cells were co-cultured with m121 ImmTAV and SL9-pulsed T2 cells then stained for perforin. Perforin distribution in CD8+ T cells was described as (a) distal (across from synapse), (b) dispersed (throughout cell) or (c) docked (next to synapse). Black and white = Sum Stack of perforin; magenta = CD8 (on DIC image background).

4.2.9 Utility of other microscopy techniques for investigation of immunological synapses

To determine whether more quantitative and/or structural information on primary CD8+ T cell synapses could be obtained by techniques other than confocal microscopy, wide-field and STED microscopy were assessed for their utility in investigating the IS. A wide-field microscope (Delta Vision Elite) was tested for its ability to illuminate the whole visual field of the chosen microscope objective, in order to improve detection of conjugates. Raw images (figure 4.20a, left) were deconvolved using built-in software to eliminate excess light (figure 4.20a, middle).

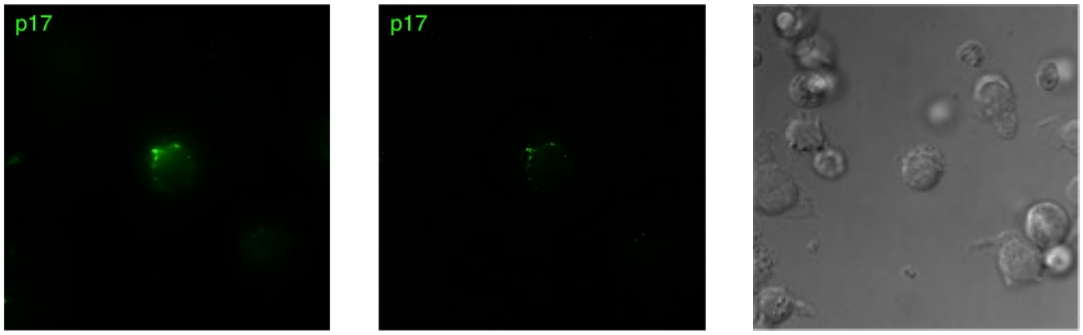

Figure 4.20: Wide-field microscopy for p17 Gag expression. HIV-infected CD4+ T cells were stained for p17 Gag and imaged using wide-field microscopy (raw = left, deconvolved = middle, DIC = right). Green = p17.

To test whether STED microscopy could improve the resolution of proteins involved in the IS, an initial assessment was performed using beads, which were imaged with and without application of the STED laser (in collaboration with Dr Jakub Chojnacki, WIMM). When the STED laser was turned on it was possible to distinguish pairs of beads as two separate objects (figure 4.21a). Additionally, the p24 expression in HIV-infected CD4+ T cells, alone or in conjugates with CD8+ T cells (with m121 ImmTAV redirection) was more defined (figure 4.21b, c).

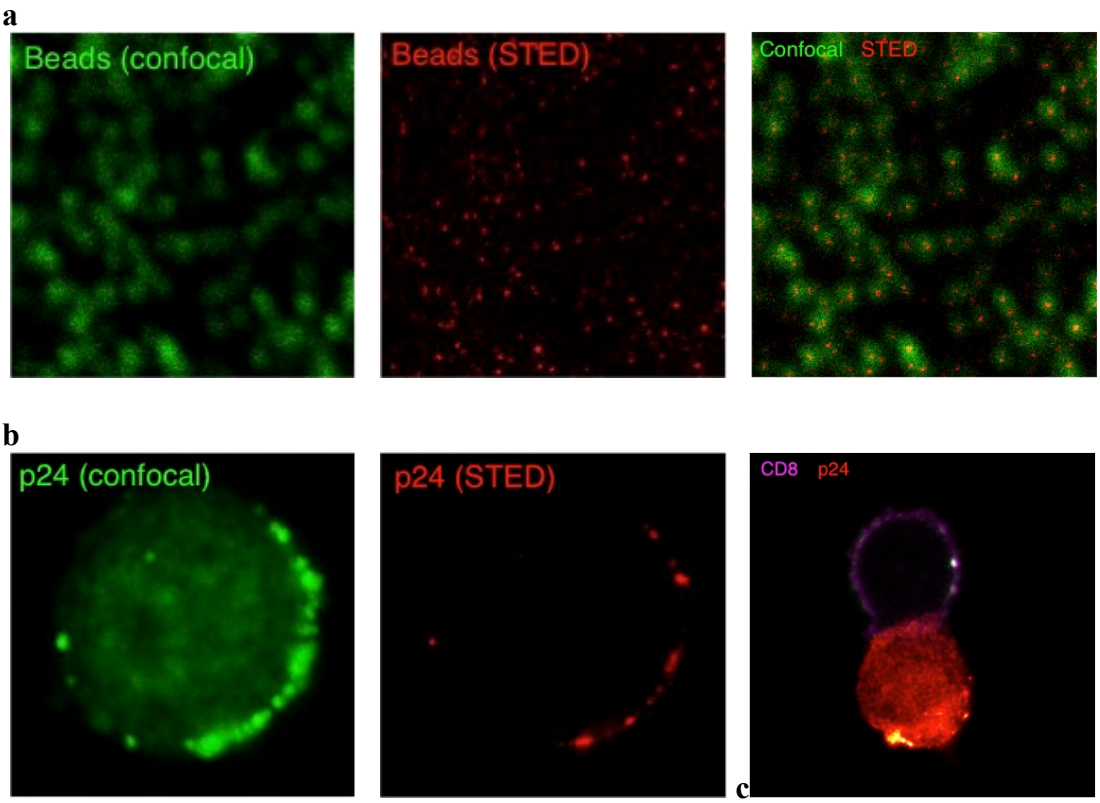

Figure 4.21: STED microscopy of p24. (a) Control 20 nm diameter crimson beads imaged using confocal (left) and STED microscopy (middle) vary in size when overlaid (right). p24 Gag expression in (b) infected single CD4+ T cells using confocal (left) and STED (right) microscopy or (c) in a conjugate using STED (STED on p24, confocal for CD8). Green = confocal (beads or p24), red = STED (beads or p24), magenta = confocal CD8.

Next, ImmTAV-redirected CD8+ T cells (10^{-9} M m121) were co-cultured with SL9-pulsed T2 cells before staining for perforin, Zap70 or F-actin. A confocal image was acquired first before the STED image for comparison. For all three stains the STED microscopy successfully increased the resolution of the acquired image, although at the cost of reduced signal intensity due to the increased photobleaching. Resulting images displayed smaller perforin or Zap70 punctae and thinner F-actin filaments (figure 4.22). Thanks to increased STED images could be used to measure the gap between contacting cells (figure 4.23a) or the diameter of Zap70 punctae (figure 4.24b). On the other hand, exposure to a high power STED laser caused increased bleaching of the fluorophore (figure 4.22d).

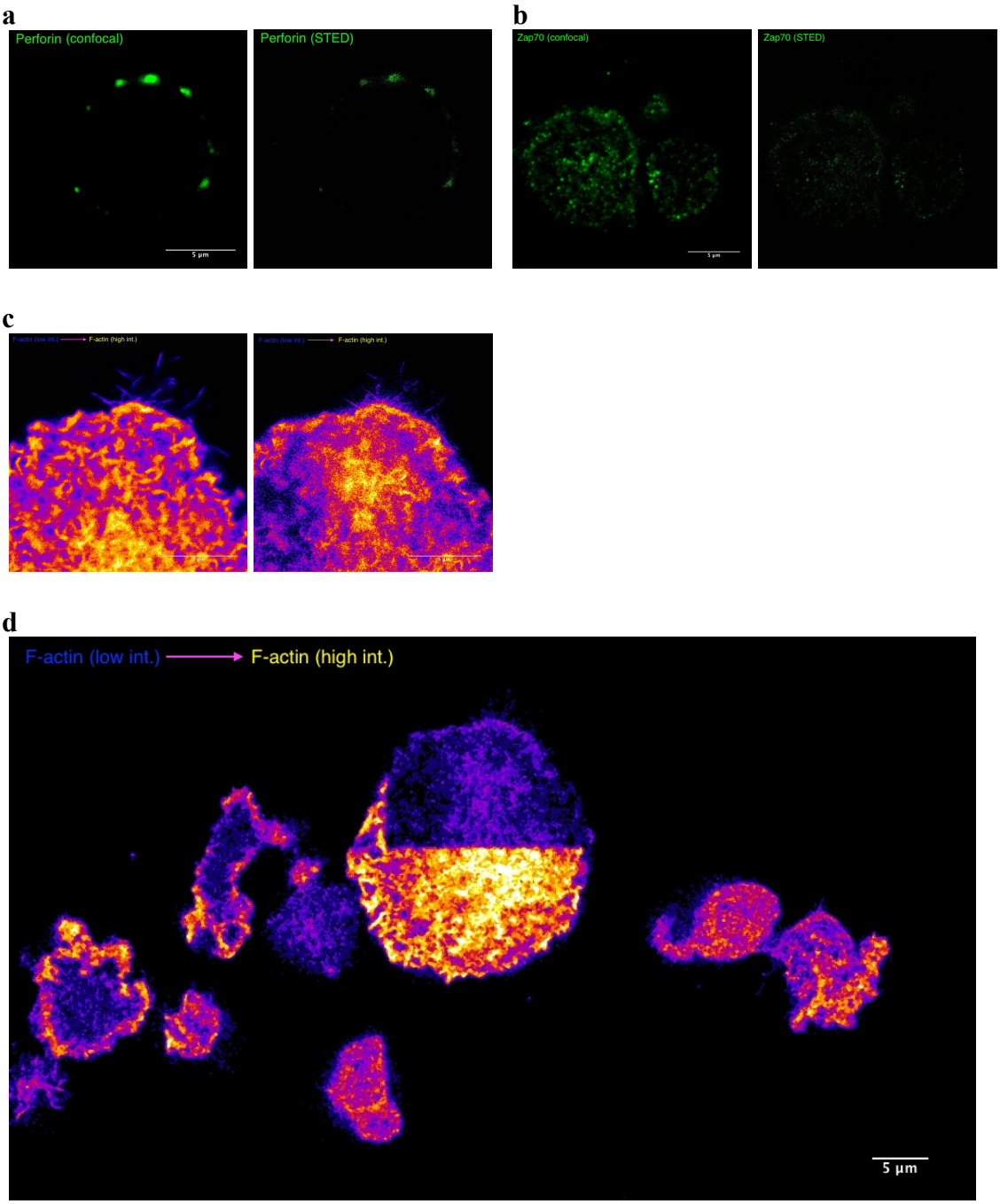

Figure 4.22: Comparison of confocal and STED for synapse analysis. CD8+ T cells were co-cultured with m121 ImmTAV and SL9-pulsed T2 cells then stained for (a) perforin, (b) Zap70 and (c) F-actin. Confocal images shown on the left, STED images on the right. (d) A confocal image (F-actin) of the bleaching that occurs after STED image acquisition of the top right corner of large cell. Fire lookup table to show intensity of F-actin – lowest = blue, brightest = white/yellow. Green = perforin in (a) or Zap70 in (b). Scale bar = 5 µM.

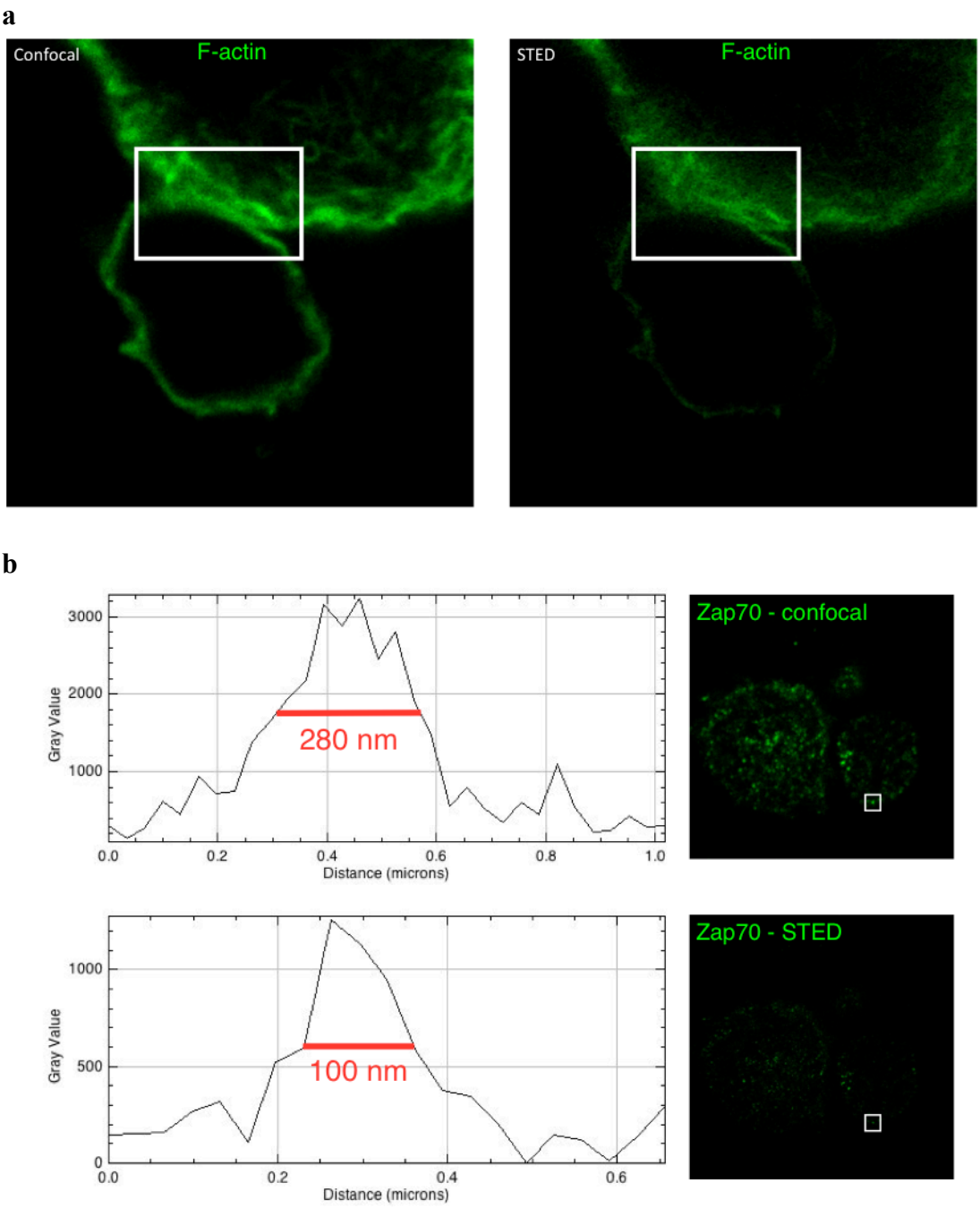

Figure 4.23: Potential applications for STED. (a) Confocal (left) and STED (right) image of F-actin staining of a T2-CD8+ T cell conjugate. (b) Intensity of Zap70 plotted as measured through Zap70 punctum (white box on image) of confocal image (top) and STED image (bottom). Green = F-actin in (a), Zap70 in (b).

4.3 Discussion

The aim of this chapter was to optimise a staining protocol for immunofluorescence imaging of the immunological synapse components. This is the first report of a protocol to study the immunological synapse formed by primary HIV-infected CD4+ T cells and primary CD8+ T cells under HIV-specific ImmTAV redirection. This method will allow for the *ex vivo* study of CD8+ T cell killing of infected T cells, indicative of the events occurring *in vivo.* To achieve this, it was necessary to develop a method suitable for use in a containment level 3 (CL3) laboratory; as there was no CL3-based confocal microscope at the time of the investigation it was necessary to work with fixed samples that could be removed from the CL3 laboratory. These requirements, to work with fixed samples and physiologically relevant cells, imposed limitations on the questions that could be addressed.

As no similar work had been done before, a critical evaluation of several other protocols was necessary to create an informed methodological design as discussed below. When formulating the immunofluorescence panel, deciding which cells and molecular markers were crucial for the synapse analysis led the design process with HIV-infected CD4+ T cell/CD8+ T cells synapses as the primary goal. As both cells involved were T cells markers were needed to distinguish the two and to identify infected cells from uninfected cells (figures 4.2, 4.3 and 4.6). The choice of a Gag antibody was based on the clarity of the signal gained and the relevance to the questions being asked. While activated infected cells were used to test the antibodies, it was also important to image synapses involving GPR cells with low Gag, but not Env, expression. Between the two Gag antibodies available the anti-p24 antibody could detect both mature (CA) and immature (CA domain of Gag – p55) forms of Gag allowing detection of Gag proteins on resting infected cells that were not producing mature virus. This resulted in labelled hazy

clouds of Gag throughout the cell, in addition to punctae at the plasma membrane seen with the anti-p17 antibody (figure 4.2a). SL9-pulsed T2 cells were also used as a more robust and simpler APC, distinguishable by cell size (figure 4.10).

Two proteins involved in early signalling events in IS formation were tested to ascertain whether either were detectable during the co-culture conditions used to observe primary T cell synapses. Lck was chosen for two reasons: it is the first tyrosine kinase to be recruited to the signalling cascade and HIV sequesters it in endosomal compartments to modulate early lymphocyte responses.[31,389,390,413–415] However, despite optimisation efforts it was difficult to achieve consistent Lck expression at the synapse as reported by other groups. Zap70, another early signalling kinase, provided a clearer signal as the antibody detected both isoforms of Zap70 and was polyclonal. Polyclonal antibodies can have higher overall affinity against the antigen allowing them to detect proteins present in low quantities but there is the potential for variability between batches or cross reactivity. However, this increased Zap70 signal came at a cost as it limited the detection of purely active Zap70 involved in signalling at the synapse.[258] Despite these issues Zap70 was chosen as a synapse marker instead of Lck.

The choice of staining method and how it affected antibody binding to the epitope of interest also impacted the quality of the immunofluorescence. For example, the mouse anti-human CD8α antibody bound an extracellular epitope of the α-chain of CD8 (aa #22 – 198, extracellular) and cells could be stained without permeabilisation. However, the rabbit anti-CD8α antibody bound amino acids in the cytoplasmic tail (aa #1 – 13, cytoplasmic) of the α-chain and thus permeabilisation was required. TX100, which acts as a non-ionic detergent, forms holes in the plasma membrane allowing the antibody access to this epitope without affecting cell surface structure. Saponin was less compatible with anti-CD8α antibodies as it allowed intracellular access by selectively removing

cholesterol from the membrane to make holes, affecting the distribution of the cell surface CD8.[416] LFA-1 was affected in the converse manner to the rabbit anti-CD8α as any permeabilisation before the primary antibody eradicated the staining; cells had to be stained for LFA-1, then permeabilised to allow staining for CD8 and/or p24.

Using primary and secondary antibodies, instead of direct conjugations, meant antibodies could be flexibly used in different panels. For all of the mouse and rabbit primary antibodies there were no concerns with the goat anti-mouse or anti-rabbit secondary antibodies as, according to the manufacturers (ThermoFisher), the antibodies were cross-adsorbed against human IgG and serum to increase the specificity of the antibodies. However, the anti-p24 antibody was of human origin and the goat anti-human secondary, while cross-adsorbed against mouse, rabbit and bovine serum, was able to non-specifically bind human epitopes on uninfected cells. While there was a statistically significant difference of the TCCF(p24) between the uninfected and infected cells (figure 4.3b) the presence of uninfected cells with staining patterns that mimicked infected cells (TCCF(p24)^{high}) posed a problem for identifying genuine synapses (figure 4.3a). By conjugating a dye to the antibody this improved the background staining; a far-red dye was chosen to avoid conflicts with the typical staining panel (Alexa Fluor 488 for synapse markers, Alexa Fluor 568 for CD8) and to make it photostable for use with STED microscopy. It was difficult to achieve a high degree of labelling and multiple conjugation steps were undertaken to ensure enough dye was attached to the primary antibody. While the dye was difficult to see with low p24-expressing cells, compared to the secondary Alexa Fluor 488, it was still able to differentiate between uninfected and infected cells (figure 4.3b and chapter three).

The optimised immunofluorescence images provided qualitative information about the IS but with the correct analysis further information was extracted from the

images. Many groups measured the percentage of conjugates that expressed a certain synapse marker pattern.[407,417–419] For example, Khaznadar et al. quantified the percentage of conjugates with polarised lytic granules using a quadrant system to define whether granules were polarised.[407] While this method provided a simple assessment of whether or not granule polarisation was evident, as granule polarisation is not discrete but on a continuum other information from the images was lost. In those cells where the granules were 'not polarised' the granules may have been located completely on the opposite side of the cell, representing no polarisation, or were en route to the synapse, representing partial polarisation. However, in this thesis by defining perforin expression as distal to, dispersed, or docked at the IS the images were better represented.[385,408] Another group assessed synapse maturation by measuring the distance between perforin and the IS.[410] However, this method was not useful for the analysis in this thesis as perforin was rarely concentrated enough in one place that the distance to the IS could be measured, unlike with the MTOC. Measurement of the distance of the MTOC (a clearly defined point of brightness) from the IS proved to be simple and robust, as well as consistent with previous data that showed that the MTOC moves closer to the IS over time.[276,277,408,420]

To measure the expression of a fluorophore multiple parameters were available including the MFI and the IntDen. Whereas the MFI might have been applicable when comparing two areas of an equal size or with uniform intensity the IntDen, which is the product of the area and the mean grey value, was useful for comparing two different sized areas with variable intensities. The IntDen was used for most assessments to compare the total amount of protein in the observed area. For example, the TCCF, used to measure the expression of p24, was a measure of the IntDen of the p24 expression with the background fluorescence subtracted to control for any variations in autofluorescence.

Another important component of image analysis was to identify and minimise the sources of bias. All slides were stained with the same concentrations of antibody and imaged using the same laser settings to allow direct comparisons of images. Parameters were set to define the synapse pairs, i.e. touching $CD8^{neg.}$/CD8+ pair, TCCF(p24) of target > mean TCCF(p24) of the uninfected cells and any alterations to the images, using software like ImageJ, were kept to a minimum to ensure artefacts were not added or removed. Marker expression at the 'equator' versus the entire Z-stack was repeatedly compared to ensure decisions to choose one over the other for ease of analysis did not affect the results greatly (figures 4.4 and 4.17).

This work highlighted the utility of confocal microscopy for investigation of the IS in primary T cells: the pinhole system restricts the amount of light that reaches the sample, limits background fluorescence and is less phototoxic to the cells.[380,421] However, one of the aims was to perform a quantitative analysis rather than just a description of IS formation and this was a particular challenge due to the rarity of conjugates in primary CD4+/CD8+ T cell co-cultures. A widefield microscope was therefore tested as it enabled imaging of a large area without the need for scanning by simultaneously illuminating the sample, thus potentially increasing statistical power and reducing bias that could occur from selection of cell conjugates that were poorly representative of the sample.[371,422,423] The widefield microscope proved useful for finding target cells and detecting fluorescence, however, built-in deconvolution software had to be used to eliminate background light in the raw images and there was less control over the depth of field. This lengthened the acquisition process and overall the microscope was less user-friendly than the confocal microscope, which was eventually adapted to automate the process of finding cell conjugates to some degree; however, restricted access to the microscope and storage capacity limited the extent to which automation methods could be applied.

STED microscopy was used to assess whether the investigation of synapse architecture would benefit from higher resolution than was achievable with the confocal microscope. Potential ideas for the application included assessing whether F-actin clearing from the cSMAC was visible (as the phalloidin stain was oversaturated in confocal images) and if perforin deposition at the cSMAC occurred in this cell system. STED was chosen because the dyes/fluorophores used with the confocal microscope were compatible with the STED laser and provided the option of using a CL3-based STED microscope. As expected, STED did improve the resolution of all the markers tested (figure 4.21 – 4.22) although the information gained from this improvement varied. p24 expression was more defined with clearer punctae, however, as p24 was only used to identify the infected cell in the conjugate the added resolution of the Gag proteins was not required. On the other hand, the improved resolution of the Zap70 punctae helped resolve two clusters of Zap70 that were close together and measure their size (figure 4.23). Due to the strength of the STED laser for dim stains, like LFA-1, molecule expression was almost non-existent (not shown) but for bright stains, like phalloidin, STED revealed structural details including gaps between the cells or thin filaments (figures 4.22 – 4.23). STED had to be carefully used as the laser could bleach the sample making it hard to discern whether bleaching or improved resolution had occurred (figure 4.22d).

While a few of the stains showed promise for use with STED the potential was limited by the methodological approach. Reported successful applications of STED for synapse analysis relied on imaging the synapse from below the cell via the use of planar bilayers or coated coverslips.[424,425] While this limited the physiological relevance of the study it did allow a full view of the interface without relying on Z-stacks. In this thesis the use of physiologically relevant targets and reliance on the ImmTAV to mediate the synapse limited the imaging orientation to the side of the synapse and Z-stacks were

difficult to acquire due to the strength of the STED laser. Other groups have also imaged multiple molecules at the synapse at once, for example F-actin and perforin, to provide reference points for the movement of each molecule.[424,425] Therefore future questions, which may be addressed with STED, such as how the cytoskeleton remodels during an ImmTAV-driven synapse or with CD8+ T cells from CHI patients, would benefit from improvements to the staining panel and orientation of cells to acquire the most information.

The work in this chapter focused on preparing a method to analyse synapse markers in parallel in fixed, primary T cell synapses using confocal microscopy. This method was limited because the cells were fixed and only one synapse marker was present in a sample at a time, however, this sets up future work for optimising multi-colour synapse panels and methods for live cell imaging. For example, co-staining of α-tubulin (MTOC) and perforin would provide information on when perforin localises to the MTOC in relation to the MTOC localising to the IS.[276,403] Live cell imaging offers the potential to investigate the kinetics of synapse formation but identification of cellular proteins would requires the use of reporter systems.[376,380,426,427] However, imaging the kinetics would be beneficial for understanding the efficiency of ImmTAV-mediated killing. For example, Foley et al. used a 3D *in vitro* model of tissue to visualise the interaction between HIV-specific CTLs with infected or peptide pulsed CD4+ T cells and found that target cells with high motility or those presenting low avidity antigens escaped killing by CTLs, suggesting that the migration of target and CD8+ T cells impacts CD8+ T cell function.[428] This investigation underlined the utility for investigating cell-to-cell contact in real time as a fixed cell experiment may not have captured the subtleties of the CTLs' attempts to kill the targets (i.e., a 'direct hit,' 'successful tether,' 'failed tether' or 'brush'). *In vivo* imaging, or 3D *in vitro* models as used by Foley et al., may better

estimate the efficiency of CTL killing as the surrounding environment, including other effectors and immune cells, may contribute to the killing process.[252,429] As primary CD8+ T cell synapse formation appeared sparse on fixed slides ensuring the IS formation is captured by real time microscopy would lengthen image acquisition times or require multiple attempts.

In conclusion, there were multiple factors that impacted the outcome of immunofluorescence staining and the quantity of information that could be gained from those images. Protein marker and antibody choice was a crucial first step for ensuring the proposed synapse questions were being investigated properly. Optimising the protocol for staining was more difficult when fixation and multi-colour panels were required, but a successfully designed panel facilitated fast and accurate imaging of the correct targets; the staining optimisation process was also applicable to imaging of other viruses including recombinant ZIKV proteins (appendix 4.1). Multiple methods for analysis then had to be tested with the proposed set up of cells to ensure the method could be repeated with minimal bias. The synapse marker panels optimised in this chapter, comprising LFA-1, Zap70, MTOC, F-actin and perforin (with p24 and CD8) were used for the comparison of primary CD8+ T cell immunological synapses in the context of HIV infection as reported in the next chapter.

4.4 Questions addressed in this chapter

- *What is the best method to detect HIV-infected cells by immunofluorescence?*

  Primary non-conjugated antibodies (with a secondary antibody) against HIV Gag p17 and p24 proteins gave a stronger signal than those against an Env gp120 protein (figure 4.2); the biggest range of expression was achieved with a human anti-p24 primary antibody. However, the directly conjugated anti-p24 antibody had less non-specific staining than the primary/secondary combination (figure 4.3; section 4.2.1).

- *What is the best staining protocol to detect immunological synapses between primary CD8+ T cells and physiologically relevant HIV-infected targets?*

  An antibody was required to mark the CD8+ T cell, the HIV-infected targets and molecules of the synapse (LFA-1/Zap70/MTOC/Perforin/F-actin). It was necessary to optimise fixation/permeabilisation methods for each of the primary antibodies used (figures 4.5 – 4.19). The best method involved fixation with 2 – 4% PFA, permeabilisation with 0.1% TX100, blockade with 2.5% goat serum and the best titration of primary antibodies and secondary antibodies (sections 4.2.2 – 4.2.8).

- *How can immunofluorescence images be used to quantify events involved in immunological synapse formation?*

  A limitation of previous work that relied on representative images was that much of the data was descriptive and raised questions about how reproducible the reported observations were. The work in this chapter developed methods that enabled capture of a larger number of events in order to be confident about the reproducibility of the observed signals and to determine if observed changes were biologically meaningful (sections 4.2.3 – 4.2.8).

- *What does super resolution microscopy add to the information gained from an immunofluorescence study of the immunological synapse?*

  STED microscopy improves the resolution of p24 and synapse marker stains compared to confocal microscopy with the potential for measuring molecule sizes and distances between molecules more accurately (figures 4.21 – 4.23). However, there was a risk of photo bleaching (figure 4.22) and the improved resolution did not provide more information about the immunological synapse in the context of the markers and analysis methods chosen (section 4.2.9).

CHAPTER FIVE: COMPARISON OF PRIMARY CD8+ T CELL IMMUNOLOGICAL SYNAPSES IN THE CONTEXT OF HIV INFECTION

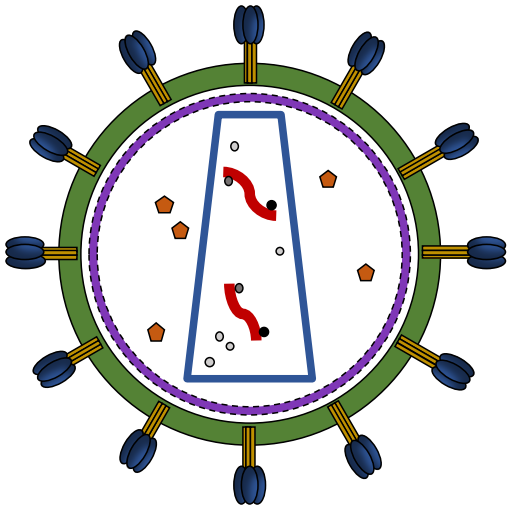

5.1 Introduction

In chapter three, the antiviral function of CD8+ T cells from HIV-positive and HIV-negative subjects was compared in a model of HIV latency. ImmTAV-redirected healthy donor (HD) and chronic HIV infected (CHI) donor CD8+ T cells could both recognise and eliminate a proportion of resting infected CD4+ T cells. However, CHI donor CD8+ T cells failed to achieve the same antiviral effects as the HD cells; ImmTAV assistance improved killing to a level just above the natural (HIV-primed) CTL responses. Due to the bispecific design, the ImmTAV is able to bring a target and effector cell in close proximity to instigate killing via the release of perforin and granzymes at the immunological synapse (IS). The mechanism underlying the impaired antiviral activity of ImmTAV-redirected CHI donor CD8+ T cells may lie in a compromised ability to form a functioning IS.

As described previously in section 1.3.1 the IS is the interface between an APC and a lymphocyte that facilitates the temporal and spatial organisation of molecules and signalling between the two cells. For most structural investigations, the IS was studied under conditions that facilitated efficient formation of the IS including super antigen-pulsed APCs and supported lipid bilayers. However, in the context of an HIV infection the formation of the IS may not be optimal. One of the viral accessory proteins, Nef, manipulates the host cell's formation of an IS to alter T cell activation. This may be an adaptation to promote viral survival by triggering enough activation for viral replication without premature cell death. In previous studies, HIV-infected CD4+ T cells formed abnormal conjugates with super antigen-pulsed B cells: T cell receptors and Lck were sequestered in endosomal compartments due to a Nef-mediated mechansim.[31] Nef not only hijacked Lck but also triggered Lck-independent signalling, promoting production of IL-2 which led to enhancement of viral spread.[30,430] In another study, in which primary

human lymphocytes were infected with HIV isolates encoding Nef proteins from various primate lentiviruses, Nef was reported to hamper cell spreading and actin ring formation by interfering with N-Wasp translocation to the periphery and subsequent activation. This mechanism allowed for the initial TCR microcluster signalling, but affected the cytoskeletal movement crucial for other molecular rearrangements within the cell. It was suggested that this modulation of IS maturation could help Nef create a modest TCR signal aimed at HIV-1 production.[278,400]

Although the signalling effects of Nef on infected CD4+ T cell synapses with APCs have been convincingly demonstrated, the effects of Nef and other HIV proteins on CD4+/CD8+ T cell synapses have not been studied. This is surprising, given that understanding how HIV may impact target cell synapses with CD8+ T cells is important because CTLs are at best only partially successful in controlling viral replication. There is currently a gap in the literature concerning the architecture of the IS between HIV-infected target cells and primary CD8+ T cells. While previously reported killing assays provide evidence for the interaction between these two cell types there are limited microscopy-based descriptions of the synapse.[89,196,245,431,432] By contrast, the interactions involved in the cell-to-cell transfer of HIV via virological synapses have been well studied: this leads to viral propagation instead of viral control.[79–81,395,433–435] Importantly, many studies of CD8+ T cell synapses have employed super antigen-pulsed APCs as the target cell; such systems may not fully recapitulate the relevant cellular interactions *in vivo*.[278,436–438]

The work described in this chapter aimed to use confocal microscopy to investigate synapses between primary CD8+ T cells and target cells under experimental conditions that were as physiologically relevant as possible. The objectives were as follows: (i) to describe synapses in which either the effectors or the targets were from

HIV-positive patients; (ii) to determine whether a specific block in synapse formation could by identified that could explain defective antiviral function; (iii) to use the HIV ImmTAV as a tool to observe synapse formation in a model system and under physiological conditions, given that it could mediate clearance of activated and resting infected cells (chapter three and previously published work in our laboratory).[245] To achieve these objectives it was necessary to choose only a few synapse proteins (see chapter four) that could collectively demonstrate the evolution and maturation of the IS.[277,278,281] While other cell types form IS these cells were beyond the scope of this investigation as the ImmTAVs are designed to redirect CD8+ T cells to target HIV-infected cells.[79,245,251,439,440]

5.2 Results

5.2.1 Kinetics of Gag expression in HIV-infected primary CD4+ T cells

To obtain a population of HIV-infected CD4+ T cell targets for IS formation, a panel of PHA-stimulated HD CD4+ T cells (n = 5, including n = 3 HLA-A2+ donors compatible with the m121 ImmTAV) were spinoculated with HIV-1_{IIIB} (MOI = 0.01). Gag p24 expression was assessed by flow cytometry on days one, two, three, four and seven post-infection (figure 5.1). Peak p24 expression (17 – 27% p24+ cells of CD3+$CD8^{neg.}$ population) occurred at days 4 – 7 in all five donors. Day six post infection was chosen as the optimal time point, as consistently high infection rates and minimal cell death were observed, similar to previously described results.[295]

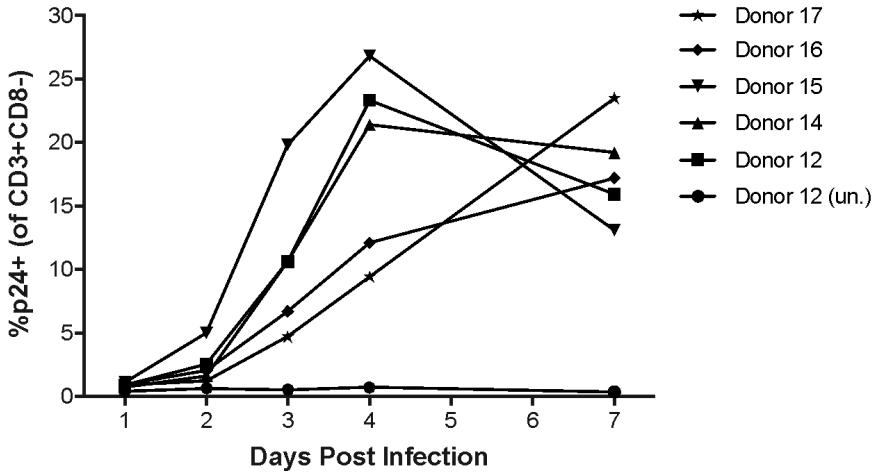

Figure 5.1: Kinetics of HIV infection in primary CD4+ T cells. Primary CD4+ T cells from five donors were stimulated with PHA for three days before spinoculating with HIV-I_{IIIB} (MOI = 0.01). The %p24+ cells (of the CD3+$CD8^{neg.}$ population) were determined by flow cytometry on days 1-7 post-spinoculation. Donor 12 was also left uninfected as a control.

5.2.2 LFA-1 localisation at the immunological synapse varies between ImmTAV-redirected CD8+ T cells from different donor groups

One of the early stages of IS formation involves the recruitment of the adhesion molecule, LFA-1, to provide stability between the interacting cells via ICAM-1 ligation and to promote T cell signalling.[246,282,441] To assess whether the HIV status affects LFA-1 localisation in CD8+ T cells during synapse formation with HIV-infected healthy donor

CD4+ T cells, the latter were co-cultured with CD8+ T cells from healthy donors (n = 3), CHI donors (n = 3) or SPARTAC trial participants who began ART during PHI (early ART, n = 3) plus m121 ImmTAV (10^{-9} M) for 30 minutes before staining for CD8, p24 and LFA-1.[293] Synapses were defined as contacts forming between HIV-infected CD4+ T cells (confirmed by measuring TCCF(p24)) and CD8+ T cells (marked by the anti-CD8 antibody) from each donor group – only these cell pairings were imaged using confocal microscopy (figure 5.2a). Based on these criteria, LFA-1 polarisation was not statistically different amongst the three donor groups (HD vs. CHI vs. Early ART, mean (SD): 17.9% (6.6) vs. 19.7% (8.1) vs. 19.4% (7.4)) (figure 5.2b).

The LFA-1 at the contact in the CD8+ T cell (percentage of total) was measured as described in chapter four. Of note, while other groups have defined whether LFA-1 was fully polarised to provide a '% of conjugates with polarised LFA-1' measurement (i.e., LFA-1 at the contact is >50% of the total LFA-1 in the cell – by visual assessment or measurement of fluorescence) based on the acquired images this was not possible for this set of data. Due to the use of primary CD4+ T cells infected with HIV-1 as targets, except for a few examples including the one in figure 5.2 most pairs of cells did not have an obvious polarisation of LFA-1 at the contact. Instead of ruling out all of these pairs as 'non synapses' leaving very few pairs left to analyse, LFA-1 polarisation at the contact as a percentage of the total LFA-1 polarisation (taken from a Z-stack summed into one image) was used to quantify LFA-1 polarisation in all the pairs that met the target and effector criteria on a continuous rather than bimodal scale.

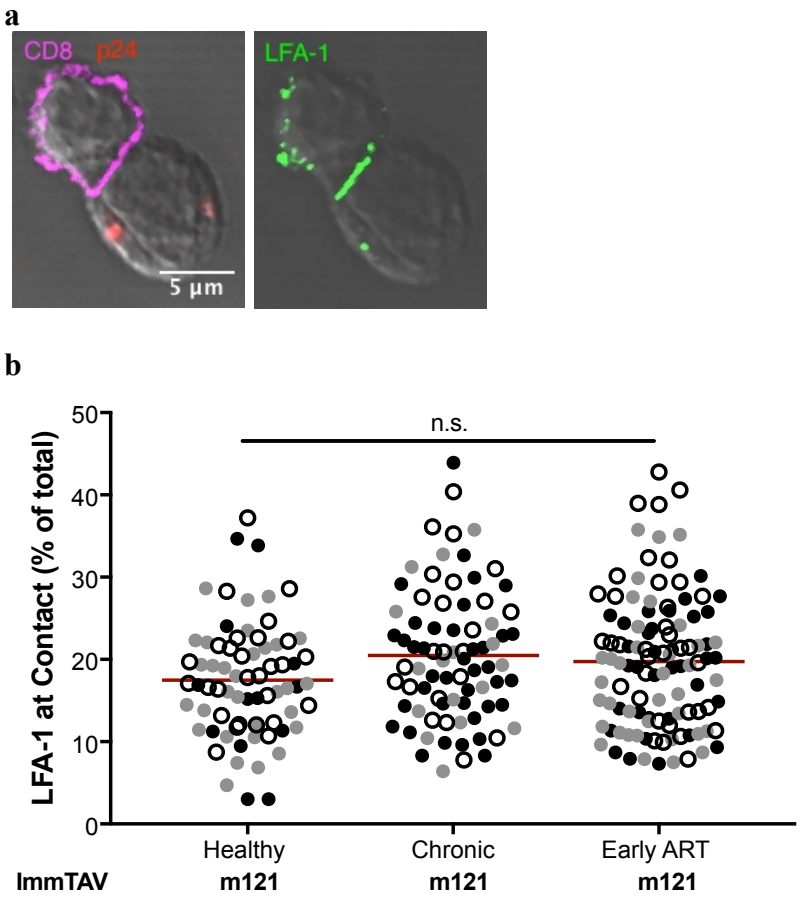

Figure 5.2: LFA-1 localisation at the immunological synapse of CD8+ T cells. m121 ImmTAV-redirected primary CD8+ T cells from three donor groups (healthy, CHI, early ART; n = 3 donors per group and n > 10 conjugates/donor – black circle, grey circle, white circle) formed conjugates with HIV-infected healthy donor CD4+ T cells. (a) Confocal image of a T cell-T cell conjugate with the most LFA-1 at the contact. Red = p24, magenta = CD8, green = LFA-1. (b) Quantification of the LFA-1 at the contact (% of total); each dot represents a conjugate imaged by microscopy. Horizontal lines represent the mean. Groups were analysed by one-way ANOVA.

5.2.3 Early ART during PHI does not fully rescue impaired antiviral activity

In the previous comparison of LFA-1 polarisation at the synapse (section 5.2.2) the CD8+ T cells from the early ART donors showed slightly more localisation of LFA-1 at the IS than the healthy donor CD8+ T cells but less than the CHI donor CD8+ T cells. As CHI patients were shown previously to have impaired CD8+ T cell-mediated antiviral activity, it was hypothesised that initiation of ART during PHI might preserve CD8+ T cell function and/or CD4+ T cell help. SPARTAC participants' PBMCs were sampled while they were still receiving ART and were used in a viral inhibition assay to assess

their antiviral activity.[442,443] Purified CD4+ T cells from the patients (n = 9) were stimulated with PHA for three days to reactivate latent HIV and then cultured with autologous CD8+ T cells (E:T of 1 or 0.1) with and without ImmTAV (irrelevant TCR ImmTAV at 10^{-9} M; m121 at 10^{-8} M and 10^{-9} M for E:T of 1; m121 at 10^{-11} M for E:T of 0.1) for six days before assessing the percentage elimination.

Without ImmTAV-redirection SPARTAC CTLs eliminated a mean (SD) 39.5% (27.4) of infected cells (figure 5.3). Only addition of m121 ImmTAV significantly increased elimination (none vs. 10^{-9} M m121 % elimination, mean (SD): 39.5% (27.4) vs. 59.9% (14.34), P = 0.04). When compared with historical data on ImmTAV effects on CD8+ T cells from CHI and healthy donor subjects CD8+ T cells from the SPARTAC participants were similar to CHI donors and were inferior to healthy donors at the higher ImmTAV concentrations (10^{-8} M) (early ART vs. CHI vs. HD, mean (SD): 60% (14) vs. 60% (21) vs. 87% (7), P = 0.002 one-way ANOVA).[245]

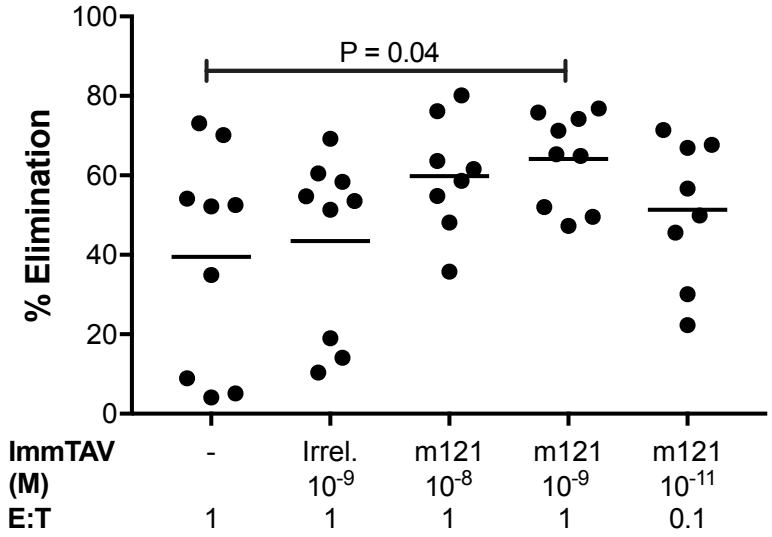

Figure 5.3: Viral inhibitory activity of CD8+ T cells from donors treated with ART during PHI. PHA-stimulated CD4+ T cells from SPARTAC patients (n = 9) were co-cultured with autologous CD8+ T cells at different E:T ratios and ImmTAV redirection (irrelevant TCR or m121). After six days, intracellular p24 was measured to calculate the % elimination. Lines represent the mean. Groups were analysed by one-way ANOVA (n.s.) with Dunnett's multiple comparisons test.

5.2.4 Antigen presentation on target cells affects LFA-1 localisation at the immunological synapse

Less LFA-1 polarised at the contact of the cell pairings than others have reported in different cell systems.[249,384] A limitation of using primary HIV-infected CD4+ T cells as the targets in this analysis was the scarcity of synapses formed with primary CD8+ T cells, irrespective of the donors' HIV status.[249] To assess whether the low LFA-1 polarisation in CD8+ T cells was related to cognate epitope density on primary CD4+ T cell targets alternative target cells were investigated. T2 cells are TAP-deficient and are only able to present HLA-A2 on the cell surface when the heavy chain and β2 microglobulin complex is stabilised by exogenously loaded peptide. Peptide-pulsed T2 cells have been used extensively as a model target cell to assess the potency of HLA-A2-restricted ImmTACs and ImmTAVs.[225,226,245] Prior to use in this work, HLA-A2 expression on T2 cells was compared after pulsing with the HIV Gag SL9 epitope (HLA-A2 restricted), a non HLA-A2 restricted influenza peptide or no peptide. While there was some background HLA-A2 expression, only the SL9 peptide increased HLA-A2 expression immediately after pulsing (figure 5.4).

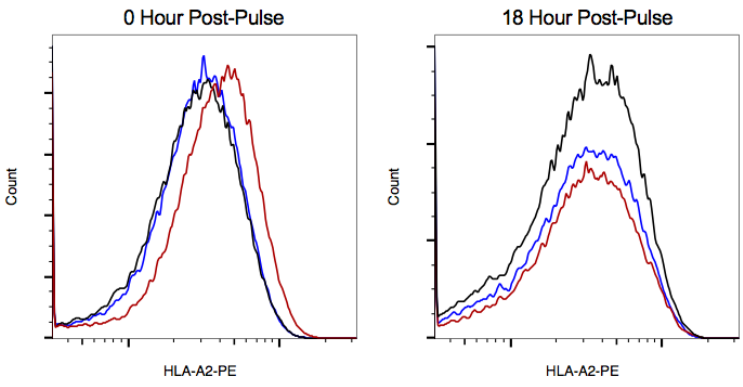

Figure 5.4: Peptide pulsing of T2 cell line. T2 cells were left unpulsed (black line) or were pulsed with flu peptide (12.5 μM; blue line) or SL9 peptide (12.5 μM; red line) for 5½ hours before staining for HLA-A2 immediately or after 18 hours. Histograms of the MFI of HLA-A2-PE is shown.

HD CD8+ T cells were then co-cultured with various target cells plus m121 ImmTAV (10^{-9} M) as follows: (i) SL9-pulsed T2 cells; (ii) resting infected HD CD4+ T

cells (latency model, chapter three); (iii) early ART-treated CD4+ T cells (SPARTAC patients) reactivated with PHA ('reactivated autologous HIV'); (iv) SEB-pulsed WJR076 B cell line cells; the latter were included as a positive control as super antigen-pulsed B cells, or other APCs, induce potent T cell activating activity (figure 5.5).[384,437,444,445] LFA-1 localisation was significantly higher in CD8+ T cells forming conjugates with the T2 cells compared to the activated infected, resting infected or reactivated autologous HIV+ CD4+ T cells (T2 vs. activated vs. resting vs. reactivated, mean (SD): 30.5% (17.0) vs. 17.9% (6.6) vs. (13.1% (4.2) vs. 15.0% (7.8), $P < 0.0001$). Although LFA-1 polarisation was higher in conjugates with activated infected CD4+ T cells compared to resting infected CD4+ T cells the difference was not significant due to the low number of resting infected conjugates (figure 5.5a). T2 cells left unpulsed or SL9-pulsed but cultured with CD8+ T cells in the absence of m121 ImmTAV did not form any conjugates (not shown).

Of the HIV-infected target cells, Gag expression (TCCF(p24) by confocal microscopy) was highest in the activated infected CD4+ T cells (activated vs. resting vs. reactivated, mean (SD): 1874 (2428) vs. 557.6 (337.8) vs. 446.2 (260.6), $P < 0.0001$; figure 5.5.b). In summary, LFA-1 localisation to the IS was highest when the target cell HIV antigen expression was predicted to be maximal, either through saturation of HLA class I molecules by exogenous peptide loading or productive infection, which required activation of CD4+ T cells.

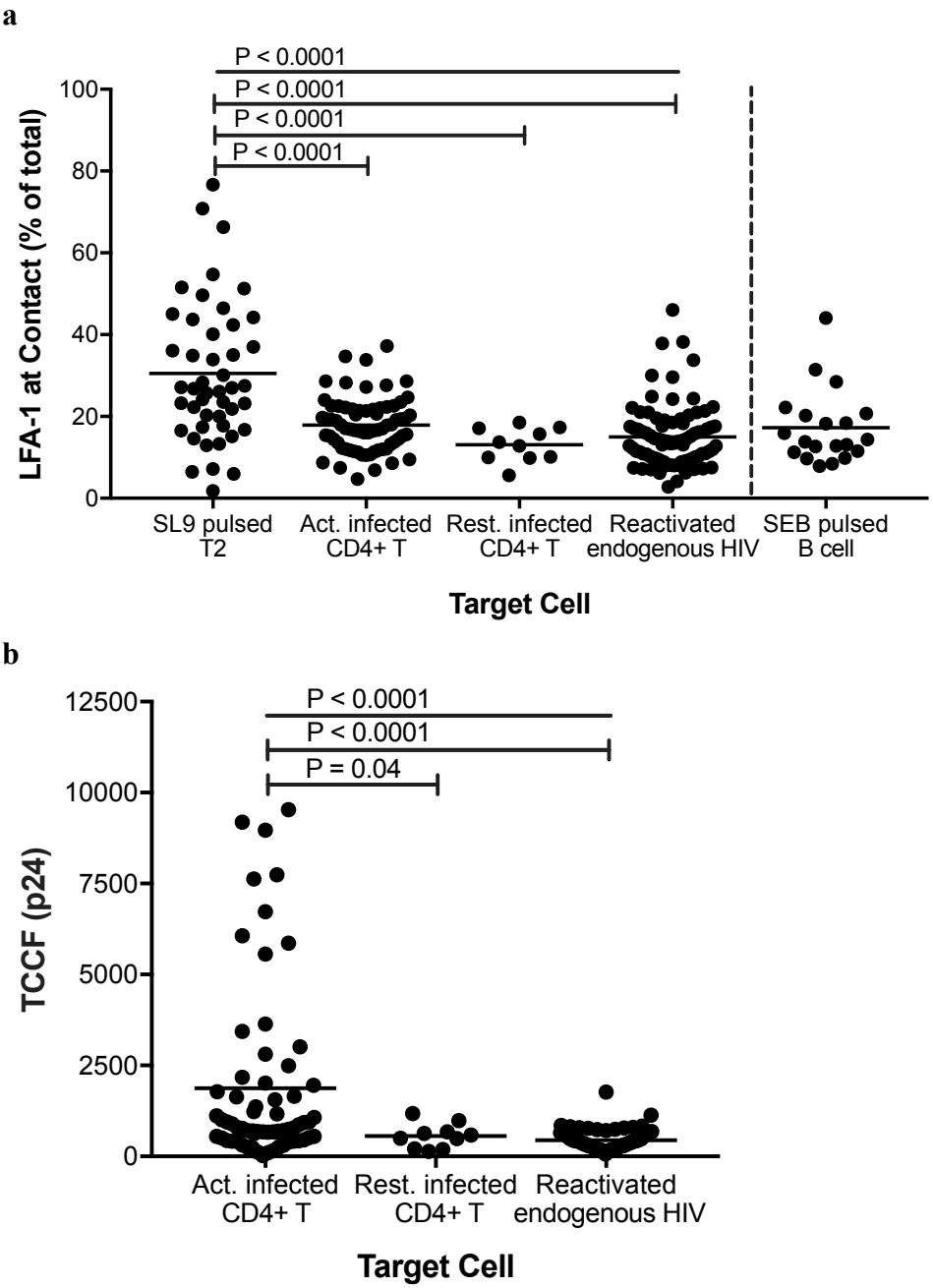

Figure 5.5: LFA-1 polarisation according to target cell type. Immunofluorescence images were used to make a comparison of (a) LFA-1 at the contact (% of total) in CD8+ T cells cultured with different target cells (n = 1, 3, 1, 3, 1 CD8+ T cell donors/group respectively with n > 9 conjugates/donor) and (b) p24 expression (TCCF(p24)) of the primary CD4+ T cell targets from (a); each dot represents a target cell. Horizontal lines represent the mean. Groups were analysed by one-way ANOVA with Tukey's multiple comparisons test.

5.2.5 SL9-pulsed T2 cells elicit reproducible immunological synapses with primary CD8+ T cells

As co-culture with SL9-pulsed T2 cells elicited greater localisation of CD8+ T cell LFA-1 at the synapse compared to infected primary CD4+ T cells, T2 cells were used for further investigation of the immunological synapse. Based on previous kinetic studies, 30 minutes may have been too late to assess peak LFA-1 recruitment to the synapse.[277,278,446] To find the optimal co-culture time, SL9-pulsed T2 cells were co-cultured with HD CD8+ T cells in the presence of m121 ImmTAV (10^{-9} M) for 5, 15 or 30 minutes. To quantify the synapses formed ten low magnification fields of view were acquired on the slide and the number of T2 cells in conjugates with CD8+ T cells was compared to the total number of T2 cells imaged (sections 2.4.5 and 2.4.18). Over time the number of synapses formed with m121 ImmTAV-redirected HD CD8+ T cells increased (5 vs. 15 vs. 30 min., mean: 11.9% vs. 27.2% vs. 42.7%), while very few synapses (3.9%) formed with the m232 control (irrelevant TCR ImmTAV) and the number did not change over the time course (figure 5.6a).

Slides were also stained for Zap70, F-actin, α-tubulin (MTOC) and perforin (figure 5.6b). Cell pairs were chosen based on the presence of a T2 cell (large morphology) and CD8-stained T cell (magenta); cells not meeting these criteria were neither imaged nor assessed for synapse marker polarisation. Zap70 polarisation at the synapse increased over time and appeared to plateau between 15 and 30 minutes (5 vs. 15 vs. 30 min., mean (SD): 15.2% (5) vs. 27.8% (11.8) vs. 28.8% (8.6), P = 0.0001). An alternative method of analysing Zap70 that involved measuring the proportion of Zap70 localised to the periphery (active), showed that the percentage of peripheral Zap70 peaked at 15 minutes (figure 5.7). F-actin polarisation significantly decreased over time (5 vs. 15 vs. 30 min., mean (SD): 57% (13.5) vs. 44.7% (14.2) vs. 36.6% (10.3), P = 0.0008). The

MTOC moved closer to the synapse over time (5 vs. 15 vs. 30 min., mean μm (SD): 4.2 (0.9) vs. 2.8 (1) vs. 2.2 (1.3), $P < 0.0001$) while perforin docking at the synapse peaked at 15 minutes (5 vs. 15 vs. 30 min., % docked: 15% vs. 47% vs. 23%). The 15-minute co-culture time was therefore chosen for all subsequent experiments as it best captured the maximal changes in the polarisation of several relevant synapse proteins, suggesting synchronization of synapse formation within the cell populations being studied. Due to limited CD8+ T cell numbers and difficulties accurately analysing F-actin polarisation at the synapse the phalloidin stain was not included in further experiments (appendix 5.1).

See next page for figure 5.6.

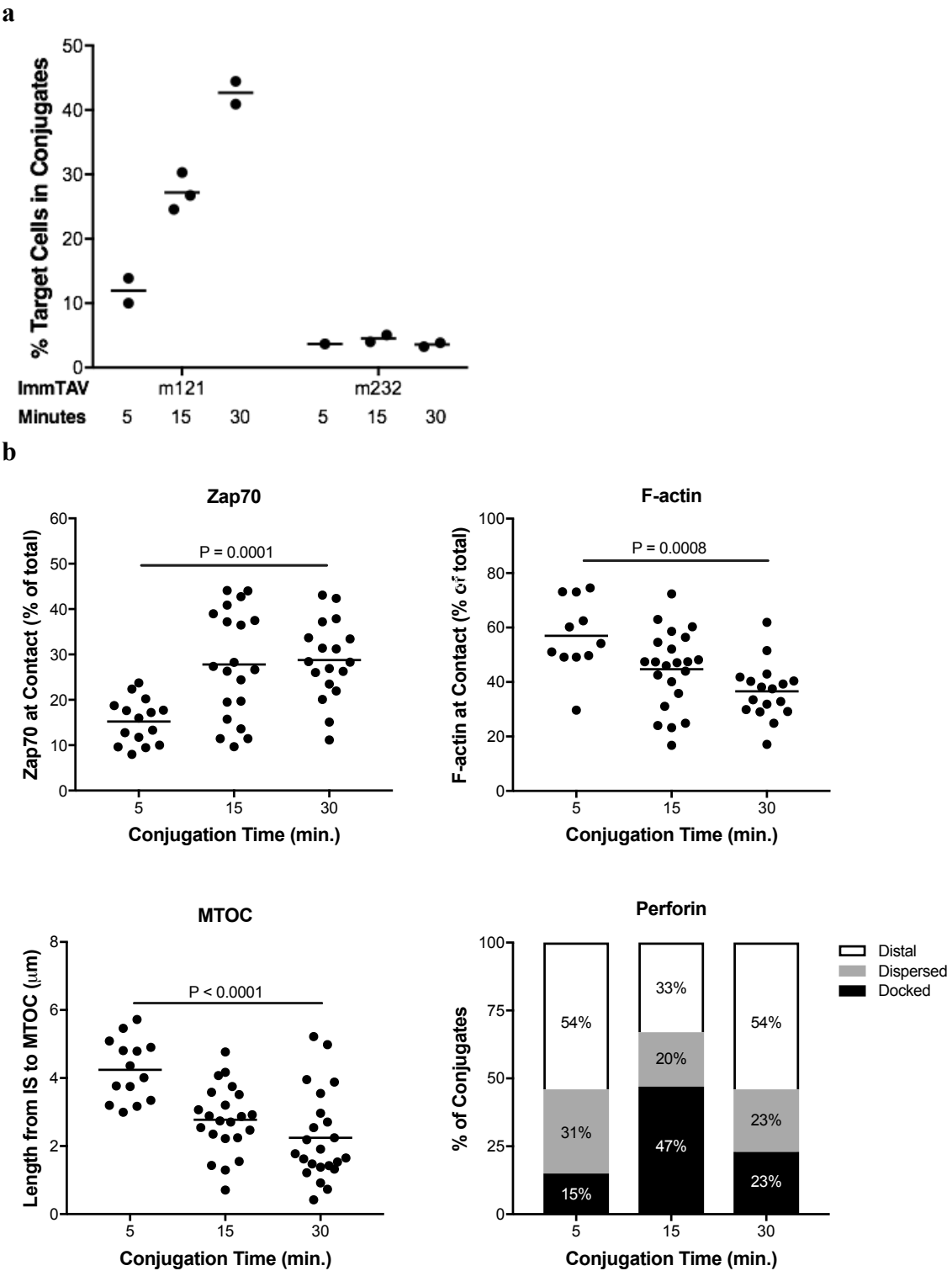

Figure 5.6: Time course of synapse formation in T2-T cell synapses. ImmTAV-redirected healthy donor CD8+ T cells (n = 1 donor) were co-cultured with SL9-pulsed T2 cells for 5, 15 or 30 minutes before (a) quantifying the percentage of T2 cells in conjugates and b) measuring Zap70 (at contact, % of total), F-actin (at contact, % of total), MTOC (μm from synapse) and perforin (% distal, docked, dispersed) polarisation in the CD8+ T cells; each dot represents a conjugate imaged by microscopy (n > 10/timepoint). Horizontal lines represent the mean. Groups were analysed by one-way ANOVA.

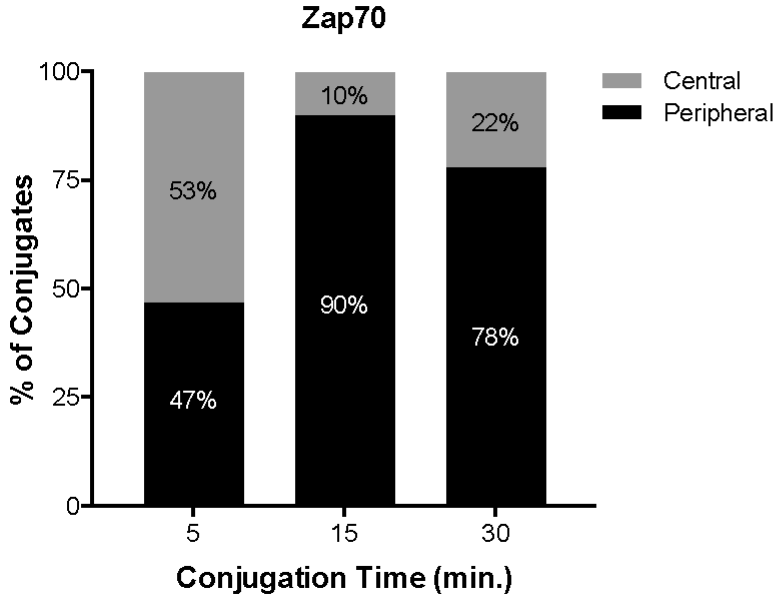

Figure 5.7: Alternate analysis of Zap70 polarisation at the immunological synapse. Zap70 polarisation in the CD8+ T cell over time (compare to figure 5.6b) was also analysed by measuring the percentage of conjugates with either CD8+ T cell central or peripheral Zap70 expression (binning method).

5.2.6 HIV ImmTAV facilitates formation of fully functional synapses with both activated infected and resting infected primary CD4+ T cells

While SL9-pulsed T2 cells present the cognate epitope for the m121 ImmTAV, they are not as physiologically relevant as an APC as HIV-infected primary T cells. The results in chapter three showed that Gag expression in HIV-infected cells varies within infected cell populations, especially between activated and latently infected cells. To assess the formation of synapses with HIV-infected primary CD4+ T cells with both low and high Gag expression, HD CD8+ T cells were co-cultured with activated infected or resting infected CD4+ T cells and ImmTAV (HIV-1_{IIIB} used at an MOI = 0.01 for both infections).

The method used to determine the number of conjugates in section 5.2.5 was found to be unsuitable for quantifying primary T cell-T cell synapses because of their scarcity; careful scanning of the slides was necessary to find the conjugates as ten random

low magnification fields of view were insufficient to capture them. A subjective observation was that it was easier to find synapses when the targets were activated infected cells than resting infected cells. In order to test this more objectively, a second method was applied. Slides were coded so that the observer was blinded to the experimental condition (active or resting infection and HIV ImmTAV or control ImmTAVs). The observer marked as many synapses as possible searching through the eyepiece for 15 minutes. Images were then acquired and the final synapse count was based on correctly paired cells only ($CD8^{neg.}$/CD8+ touching cells, TCCF(p24) of target > uninfected controls). After 15 minutes 12 conjugates were found on the slide with activated infected targets, in contrast to six on the slide with the resting infected cells (figure 5.8); a negligible number of synapses were found on slides with no ImmTAV or with the m231 or m232 ImmTAV controls.

ImmTAV, infection	Conjugates
m121 resting	6
m121 active	12
m231 active	0
m232 active	1
- active	0

Figure 5.8: Quantification of T cell-T cell synapses. Healthy donor CD8+ T cells were co-cultured with ImmTAVs and either resting infected or activated infected CD4+ T cells before counting for 15 minutes the number of conjugates that could be found under each condition (blinded).

The slides prepared with m121 ImmTAV-redirected CD8+ T cells were also stained for synapse proteins, CD8 and Gag before images were acquired by confocal microscopy. Target cells with a TCCF(p24) lower than that of the stained, uninfected cells were not considered for further analysis (appendix 5.2). Gag expression was significantly higher in the activated infected target cells (active vs. resting, median: 2819 vs. 1264, P = 0.003) in keeping with the TCCF data from chapter three (section 3.2.3). While all target cells in the synapses that were included in the final analysis were

confirmed as infected according to the TCCF measurements, Gag could be also seen by eye in activated infected cells (figure 5.9); this was not often the case for resting infected cells (not shown).

a **b**

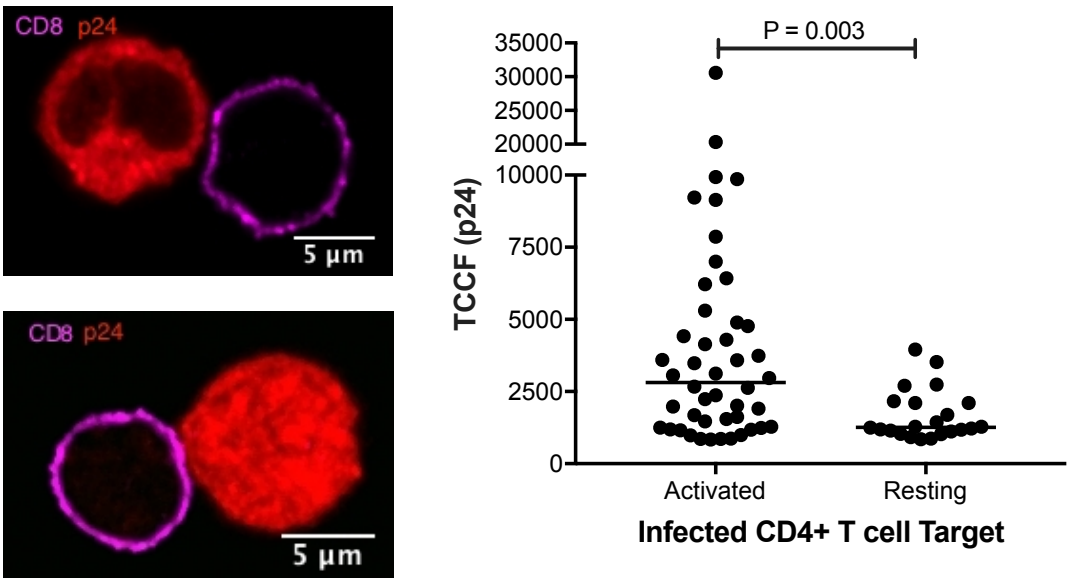

Figure 5.9: HIV Gag expression in the target cells of T cell-T cell synapses. (a) Immunofluorescence images of ImmTAV-redirected HD T cell-T cell conjugates with both activated and resting infected CD4+ T cell targets (images not shown for resting infected targets as p24 expression was not visible in images). Red = p24, magenta = CD8. (b) Measurements of the TCCF(p24) of the target cells (target cells with a TCCF(p24) less than the TCCF(p24) for the uninfected cells were not considered for further analysis and are not shown here); each dot represents a conjugate imaged by microscopy (n = 3 donors/condition with n > 20 conjugates/condition). Horizontal lines represent the median. Groups were analysed by Mann Whitney test.

In view of the difference in Gag expression in activated and resting target cells, its impact on recruitment of synapse proteins in the CD8+ T cells was explored. Zap70 localisation at the synapse was not significantly different (activated vs. resting, mean (SD): 11.3% (2.7) vs. 12.7% (3.2)) and peripheral polarisation of Zap70 was prominent in both groups (figure 5.10). The MTOC was significantly closer to the IS in CD8+ T cells forming conjugates with resting infected T cells (activated vs. resting, mean µm (SD): 3.6 (0.8) vs. 2.7 (0.9), P = 0.048) although further donors would be needed to confirm this as

only nine synapses were found for the resting infected targets (figure 5.11). Analysis of MTOC location at 5, 15 and 30 minutes also confirmed that the synapse progression with activated infected T cell targets was similar to that seen with T2 cell targets (appendix 5.3). 14.3% of activated infected cell synapses expressed docked perforin compared to 27.3% of resting synapses, although perforin polarisation in both groups was primarily located dispersed throughout the cell (figure 5.12).

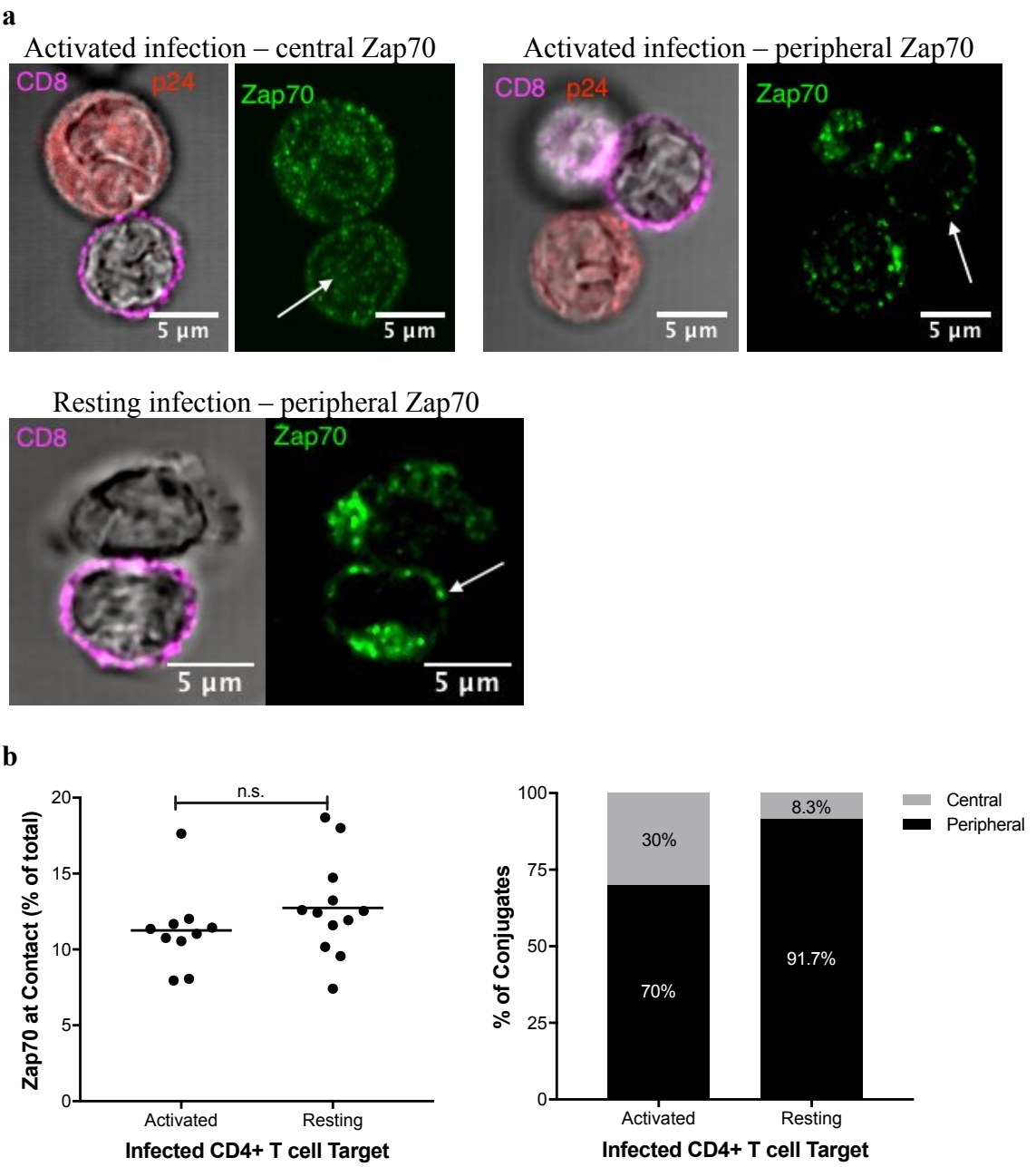

Figure 5.10: Zap70 polarisation in T cell-T cell immunological synapses. (a) Immunofluorescence images of ImmTAV-redirected HD T cell-T cell conjugates with both activated (top) and resting (bottom) infected CD4+ T cell targets. Red = p24, magenta = CD8, green = Zap70; p24 intensity in resting infected cells is low enough it does not show up visibly in images. (b) Measurements of the Zap70 at contact (% of total; left) or % of conjugates with central versus peripheral Zap70 polarisation (right) in the CD8+ T cells; each dot represents a conjugate imaged by microscopy (n = 1 donor, n > 9 conjugates/condition). Horizontal lines represent the mean. Groups were analysed by unpaired t test.

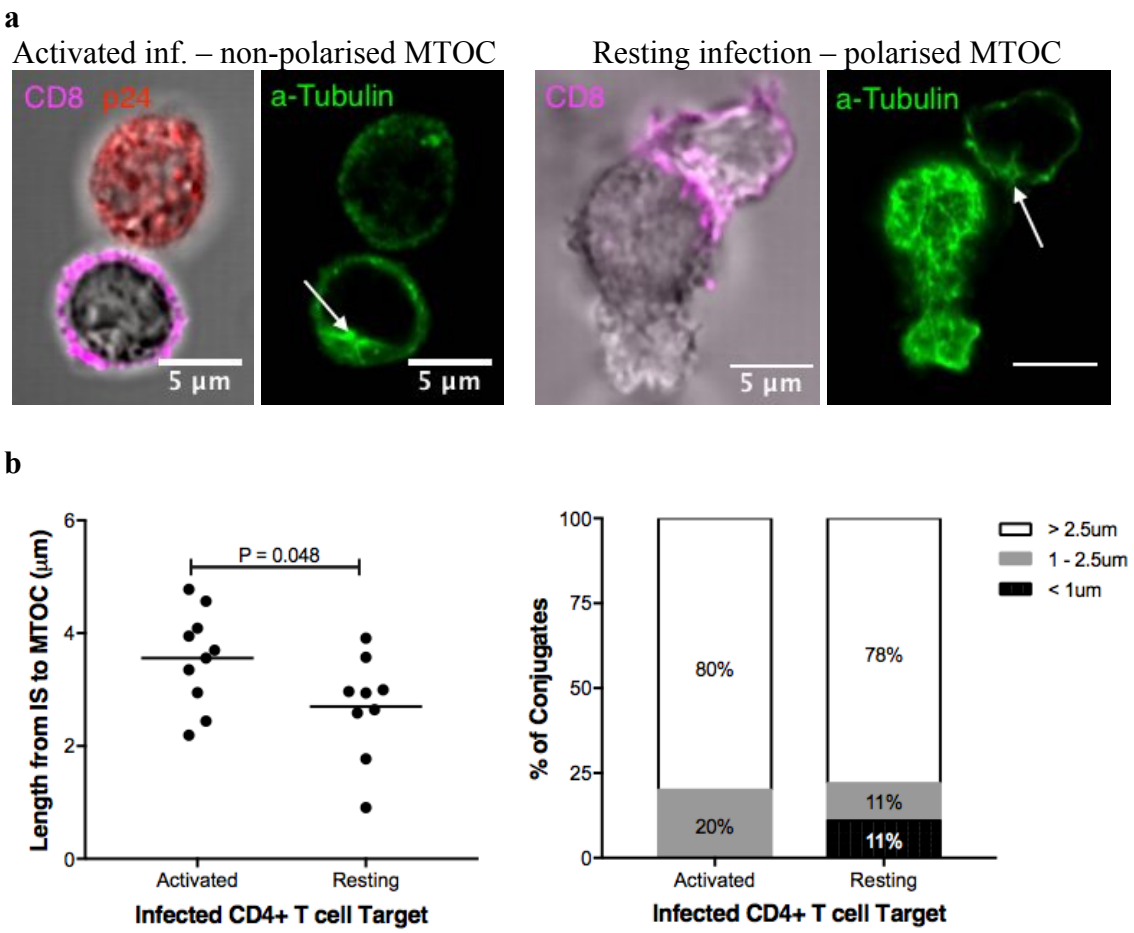

Figure 5.11: MTOC polarisation in T cell-T cell immunological synapses. (a) Immunofluorescence images of ImmTAV-redirected HD T cell-T cell conjugates with both activated (left) and resting (right) infected CD4+ T cell targets. Red = p24, magenta = CD8, green = MTOC (α-tubulin, arrow), black/white = DIC. (b) Measurements of the length (µm) from the immunological synapse to the MTOC (left) which were binned into three categories (right; <1 µm, 1 – 2.5 µm, >2.5 µm); each dot represents a conjugate imaged by microscopy (n = 1 donor, n > 8 conjugates/condition). Horizontal lines represent the mean. Groups were analysed by unpaired t test.

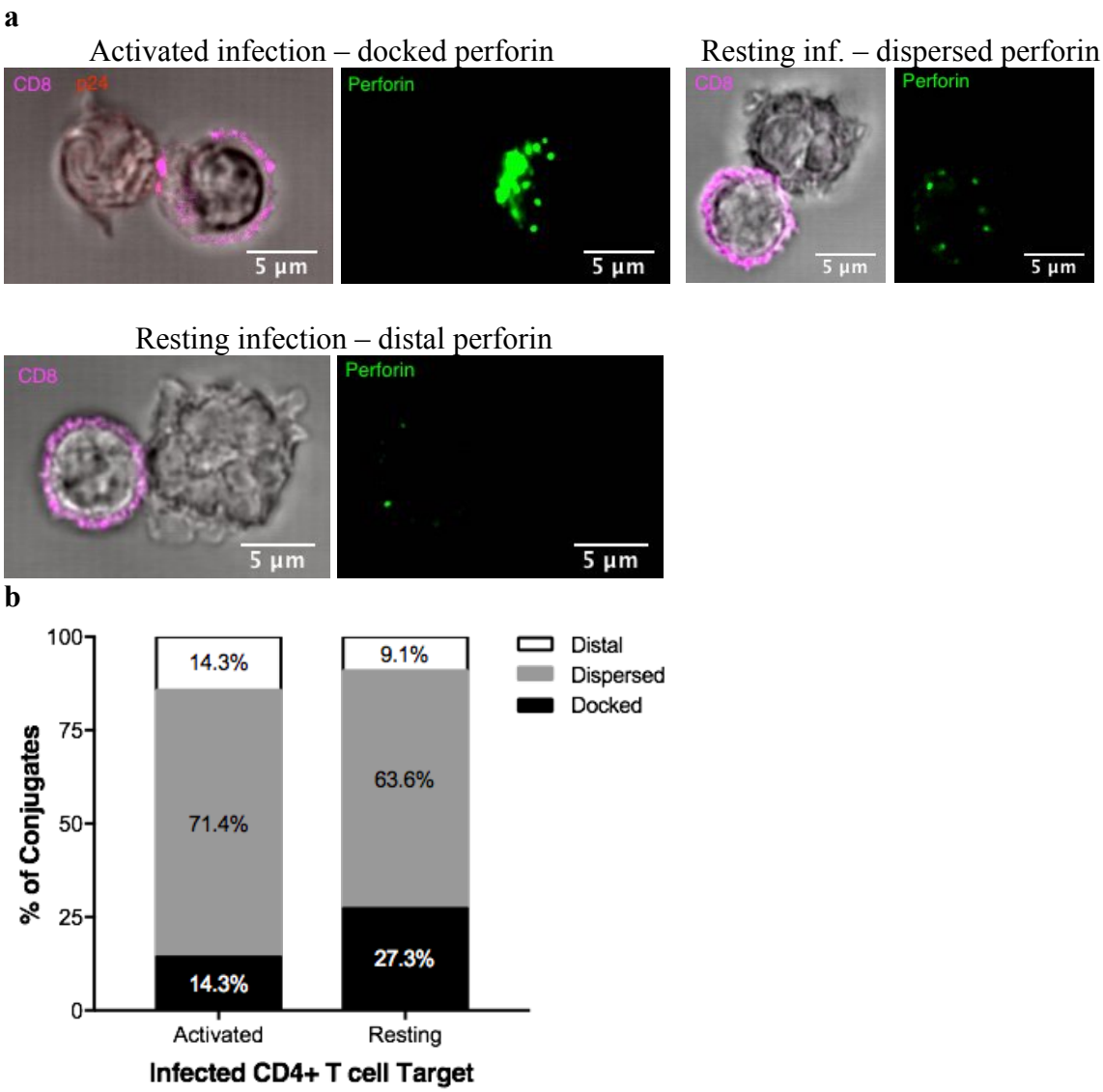

Figure 5.12: Perforin polarisation in T cell-T cell immunological synapses. (a) Immunofluorescence images of ImmTAV-redirected HD T cell-T cell conjugates with both docked, dispersed and distal perforin polarisation. Red = p24, magenta = CD8, green = perforin, black/white = DIC. (b) Perforin polarisation was categorised into distal, dispersed and docked regions (n = 1 donor, n > 9/condition).

5.2.7 Enrichment of the SL9-specific cytotoxic T lymphocyte population does not alter synapse protein polarisation

While the viral epitope expression on the target cell may affect the number of immunological synapses that form, the impaired antiviral activity of CD8+ T cells from CHI (and PHI) donors compared to healthy donors suggests that the effector cell is also implicated in synapse maturation.[89,245] The m121 ImmTAV was able to redirect HIV-

naïve or non-HIV specific CD8+ T cells towards SL9-pulsed T2 cells or HIV-infected primary CD4+ T cells, resulting in killing of the target cells.[245] To assess whether naturally primed CTLs from PLWH were able to form synapses with target cells, CHI donors with pre-existing SL9-specific CTLs were chosen. The frequency of SL9-specific CD8+ T cells in the peripheral blood was assessed by dextramer staining. To improve the chances of finding natural synapses a short-term cell line (STCL) was created for each SL9-responding CHI donor; for example, this increased the SL9-dextramer positive population from 0.65% to 1.68% in one donor (figure 5.13a). Enriching the CD8+ T cell population for SL9-specific cells increased the percentage of peptide-pulsed T2 cells in conjugates from 5.7% to 17.5% (figure 5.13b).

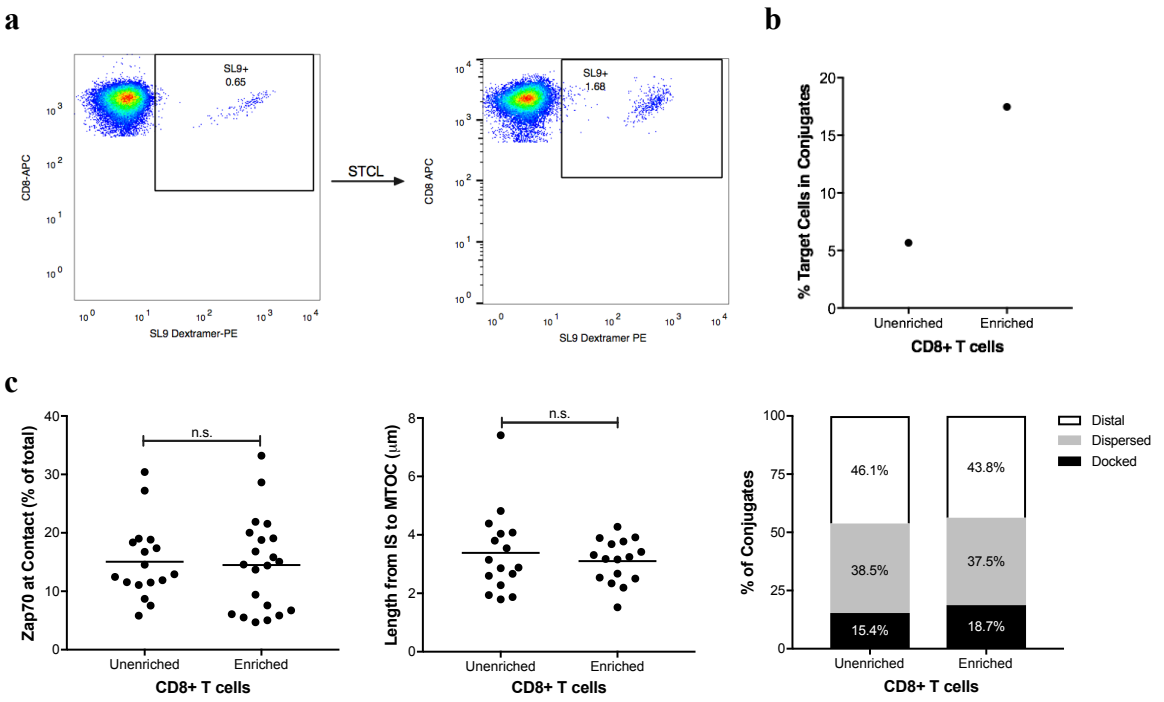

Figure 5.13: Enrichment of SL9-specific CTLs from CHI donors. (a) A STCL ('enriched') was created to enrich for SL9-specific CD8+ T cells from the CHI donors and the SL9-specific population was measured with SL9-dextramer staining (one representative donor shown). Unenriched and SL9-enriched CD8+ T cells from a CHI donor (n = 1) were co-cultured with SL9-pulsed T2 cells before (b) quantifying the number of T2 conjugates that formed and (c) measuring the polarisation of Zap70, MTOC and perforin as previously described; each dot represents a conjugate imaged by microscopy (n = 1 donor, n > 10 conjugates /condition). Horizontal lines represent the mean. Groups were analysed by unpaired t test.

To determine whether the enrichment process, which includes peptide stimulation and *in vitro* expansion over a 10-day period, might enhance synapse formation the three chosen proteins were compared in synapses using unenriched (*ex vivo* CD8+ T cells) and enriched (SL9-STCL) CD8+ T cells without ImmTAV redirection (n = 1). There was no significant difference between the two groups for Zap70 localisation, length from the IS to the MTOC as determined by α-tubulin staining or perforin polarisation (figure 5.13c). Additional experiments with the CHI donor's CD8+ T cells showed that increasing the E:T ratio increased the number of conjugates but did not improve MTOC localisation. By contrast, addition of the m121 ImmTAV to the co-culture increased the number of conjugates by more than 2-fold and also significantly polarised the MTOC towards the synapse (figure 5.14).

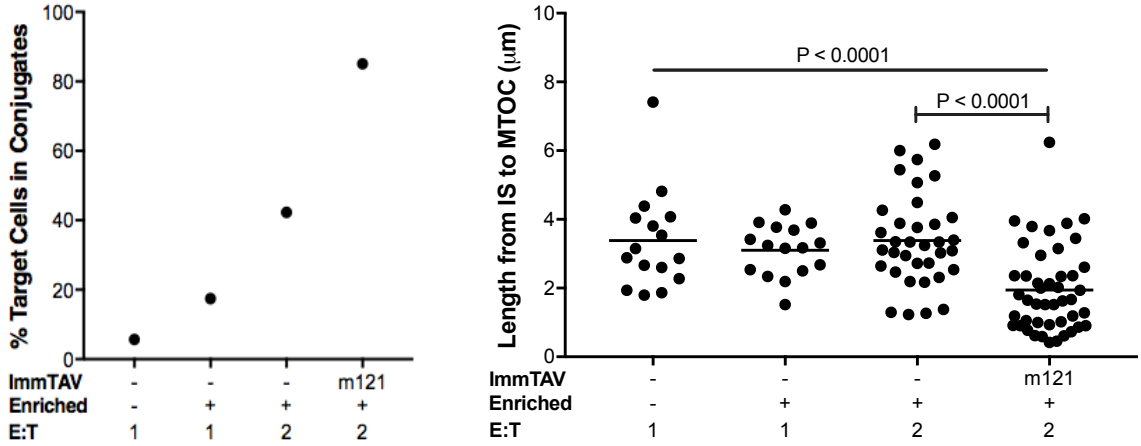

Figure 5.14: Effect of enrichment, E:T ratio and ImmTAV on synapse formation (extension of figure 5.13). Enriching for SL9-specific CTLs, increasing the E:T ratio and adding the m121 ImmTAV all increased the number of conjugates that formed (left; each dot represents a slide with n = 1 donor) but only adding the ImmTAV improved the localisation of the MTOC (right; each dot represents a conjugate imaged by microscopy with n = 1 donor). Horizontal lines represent the mean. Groups were analysed by one-way ANOVA and Tukey's multiple comparisons test.

5.2.8 IS protein polarisation varies between ImmTAV-redirected CD8+ T cells from HIV-positive and negative donors

Previously reported functional data suggested that CD8+ T cells from CHI patients failed to achieve the same levels of viral inhibitory activity of HD CD8+ T cells

when redirected by the HIV ImmTAV.[245] To assess whether defective synapse formation and/or maturation could account for these functional differences, CD8+ T cells from HD (n = 3, m121 ImmTAV redirected) and CHI patients (n = 3, SL9-enriched, +/- m121 ImmTAV redirection) were co-cultured with SL9-pulsed T2 cells for 15 minutes before immunofluorescence staining for Zap70, α-tubulin (MTOC) or perforin. The m231, m232 and no ImmTAV controls were not included for either donor group for synapse marker analysis due to limiting CD8+ T cell numbers and the lack of conjugate formation seen in figure 5.8.

The number of synapses that formed under the different conditions is shown in figure 5.15. As expected, ImmTAV redirection increased the number of synapses formed regardless of whether the CD8+ T cells were from HIV-negative or HIV-positive donors. 27.2% of the target cells were in conjugates with HD CD8+ T cells compared to 21.8% with non-ImmTAV redirected CHI donor cells and 42.6% with ImmTAV-redirected CHI donor cells. ImmTAV redirection was specific to SL9-presenting targets because healthy donor CD8+ T cells without HIV ImmTAV redirection or with the non-SL9 specific m232 ImmTAV did not form a significant number of synapses (figure 5.15).

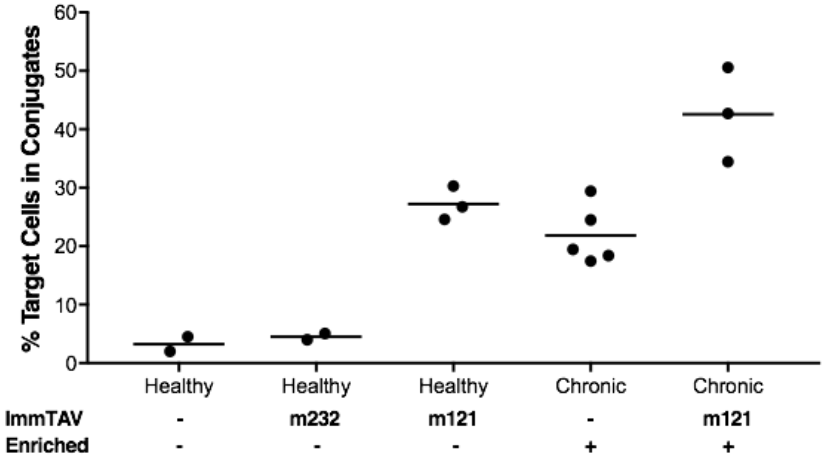

Figure 5.15: Quantification of T2-T cell synapses with CD8+ T cells from different donors. SL9-pulsed T2 cells were co-cultured with CD8+ T cells from healthy and CHI donors with and without ImmTAV redirection to quantify the percentage of T2 cells in conjugates (n > 50 T2 cells counted/slide); each dot represents a slide that was imaged (n = at least 2 donors/condition). Horizontal lines represent the mean.

Zap70 localisation at the synapse was significantly higher in ImmTAV-redirected HD CD8+ T cells than CHI donor CD8+ T cells without ImmTAV redirection (HD/m121 vs. CHI/-, mean (SD): 18.8% (8) vs. 12.4% (7), P = 0.0002); using the binning analysis method more HD CD8+ T cells expressed peripheral Zap70 as well (HD/m121 vs. CHI/-, mean: 85% vs. 17.2%; figure 5.16). Unfortunately, there were not enough CD8+ T cells from these CHI patients to assess the impact of ImmTAV-redirection on Zap70 polarisation. However, it was possible to assess MTOC polarisation and perforin polarisation in enriched SL9-specific CD8+ T cells from CHI donors with and without ImmTAV redirection. The MTOC of the non-ImmTAV redirected CHI donor CD8+ T cells was significantly further away from the synapse compared to ImmTAV-redirected CHI donor or HD CD8+ T cells, however there was no significant difference in the location of the MTOC between the two ImmTAV-redirected groups (HD/m121 vs. CHI/- vs. CHI/m121, mean μm (SD): 2.4 (1.3) vs. 4.7 (2.6) vs. 2.8 (2.1), P < 0.0001 CHI/- vs. HD/121 or CHI/m121; figure 5.17). Polarisation of perforin docked at the synapse was highest in HD CD8+ T cells compared to either CHI donor CD8+ T cell condition (HD/m121 vs. CHI/- vs. CHI/m121, mean: 38.9% vs. 19.2% vs. 18.1%; figure 5.18). The number of conjugates, Zap70 localisation, MTOC polarisation and perforin polarisation were consistent amongst the three healthy donors, illustrating the robustness of the measurements used to assess synapse formation (appendix 5.4). A preliminary analysis of CD8+ T cells from one patient who initiated ART during PHI (RIVER donor) was also used to assess synapse formation. In a comparison with the healthy donor CD8+ T cells from the early ART donor exhibited impaired synapse formation (appendix 5.5) but due to bead contamination (magnetic separation beads aggregated on CD8+ T cells and T2 cells hindering identification of synapses) additional donors were not available or further comparison.

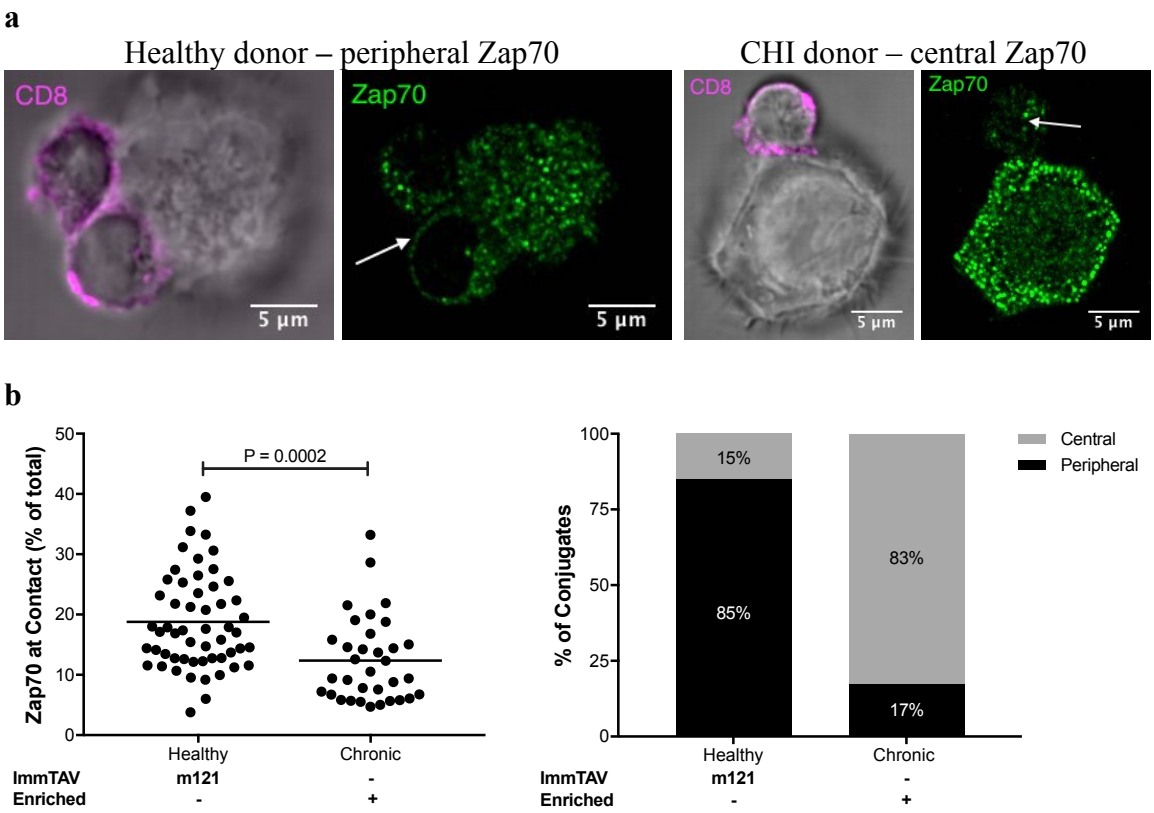

Figure 5.16: Zap70 polarisation in T2-T cell immunological synapses. SL9-pulsed T2 cells were cultured with ImmTAV-redirected HD CD8+ T cells (n = 3) or SL9-enriched CHI patient CD8+ T cells (n = 3). (a) Immunofluorescence images of Zap70 polarisation (left = peripheral, right = central Zap70). Magenta = CD8, green = Zap70. (b) Measurements of the Zap70 at the contact (% of total) (left) or % of conjugates with central versus peripheral Zap70 polarisation (right) in the CD8+ T cells; each dot represents a conjugate imaged by microscopy (n > 10/donor). Horizontal lines represent the mean. Groups were analysed by unpaired t test.

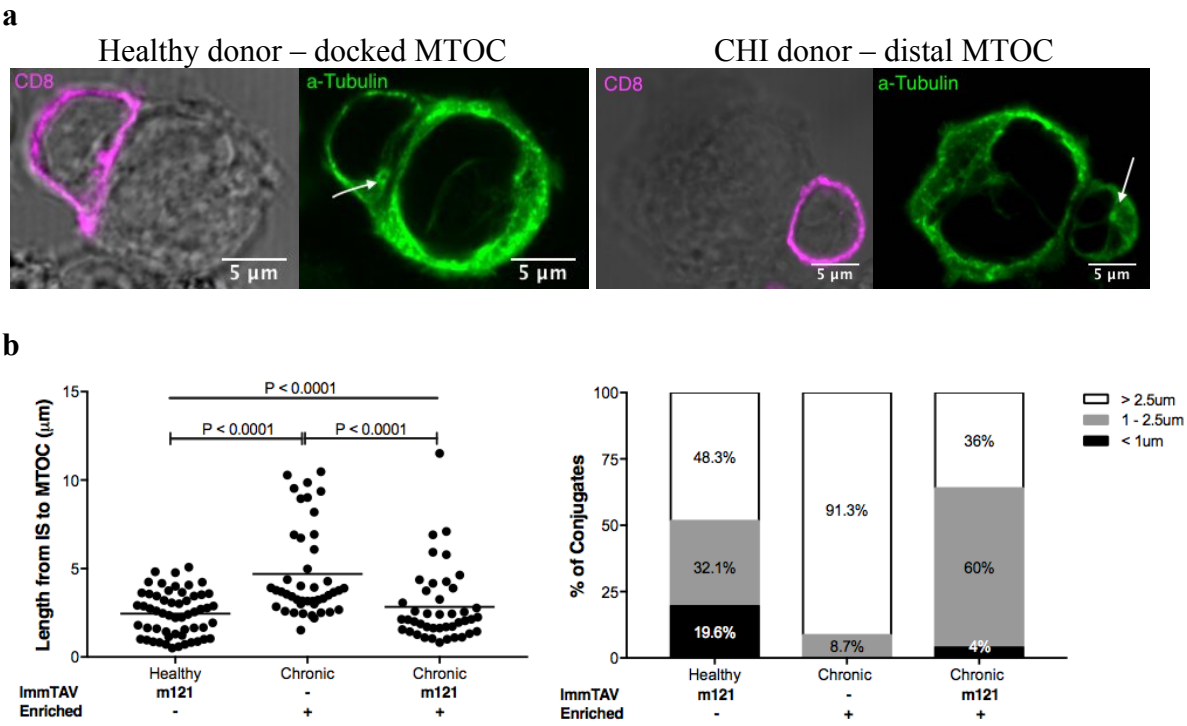

Figure 5.17: MTOC polarisation in T2-T cell immunological synapses. SL9-pulsed T2 cells were cultured with ImmTAV-redirected HD CD8+ T cells (n = 3) and ImmTAV-redirected or naturally occurring SL9-enriched CHI patient CD8+ T cells (n = 3). (a) Immunofluorescence images of the MTOC showing docked (left) and distal (right) MTOC (arrow). Magenta = CD8, green = MTOC. (b) Measurements of the length (µm) from the immunological synapse to the MTOC (left) which were binned into three categories (right; <1 µm, 1 – 2.5 µm, >2.5 µm); each dot represents a conjugate imaged by microscopy (n > 10/donor). Horizontal lines represent the mean. Groups were analysed by one-way ANOVA with Tukey's multiple comparisons test.

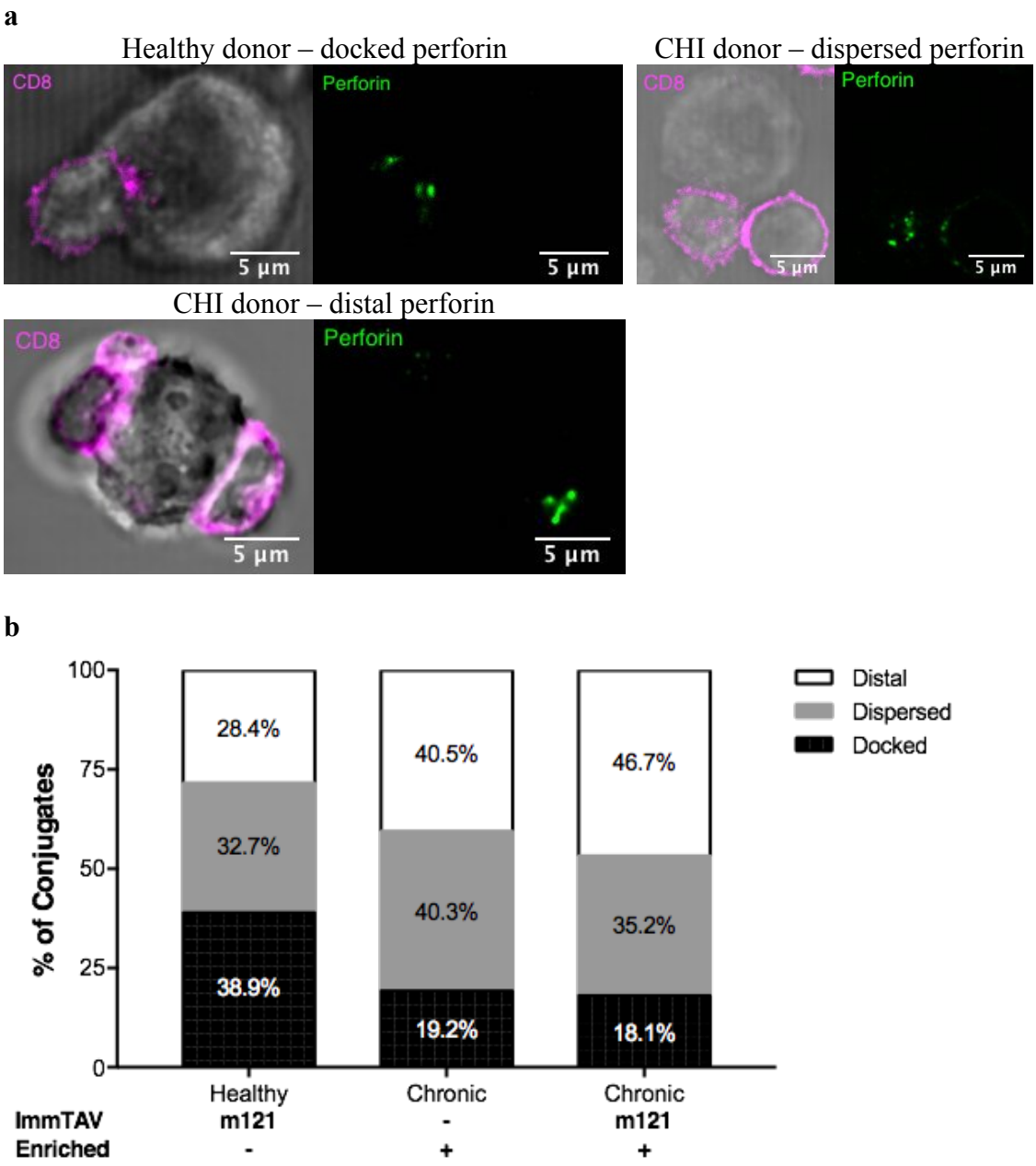

Figure 5.18: Perforin polarisation in T2-T cell immunological synapses. SL9-pulsed T2 cells were cultured with ImmTAV-redirected HD CD8+ T cells (n = 3) and ImmTAV-redirected or naturally occurring SL9-enriched CHI patient CD8+ T cells (n = 3). (a) Immunofluorescence images of perforin polarisation (docked, dispersed and distal). Magenta = CD8, green = perforin, black/white = DIC. (b) Perforin polarisation was binned into docked, dispersed and distal regions (n > 10/donor).

5.2.9 Live cell imaging of the formation of primary CD8+ T cell synapses

To capture the kinetics of synapse formation and target cell killing, the interaction between primary CD8+ T cells and HIV-infected T cells was studied using time-lapse microscopy (in collaboration with Dr Jakub Chojnacki, WIMM). HLA-A2 transfected

cell lines were chosen as potential target cells due to their large size compared to CD8+ T cells and potential to support a high level of infection – both traits that would facilitate detection of synapses (figure 5.19a). Jurkat cells were larger than the other target cells and, more importantly, also larger that CD8+ T cells (Jurkat vs. C8166 vs. T0 vs. T2 vs. CD8+ T, mean (SD): 13.6 (1.7) vs. 9.5 (1.7) vs. 10.9 (1.9) vs. 12.2 (1.5) vs. 7.2 (1.4), P = 0.0001 Jurkat vs. CD8+ T; figure 5.19b). Additionally, Jurkat cells retained a consistent appearance and high viability after infection in contrast to the other cell types, which clustered together and began to die (figure 5.19a).

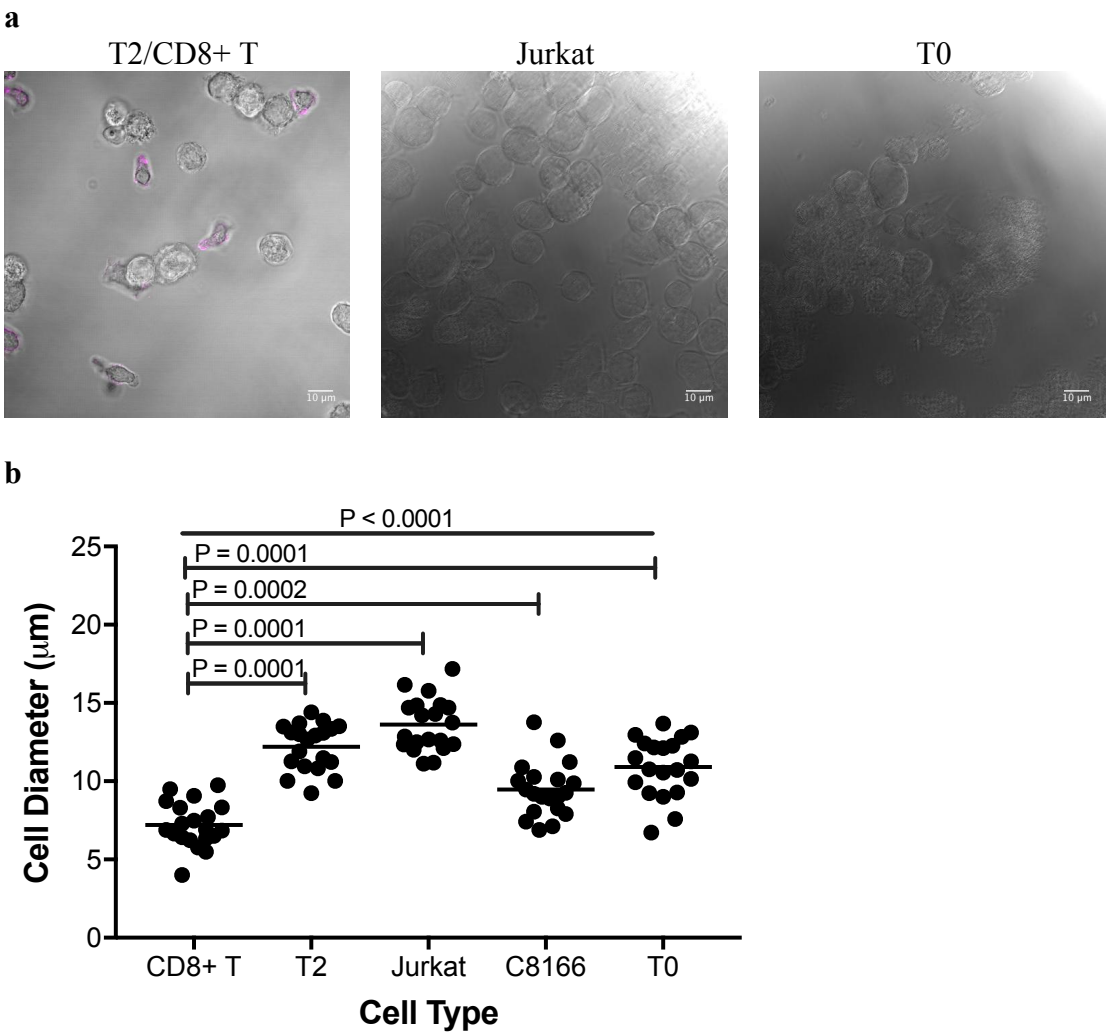

Figure 5.19: Comparison of target cell sizes. Various cell lines (all HIV-infected except for T2 cells, which were SL9 peptide-pulsed) were (a) imaged (from left to right: T2 with primary CD8+ T cells, Jurkats, T0 cells) and (b) measured to determine the average diameter of the target cells in comparison to the size of CD8+ T cells. Magenta = CD8 on DIC image. Horizontal lines represent the mean. Groups were analysed by one-way ANOVA with Dunnett's multiple comparisons test.

Previous studies in our group showed that peak infection of Jurkat cells was attained at around 10 days post-spinoculation (>80% Gag-positive cells by intracellular staining; Dr Hongbing Yang, unpublished results). However, elimination of infected Jurkat cells by ImmTAV-redirected CD8+ T cells was sub-optimal at a concentration of 10^{-9} M, possibly due to the high expression of CD3 on their surface (Dr Hongbing Yang, unpublished results), which may have sequestered the ImmTAV away from the CD8+ T cells. However, clearance of the infected Jurkat cells reached over 90% after seven days co-culture when the ImmTAV concentration was increased to 10^{-8} M (Dr Hongbing Yang, unpublished results). For live cell imaging, infected Jurkat cells were therefore co-cultured with primary CD8+ T cells (E:T of 1) and 10^{-8} M m121 ImmTAV in a well of a chambered coverglass. After five minutes in the incubator chamber of the microscope to calibrate the temperature the microscope ocular was used to find a potential field of view with both cell types visible and images were taken every two seconds for 30 minutes. Figure 5.20 illustrates single images taken from one example time-lapse video (appendix 5.6). This video began 15 minutes after co-culture and shows the complete formation of a synapse (conjugate one – white arrows) and the completion of an already formed synapse (conjugate two – black arrows). For conjugate one, the CD8+ T cell migrated around the slide (figure 5.20a), scanned the Jurkat cell (figure 5.20b), formed a contact with the Jurkat cell (figure 5.20c), remained tightly attached to the Jurkat cell with minor membrane fluctuations (figure 5.20d) and began roaming around the Jurkat cell (figure 5.20e) before the Jurkat's cellular membrane began blebbing at ~21 minutes post-contact (figure 5.20f). The CD8+ T cell of conjugate two had already bound the Jurkat at the start of imaging and the Jurkat's cellular membrane blebbing began ~19 minutes after imaging began.

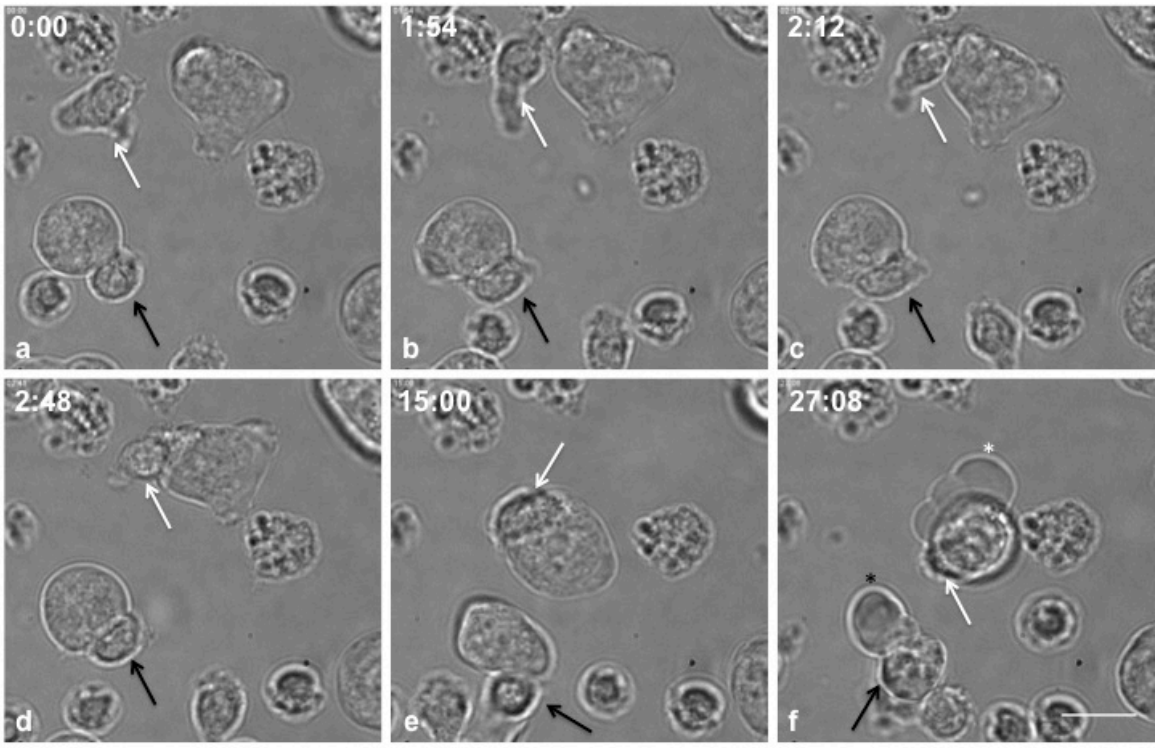

Figure 5.20: Live cell imaging of the formation of primary CD8+ T cell immunological synapses. Selected images taken from the time-lapse microscopy shown in appendix 5.6. HIV-infected, HLA-A2 transfected Jurkat cells were co-cultured with HD CD8+ T cells (E:T of 1) and m121 ImmTAV (10^{-8} M). Timestamp on each image is in relation to the start of imaging at 0:00, 15 minutes after co-culture began. Images show stages of synapse formation for top conjugate (white arrow marking CD8+ T cell) including (a) the migration of the CD8+ T cell, (b) the CD8+ T cell scanning the target, (c) the CD8+ T cell making contact with the target, (d) the formation of a tight synapse, (e) the CD8+ T cell roaming around the target and (f) the blebbing of the cell membrane of the target (*). Second conjugate already formed at 0:00 marked in black. Scale bar represents 10 μm.

5.3 Discussion

The work described in this chapter provides, to my knowledge, the first description of immunological synapses between primary CD8+ T cells and primary HIV antigen-expressing CD4+ T cells. The HIV ImmTAV (m121), a potent bispecific retargeting molecule, enabled demonstration of CD8+ T cell recruitment, activation and killing of HIV-peptide pulsed or virus-infected target cells by fixed and live cell confocal microscopy. As spontaneous synapses between 'natural,' i.e. HIV-primed CTL, and virus-infected targets were found to be rare events, this could explain the lack of published data on IS development in the context of HIV infection. The HIV ImmTAV promotes rapid and efficient effector-target conjugate formation and thus provided a unique opportunity to explore the impact of both viral antigen expression on target cells and CD8+ T cell functional capacity on synapse formation and maturation, with minimal manipulation of the cell populations *in vitro*.[280,284]

Previous studies of the IS suggested that the accumulation of LFA-1 at the IS, or even the virological synapse, stabilises the interaction between the effector and target cells, which promotes synapse maturation.[79,280,384,447] The importance of LFA-1/ICAM-1 interactions in initiating CD8+ T cell effector functions was demonstrated by blockade of LFA-1 on tumour-infiltrating lymphocytes. This led to inhibition of actin clearance and reduced cytotoxic activity.[384] ImmTAV-redirected CD8+ T cells from healthy donors, CHI donors and early ART donors all expressed a similar percentage of LFA-1 at the contact with the HIV-infected target cells (figure 5.2). It was hypothesized that the CD8+ T cells from the CHI donors might express less LFA-1 at the contact (as a consequence of chronic antigenic stimulation and dysregulation of TCR signalling), which could result in unstable immunological synapses and reduced killing. While there is no difference seen in figure 5.2 this may be because all of the contacts formed were mediated by the m121

ImmTAV; as none of the CHI or early ART donors were HLA-A2+ the natural synapses formed by CTLs could not be directly compared with those mediated by the ImmTAV which recognises an HLA-A2 presented peptide. The ImmTAV, in binding the target cell's pHLA with picomolar affinity and recruiting CD8+ T cells via the binding of their CD3 may normalise the signalling received by the effector cells resulting in a similar level of LFA-1 recruitment to the contact. Further work with natural, non-ImmTAV redirected, HIV-specific CTL synapses would be required to see what effect the ImmTAV had on LFA-1 localisation and adhesion and if any pre-existing defect occurs in CHI donor cells in relation to LFA-1 recruitment.[187,189,193]

LFA-1 polarisation to the contact site was not as complete as has been described in the literature; the number of conjugates with LFA-1 at the contact reaching more than 50% of the total was limited (figure 5.2).[79,384,398,409,447] However, the experimental design reported here differed from that in the literature and may contribute to the differing LFA-1 pattern. First, an antibody was used to measure total LFA-1 polarisation, yet LFA-1 recruitment to the synapse does not necessarily indicate a functional role in adhesion.[79] Others have used an antibody specific for the high-affinity conformation of LFA-1 that detects LFA-1 bound to ICAM-1 which requires it to adopt an open conformation.[384,405] Secondly, *in vitro* HIV-infected CD4+ T cells were used as targets whereas in other investigations showing total LFA-1 polarisation to the synapse the observations were based on IS formation with super antigen-pulsed B cells as APCs.[249,384,409,448] Super antigens are able to cross-link HLA class II and TCR molecules, bypassing classical HLA-restricted antigen presentation, in addition to binding co-stimulatory molecules. This creates a more stable interaction that leads to polyclonal T cell activation on a massive scale, circumventing normal regulatory mechanisms.[419,449] When peptide-pulsed T2 cells were used as targets, LFA-1 polarisation in CD8+ T cells at the synapse was

higher than that observed with HIV-infected CD4+ T cells, which suggests that LFA-1 recruitment may be a function of pHLA density on the target cell. However, even with SL9-pulsed T2s the number of conjugates where LFA-1 at the contact was over 50% ('polarised') was still minimal (figure 5.3) suggesting even this relevant positive control for HIV-infected targets still forms less stable and artificial conjugates compared to sAg-pulsed B cells.

The picomolar affinity of the HIV-specific TCR component of the m121 ImmTAV confers exquisite sensitivity to pHLA on the target cell (several orders of magnitude higher than the affinity of a natural TCR). This enabled it to detect resting infected CD4+ T cells, despite the low density of Gag antigen (and possibly HLA-A2-SL9 peptide complexes). Detection of resting infected cells by microscopy was difficult as many of the $CD8^{neg.}$ (CD4+) cells in the conjugate were designated 'uninfected' using the TCCF(p24) cut-off derived from uninfected cells. This could be because the cells were genuinely uninfected but were in transient conjugates that did not progress to mature synapses, which might represent a non-specific effect of the ImmTAV. More likely, however, is the dye-conjugated Gag antibody (or the microscope's detectors) was not sensitive enough to detect such low levels of Gag above non-specific staining. As such there may be a population of very low Gag-expressing cells that were eliminated from analysis as they did not meet the acceptance criteria. A second marker for the target cell (e.g. CD4) would improve detection of correctly paired conjugates upon the slide. Despite this, immunological synapses involving resting infected cells were detected, although less frequently than with activated infected cells; increasing the MOI of virus to 0.05 to increase the rate of infection (as used in chapter three) may result in the detection of more resting synapses. Interestingly, the resting cell synapses did not differ greatly from those formed with activated infected cells with respect to Zap70 recruitment, MTOC

polarisation and perforin mobilisation. Contrary to expectations, according to these criteria there was a trend towards enhanced synapse maturation with resting infected targets. This requires confirmation with further donors, but raises questions as to whether IS maturation is impaired by viral products expressed in productively infected CD4+ T cells. Taken together, the detection of functional resting infected cell synapses demonstrates the sensitivity and potency of the m121 ImmTAV.

To appreciate the impact of the ImmTAV on synapse formation it was important to examine the development of 'natural' synapses, i.e. those formed by circulating HIV-specific CTLs upon encounter with targets expressing viral antigens. The three CHI patients chosen for this work had been shown previously to have pre-existing SL9 responses and to exhibit antiviral activity ranging from ~40 – 80% when their unstimulated CD8+ T cells were co-cultured with autologous reactivated CD4+ T cells at an E:T of 1 in a viral inhibition assay.[245] While the principal objective of this work was to develop the most physiologically relevant method to investigate CD8+ T cell synapses, in the present study SL9-pulsed T2 cells were used as a model APC to ensure that any observed differences between natural and ImmTAV-mediated synapses would not be confounded by variability in target antigen expression. The LFA-1 data with HIV-infected CD4+ T cells as targets also prompted this switch to a T2 cell line. *Ex vivo* CD8+ T cells from these individuals (SL9-specific CTLs were not sorted due to low frequencies) did form synapses with SL9-pulsed T2 cells but were rare (figure 5.13b). To enrich for SL9-specific CTLs a STCL was generated; this increased the proportion of SL9-specific cells by ~150% (but they still accounted for < 2% of CD8+ T cells) but had no effect on the synapse formation (figure 5.13). As predicted, addition of the m121 ImmTAV increased the number of synapses formed as it redirected CD8+ T cells to the target cells, independently of their specificity. However, its impact on synapse formation

was limited: MTOC polarisation was enhanced but perforin docking was similar to that observed in the absence of the ImmTAV (figures 5.15 – 5.18). In summary, based on the Zap70, MTOC and perforin staining there was evidence of defective synapse formation in the context of both naturally primed SL9-specific CD8+ T cells and ImmTAV-redirected CD8+ T cells from CHI patients.

In previous studies recruitment of Zap70 occurred 5 – 7 minutes after conjugate formation and persisted at the synapse for up to 30 minutes; the activated form of Zap70 was mainly found at the periphery of immature synapses and polarisation decreased as the synapse matured.[258,450] Zap70 polarisation at the synapse/periphery was higher in the ImmTAV-redirected HD CD8+ T cells than the CHI donor SL9-enriched CD8+ T cells, consistent with functional data showing superior killing of virus-infected targets by the former (figure 5.16).[245] For this study the antibody used to mark Zap70 bound both isoforms – isoform one concentrates at the synapse after antigen stimulation, and isoform two remains cytoplasmic (ab134509, Abcam). However, the use of an antibody against the non-phosphorylated/non-activated form of Zap70 limited detection of the early activated forms of Zap70. In addition, it was not possible to assess whether ImmTAV redirection of CHI donor CD8+ T cells could enhance Zap70 recruitment as cell samples were limited. Impaired Zap70 recruitment requires further investigation; it could reflect increased Zap70 degradation due to chronic immune activation or sequestration in the cytoplasm.[402,450,451] Jenkins et al. showed that when Zap70 catalytic activity was switched off in a Zap70(AS) mouse model (mice expressing a Zap70 mutant, the catalytic activity of which can be stopped with an inhibitor) the resultant abrogation of killing was associated with an MTOC that began, but did not finish, its migration and granules that did not polarise completely to the synapse. Similarly, using Zap70-deficient cells Blanchard et al. described that Zap70 signalling controls the TCR-dependent polarisation

of the MTOC to the synapse as well as being involved in the supply of PKCθ and LAT signalling molecules.[278,386,448] Defective or slowed Zap70 activity in CHI donor CD8+ T cells could affect the completion of MTOC and granule polarisation to the synapse, which might explain the differences in MTOC distance from the synapse and perforin polarisation between HD and CHI CD8+ T cells.

One of the major mechanisms of cytotoxicity is the release of pore-forming proteins such as perforin and granzymes to destroy the target cells.[247,278,408,426] For this study perforin was chosen as a marker of synapse completion because its morphology and abundance made it readily detectable by confocal microscopy.[284,403,417] 50% more HD CD8+ T cells expressed perforin at the synapse than CD8+ T cells from CHI patients, whether the latter were tested alone or in the presence of the ImmTAV. The failure of ImmTAV-redirection to mobilise perforin to the same extent as in HD CD8+ T cells suggests that CHI CD8+ T cells may be globally depleted of perforin. A recent study of CD8+ T cell functional evolution from primary to chronic HIV infection found that following HIV infection perforin+ CD8+ T cells expanded but then decreased after the resolution of viraemia. It was suggested that the loss of cytolytic potential was due to transcriptional dysregulation as the population of T-bet^{low}Eomes^{hi} cells, which express little to no perforin, expanded. This loss of perforin polarisation would explain why CHI donor CD8+ T cells express less docked perforin than HD CD8+ T cells and why, despite facilitating the formation of conjugates and migration of the MTOC, the ImmTAV has no effect on perforin localisation in CHI donor CD8+ T cells (figures 5.15, 5.17 and 5.18).[452] Additionally, while MTOC polarisation is useful for delivery of granules to the synapse the recruitment of granules, not the MTOC, to the synapse is the predictor of cytotoxicity.[278] As ImmTAV-redirection did not enhance CHI patients' CD8+ T cell antiviral activity to levels observed with healthy donor effectors in killing assays with

resting (chapter three) or reactivated CD4+ T cells, this suggests that HIV ImmTAVs alone may be insufficient to facilitate elimination of virus-infected cells.[245] Other agents may be required to correct defects in lytic granule mobilisation.

An alternative explanation is that differences in perforin migration may explain the variation in perforin polarisation. Beal et al. analysed patterns of granule polarisation in CTLs and discovered that granules can take a short, direct path to the cSMAC resulting in a concentration of granules at the cSMAC (as in many CD8+ CTLs) or a longer, delayed path with a spread of granules finishing at the pSMAC (as seen in less efficient CD4+ CTLs). If this slower path were dominant in the CHI donor synapses the 15-minute time point may have missed the maximal accumulation of the granules. In addition, upstream events such as impaired early signalling, as suggested by differences in Zap70 polarisation in healthy and CHI donor CD8+ T cells, could have had an impact on granule polarisation to the synapse.[284] As perforin has been described as localising to the MTOC before the MTOC moves to the synapse dual staining of these proteins may provide more evidence as to why perforin was not fully recruited to the synapse.[246,284]

The defective killing and synapse formation by the CD8+ T cells from CHI donors may be a result of the chronic antigenic stimulation-induced exhaustion state described in chapter three. Indeed, other groups have described changes to TCR and cytokine signalling pathways and expression of genes involves in adhesion and migration as a result of persistent antigen exposure. Singh et al. reported that monoclonal naïve T cells modulated their responsiveness after exposure to persistent antigen resulting in cells with an impaired proliferative ability, TCR signalling and cytokine production after restimulation.[453] This phenomenon has also been described in the context of chronic viral infection by comparing the gene expression profile of exhausted LCMV-specific CD8+ T cells from chronic infection with functional LCMV-specific CD8+ T cells after acute

infection. The exhausted cells overexpressed inhibitor receptor genes with ITIM motifs (delivery of negative signals), downregulated signalling molecules like Lck (early kinase required for IS formation), did not upregulate perforin (required for cytotoxicity), had an altered expression of genes required for cytokine signalling and exhibited a profile pattern suggestive of metabolic and bioenergetics deficiencies (see section 7.2).[195] This molecular signature of CD8+ T cell exhaustion during chronic LCMV infection suggests that the antigen exposure in chronic HIV infection could push T cells to adapt by altering expression of genes involved in TCR signalling and immunological synapse formation as seen by the results in this chapter.

Advances in microscopy have allowed for improved resolution and capture of the unique dynamics of synapse formation. Live cell imaging of CTLs has captured complete cycles of activation and degranulation, that can occur within a few minutes.[256,454] Bertrand et al. described CTLs that were able to secrete lytic granules within 40 – 60 seconds after target cell encounter, even when MTOC polarisation had been inhibited.[403] In this thesis I have described how HIV-infected Jurkat cells were used to capture synapse formation in real time (figure 5.20). While this method required the use of a different target from those used for confocal microscopy, it provided additional evidence for effective synapse formation between HIV-infected CD4+ T cells and ImmTAV-redirected CD8+ T cells. Evolving synapses were observed from 5 – 45 minutes post co-culture; synapses could be found at different stages at a given time point. While contacting their targets the CTLs appeared very motile, forming the 'kinapses' described by Halle et al. in their study of CTL killing of virus infected targets.[455] Additionally, not all conjugates culminated in cytolysis of the target cell – some CD8+ T cells made contact with the target but subsequently detached or sampled the entire surface of the Jurkat cell without killing. However, a comparison of the slide directly after co-culture

and after 60 minutes demonstrated that widespread killing had occurred as the previously intact Jurkats had been replaced with debris. In the conjugate shown in figure 5.20 the time from cell contact to blebbing of the target cell's membrane was ~21 minutes. While this is a longer killing time than described by Bertrand et al. (< 1 minute) or Stinchcombe et al. (< 6 minutes) in their CTL studies this is only one synapse (a heterogeneous population of CTLs could result in a range of killing times) and HIV-infected targets and human CTLs were used in contrast to the mouse CTLs used by Stinchcombe et al. and the peptide-HLA coated surfaces ('targets') used by Bertrand et al.[256,281,403,445] Acquisition of further real-time data on CTL synapse formation would allow for the calculation of the '*per capita* killing rate,' i.e. the number of targets that are killed during a set time by one CTL with ImmTAV redirection.[429,455] While further development of this work, incorporating HIV-specific and synapse protein-specific tags, is needed in order to capitalise on the potential of live cell imaging to provide detailed kinetic information, this proof of principle experiment illustrated the utility of the m121 ImmTAV.

To conclude, CD8+ T cells from CHI patients form defective immunological synapses compared to healthy donors; while the number of synapses that formed were similar the resulting molecular rearrangements were inhibited in CHI donor CD8+ T cells (figure 5.21). Further studies with co-staining of synapse proteins and live cell imaging could help define more precisely at what stage the signalling cascade falters in CHI CTLs and thus identify new targets for therapeutic intervention.[256,276,284,385,408] The ImmTAV was found to be an effective tool for studying synapses as it permitted the use of more relevant experimental conditions than those used to date, such as *ex vivo* primary T cell co-cultures and expression of native viral antigens. The data reported here provide the foundation for further study of immunological synapses to determine the impact of novel

interventions for HIV eradication, including immune checkpoint blockade and other immunomodulators.

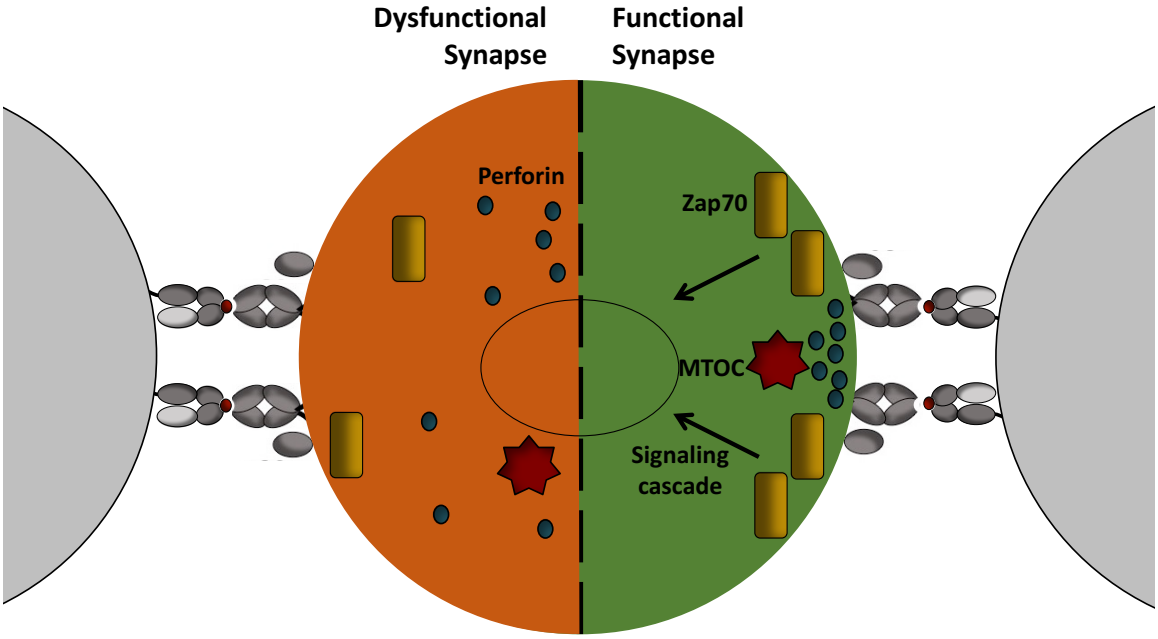

Figure 5.21: Dysfunctional versus functional synapses. During the formation of a functional synapse (as seen with ImmTAV-redirected healthy donor CD8+ T cells) upon TCR complex engagement with the pHLA complex intracellular signalling (arrow) facilitates the recruitment of Zap70 (yellow), MTOC (red) and perforin (blue) to the synapse for lysis of the infected cell. In dysfunctional synapses, like those formed by CTLs from CHI donors, there is less Zap70 at the synapse and the MTOC and perforin are found further away. This may result in the impaired antiviral response reported in chronic HIV infected patients.

5.4 Questions addressed in this chapter

- *Can immunological synapses be observed between primary CD4+ T cells and CD8+ T cells from HIV-positive patients?*

  Yes. T cell-T cell synapses were observed using ImmTAV-redirected CD8+ T cells from CHI and early ART donors in combination with HIV-infected healthy donor CD4+ T cells (figure 5.2; section 5.2.2). However, SL9-pulsed T2 cell targets were used for further investigation of synapse formation by HIV-positive patient CD8+ T cells to ensure the observed differences between natural and ImmTAV-mediated synapses would not be confounded by variability in target antigen expression (figure 5.5; section 5.2.4).

- *How does the immunological synapse change over time?*

  Over the course of 30 minutes conjugates between primary CD8+ T cells and SL9-pulsed T2 cells accumulated (figure 5.6). Zap70 recruitment, MTOC and perforin migration towards the synapse and F-actin clearing peaked between 15 and 30 minutes (figure 5.6). The 15-minute time point was chosen for further studies as it best captured the critical events, suggesting that synapse synchronisation was maximal at this time (section 5.2.5).

- *How does enriching for SL9-specific CTLs affect synapse formation?*

  Enriching for SL9-specific CTLs via the generation of a STCL increased the percentage of SL9+ cells by dextramer staining and the number of synapses that formed (figure 5.13). The peptide stimulation did not affect the synapse parameters measured (section 5.2.7). However, even after enrichment, the proportion of SL9-specific CTLs was very low, therefore, sorting the cells to achieve higher purity would be needed to address this question fully.

- *Can the T2-T cell model be applied to HIV-infected T cell-T cell synapses?*

  Yes. While fewer synapses were found using primary T cell targets the progression of MTOC localisation over time was similar to that seen in T2-T cell conjugates (figure 5.8 and appendix 5.3). Synapse marker polarisation was normal in HD CD8+ T cells forming synapses with either activated infected or resting infected CD4+ T cells despite the difference in Gag expression (figures 5.9 – 5.12; section 5.2.6). Furthermore, live cell imaging showed the redirection of healthy donor CD8+ T cells towards infected Jurkat cells and their subsequent death (figure 5.20; section 5.2.9).

- *Is there a difference in the development of immunological synapses formed by CD8+ T cells from HIV-positive and HIV-negative donors?*

  Yes. While there was no apparent defect in conjugate formation, i.e. the number of T2-T cell synapses that formed (figure 5.15), both spontaneous and ImmTAV-mediated synapse maturation were hindered when the effectors were CD8+ T cells from CHI donors; there was less Zap70 recruitment as well as MTOC and perforin polarisation to the synapse in CD8+ T cells from CHI donors compared to ImmTAV-redirected healthy donor CD8+ T cells (figures 5.16 – 5.18; section 5.2.8).

- *Does early ART improve the formation of CD8+ T cell immunological synapses?*

  This was only partially explored due to sample availability and conclusions are limited. In a comparison of ImmTAV-redirected CD8+ T cells in conjugates with primary HIV-infected CD4+ T cells, LFA-1 polarisation in CD8+ T cells was unexpectedly higher in early ART treated subjects than healthy donors and higher still in CHI patients (figure 5.2). The trend was contrary to expectations as LFA-1 polarisation is indicative of a more functioning synapse, yet CHI CD8+ T cells

were dysfunctional in viral inhibition assays. This may be due to the use of primary T cell targets (figure 5.5), characteristics of the anti-LFA-1 antibody used or the 30-minute time point chosen to analyse LFA-1 polarisation (sections 5.2.2 – 5.2.4). Likewise, the synapses formed with SL9-pulsed T2 cells by the CD8+ T cells from another early ART donor were not as mature as those formed by HD CD8+ T cells in a comparison of Zap70 polarisation, MTOC migration and perforin polarisation (appendix 5.5).

CHAPTER SIX: THE EFFECT OF ZIDOVUDINE ON MITOCHONDRIAL TURNOVER IN PRIMARY T CELLS

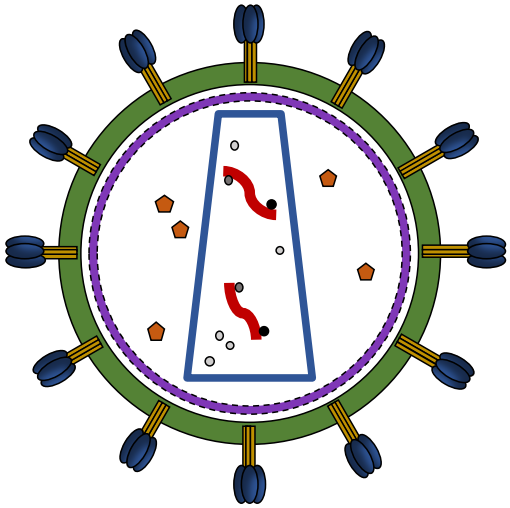

6.1 Introduction

Since the identification of the Human Immunodeficiency Virus as the causative agent of AIDS, researchers have developed at least 20 drugs that inhibit virus replication. Previously developed as a treatment of the Friend virus, zidovudine (ZDV, also known as azidothymidine or AZT) became the first approved agent for the treatment of HIV in adults, and soon after in children and for mother-to-infant transmission.[456,457] ZDV functions as a thymidine analogue and was the first of the nucleoside reverse transcriptase inhibitor (NRTI) class of drugs that include thymidine, cytidine, guanosine and adenosine analogues. Within the cell kinases convert ZDV to the active 5'-triphosphate form. This competes with the naturally occurring thymidine triphosphate as a substrate for HIV's reverse transcriptase. Once ZDV is incorporated into the growing DNA strand the chain terminates due to a modification of the 3'-hydroxy group into an azido group. As HIV lacks the genes required to synthesise enzymes to metabolize purine and pyrimidine nucleotides the modification prevents further phosphodiester linkages needed to complete the growing chain.[458,459] Without the ability to reverse transcribe the viral RNA into DNA the virus is unable to replicate using the host cell's machinery and viral spread is halted.

Despite the initial clinical benefit for some PLWH, newer antiretrovirals replaced ZDV due to its toxicity. In addition, the emergence of drug-resistant variants became apparent with ZDV monotherapy and was a consequence of error prone reverse transcription; ZDV resistance mutations reduced binding of the drug to reverse transcriptase and/or released the analogue, allowing for further chain extension.[460,461] Several metabolic toxicities also emerged with long-term use including fat redistribution (leading to facial and limb lipoatrophy and central adiposity) hepatic steatosis, myopathy and lactic acidosis.[462–464] Many of these side effects have been attributed to the mechanism of action of the drug – despite having a 100-fold greater affinity for reverse

transcriptase ZDV can bind and inhibit the cellular mitochondrial DNA polymerase-γ (Pol- γ) as well.[465] The 'Pol-γ hypothesis' proposes that the interference of ZDV with the host cell nucleotides, mitochondrial DNA (mtDNA) production and Pol-γ proof-reading activity can cause compromised mitochondrial function and mtDNA depletion especially in cells with excess drug.[461,466] mtDNA depletion produces defective electron transport chain complexes and the resulting ATP production failures can cause dysfunction in the tissues.[463,467] However, the mitochondrial toxicity does not correlate with the inhibitory effect of ZDV on Pol-γ when compared to other NRTIs.[461,468–470] Furthermore, mtDNA depletion does not inevitably lead to clinically apparent toxicity as mtDNA depletion has been reported in asymptomatic and treatment naïve patients. The conflicting data suggests that the mechanism of ZDV toxicity is not fully explained by its activity as a thymidine analogue.

Previous studies suggested that an alternative mechanism for the mitotoxicity of ZDV (and stavudine, another thymidine analogue) is their ability to inhibit autophagic flux.[471,472] Autophagy (macroautophagy) is a homeostatic mechanism, upregulated in times of stress, used by the cell to degrade and recycle cellular contents such as excess organelles. Autophagy begins with a double membrane phagophore that forms around the cellular components. Microtubule-associated protein 1 light chain 3 (LC3) proteins are post-translationally modified to a lipidated form, LC3-II, and are incorporated into the forming autophagosome (figure 6.1). The fully formed autophagosome fuses with a lysosome to form the autolysosome and the internal components are degraded by acid hydrolases, while the LC3 is recycled.[473,474] Any blockage of this catabolic pathway can result in the accrual of damaging reactive oxygen species (ROS) and defective mitochondria within the cell.[475] Stankov et al. reported that thymidine analogues interfered with recycling of toxic cellular components in hepatocyte and adipocyte cell

lines, which led to increased apoptosis, decreased proliferation and an accumulation of intracellular lipids.[471,472] These results provide a possible mechanism to account for the hepatotoxicity and lipoatrophy associated with thymidine analogue exposure *in vivo*. However, whether ZDV adversely affects other tissues via the same mechanism has not been explored.

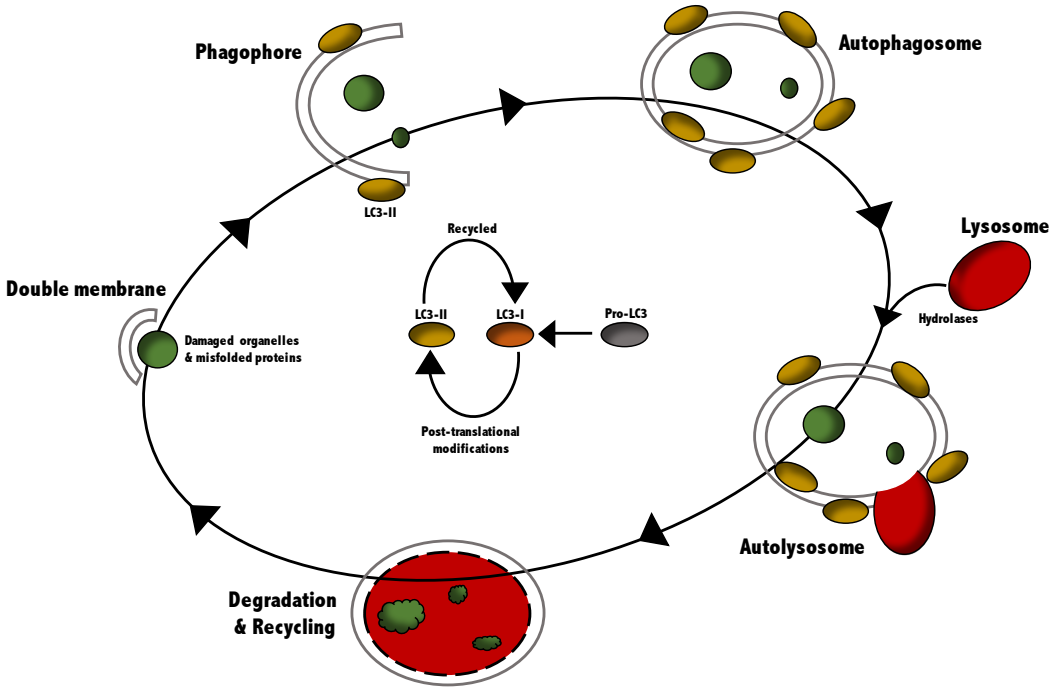

Figure 6.1: The cycle of autophagy. In order to recycle excess or damaged cellular components the cell utilises the cyclical process of autophagy. A double membrane *phagophore* begins to form around the cellular components and the post-translationally lipidated *LC3-II* protein is incorporated into the membrane. The membrane fully encircles the cellular components to form the *autophagosome* and it fuses with a *lysosome* to form the *autolysosome*. The acidic hydrolases within the lysosome degrade the cellular components and the whole vesicle is recycled.

As ZDV accumulates in T cells, these are potentially susceptible to drug-related toxicity. A Southern African multi-centre cohort study showed that patients on ZDV-containing ART regimens exhibited impaired immunological recovery compared to patients on ZDV-sparing regimens. CD4+ T cell counts from over 70,000 patients were tracked over the course of five years. Despite, higher CD4+ cell counts at baseline, those on ZDV-containing regimens were more likely to show severely impaired immunological

recovery (defined as < 100 CD4+ T cells/μl) after one year than those without ZDV exposure.[476] This finding suggests that ZDV could have an effect on T cell proliferation and function.[477] The aim of the work described in this chapter was to explore the consequences of ZDV exposure in primary T cells, *in vitro* and *in vivo*, focusing on mitochondrial turnover, autophagic flux and antiviral T cell function.

6.2 Results

6.2.1 Assay optimisation: mitotoxicity

As ZDV is reported to be mitotoxic, parameters of mitochondrial function were assessed by flow cytometry using two separate staining panels – one incorporating the MitoSOX dye (mtROS) and one the MitoTracker stain (mtMass). The staining panel containing the MitoSOX dye presented smeared CD3 and CD4 surface staining. This problem was resolved by titrating the CD3 and CD4 antibodies and MitoSOX dye in addition to reversing the surface stain and MitoSOX staining order (figure 6.2).

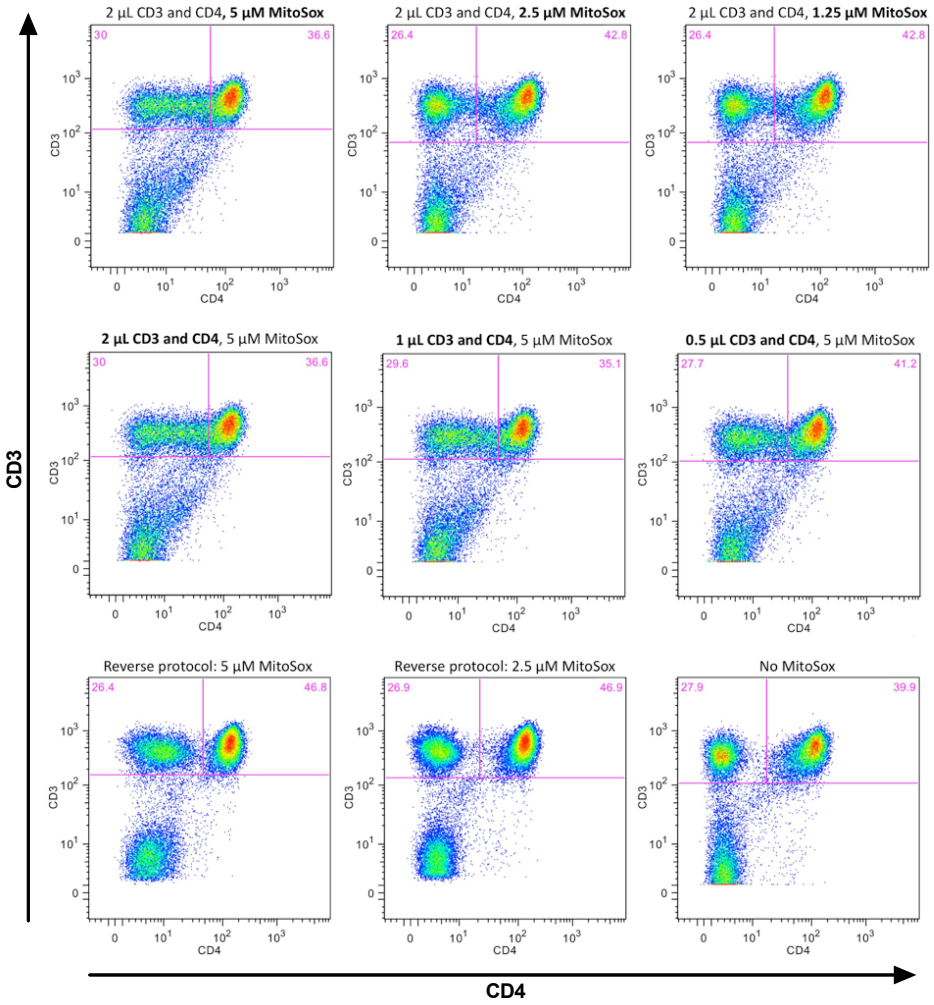

Figure 6.2: MitoSOX surface staining optimisation. Surface stain (CD3 vs. CD4) flow cytometry plots of PBMCs stained with decreasing concentrations of MitoSOX (5, 2.5, 1.25 µM; top row), decreasing amounts of surface stains (2, 1, 0.5 µL each antibody; middle row) and staining with MitoSOX before surface stains (5, 2.5 µM MitoSox 'reverse protocol' – bottom row, 1st and 2nd boxes) as compared to MitoSOX-negative sample (bottom row, 3rd box).

As it was a safety requirement to treat PBMC samples from PLWH with a fixative before acquisition on the flow cytometer, it was necessary to check first for any effect of the fixation process on MitoSOX and MitoTracker staining. PBMCs stained using either the MitoSOX or MitoTracker panels were fixed with 2% or 4% PFA and compared to unfixed counterparts. Fixation of cells stained with MitoSOX inflated the MitoSOX+ population and caused a recurrence of the surface stain smearing (figure 6.3a). Fixation of MitoTracker stained cells destroyed the MitoTracker signal (figure 6.3b). Consequently, it was necessary to perform all analyses of MitoTracker-stained HIV+ samples without fixation on a designated cytometer.

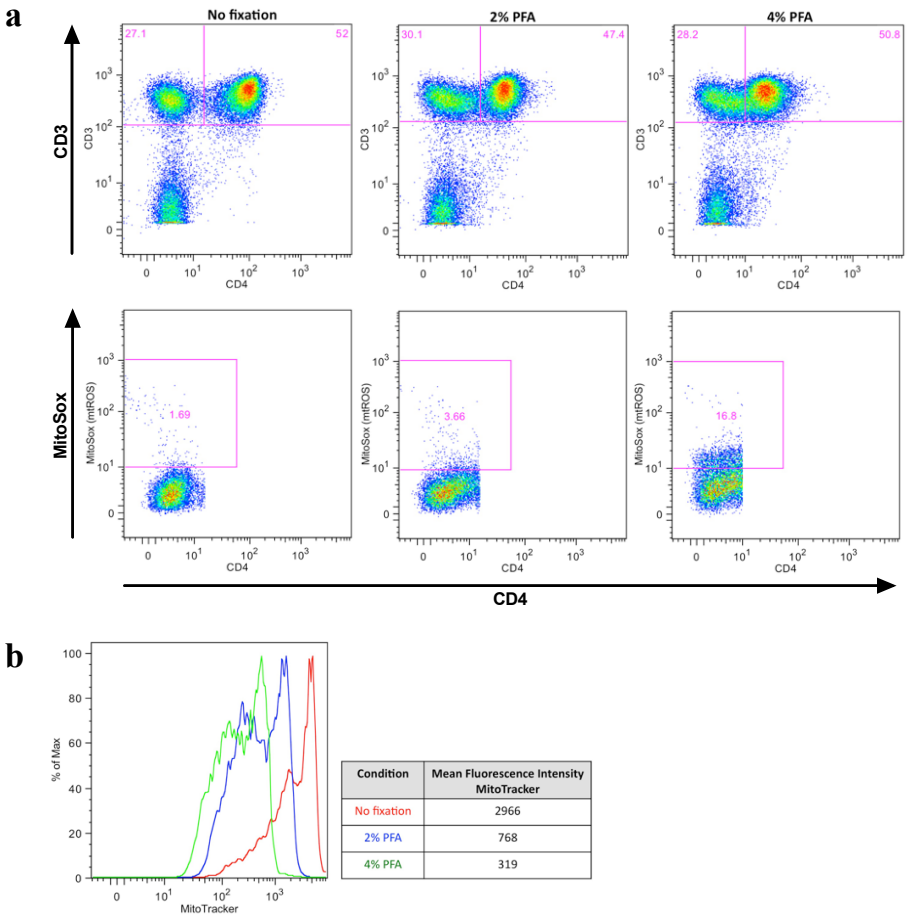

Figure 6.3: PFA fixation alters MitoSOX and MitoTracker staining. (a) Surface stains (top row) and MitoSOX stain (bottom row) from MitoSox panel and (b) MFI MitoTracker histograms for PBMCs left unfixed (left column or red) or fixed with 2% PFA (middle column or blue) or 4 % PFA (right column or green).

Finally, to assess the effect of cryopreservation on mitochondrial staining fresh and frozen PBMCs from healthy donors were tested in parallel: cells were rested overnight and treated with ZDV for six hours to induce mtROS production. MitoSOX staining showed that fresh cells produced more mtROS than frozen samples for both CD8+ T cells (5 μM fresh vs. frozen % MitoSox+, mean (SD): 43.7% (6.1) vs. 13% (4.5), $P < 0.0001$) and CD4+ T cells (5 μM fresh vs. frozen % MitoSox+, mean (SD): 30% (9.2) vs. 10.8% (4.6), $P < 0.0001$; figure 6.4). The cell viability of the total T cells (% LIVE/DEAD$^{neg.}$) decreased upon the addition of 10 μM ZDV for both fresh (0 – 5 μM vs. 10 μM ZDV, mean: 95.9% vs. 35%) and frozen (0-5 μM vs. 10 μM ZDV, mean: 93.6% vs. 63%) conditions.

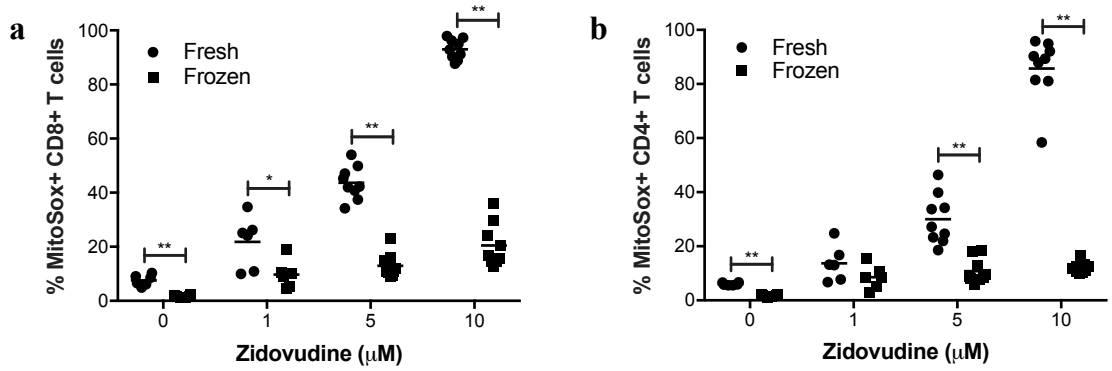

Figure 6.4: Fresh cells produce more mtROS than frozen cells when exposed to increasing concentrations of ZDV. PBMCs were separated from the blood of healthy donors (n = 6 – 9) and either used fresh or were frozen and cryopreserved for at least one week. Both fresh and thawed PBMCs were cultured with 0, 1, 5 and 10 μM of ZDV for six hours before staining for mtROS. % MitoSOX+ cells of (a) CD8+ T cells and (b) CD4+ T cells is shown for fresh (circle) and frozen cells (square). Horizontal lines represent the mean. Groups were analysed by multiple t tests (*P = 0.02; **P < 0.0001).

6.2.2 ZDV recapitulates the effects of autophagic flux inhibitors

Previous studies suggested that ZDV can inhibit autophagic flux (or mitophagy when this occurs with mitochondria) resulting in a build-up of normally recycled mitochondrial contents.[471,472] To begin to assess whether such effects could be observed in T cells mtROS expression and mtMass were analysed in PBMCs from healthy donors

(n = 3) cultured with ZDV and known flux inhibitors, E64d/Pepstatin A or chloroquine. Although not significant, ZDV caused the biggest increase in mtROS, as measured by percentage MitoSOX+ CD8+ T cells (ZDV vs. control vs. untreated, median: 43.8% vs. 12.9% vs. 4.5%) and CD4+ T cells (ZDV vs. control vs. untreated, median: 19.2% vs. 5.8% vs. 2.9%). mtMass, as measured by the percentage change to control of MitoTracker MFI was also affected by ZDV in CD8+ T cells (ZDV vs. control, median: 35.9% vs. -1%) and CD4+ T cells (ZDV vs. control, median: 41.1% vs. 3.4%; figure 6.5). Chloroquine, a known lysosomal inhibitor, also caused a non-significant increase in both the MitoSOX+ population (CD8+ T cells chloroquine vs. control, median: 21.5% vs. 10.2%; CD4+ T cells chloroquine vs. control, median: 13.8% vs. 3.7%) and percentage change to control MitoTracker (CD8+ T cells chloroquine vs. control, median: 43.5% vs. 1.9%; CD4+ T cells chloroquine vs. control, median: 34.1% vs. 2.4%). However, there was little change with E64d/Pepstatin A compared to the respective control for percentage MitoSOX+ populations in CD8+ T cells (E64d/Pepstatin A vs. ethanol control, median: 8.9% vs. 17.1%) and CD4+ T cells (E64d/Pepstatin A vs. ethanol control CD4+ T cells, median: 4.4% vs. 5%) or percentage change to control MitoTracker MFI in CD8+ T cells (E64d/Pepstatin A vs. control, median: 15.5% vs. -4.3%) and CD4+ T cells (E64d/Pepstatin A vs. control, median: 16.4% vs. -1.8%), possibly due to the high ethanol concentration (figure 6.5). In summary, ZDV appeared to recapitulate the effect of flux inhibitors suggesting that ZDV may also interfere with mitophagy.

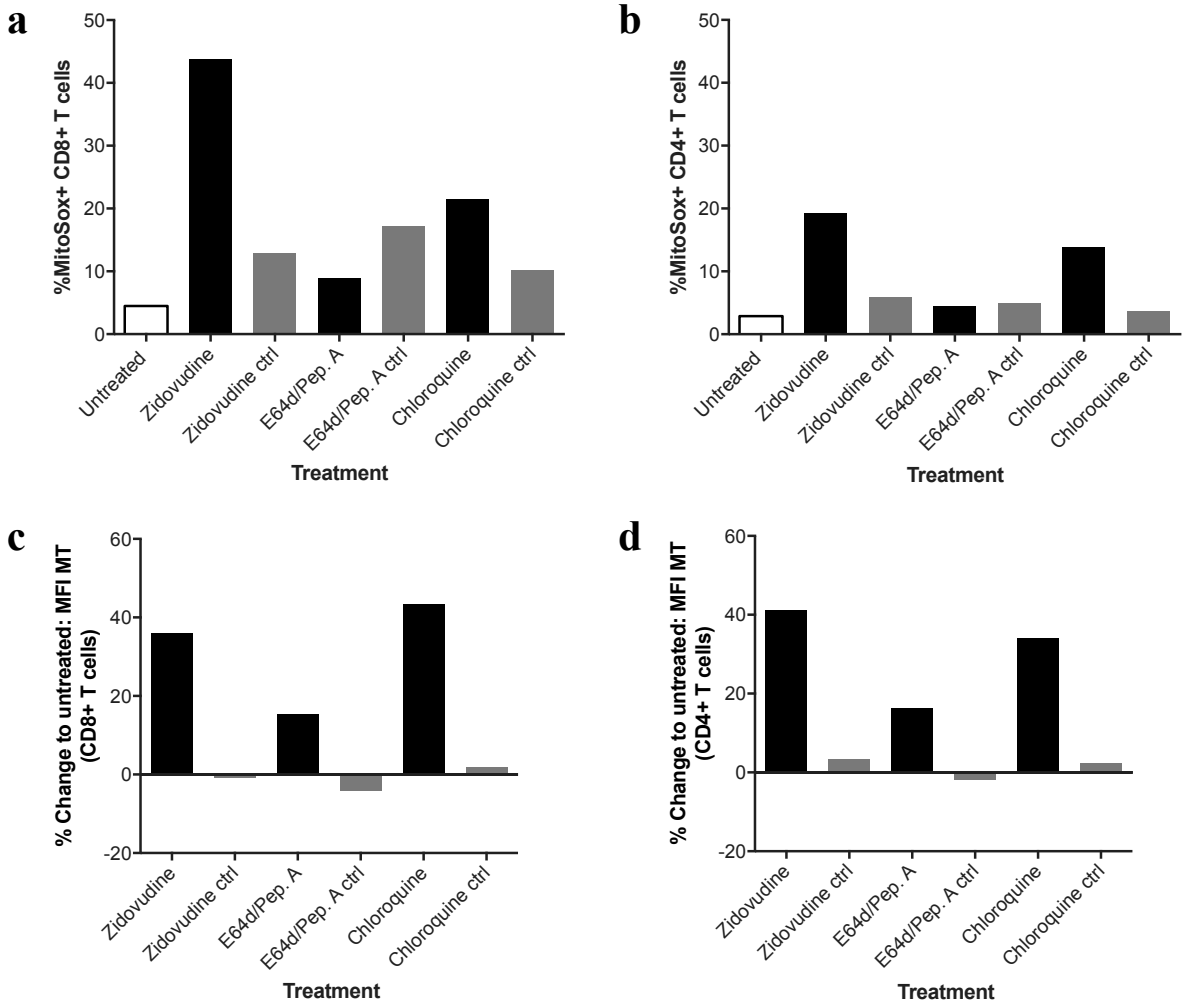

Figure 6.5: Zidovudine recapitulates the effects of autophagic flux inhibitors. PBMCs from healthy donors (n = 3) were cultured for 18 hours with media alone, zidovudine (5 μM), E64d/Pepstatin A (10 μg/ml), chloroquine (15 μM) or the appropriate controls (PBS, ethanol or water of the same volumes respectively) before staining for mtROS or mtMass. % MitoSOX+ cells shown for (a) CD8+ T cells or (b) CD4+ T cells. MFI MitoTracker for each condition compared to the untreated samples to calculate % change to untreated for (c) CD8+ T cells and (d) CD4+ T cells. Each bar represents the median of 3 donors (no significant differences).

6.2.3 *In vitro* exposure to ZDV, but not tenofovir disoproxil fumarate or darunavir, increases mtROS in T cells

Next, the effects of ZDV and two other antiretroviral drugs (tenofovir, TDF; darunavir, DNV) on mitochondria were investigated in PBMCs from healthy donors. PBMCs (n = 10) were cultured with therapeutic concentrations of ZDV (tNRTI), TDF (aNRTI) or DNV (protease inhibitor) for six hours before quantification of mtROS and mtMass using previously described assays (section 6.2.1). ZDV exposure led to a

significant increase in mtROS+ T cells for both CD8+ T cells (ZDV vs. control, mean (SD): 17.5% (9.7) vs. 7.1% (5.0), P = 0.008) and CD4+ T cells (ZDV vs. control, mean (SD): 12.1% (10.1) vs. 4.7% (2.7), P = 0.048; figure 6.6). This effect was dose dependent, although concentrations of ZDV higher than 5 μM, which is estimated to reflect therapeutic dosing levels, resulted in excessive cell death (figure 6.4). No change in the mtROS+ T cell population was seen for TDF or DNV compared to their controls (figure 6.6). Change in mtMass, assessed by percentage change in the MitoTracker MFI upon drug exposure, was slightly higher in ZDV-exposed than TDF- or DNV-exposed CD8+ T cells (% change ZDV vs. TDF vs. DNV, mean (SD): 22.3% (26.8) vs. 7.6% (19.9) vs. 0.6% (18) respectively) and CD4+ T cells (% change ZDV vs. TDF vs. DNV, mean (SD): 16.6% (22.9) vs. 0.8% (24.7) vs. 0% (17.7)) but the differences were not statistically significant (figure 6.6).

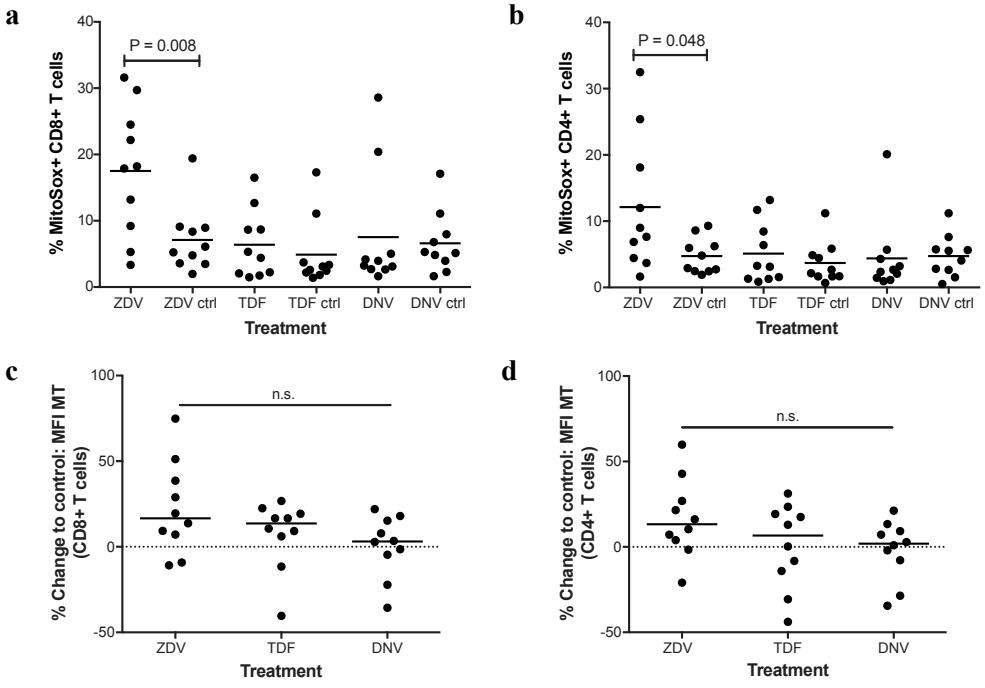

Figure 6.6: *In vitro* exposure to ZDV increases mtROS expression in primary T cells. PBMCs from healthy donors (n = 10) were cultured with zidovudine (5 μM), tenofovir (10 μM), darunavir (10 μM) or PBS controls of equal volume for six hours before being stained for mtROS or mtMass. %MitoSOX+ cells shown for (a) CD8+ T cells or (b) CD4+ T cells. % change to control of mtMass (MFI (MitoTracker) for (c) CD8+ T cells and (d) CD4+ T cells. Horizontal lines represent the mean. Groups were analysed by paired t test for two groups and one-way ANOVA for three groups.

6.2.4 T cells from HIV patients on ZDV-containing ART regimens express more mtROS than those from patients on ZDV-sparing regimens

ZDV toxicity may develop over months and years of exposure and could be underestimated in a short term *in vitro* exposure. The effect of long-term exposure to the drug was investigated by assessing mtROS and mtMass in *ex vivo* T cells from patients who had been treated with a ZDV-containing regimen for at least one year (n = 10). Patients on ZDV-sparing regimens who were age and ART duration matched (n = 10) were studied as controls (Table 6.1). Because fresh blood samples from patients on ZDV-containing regimes were not available all comparisons made in this study were with frozen samples. There was a significantly higher frequency of mtROS+ cells within the CD4+ T cell subset in the ZDV-treated group than the ZDV-spared group (ZDV+ vs. ZDV-, mean (SD): 8.7% (3.4) vs. 6.0% (2.0), P = 0.046). While not significant, the mtROS+ cells were 2-fold more frequent among CD8+ T cells in the ZDV-containing regimes (ZDV+ vs. ZDV-, mean (SD): 23.6% (21.2) vs. 11.7% (12.0); figure 6.7). There was no correlation between the duration on ART and the frequency of mtROS+ cells in the ZDV-treated or ZDV-spared groups (not shown).

Based on the autophagic flux inhibition hypothesis of Stankov et al. it is possible that ZDV exposure *in vivo* would result in the accumulation of defective mitochondria, leading to an increase in mtMass.[471] Previous groups suggested the existence of a discrete $mtMass^{high}$ population, similar to the mtROS+ population, consistent with accumulations of defective mitochondria;[478] however, this population was not visible in the patient samples and a difference between ZDV-exposed and spared groups could not be discerned. As the MitoTracker MFI values could not be directly compared due to the ZDV+ and ZDV- cohort samples being acquired separately a long-term effect of ZDV on mtMass was not confirmed (figure 6.7).

Table 6.1: Clinical information on ART-treated subjects

	Patient ID #	Age (years)	Gender	CD4 (cells/µl)	Duration of ART (years)	ART regimen
ZDV+	3	53	F	400	6	ZDV/TDF/R/DNV
	14	52	F	410	3	ZDV/*NRTI/NNRTI*
	26	49	M	400	2	ZDV/*NRTI/PI*
	27	42	M	1130	2	ZDV/*NRTI/PI*
	50	36	F	610	8	ZDV/3TC/NVP
	56	38	M	490	1	ZDV/3TC/NVP
	61	66	M	520	9	ZDV/3TC/NVP
	63	43	M	400	7	ZDV/3TC/TDF/R/LPV
	78	69	M	550	8	ZDV/*NRTI/NNRTI*
	97	49	M	450	14	ZDV/*NRTI/PI*
Mean (SD)		**50 (11)**		**536 (221)**	**6 (4)**	
ZDV-	28	40	F	560	7	*Dual NRTI/NNRTI*
	30	50	M	410	2	TDF/FTC/R/DNV
	32	47	F	790	2	TDF/*NRTI/NNRTI*
	40	68	M	820	5	TDF/FTC/EFV
	62	39	F	380	8	ABC/3TC/NVP
	67	55	M	710	2	TDF/FTC/EFV
	81	64	M	600	10	ABC/3TC/NVP
	93	53	M	670	15	ABC/TDF/NVP
	113	37	M	420	1	*Dual NRTI/PI*
	123	54	F	600	6	*Dual NRTI/NNRTI*
Mean (SD)		**51 (10)**		**596 (156)**	**6 (4)**	

ZDV – zidovudine; TDF – tenofovir; 3TC – lamivudine; FTC – emtricitabine; ABC – abacavir; NVP – nevirapine; EVF – efavirenz; R – ritonavir (booster dose); DNV – darunavir; LPV – lopinavir; where information on regimen composition was not available, this is indicated by italics.

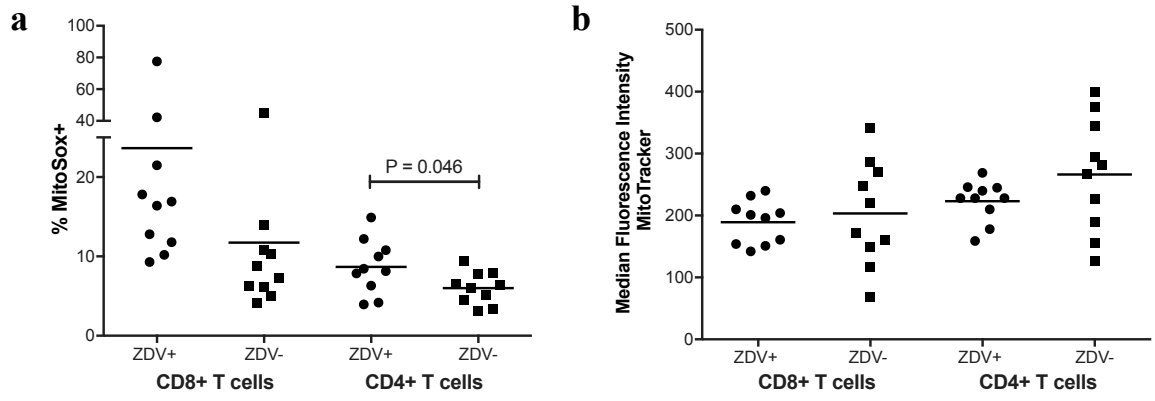

Figure 6.7: *In vivo* exposure to zidovudine increases mtROS in CD4+ T cells. PBMCs from patients on ZDV-containing and ZDV-sparing ART regimens (n = 10 each) were assessed for (a) mtROS (% MitoSox+ of CD8+ and CD4+ T cells) and (b) mtMass (Raw MFI MitoTracker of CD8+ and CD4+ T cells). No statistical tests were completed for mtMass because the MFI MitoTracker could not be directly compared between patient groups due to acquisition at different times. Horizontal lines represent the mean. Groups were analysed by paired t test.

6.2.5 Assay optimisation: autophagy

Quantification of autophagy in primary cells is challenging because of the cyclical nature of the process, the difficulty in using GFP-labelled constructs of LC3 and the heterogeneity of autophagic flux.[473,479] Previous work with an ImageStream-based assay showed that changes to autophagic flux in primary T cells are subtle and there is wide inter-donor variation.[473] Instead, a flow cytometry-based assay was chosen to assess the effect of ZDV on autophagic flux in T cells; this assay uses an LC3-specific FITC-conjugated antibody that binds LC3-I/II but the application of a selective permeabilisation reagent (Autophagy Reagent B) that extracts cytosolic LC3-I enables detection of autophagosome-bound LC3-II alone. Treating samples with a lysosomal inhibitor prevents degradation of LC3, amplifying the signal for detection with flow cytometry. From the MFI of the LC3 in an untreated and treated sample the Autophagy Activity Factor (AAF) can be calculated (section 2.10.5). The AAF normalises the autophagic flux of the treated condition to the untreated or basal autophagy activity; the higher the AAF the more autophagosome formation or autophagic flux inhibition has occurred.

Autophagy Reagent A (ARA) is a proprietary agent of unknown composition so its autophagic activity was first compared with that of a known lysosomal inhibitor, chloroquine. The ARA had a comparable effect on autophagic flux to chloroquine, with no effect from the control in CD8+ T cells (AAF for ARA vs. chloroquine vs. control, mean (SD): 0.96 (0.23) vs. 0.68 (0.12) vs. 0.002 (0.05), $P < 0.0001$) and CD4+ T cells (AAF for ARA vs. chloroquine vs. control, mean (SD): 0.69 (0.22) vs. 0.51 (0.09) vs. -0.008 (0.06), $P < 0.0001$; figure 6.8). Importantly, the recommended maximum number of cells was 150,000 per well of a 96-well plate (in contrast to the manufacturer's higher cell number recommendation) to ensure complete permeabilisation and consistent LC3 staining (figure 6.9). Finally, to ensure this assay could be used with HIV+ samples the

assay was tested with and without a 2% PFA fixation step. Even though fixation caused a slight loss of LC3 intensity the drop was consistent amongst all controls and still allowed the agents to amplify the LC3 signal (figure 6.10).

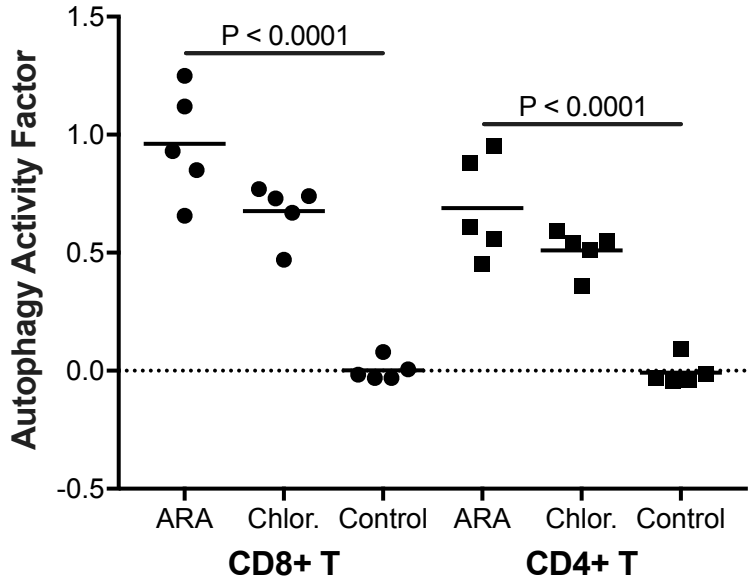

Figure 6.8: Autophagy Reagent A compares to chloroquine as a lysosomal inhibitor in flow cytometry-based autophagy assay. ARA, as supplied in the FlowCellect Autophagy LC3 Antibody-based Assay Kit from Millipore, was compared to chloroquine, a known late stage autophagy inhibitor, by culturing healthy donor PBMCs (n = 5) in media alone, ARA (1:1000), chloroquine (15 μM) or diluent control. The AAF was calculated for both CD8+ T cells (circles) and CD4+ T cells (squares). Horizontal lines represent the mean. Groups were analysed by one-way ANOVA.

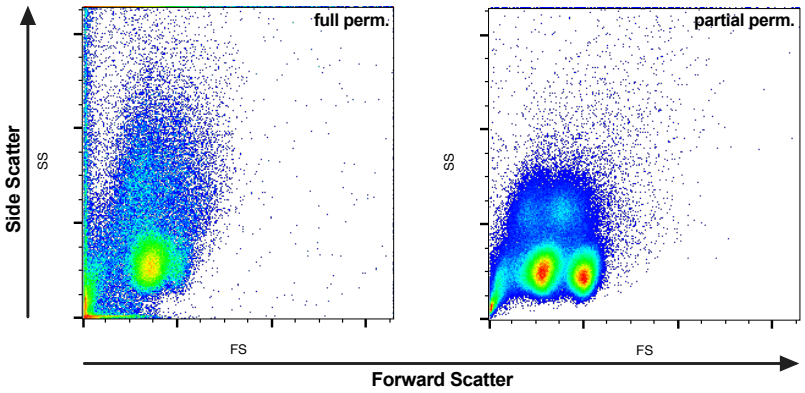

Figure 6.9: Excessive cell numbers results in partial permeabilisation. Flow cytometry forward scatter/side scatter plots of ~150,000 PBMCs (left) and ~1 million PBMCs (right) used with the recommended amount of Autophagy Reagent B permeabilisation reagent (100 μL 1x/sample). Lymphocytes should be in one cluster as on the left but partial permeabilisation results in two different sized groups of cells.

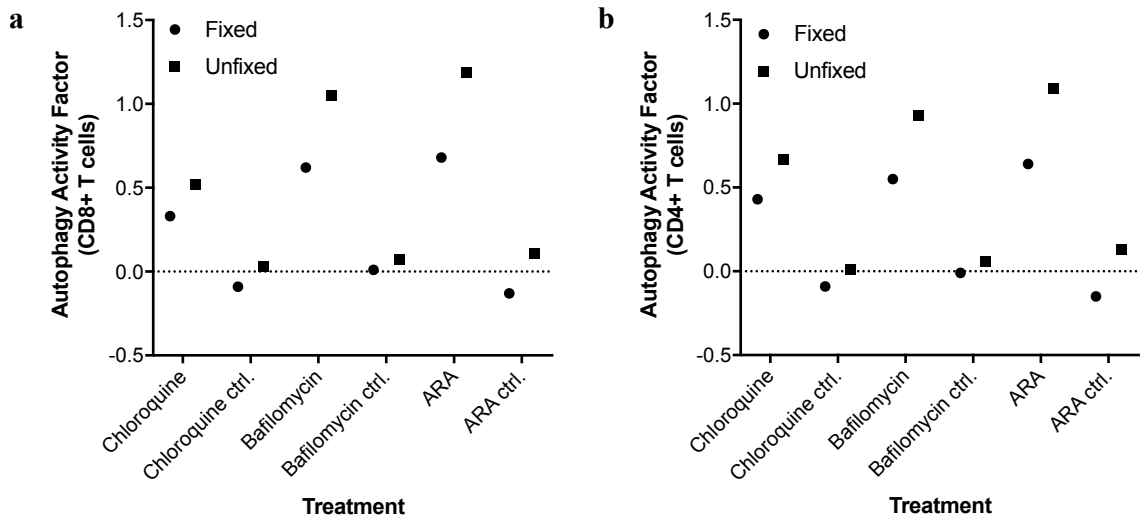

Figure 6.10: Fixation slightly decreases the AAF in primary T cells. PBMCs, cultured with chloroquine (15 μM), bafilomycin (0.1 μM), ARA (1:1000) or the appropriate diluent controls were stained for LC3 then either left unfixed or were fixed with 2% PFA. AAF is shown for (a) CD8+ T cells and (b) CD4+ T cells that were fixed (circles) and unfixed (squares) after staining.

6.2.6 *In vitro* exposure to ZDV does not affect autophagic flux in T cells

As defective and excess mitochondria are normally cleared by mitophagy to prevent cellular damage, the association between ZDV and mtROS production could be due to impaired autophagic flux.[472,480] To assess the short-term effect of ZDV on autophagy PBMCs from five donors were cultured with ZDV, ARA (autophagic flux inhibitor control) or PBS control for two or six hours followed by staining for LC3-II. The AAF did not differ significantly in the ZDV-exposed cells compared to the PBS control after either two or six hours for CD8+ T cells (six hour AAF ZDV vs. control, mean (SD): 0.02 (0.157) vs. -0.05 (0.03)) or CD4+ T cells (six hour AAF ZDV vs. control, mean (SD): 0.14 (0.18) vs. -0.05 (0.04); figure 6.11). The ARA positive control did increase the AAF as expected, with a significant increase between two and six hours for CD8+ T cells (ARA two vs. six hours, mean (SD): 0.96 (0.23) vs. 1.8 (0.26), P = 0.0006) and CD4+ T cells (ARA two vs. six hours, mean (SD): 0.69 (0.22) vs. 1.52 (0.22), P = 0.0003; figure 6.11).

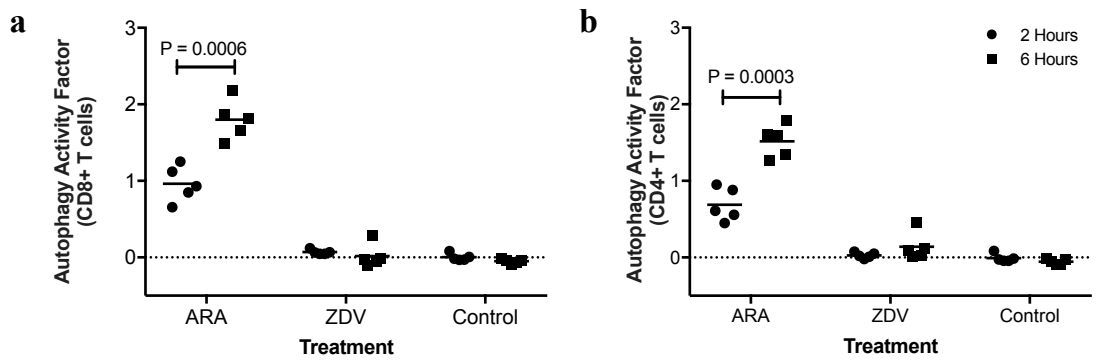

Figure 6.11: *In vitro* exposure to zidovudine does not alter autophagic activity

PBMCs from healthy donors (n = 5) were cultured with ARA (1:1000), zidovudine (5μM) or diluent control for two or six hours before staining for LC3. AAF is shown for (a) CD8+ T cells and (b) CD4+ T cells for the two hour (circle) and six hour (square) time points. Horizontal lines represent the mean. Groups were analysed by multiple t tests.

6.2.7 No difference in autophagic flux seen in T cells from patients on ZDV-containing or ZDV-sparing ART regimens

The effect of ZDV on autophagy may only be evident after long-term exposure. To investigate this, PBMCs from patients in the same ZDV-containing (n = 9) and ZDV-sparing (n = 10) ART cohorts as used previously (section 6.2.4) were cultured with and without ARA for 2 ½ hours. There was no significant difference in the AAF between the two groups for either CD8+ (AAF ZDV+ vs. ZDV-, mean (SD): 0.7 (0.12) vs. 0.8 (0.26)) or CD4+ T cells (ZDV+ vs. ZDV-, mean (SD): 0.62 (0.29) vs. 0.67 (0.26); figure 6.12).

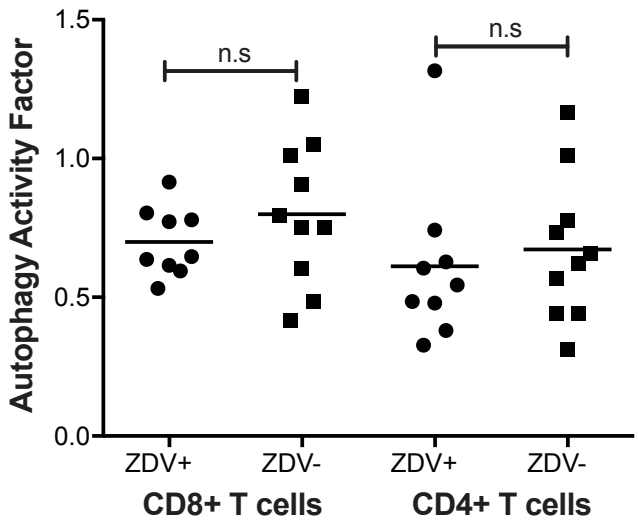

Figure 6.12: Autophagic flux does not vary in primary T cells from patients on ZDV-containing versus ZDV-sparing ART regimens. PBMCs from patients on ZDV-containing and ZDV-sparing regimens were cultured with and without then stained for LC3. The AAF, calculated by comparing the treated and untreated cells is shown for both CD8+ and CD4+ T cells from ZDV+ patients (circle) and ZDV- patients (squares). Horizontal lines represent the means. Groups were analysed by paired t tests.

6.2.8 Assay optimisation: apoptosis

Despite having no apparent effect on autophagy in *ex vivo* primary T cells, ZDV exposure may increase their susceptibility to apoptosis as the intrinsic pathway of apoptosis is linked to both mitochondrial damage and autophagy.[481] A previous report suggested that HIV-specific CTLs were preferentially primed for apoptosis and HIV-specific CTLs from elite controllers were more resistant to apoptosis compared to those from ART-treated chronic patients.[482] To distinguish any effect of ZDV on the HIV-specific versus total population of T cells, HIV-specific cells were identified by measurement of intracellular IFNγ after stimulation with HIV Gag peptide pools. Using unstimulated and SEB-stimulated PBMCs the appropriate concentration of the IFNγ antibody was determined following a titration (figure 6.13a). Induction of apoptosis was measured by expression of activated caspase-3. An FMO panel was initially used to set the caspase-3+ gate but this gate did not accurately capture the caspase-3+ population when applied to the fully stained sample; gates were better set on the negative control before applying to the samples (figure 6.13b – c).

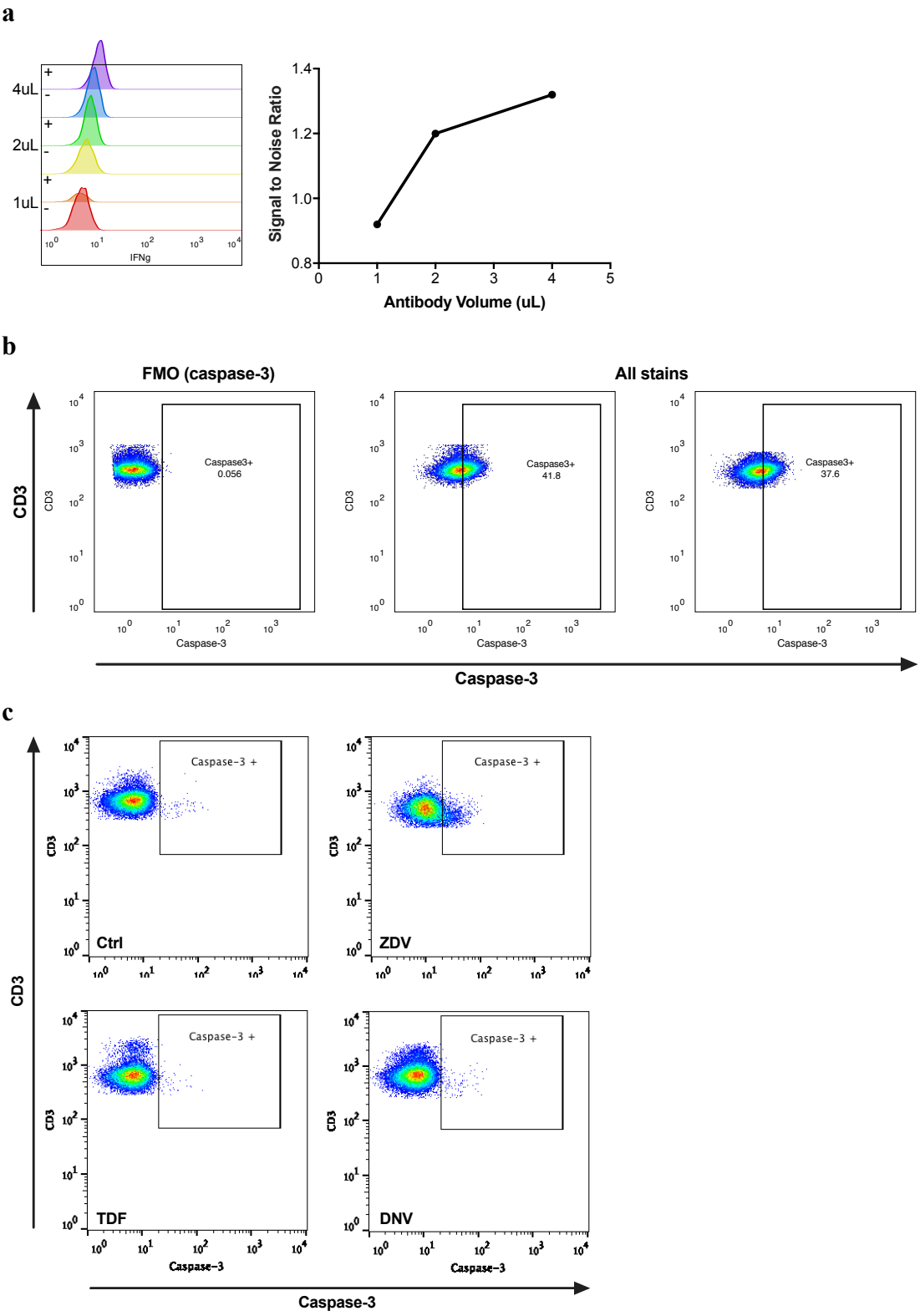

Figure 6.13: Optimisation of intracellular staining for IFNγ and caspase-3. (a) IFNγ-FITC antibody was titrated using unstimulated and SEB-stimulated PBMCs; the signal to noise ratio was calculated by comparing the MFI(IFNγ) of the positive and negative controls. (b) Originally to gate on the caspase-3+ population a caspase-3-PE FMO was applied to samples but the gate unnaturally bisected the T cell population. As a result, (c) gating on the caspase-3+ population was based on the untreated T cell population.

6.2.9 *In vitro* exposure to ZDV increases apoptosis in T cells

To assess the effect of ZDV on spontaneous apoptosis in T cells, healthy donor PBMCs (n = 6) were cultured with ZDV, TDF or DNV for six hours. The frequencies of caspase-3+ cells within the entire CD8+ and CD4+ T cell subsets were measured using flow cytometry. Short-term exposure to ZDV significantly increased caspase-3 expression compared to TDF, DNV or the PBS control in both CD8+ T cells (ZDV vs. TDF vs. DNV vs. control, mean (SD): 12.1% (7.1) vs. 0.8% (0.6) vs. 1.2% (2.0) vs. 0.7% (0.6), P = 0.008) and CD4+ T cells (ZDV vs. TDF vs. DNV vs. control, mean (SD): 5.1% (2.5) vs. 0.5% (0.3) vs. 0.4% (0.2) vs. 0.5% (0.4), P = 0.006; figure 6.14a). Caspase-3 expression was also confirmed by confocal microscopy of ZDV-exposed CD8+ T cells (figure 6.14b).

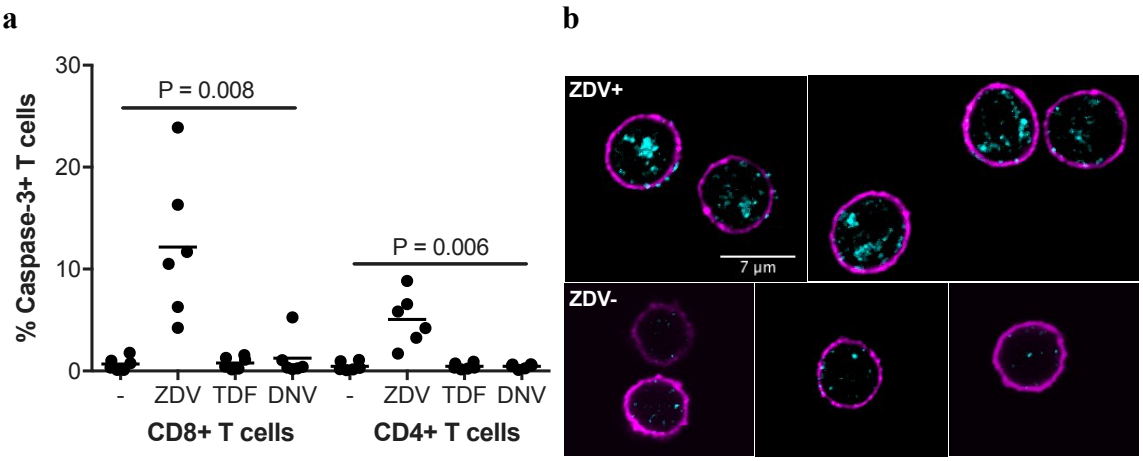

Figure 6.14: *In vitro* exposure to ZDV increases susceptibility to apoptosis in T cells. Healthy donor PBMCs (n = 6) were cultured in media alone (-), zidovudine (5 μM), tenofovir (10 μM) or darunavir (10 μM) for six hours before intracellular staining for caspase-3. (a) The % caspase-3+ CD8+ T cells and CD4+ T cells are shown. (b) Representative confocal image of CD8+ T cells exposed to zidovudine (ZDV+) or media alone (ZDV-); cyan = caspase-3, magenta = CD8. Horizontal bars represent the mean. Groups were analysed by one-way ANOVA.

6.2.10 *Ex vivo* T cells from HIV patients on ZDV-containing ART regimens demonstrate increased apoptosis compared to those from patients on ZDV-sparing regimens

To assess the susceptibility to apoptosis of T cells exposed to ZDV long-term *ex vivo* PBMCs from patients on ZDV-containing (n = 6) and ZDV-sparing ART (n = 7) regimens were cultured with PBS (negative control), SEB (positive control) or a pool of overlapping HIV Gag peptides (representing the full Gag protein sequence and split into pool A and pool B – appendix 2.2) for six hours. After stimulation, the samples were analysed for caspase-3 expression in Gag-specific (IFNγ+) and total CD8+ T cell and CD4+ T cell populations. Unfortunately, the IFNγ+ populations were too small to gate accurately on the caspase-3+ subset; as a result, the caspase-3 populations reported are the total CD8+ or CD4+ T cell populations from the negative control with 'spontaneous apoptosis.' The samples from patients on ZDV regimens had a significantly greater proportion of T cells that were programmed for spontaneous apoptosis for both CD8+ (ZDV+ vs. ZDV-, mean (SD): 0.13% (0.06) vs. 0.05% (0.03), P = 0.012) and CD4+ T cell subsets (ZDV+ vs. ZDV-, mean (SD): 0.22% (0.03) vs. 0.06% (0.04), P < 0.0001; figure 6.15). These data indicate that CD4+ T cells were more affected than CD8+ T cells (P = 0.01). However, the proportion of apoptotic cells was less than after *in vitro* ZDV exposure (figure 6.14).

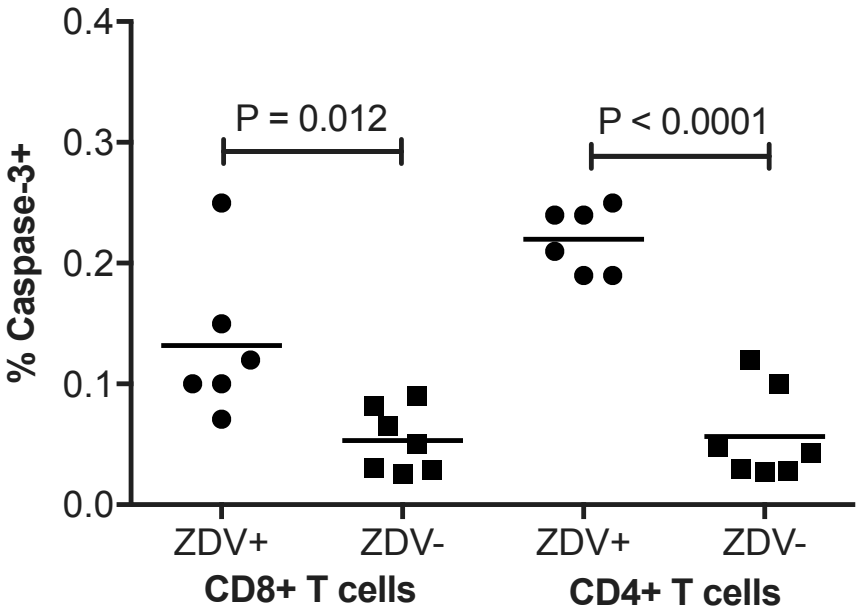

Figure 6.15: T cells from ZDV-exposed patients show increased susceptibility to apoptosis. PBMCs from patients on ZDV-containing (n = 6) and ZDV-sparing (n = 7) regimens were stained for caspase-3 expression. % Caspase-3+ CD8+ T cells and CD4+ T cells are shown. Horizontal bars represent the mean. Groups were analysed by unpaired t test.

6.2.11 Exposure to ZDV *in vivo* does not affect the viral inhibitory activity of CD8+ T cells

ART-treated patients exhibit impaired CD8+ T cell antiviral activity as compared to the rare individuals who spontaneously control HIV (elite controllers).[196,432,483] Whether this reflects immune compromise that necessitates initiation of ART in these patients or incomplete immune reconstitution during ART is still unresolved. To assess whether the toxic effects of ZDV on CD8+ T cells, as indicated by increased mtROS and susceptibility to apoptosis, were associated with impaired viral inhibitory activity T cells from the previously mentioned patient cohorts were used in a viral inhibition assay. The frequency of p24+ CD4+ T cells of HIV-infected CD4+ T cell samples cultured alone or with autologous CD8+ T cells was used to calculate the percentage elimination (section 2.7). There was no significant difference in the viral inhibitory activity between CD8+ T

cells from patients on ZDV-containing (n = 9) or ZDV-sparing regimens (n = 10) (ZDV+ vs. ZDV-, mean % elimination (SD): 48.77% (23.32) vs. 53.74% (24.52); figure 6.16).

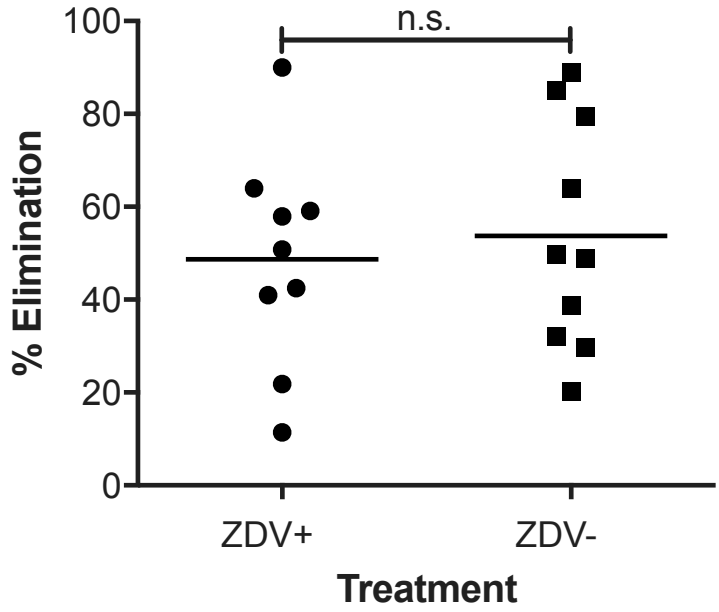

Figure 6.16: Long-term exposure to ZDV does not affect CTL viral inhibitory activity. CD4+ T cells from patients on ZDV-containing (n = 9) and ZDV-sparing (n = 10) ART regimens were superinfected with HIV-1_{IIIB} (MOI = 0.01) then cultured with and without autologous CD8+ T cells at an E:T ratio of 2. After a six day co-culture the samples were stained for p24 Gag and the % elimination was calculated. Horizontal lines represent the mean. Groups were analysed by unpaired t test.

6.3 Discussion

The work in this chapter sought to investigate the effect of therapeutic concentrations of ZDV on the mitochondrial turnover and function of primary T cells after both short and long-term exposure. To explore the possibility that ZDV has other means of toxicity than mtDNA depletion the mitochondrial turnover in cells exposed to ZDV was investigated. T cells exposed *in vitro* to ZDV produced a significantly higher quantity of mtROS than cells exposed to either tenofovir, an aNRTI, or darunavir, a protease inhibitor, suggesting the mechanism was thymidine analogue-specific. The effect could be seen after only six hours of culture with the drug (figure 6.6), significantly less time than the 15 days reported by Yamaguchi et al. for their investigation of ZDV-altered mitochondrial energy production in cultured lymphoid cells.[484] Their study also highlights the possibility that ZDV's mitotoxic effects could be due to inhibition of the election transport chain as the ZDV-exposed human lymphoid cells exhibited decreased ATP production in addition to the mtROS accumulation reported in this chapter.[463,484]

For the patients on ZDV-containing and ZDV-sparing regimens there was only a significant increase in mtROS in CD4+ T cells, although the trend was present for CD8+ T cells (figure 6.7); the standard deviation for the CD8+ T cells was much higher highlighting the heterogeneity of the mtROS+ expression. These patients were on ART for a median of six years at the time of sampling and thus would have all had long-term exposure to ZDV. The other drugs in the backbone, as well as the time on treatment, were matched between cohorts as best as possible to limit any other confounding factors. It is interesting to note the difference in mitochondrial turnover between CD8+ T cells and CD4+ T cells. Under both *in vitro* and *in vivo* exposure to ZDV CD8+ T cells expressed higher proportions of mtROS+ cells. During T cell development CD8+ T cells reduce their mitochondria by 80%, compared to double positive thymocytes, while CD4+ T cells

only reduce their mitochondria by 50%.[480,485] This increased elimination may reflect a lower tolerance for superfluous and damaged mitochondria and suggest why CD8+ T cells exposed to ZDV express more mtROS.

If the mtROS+ cell accumulation was caused by a downstream effect on autophagy (mitophagy) there should be a concomitant increase in mitochondrial mass. While the ZDV-exposed cells did express a higher mtMass the change was not significant compared to the effects of other antiretroviral drugs (figure 6.6). This may be because mtMass was only measured after six hours and it could take longer for damaged mitochondria to significantly amass.[472,486] Unfortunately, mitochondrial mass could not be compared in the patient samples, due to the lack of a $mtMass^{high}$ population to compare, so any additive effects from long term exposure could not be measured (figure 6.7).

Previous studies concluded that ZDV's toxicity in hepatocytes and adipocytes derived from its ability to inhibit autophagic flux; inhibiting the late stages of autophagy prevents the final recycling of damaged mitochondria, facilitating their accrual, and the accumulation of mtROS. However, the work in this chapter showed that ZDV did not affect autophagic flux in primary T cells either through short term *in vitro* culture or through long term *in vivo* exposure (figures 6.11 – 6.12). The discrepancies between the work of Stankov et al. and the work in this thesis may lie in the experimental design differences. Stankov's findings were primarily in hepatocyte and adipocyte cell lines, which were used as a tool to study the mechanisms underlying the reported morbidities such as lipoatrophy and hepatic steatosis.[466,468,469,487,488] These cells were able to withstand concentrations of ZDV above the estimated clinical concentration for longer exposure times without deleterious effects, resulting in a larger effect on autophagy than seen in this chapter. Additionally, the effects on autophagy were less pronounced when

primary hepatocytes were tested so the relevance of these findings to clinical use of the drug may be questionable.[471,472] For the work in this chapter, any attempt to expose primary T cells to concentrations higher than the clinical range, or for longer than 24 hours, resulted in excessive cell death. Additionally, the assay used may not have been sensitive enough to detect any effect on autophagy under these clinically relevant conditions. Thus the effects reported by Stankov et al. may be specific to the cell types they studied or any effects on T cells *in vivo* are subtle and only investigating total T cell populations has diluted them. Further investigation of effector and memory subsets may uncover different susceptibilities to ZDV's effect on autophagy as CD8+ T cells utilise autophagy differently during effector and memory cell differentiation.[489]

Detecting changes in autophagy in primary T cells poses methodological difficulties based on the cyclical nature of the process. Most autophagy assays quantify the accumulation or loss of the major autophagic proteins such as LC3-I, LC3-II or p67. As autophagic proteins are naturally recycled combinations of known pharmacological autophagy activators and inhibitors must be used in combination to determine whether an accumulation of LC3-II, for example, relates to an increase in autophagy or a late-stage block.[479,490,491] Primary T cells, which exhibit varied but high basal levels of autophagy, do not always react to known autophagy-altering agents the same way (or to the extent of cell lines) so careful consideration must be taken when choosing appropriate controls for an experiment. Initially a combination of E64d/Pepstatin A was tested as a positive control but these late-stage inhibitors only had a modest effect on autophagic flux, which made interpretation of the effects of ZDV difficult. Additionally, the diluents used contained DMSO or ethanol, which can each have their own effects on autophagy; this may have contributed to the minimal difference seen between E64d/Pepstatin A and the diluent control (ethanol) in the mitochondrial turnover assays (figure 6.5). Chloroquine,

diluted in water, proved to be a more potent late-stage positive control, eliciting a clearer LC3-II signal that could be readily measured by multiple assays.

Previous studies have used fluorescently tagged LC3 proteins, organelle specific dyes or antibodies to trace the generation and loss of autophagosomes via microscopy, immunoblotting or flow cytometry.[490,491] The utility of these approaches, often only semi-quantitative, depends on the sensitivity of the antibodies, required expertise (as in the case of morphological quantification) and quantity of cells required. For example, Western blots cannot differentiate between cell types in a mixed population unless cells are pre-sorted; however, this has been widely used in animal models where genetic modification of the autophagy genes has caused a significant loss or gain of function.[471,480,485,491,492] For detecting autophagy in PBMC samples flow cytometry methods are more applicable because they facilitate sorting of cell populations and the antibody staining provides a more quantitative method. Previously an ImageStream-based assay was tested for its ability to measure autophagic flux. Originally reported by Phadwal et al. this assay provided quantitative autophagy readouts of different cell subsets by combining flow cytometry with individual cell imaging at a high resolution.[473] Measurement of the co-localisation of two probes in a cell (reported as the Bright Detail Similarity, (BDS)) was applied for the detection of autolysosomes using a reagent panel to mark LC3 and lysosomal proteins. Induction of autophagy, as by starvation, or inhibition, as by flux inhibitors, increased the number of autolysosomes and thus the BDS. However, overall this assay was unsuitable for further analysis of autophagy as it lacked the sensitivity to detect the small effects that are observed in primary cells with intact autophagic capacity; also, the requirement for a large quantity of cells restricted its use when working with limited patient samples. The greater sensitivity of the flow cytometry based assay applied in this chapter allowed for the use of smaller sample sizes than those required for

ImageStream, with simultaneous identification of T cell subsets. However, the completeness of the selective permeabilisation reagent (designed to selectively remove LC3-1) is unknown and it is possible that LC3-1 may remain within the cells affecting the intensity ratios.

Cells exposed to ZDV not only showed an increase in mtROS but also activated caspase-3, a marker of programed cell death (figures 6.14 – 6.15). This is not surprising as mitochondrial metabolism and apoptosis are intimately linked through their association with autophagy. While the relationship between apoptosis and autophagy is multifaceted, in many cases autophagy represents as adaptation to stress that suppresses apoptosis to avoid cell death (reviewed in [493–495]). During nutrient-rich states basal levels of autophagy act as a quality control mechanism ensuring that excess and irreversibly damaged organelles, such as mitochondria, are recycled (mitophagy). In times of stress such as starvation, ER stress or hypoxia autophagy is upregulated to limit the damage caused by mtROS and to recycle macomolecules.[496] Without the regulation by autophagy the intrinsic signalling pathway of apoptosis can be triggered. The intrinsic pathway of apoptosis relies on non-receptor mediated stimuli, including absence of growth factors and hormones or the presence of toxins, free radicals and viral infections, to produce intracellular signals that act on targets within the cell.[497] These stimuli cause changes in the inner mitochondrial membrane eventually resulting in the release of pro-apoptotic proteins into the cytosol.[498] These proteins then trigger a cascade that results in effector proteins, such as caspase-3, which cleave key cellular components leading to the controlled dismantling of the cell (apoptosis).[497]

T cells from mice lacking critical autophagy-related genes (ATG) expressed increased ROS and mitochondrial mass and were more susceptible to apoptosis.[480,485] Additionally, Watanabe et al. reported that autophagy-defective human T cells

(transfected with vectors encoding ULK1 K461, a kinase dead mutant that blocks autophagy) accumulated mitochondria and mtROS, eventually resulting in enhanced apoptosis.[499] This work suggests that the homeostatic mechanism of autophagy may feed into an intrinsic cell death pathway. While the work in this chapter suggests ZDV did not reduce autophagy in T cells from CHI patients, a possible explanation for the effect of ZDV exposure on caspase-3 expression is that ZDV is preferentially phosphorylated in activated T cells and thus may compound the known effect of HIV on activation-induced apoptosis.[500–502] However, the functional outcome of these effects did not impact the antiviral activity of CTLs from CHI patients (figure 6.16). Even if ZDV was causing spontaneous apoptosis in CD8+ T cells from HIV patients the death was not significant enough that an effect was seen on top of the chronic CTL exhaustion phenotypically characterised in CHI patients.

Further investigation is required to uncover the causal mechanism behind increased mtROS production in ZDV-exposed T cells, as the effect was not related to an autophagy-dependent mechanism. Testing a larger range of ZDV concentrations and time courses, possibly requiring a T cell line to withstand the toxicity, might help determine the limits, if any, of ZDV's effect on autophagy. As the toxicity is definitely affecting the mitochondria, further tests examining the morphology and function of the mitochondria, especially in relation to triggering apoptotic pathways, would be useful to map the chain of events leading to the failed immune reconstitution.

This investigation highlighted the complexities of the mechanism of ZDV toxicity in exposed primary T cells. While ZDV is no longer part of current adult ART regimens this work has relevance as ZDV is still widely used for post-exposure prophylaxis and in low resourced settings for treatment of vertically acquired HIV infection. It has been reported that infants exposed to the drug *in utero* can exhibit symptoms of mitochondrial

dysfunction such as neurological abnormalities. T cell toxicity or impaired immune reconstitution could thus have dangerous impacts on long term health for the infants.[503–506] Improvements to in the safety of ART regimens have benefited adults more than children and this needs to be urgently addressed.

6.4 Questions addressed in this chapter

- *How does zidovudine affect mitochondrial turnover in primary T cells?*

  In vitro and *in vivo* exposure to ZDV increased mitochondrial reactive oxygen species in T cells compared to exposure to other ART regimens; assessment of mitochondrial mass was inconclusive (figures 6.6 – 6.7). However, exposure to ZDV did not affect autophagic flux compared to positive controls (figures 6.11 – 6.12). The autophagic flux assay may not have been sensitive enough to detect the small changes in autophagic activity in the highly variable primary T cells (sections 6.2.2 – 6.2.7).

- *Did exposure to ZDV increase the susceptibility to apoptosis in T cells?*

  Yes. *In vitro* and *in vivo* exposure to ZDV increased the percentage of caspase-3+ T cells (figures 6.14 – 6.15; sections 6.2.9 – 6.2.10).

- *Did exposure to ZDV affect the viral inhibitory activity of CD8+ T cells?*

  No. There was no difference in viral inhibitory activity using CD8+ T cells from patients on ZDV-containing versus ZDV-sparing regimens despite the increased susceptibility to apoptosis and mtROS after exposure to ZDV (figure 6.16; section 6.2.11).

CHAPTER SEVEN: FINAL DISCUSSION

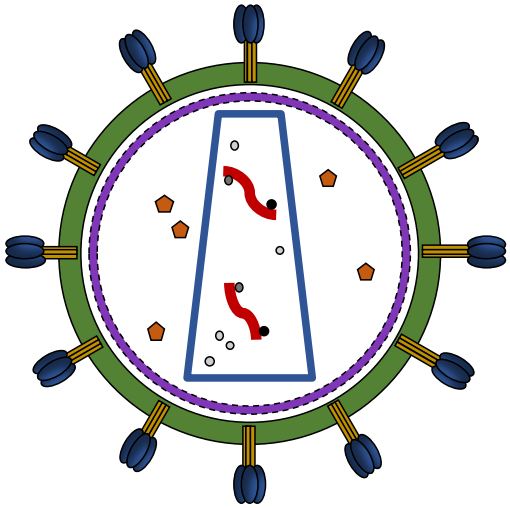

For the work in this thesis engineered bispecific T cell receptors (ImmTAVs) were applied to investigate the failure of CTLs to kill HIV-infected CD4+ T cells. The inability of CTLs to completely control the virus in most PLWH has been well documented both *in vivo* and *in vitro*.[74,187,245,507] Because initial responses that attempt to clear the virus during PHI fail, persistent viraemia results in a chronically stimulated population of CTLs with impaired function. Integration of HIV DNA into host cell chromosomes before CTL responses are fully developed also results in the establishment of a viral reservoir of latently infected cells that conventional ART is unable to clear.[116,117,330,508–510] To address these aspects of HIV persistence, firstly, a primary T cell model of latency was used to examine the Gag expression in resting CD4+ T cells, which constitute the largest component of the HIV reservoir, and their susceptibility to a 'shock and kill' intervention. Secondly, a microscopy-based method was extensively developed in order to compare the immunological synapses formed by HIV antigen-expressing T cells and primary CD8+ T cells from healthy donors and patients with chronic HIV infection, both naturally and under redirection by ImmTAVs. Finally, *in vivo* and *in vitro* exposure to different antiretrovirals, especially zidovudine, were compared in primary T cells to measure the mitotoxic effects of ART and the impact on CTL function.

7.1 Immunological synapses and the HIV reservoir

To investigate the potential heterogeneity of the latent reservoir and implications for immune targeting, direct infection of resting CD4+ T cells was employed to create a population of HIV-infected T cells that had low Gag expression but that did not spread infection. Despite the reduced antigen presentation compared with infection of activated CD4+ T cells, the HIV-specific ImmTAV, m121, was able to redirect healthy donor CD8+ T cells to eliminate up to 40% of the infected cells without the need for latency reversal. This suggests that the paradigm of latency as a state of transcriptional silence

needs revision. Addition of LRAs did reactivate virus in this model but did not improve elimination of latently infected cells, possibly because the LRAs did not increase the SL9 epitope density on the surface. A further observation from the resting cell model was that CTLs from CHI donors were able to eliminate less than 6% of the resting infected cells naturally and ImmTAV-redirection did not restore the antiviral activity to that of the ImmTAV-redirected HD CD8+ T cells (chapter three). Importantly, the immunological synapses formed by the ImmTAV-redirected HD CD8+ T cells appeared more mature than those with the CHI donor CD8+ T cells: more Zap70 localised to the synapse, the MTOC moved closer to the synapse and more cells had perforin docked at the synapse. With ImmTAV redirection MTOC localisation was found to be normal in the CHI donor CD8+ T cells but perforin mobilisation was reduced (chapter five). Collectively these results suggest that a subset of the cells of the HIV reservoir may be susceptible to elimination but persistent defects in HIV-specific CTLs and to a lesser extent, all other CD8+ T cells of CHI patients, render them unable to form fully functional synapses to clear these cells.

In addition to contributing to the failure to clear latently infected cells, *in vivo* the immunological synapse may also play a role in the induction and maintenance of latency. An APC can direct the fate of an interacting lymphocyte and could condition a CTL to have a less effective antiviral response or change the biology of a latently infected CD4+ T cell to prolong latency.[511] When Evans et al. investigated the relationship between myeloid DCs and latently infected memory CD4+ T cells they found that cell-to-cell contact increased the frequency of HIV DNA integration and latent HIV infection. Blocking of CD18, the β chain of LFA-1, which binds to ICAM-1, reduced the number of latently infected cells, thus demonstrating the importance of a stable IS for DC-induced T cell latency. Examination of gene transcriptional changes suggested that the cell-cell

interaction impacted two main nodes: up-regulation of type I interferons, inhibiting viral replication, and down-regulation of NF-κB, inducing further T cell quiescence.[512] As resting CD4+ T cells can be found in lymphoid tissue where DCs are also frequent, the importance of this cell-cell contact for inducing latency presents a difficult mechanism to target. Other groups also confirmed the importance of cell-to-cell contact for inducing latency as latent infection was more commonly found in resting lymphoid cell aggregates and in co-cultures of resting CD4+ T cells and endothelial cells; the stimulation provided by the endothelial cells (possibly mediated by the interaction of the endothelial cell costimulatory molecule, CD58, interacting with CD2 on the T cell) rendered the resting CD4+ T cells, particularly the memory T cell subset, permissible to latent infection.[345,511–515]

The maintenance of latency through contact with an APC at the IS may be achieved through the promotion of signals to induce stem cell-like qualities in the infected cell. Memory CD4+ T cells are ideal reservoirs of latent virus because of their ability to survive long-term, self-renew and differentiate upon stimulation – all of which are stem cell-like properties. The self-renewal of embryonic stem cells relies on the transcriptional coactivator, Yes-associated protein (YAP). However, YAP expression was also sustained in T cells after the activation of PD-1, suggesting that the IS could induce a long-lived stem cell-like memory phenotype in infected CD4+ T cells.[511,516,517] Indeed, more integrated HIV DNA was found in PD-1^{high} cells compared to PD-1^{low} cells from viraemic donors.[511,518] The PD-1/PD-L1 pathway inhibits T cell activation via the dephosphorylation of signalling molecules such as Zap70. As the viral reservoir is established during the first days of primary infection, negative signals from inhibitory molecules like PD-1 could push the cell towards a quiescent phenotype by limiting the cellular transcription factors needed for active HIV gene expression. Addition of an anti-

PD-1 blocking antibody in an *in vitro* system could provide information on whether limiting this signal reduces the state of latency and makes the cells more susceptible to elimination; attenuation of PD-1 signalling during PHI could limit seeding of the reservoir although there is the risk of catastrophic immune activation.

Future work with a latency model that includes other participating cells could provide more information on the effect of cell-to-cell induced latency on HIV protein expression and susceptibility to clearance of reservoir cells. This could also include the influence of regulatory cells on clearance of reservoir cells as Siewe et al. reported that regulatory B cells may play a role in attenuating CTL responses after reactivation of HIV latent reservoirs.[519] Additionally, other cell populations contribute to the latent reservoir, such as cells of monocytic lineage, which can become infected with virus but survive long-term as they do not generally support viral replication.[100–102,105,520] While the work presented in this thesis focused on the impact of HIV infection on the effector arm of the immune response, further experiments with diverse cell targets and virus would provide more information about how latent infection of an APC could influence synapses with CD8+ T cells. A recently reported marker of latently infected cells, CD32a, could be used to identify potential synapses with latently infected cells.[521]

7.2 CTL exhaustion and metabolism

PLWH must remain on life-long ART to suppress viral replication but the chronic use of different antiretrovirals may be associated with adverse effects in the long-term. While these are less common with modern ART, older agents in the NRTI and PI classes, especially zidovudine (ZDV) and stavudine, have been linked to morbidities including metabolic syndrome, impaired immune reconstitution and mitochondrial toxity.[468,487,522,523] In this thesis, ZDV-exposed T cells were shown to be more prone to mtROS production and spontaneous apoptosis. Despite previous studies that linked

ZDV's mitotoxic effects to an inhibition of autophagic flux, autophagy assays were not sensitive enough to detect any changes in the primary T cells exposed to clinically relevant concentrations of ZDV. There was no difference in the antiviral activity of CD8+ T cells from either ZDV-exposed or ZDV-spared patients (chapter six); however, any effect may have been masked by the generalised dysfunction of CD8+ T cells from CHI donors that was evident from the analysis of immunological synapse formation (chapter five) and resting cell infection viral inhibition assays (chapter three). Furthermore, CD39 expression, an identifier of exhausted cells, was higher in CD8+ T cells from CHI donors compared to healthy donors, consistent with previously published data (chapter three).[187,336]

The dysfunction described in the CTLs of CHI patients in this thesis may be a result of the HIV-induced chronic antigenic stimulation from HIV altering the metabolic profile of the T cells. Under normal conditions the metabolic requirements of a T cell change upon encounter with antigen. Naïve T cells rely on oxidative phosphorylation (OXPHOS) or fatty acid oxidation (FAO) to produce the required ATP. Without TCR ligation ATP production, mitochondrial potential and metabolic substrates decrease leading to apoptosis.[524] Once a naïve T cell is activated the requirement to rapidly divide favours the switch to glycolysis to incorporate nucleotides, amino acids and lipids into the biomass.[525,526] This switch requires ligation of the TCR and costimulatory molecules, which signal for the cell to increase glucose transporter 1 (GLUT1) expression to promote glucose uptake.[527] mTOR integrates signals from the intracellular environment and the pathway is required to sustain glycolysis in CTLs.[528] Finally, when a T cell begins to transition to a memory state its metabolism switches to FAO, which allows for rapid ATP generation upon secondary antigenic challenge.[529] Just as a T cell's metabolic needs change after antigenic stimulation a stimulated T cell also has different autophagic

requirements. Using *Atg7*$^{fl/fl}$*Gzmb*-Cre mice, in which antigenic stimulation results in the deletion of *Atg*7 in granzyme B-expressing CD8+ T cells, Xu et al. reported that there was no difference in T cell proliferation and differentiation (into functional effector T cells) between the wild type and autophagy-deficient virus-specific CD8+ T cells after infection with lymphocytic choriomeningitis virus (LCMV); however, few autophagy-deficient antigen-specific T cells survived the contraction phase to transition into memory cells. A metabolite analysis of *Atg7*-sufficient versus *Atg7*-deficient cells found that pathways involved in lipid biosynthesis and FAO were dysregulated in the absence of Atg7. These results suggest that while T cells may have low autophagy requirements for anabolic processes, autophagy is required for the survival of effector CD8+ T cells; autophagy may be used to produce the lipid substrates necessary for FAO or to remove damaging ROS and defective mitochondria to promote the longevity of the memory T cell population.[489,530]

T cells adapt their metabolism to meet the energetic requirements of each stage of their development but chronic antigenic stimulation has been shown to alter this tightly regulated programme of metabolism. Bengsch et al. compared the metabolic profiles of murine T cells infected with an acutely cleared strain (Arm) and a chronic strain (clone 13) of LCMV. Chronic antigenic stimulation drove high mTOR activity early in infection, which increased the dependence on glycolysis and OXPHOS. However, with limited glucose uptake the exhausted T cells (T_{ex}) could not meet the bioenergetic demand. This early metabolic dysfunction resulted in ROS production, mitochondrial depolarisation, fused mitochondria and consequently, the exhausted effector function described during chronic infection. Despite transcriptional upregulation of genes necessary for metabolic pathways, the T_{ex} did not switch to OXPHOS in the absence of glucose.[531] In a separate study investigating T cell exhaustion in HBV patients, metabolic

dysregulation related to glycolysis dependence also preceded major mitochondrial and functional changes in exhausted HBV-specific T cells; this was in contrast to CMV-specific T cells from the same patients which were able to switch to OXPHOS in the absence of glucose.[532] An overreliance on glycolysis and a failure to switch to OXPHOS in the absence of appropriate glucose supplies may drive the dysfunction in exhausted HIV-specific CTLs; an analysis of the GLUT1 expression and glucose dependence of CD8+ T cells from patients with divergent clinical outcomes could uncover a mechanism behind the impaired antiviral activity and defective synapse formation described in this thesis. Further investigation of the T cell subsets recruited to the infected targets, their metabolic requirements and their mitochondrial health (as measured in chapter six) could be important for identifying new therapeutic targets. Reversal of generalised CD8+ T cell exhaustion will be essential for achieving maximal therapeutic benefit from ImmTAVs and other retargeting agents in HIV cure strategies.

PD-1 has also been implicated in the reported metabolic dysfunction of CD8+ T cells; PD-1 blockade is a heavily favoured method to reverse T cell exhaustion because of its upregulation during chronic HIV infection. Bengsch et al. reported that PD-1 negatively regulated PGC-1α, a key transcriptional regulator of genes involved with metabolism and mitochondrial biogenesis.[531] The metabolomic analysis reported in the LCMV model by Bengsch et al. suggests that the mechanism underlying the efficacy of PD-1 blockade in reversing CD8+ T cell exhaustion is linked to PD-1's dysregulation of the metabolism of an effector T cell; blocking the PD-1 pathway relieved the metabolic limitations and allowed the cell to meet the bioenergetic demands crucial for proliferation. However, PD-1's apparent unwanted effects may be crucial for cell survival, allowing chronically stimulated cells to survive as terminally differentiated CTLs with adapted metabolic requirements, albeit at the cost of their effector function.[533]

This raises the possibility of treating T cell exhaustion by normalising the regulation of metabolism in effector T cells. If achieved early in the course of HIV infection, T cell dysfunction could be averted.[531] In future work it would be interesting to explore the effects of manipulating glucose availability in culture on the antiviral function of exhausted CD8+ T cells.

7.3 HIV in perspective

Understanding the impact of chronic infection on T cell effector function is crucial for the development of targeted therapeutics against HIV. Many PLWH are unaware of their status and encouraging testing does not always reach the groups most at risk. Even on an effective ART regimen, PLWH must cope with daily side-effects.[534] If achieved, the UN's ambitious 90-90-90 goal – ensuring 90% of PLWH know their status, starting 90% of them on ART and achieving viral suppression in 90% of those people – could help curb the HIV epidemic but it faces many hurdles that are both culturally and economically dependent.[1,535] While some antiretrovirals are nearing the end of their patent, opening up the opportunity for cheaper generics, the cost of HIV to healthcare systems is still great; HIV treatment costs ~£360,800 per person in the United Kingdom and ART makes up the majority of these healthcare costs.[536] A functional cure for HIV, such that PLWH could maintain control of the virus without daily ART, would have enormous benefits on the health and wellbeing of PLWH and would alleviate the burden on healthcare systems. The m121 ImmTAV used in this thesis was specific for the HLA-A2-presented SL9 epitope of HIV's Gag, however, there is the potential to broaden the application of the ImmTAV through the development of additional ImmTAVs. ImmTAVs targeting different HIV epitopes could be used at the same time to eliminate a more diverse population of infected cells, expressing non-SL9 epitopes, and ImmTAVs specific for epitopes presented by different HLA alleles could be applied to a larger

population of PLWH. As the work presented in this thesis provides proof of concept for using ImmTAVs to target resting infected cells there is the potential to eliminate a proportion of the HIV reservoir, one of the key barriers to an HIV cure.

REFERENCES

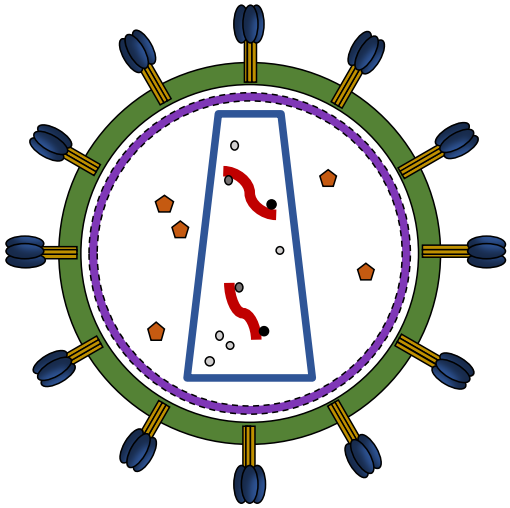

1. UNAIDS (2014). *90-90-90*.

2. WHO (2016). *Progress Report 2016: Prevent HIV, test and treat all*.

3. D'arc, M, Ayouba, A, Esteban, A, Learn, GH, Boué, V, Liegeois, F, *et al.* (2015). Origin of the HIV-1 group O epidemic in western lowland gorillas. *Proc. Natl. Acad. Sci.* **112**: E1343–E1352.

4. Sharp, PM and Hahn, BH (2011). Origins of HIV and the AIDS pandemic. *Cold Spring Harb. Perspect. Med.* **1**: 1–22.

5. Hahn, BH, Shaw, GM, De Cock, KM and Sharp, PM (2000). AIDS as a zoonosis: scientific and public health implications. *Science* **287**: 607–14.

6. Kanki, P, Traver, K, MBoup, S, Hsieh, C-C, Marlink, R, Gueye-NDiaye, A, *et al.* (1994). Slower heterosexual spread of HIV-2 than HIV-1. *Lancet* **343**.

7. Marlink, R, Kanki, P, Thior, I, Travers, K, Eisen, G, Siby, T, *et al.* (1994). Reduced Rate of Disease Development After HIV-2 Infection as Compared to HIV-1. *Science* **265**.

8. Reeves, JD, Hibbitts, S, Simmons, G, Mcknight, I, Azevedo-Pereira, JM, Moniz-Pereira, J, *et al.* (1999). Primary Human Immunodeficiency Virus Type 2 (HIV-2) Isolates Infect CD4-Negative Cells via CCR5 and CXCR4: Comparison with HIV-1 and Simian Immunodeficiency Virus and Relevance to Cell Tropism In Vivo. *J. Virol.* **73**: 7795–7804.

9. Sundquist, WI and Kräusslich, H-G (2012). HIV-1 assembly, budding, and maturation. *Cold Spring Harb. Perspect. Med.* **2**: a006924.

10. Kaushik, R and Ratner, L (2004). Role of human immunodeficiency virus type 1 matrix phosphorylation in an early postentry step of virus replication. *J. Virol.* **78**: 2319–26.

11. Solbak, SMO, Reksten, TR, Hahn, F, Wray, V, Henklein, P, Henklein, P, *et al.*

(2013). HIV-1 p6 - A structured to flexible multifunctional membrane-interacting protein. *Biochim. Biophys. Acta - Biomembr.* **1828**: 816–823.

12. Pettit, SC, Moody, MD, Wehbie, RS, Kaplan, AH, Nantermet, P V, Klein, CA, *et al.* (1994). The p2 domain of human immunodeficiency virus type 1 Gag regulates sequential proteolytic processing and is required to produce fully infectious virions. *J. Virol.* **68**: 8017–27.
13. Kräusslich, HG, Fäcke, M, Heuser, AM, Konvalinka, J and Zentgraf, H (1995). The spacer peptide between human immunodeficiency virus capsid and nucleocapsid proteins is essential for ordered assembly and viral infectivity. *J. Virol.* **69**: 3407–19.
14. Wiegers, K, Rutter, G, Kottler, H, Tessmer, U, Hohenberg, H and Kräusslich, HG (1998). Sequential steps in human immunodeficiency virus particle maturation revealed by alterations of individual Gag polyprotein cleavage sites. *J. Virol.* **72**: 2846–2854.
15. Pancera, M, Majeed, S, Ban, Y-EA, Chen, L, Huang, C -c., Kong, L, *et al.* (2010). Structure of HIV-1 gp120 with gp41-interactive region reveals layered envelope architecture and basis of conformational mobility. *Proc. Natl. Acad. Sci.* **107**: 1166–1171.
16. Harrich, D, Ulich, C and Gaynor, RB (1996). A critical role for the TAR element in promoting efficient human immunodeficiency virus type 1 reverse transcription. *J. Virol.* **70**: 4017–4027.
17. Zack, JA, Arrigo, SJ, Weitsman, SR, Go, AS, Haislip, A and Chen, ISY (1990). HIV-1 entry into quiescent primary lymphocytes: Molecular analysis reveals a labile, latent viral structure. *Cell* **61**: 213–222.
18. Müller, HP and Varmus, HE (1994). DNA bending creates favored sites for

retroviral integration: an explanation for preferred insertion sites in nucleosomes. *EMBO J.* **13**: 4704–14.

19. Ashorn, P, McQuade, TJ, Thaisrivongs, S, Tomasselli, AG, Tarpley, WG and Moss, B (1990). An inhibitor of the protease blocks maturation of human and simian immunodeficiency viruses and spread of infection. *Proc. Natl. Acad. Sci. U. S. A.* **87**: 7472–6.

20. Feinberg, MB, Baltimore, D and Frankel, AD (1991). The role of Tat in the human immunodeficiency virus life cycle indicates a primary effect on transcriptional elongation. *Proc. Natl. Acad. Sci. U. S. A.* **88**: 4045–9.

21. Kao, S-Y, Calman, AF, Luciw, PA and Peterlin, BM (1987). Anti-termination of transcription within the long terminal repeat of HIV-1 by tat gene product. *Nature* **330**: 489–493.

22. Pollard, VW and Malim, MH (1998). The HIV-1 Rev Protein. *Annu. Rev. Microbiol.* **52**: 491–532.

23. Felber, BK, Drysdale, CM and Pavlakis, GN (1990). Feedback regulation of human immunodeficiency virus type 1 expression by the Rev protein. *J. Virol.* **64**: 3734–41.

24. Perkins, a, Cochrane, a W, Ruben, SM and Rosen, C a (1989). Structural and functional characterization of the human immunodeficiency virus rev protein. *J. Acquir. Immune Defic. Syndr.* **2**: 256–263.

25. Chaudhuri, R, Lindwasser, OW, Smith, WJ, Hurley, JH and Bonifacino, JS (2007). Downregulation of CD4 by Human Immunodeficiency Virus Type 1 Nef Is Dependent on Clathrin and Involves Direct Interaction of Nef with the AP2 Clathrin Adaptor. *J. Virol.* **81**: 3877–3890.

26. Schindler, M, Schmökel, J, Specht, A, Li, H, Münch, J, Khalid, M, *et al.* (2008).

Inefficient Nef-mediated downmodulation of CD3 and MHC-I correlates with loss of CD4+ T cells in natural SIV infection. *PLoS Pathog.* **4**.

27. Schindler, M, Münch, J, Kutsch, O, Li, H, Santiago, ML, Bibollet-Ruche, F, *et al.* (2006). Nef-Mediated Suppression of T Cell Activation Was Lost in a Lentiviral Lineage that Gave Rise to HIV-1. *Cell* **125**: 1055–1067.

28. Kirchhoff, F, Schindler, M, Specht, A, Arhel, N and Münch, J (2008). Role of Nef in primate lentiviral immunopathogenesis. *Cell. Mol. Life Sci.* **65**: 2621–2636.

29. Simmons, A, Aluvihare, V and McMichael, A (2001). Nef triggers a transcriptional program in T cells imitating single-signal T cell activation and inducing HIV virulence mediators. *Immunity* **14**: 763–777.

30. Pan, X, Rudolph, JM, Abraham, L, Habermann, A and Haller, C (2012). HIV-1 Nef compensates for disorganization of the immunological synapse by inducing TGN-associated Lck signaling HIV-1 Nef compensates for disorganization of the immunological synapse by inducing TGN-associated Lck signaling. *Blood* **119**: 786–798.

31. Thoulouze, MI, Sol-Foulon, N, Blanchet, F, Dautry-Varsat, A, Schwartz, O and Alcover, A (2006). Human immunodeficiency virus type-1 infection impairs the formation of the immunological synapse. *Immunity* **24**: 547–61.

32. Miller, BMD, Warmerdam, MT, Gaston, I, Greene, W and Feinberg, M (1994). The Human Immunodeficiency Virus-1 nef Gene Product: A Positive Factor for Viral Infection and Replication in Primary Lymphocytes and Macrophages. *J Exp. Med.* **179**.

33. Aiken, C, Konner, J, Landau, NR, Lenburg, ME and Trono, D (1994). Nef induces CD4 endocytosis: Requirement for a critical dileucine motif in the membrane-proximal CD4 cytoplasmic domain. *Cell* **76**: 853–864.

34. Luria, S, Chambers, IAN and Berg, P (1991). Expression of the type 1 human immunodeficiency virus Nef protein in T cells prevents antigen receptor-mediated induction of interleukin 2 mRNA. *Pnas* **88**: 5326–5330.

35. Rosa, A, Chande, A, Ziglio, S, De Sanctis, V, Bertorelli, R, Goh, SL, *et al.* (2015). HIV-1 Nef promotes infection by excluding SERINC5 from virion incorporation. *Nature* **526**: 212–217.

36. Usami, Y, Wu, Y and Göttlinger, HG (2015). SERINC3 and SERINC5 restrict HIV-1 infectivity and are counteracted by Nef. *Nature* **526**: 218–223.

37. Strebel, K, Daugherty, D, Clouse, K, Cohen, D, Folks, T and Martin, M a (1987). The HIV 'A' (sor) gene product is essential for virus infectivity. *Nature* **328**: 728–730.

38. Miller, JH, Presnyak, V and Smith, HC (2007). The dimerization domain of HIV-1 viral infectivity factor Vif is required to block virion incorporation of APOBEC3G. *Retrovirology* **4**.

39. Sheehy, AM, Gaddis, NC and Malim, MH (2003). The antiretroviral enzyme APOBEC3G is degraded by the proteasome in response to HIV-1 Vif. *Nat. Med.* **9**: 1404–1407.

40. Vodicka, MA, Koepp, DM, Silver, PA and Emerman, M (1998). HIV-1 Vpr interacts with the nuclear transport pathway to promote macrophage infection. *Genes Dev.* **12**: 175–185.

41. Goh, WC, Rogel, ME, Matthew Kinsey, C, Michael, SF, Fultz, PN, Nowak, MA, *et al.* (1998). HIV-1 Vpr increases viral expression by manipulation of the cell cycle: A mechanism for selection of Vpr in vivo. *Nat. Med.* **4**: 65–71.

42. Klimkait, T, Strebel, K, Hoggan, MD, Martin, MA and Orenstein, JM (1990). The human immunodeficiency virus type 1-specific protein vpu is required for efficient

virus maturation and release. *J. Virol.* **64**: 621–629.

43. Schubert, U, Bour, S, Ferrer-Montiel, A V, Montal, M, Maldarell, F and Strebel, K (1996). The two biological activities of human immunodeficiency virus type 1 Vpu protein involve two separable structural domains. *J. Virol.* **70**: 809–19.

44. Estrabaud, E, Le Rouzic, E, Lopez-Vergès, S, Morel, M, Belaïdouni, N, Benarous, R, *et al.* (2007). Regulated degradation of the HIV-1 Vpu protein through a βTrCP-independent pathway limits the release of viral particles. *PLoS Pathog.* **3**: 0995–1004.

45. Hauser, H, Lopez, LA, Yang, SJ, Oldenburg, JE, Exline, CM, Guatelli, JC, *et al.* (2010). HIV-1 Vpu and HIV-2 Env counteract BST-2/tetherin by sequestration in a perinuclear compartment. *Retrovirology* **7**: 51.

46. Neil, SJD, Zang, T and Bieniasz, PD (2008). Tetherin inhibits retrovirus release and is antagonized by HIV-1 Vpu. *Nature* **451**: 425–430.

47. Korber, B, Hraber, P, Wagh, K and Hahn, BH (2017). Polyvalent vaccine approaches to combat HIV-1 diversity. *Immunol. Rev.* **275**: 230–244.

48. Robertson, DL, Anderson, JP, Bradac, JA, Carr, JK, Foley, B, Funkhouser, RK, *et al.* (2000). HIV-1 Nomenclature Proposal HIV-1. *Science* **288**.

49. Spira, S, Wainberg, MA, Loemba, H, Turner, D and Brenner, BG (2003). Impact of clade diversity on HIV-1 virulence, antiretroviral drug sensitivity and drug resistance. *J. Antimicrob. Chemother.* **51**: 229–240.

50. Jeeninga, RE, Hoogenkamp, M, Armand-Ugon, M, de Baar, M, Verhoef, K and Berkhout, B (2000). Functional Differences between the Long Terminal Repeat Transcriptional Promoters of Human Immunodeficiency Virus Type 1 Subtypes A through G. *J. Virol.* **74**: 3740–3751.

51. Montano, M a, Novitsky, V a, Blackard, JT, Cho, NL, Katzenstein, D a and Essex,

M (1997). Divergent transcriptional regulation among expanding human immunodeficiency virus type 1 subtypes. *J. Virol.* **71**: 8657–65.

52. Hraber, P, Korber, BT, Lapedes, AS, Bailer, RT, Seaman, MS, Gao, H, *et al.* (2014). Impact of Clade, Geography, and Age of the Epidemic on HIV-1 Neutralization by Antibodies. *J. Virol.* **88**: 12623–12643.

53. Bleul, CC, Wu, L, Hoxie, JA, Springer, TA and Mackay, CR (1997). The HIV coreceptors CXCR4 and CCR5 are differentially expressed and regulated on human T lymphocytes. *Proc. Natl. Acad. Sci.* **94**: 1925–1930.

54. Scarlatti, G, Tresoldi, E, Björndal, A, Fredriksson, R, Colognesi, C, Deng, HK, *et al.* (1997). In vivo evolution of HIV-1 co-receptor usage and sensitivity to chemokine-mediated suppression. *Nat. Med.* **3**: 1259–65.

55. Kwong, PD, Wyatt, R, Robinson, J, Sweet, RW, Sodroski, J and Hendrickson, W a (1998). Structure of an HIV gp120 envelope glycoprotein in complex with the CD4 receptor and a neutralizing human antibody. *Nature* **393**: 648–59.

56. Alkhatib, G (2009). The biology of CCR5 and CXCR4. *Curr. Opin. HIV AIDS* **4**: 96–103.

57. Ghosn, J, Bayan, T, Meixenberger, K, Tran, L, Frange, P, Monforte, A d. A, *et al.* (2017). CD4 T cell decline following HIV seroconversion in individuals with and without CXCR4-tropic virus. *J. Antimicrob. Chemother.* **72**: 2862–2868.

58. Van't Wout, AB, Kootstra, NA, Mulder-Kampinga, GA, Albrecht-Van Lent, N, Scherpbier, HJ, Veenstra, J, *et al.* (1994). Macrophage-tropic variants initiate human immunodeficiency virus type 1 infection after sexual, parenteral, and vertical transmission. *J. Clin. Invest.* **94**: 2060–2067.

59. Laguette, N, Brégnard, C, Bouchet, J, Benmerah, A, Benichou, S and Basmaciogullari, S (2009). Nef-induced CD4 endocytosis in human

immunodeficiency virus type 1 host cells: role of p56lck kinase. *J. Virol.* **83**: 7117–28.

60. Goldstone, DC, Ennis-Adeniran, V, Hedden, JJ, Groom, HCT, Rice, GI, Christodoulou, E, *et al.* (2011). HIV-1 restriction factor SAMHD1 is a deoxynucleoside triphosphate triphosphohydrolase. *Nature* **480**: 379–382.

61. Baldauf, HM, Pan, X, Erikson, E, Schmidt, S, Daddacha, W, Burggraf, M, *et al.* (2012). SAMHD1 restricts HIV-1 infection in resting CD4 + T cells. *Nat. Med.* **18**: 1682–1687.

62. Ruffin, N, Brezar, V, Ayinde, D, Lefebvre, C, Wiesch, JS Zur, van Lunzen, J, *et al.* (2015). Low SAMHD1 expression following T-cell activation and proliferation renders CD4+ T cells susceptible to HIV-1. *Aids*: 1doi:10.1097/QAD.0000000000000594.

63. Coiras, M, López-Huertas, MR, Pérez-Olmeda, M and Alcamí, J (2009). Understanding HIV-1 latency provides clues for the eradication of long-term reservoirs. *Nat. Rev. Microbiol.* **7**: 798–812.

64. Schröder, ARW, Shinn, P, Chen, H, Berry, C, Ecker, JR, Bushman, F, *et al.* (2002). HIV-1 integration in the human genome favors active genes and local hotspots. *Cell* **110**: 521–9.

65. Hughes, S and Coffin, J (2016). What integration sites tell us about HIV persistence. *Cell Host Microbe* **19**: 588–598.

66. Jouvenet, N, Zhadina, M, Bieniasz, P and Simon, S (2011). Dynamics of ESCRT protein recruitment during retroviral assembly. *Nat Cell Biol* **13**: 394–401.

67. Van Engelenburg, SB, Shtengel, G, Sengupta, P, Waki, K, Jarnik, M, Ablan, SD, *et al.* (2014). Distribution of ESCRT Machinery at HIV Assembly Sites Reveals Virus Scaffolding of ESCRT Subunits. *Science* **343**: 653–656.

68. Engelman, A and Cherepanov, P (2012). The structural biology of HIV-1: mechanistic and therapeutic insights. *Nat. Rev. Microbiol.* **10**: 279–90.

69. Fanales-Belasio, E, Raimondo, M, Suligoi, B and Butto, S (2010). HIV virology and pathogenic mechanisms of infection: a brief overview. *Ann. Ist. Super. Sanita* **46**: 5–14.

70. Patel, P, Borkowf, CB, Brooks, JT, Lasry, A, Lansky, A and Mermin, J (2014). Estimating per-act HIV transmission risk. *AIDS* **28**: 1509–1519.

71. Galvin, SR and Cohen, MS (2004). The role of sexually transmitted diseases in HIV transmission. *Nat. Rev. Microbiol.* **2**: 33–42.

72. Loutfy, MR, Wu, W, Letchumanan, M, Bondy, L, Antoniou, T, Margolese, S, *et al.* (2013). Systematic Review of HIV Transmission between Heterosexual Serodiscordant Couples where the HIV-Positive Partner Is Fully Suppressed on Antiretroviral Therapy. *PLoS One* **8**.

73. Quinn, T, Wawer, M, Sewankambo, N, Serwadda, D, Li, C, Wabwire-Mangen, F, *et al.* (2000). Viral load and heterosexual transmission of human immunodeficiency virus type 1. *N. Engl. J. Med.* **342**: 921–929.

74. McMichael, AJ, Borrow, P, Tomaras, GD, Goonetilleke, N and Haynes, BF (2009). The immune response during acute HIV-1 infection: clues for vaccine development. *Nat. Rev. Immunol.* **10**: 11–23.

75. Keele, BF, Giorgi, EE, Salazar-Gonzalez, JF, Decker, JM, Pham, KT, Salazar, MG, *et al.* (2008). Identification and characterization of transmitted and early founder virus envelopes in primary HIV-1 infection. *Proc. Natl. Acad. Sci.* **105**: 7552–7557.

76. Salazar-Gonzalez, JF, Bailes, E, Kimmy, T, Salazar, MG, Guffey, MB, Keele, BF, *et al.* (2008). Deciphering Human Immunodeficiency Virus Type 1 Transmission

and Early Envelope Diversification by Single-Genome Amplification and Sequencing Deciphering Human Immunodeficiency Virus Type 1 Transmission and Early Envelope Diversification by Single-Genome. *J. Virol.* **82**: 3952–3970.

77. Konrad, B, Taylor, D, Conway, J, Ogilvie, G and Coombs, D (2017). On the duration of the period between exposure to HIV and detectable infection. *Epidemics*.

78. Perelson, AS, Neumann, AU, Markowitz, M, Leonard, JM and Ho, DD (1996). HIV-1 Dynamics in Vivo: Virion Clearance Rate, Infected Cell Life-Span, and Viral Generation Time. *Science* **271**: 1582–1586.

79. Jolly, C, Mitar, I and Sattentau, QJ (2007). Adhesion molecule interactions facilitate human immunodeficiency virus type 1-induced virological synapse formation between T cells. *J. Virol.* **81**: 13916–13921.

80. Martin, N, Welsch, S, Jolly, C, Briggs, J a G, Vaux, D and Sattentau, QJ (2010). Virological synapse-mediated spread of human immunodeficiency virus type 1 between T cells is sensitive to entry inhibition. *J. Virol.* **84**: 3516–27.

81. Jolly, C, Kashefi, K, Hollinshead, M, Sattentau, QJ, Laboratories, JT, Henry, T, *et al.* (2004). HIV-1 Cell to Cell Transfer across an Env-induced , Actin-dependent Synapse. *J. Exp. Med.* **199**.

82. Groppelli, E, Starling, S and Jolly, C (2015). Contact-Induced Mitochondrial Polarization Supports HIV-1 Virological Synapse Formation. *J. Virol.* **89**: 14–24.

83. Pope, M and Haase, AT (2003). Transmission, acute HIV-1 infection and the quest for strategies to prevent infection. *Nat. Med.* **9**: 847–52.

84. McMichael, AJ and Rowland-jones, SL (2001). Cellular immune responses to HIV. *Nature* **410**.

85. Brenchley, JM, Schacker, TW, Ruff, LE, Price, DA, Taylor, JH, Beilman, GJ, *et*

al. (2004). CD4 $^{+}$ T Cell Depletion during all Stages of HIV Disease Occurs Predominantly in the Gastrointestinal Tract. *J. Exp. Med.* **200**: 749–759.

86. Mattapallil, JJ, Douek, DC, Hill, B, Nishimura, Y, Martin, M and Roederer, M (2005). Massive infection and loss of memory CD4+ T cells in multiple tissues during acute SIV infection. *Nature* **434**: 1093–1097.

87. Veazey, R, Demaria, M, Chalifoux, L, Shvetz, D, Pauley, D, Knight, H, *et al.* (1998). Gastrointestinal Tract as a Major Site of CD4+ T Cell Depletion and Viral Replication in SIV Infection. *Science* **280**: 427–431.

88. Migueles, SA, Sabbaghian, MS, Shupert, WL, Bettinotti, MP, Marincola, FM, Martino, L, *et al.* (2000). HLA B*5701 is highly associated with restriction of virus replication in a subgroup of HIV-infected long term nonprogressors. *Proc. Natl. Acad. Sci.* **97**: 2709–2714.

89. Migueles, SA and Connors, M (2015). Success and failure of the cellular immune response against HIV-1. *Nat. Immunol.* **16**: 563–570.

90. Fellay, J, Shianna, K V., Ge, D, Colombo, S, Ledergerber, B, Weale, M, *et al.* (2007). A Whole-Genome Association Study of Major Determinants for Host Control of HIV-1. *Science* **317**: 944–947.

91. Bacchetti, P and Moss, AR (1989). Incubation period of AIDS in San Francisco. *Nature* **338**: 251–3.

92. Buckheit, RW, Siliciano, RF and Blankson, JN (2013). Primary CD8+ T cells from elite suppressors effectively eliminate non-productively HIV-1 infected resting and activated CD4+ T cells. *Retrovirology* **10**: 68.

93. Perreau, M, Levy, Y and Pantaleo, G (2013). Immune response to HIV. *Curr Opin HIV AIDS* **8**: 333–340.

94. Cartwright, EK, Spicer, L, Smith, SA, Lee, D, Fast, R, Paganini, S, *et al.* (2016).

CD8+Lymphocytes Are Required for Maintaining Viral Suppression in SIV-Infected Macaques Treated with Short-Term Antiretroviral Therapy. *Immunity* **45**: 656–668.

95. Chomont, N, El-Far, M, Ancuta, P, Trautmann, L, Procopio, F a, Yassine-Diab, B, *et al.* (2009). HIV reservoir size and persistence are driven by T cell survival and homeostatic proliferation. *Nat. Med.* **15**: 893–900.

96. Geeraert, L, Kraus, G and Pomerantz, RJ (2008). Hide-and-seek: the challenge of viral persistence in HIV-1 infection. *Annu. Rev. Med.* **59**: 487–501.

97. Bullen, CK, Laird, GM, Durand, CM, Siliciano, JD and Siliciano, RF (2014). New ex vivo approaches distinguish effective and ineffective single agents for reversing HIV-1 latency in vivo. *Nat. Med.* **20**: 425–9.

98. Margolis, DM, Garcia, J V., Hazuda, DJ and Haynes, BF (2016). Latency reversal and viral clearance to cure HIV-1. *Science* **353**: aaf6517-aaf6517.

99. Siliciano, RF and Greene, WC (2011). HIV Latency. *Cold Spring Harb. Perspect. Med.*: 1–19doi:10.1101/cshperspect.a007096.

100. Arfi, V, Rivière, L, Jarrosson-Wuillème, L, Goujon, C, Rigal, D, Darlix, J-L, *et al.* (2008). Characterization of the early steps of infection of primary blood monocytes by human immunodeficiency virus type 1. *J. Virol.* **82**: 6557–65.

101. Sonza, S, Mutimer, HP, Oelrichs, R, Jardine, D, Harvey, K, Dunne, a, *et al.* (2001). Monocytes harbour replication-competent, non-latent HIV-1 in patients on highly active antiretroviral therapy. *AIDS* **15**: 17–22.

102. McElrath, MJ, Steinman, RM and Cohn, ZA (1991). Latent HIV-1 infection in enriched populations of blood monocytes and T cells from seropositive patients. *J. Clin. Invest.* **87**: 27–30.

103. Groot, F, Welsch, S and Sattentau, QJ (2008). Efficient HIV-1 transmission from

macrophages to T cells across transient virological synapses. *Blood* **111**: 4660–3.

104. Abbas, W, Tariq, M, Iqbal, M, Kumar, A and Herbein, G (2015). Eradication of HIV-1 from the Macrophage Reservoir: An Uncertain Goal. *Viruses* **7**: 1578–1598.

105. Perno, CF, Newcomb, FM, Davis, DA, Aquaro, S, Humphrey, RW, Calio, R, *et al.* (1998). Relative potency of protease inhibitors in monocytes/macrophages acutely and chronically infected with human immunodeficiency virus. *J Infect Dis* **178**: 413–422.

106. Duncan, CJ a, Williams, JP, Schiffner, T, Gärtner, K, Ochsenbauer, C, Kappes, J, *et al.* (2014). High-multiplicity HIV-1 infection and neutralizing antibody evasion mediated by the macrophage-T cell virological synapse. *J. Virol.* **88**: 2025–34.

107. Thornhill, J, Fidler, S and Frater, J (2015). Advancing the HIV cure agenda: the next 5 years. *Curr. Opin. Infect. Dis.* **28**: 1–9.

108. North, TW, Higgins, J, Deere, JD, Hayes, TL, Villalobos, A, Adamson, L, *et al.* (2010). Viral Sanctuaries during Highly Active Antiretroviral Therapy in a Nonhuman Primate Model for AIDS. *J. Virol.* **84**: 2913–2922.

109. Chun, T, Nickle, DC, Justement, JS, Meyers, JH, Roby, G, Hallahan, CW, *et al.* (2008). Persistence of HIV in Gut-Associated Lymphoid Tissue despite Long-Term Antiretroviral Therapy. *J. Infect. Dis.* **197**: 714–720.

110. Thompson, KA, Cherry, CL, Bell, JE and McLean, CA (2011). Brain cell reservoirs of latent virus in presymptomatic HIV-infected individuals. *Am. J. Pathol.* **179**: 1623–1629.

111. Lorenzo-Redondo, R, Fryer, H, Bedford, T, Kim, E-Y, Archer, J, Pond, S, *et al.* (2016). Persistent HIV-1 replication maintains the tissue reservoir during therapy. *Nature* **530**: 51–56.

112. Ananworanich, J, Chomont, N, Eller, LA, Kroon, E, Tovanabutra, S, Bose, M, *et*

al. (2016). HIV DNA Set Point is Rapidly Established in Acute HIV Infection and Dramatically Reduced by Early ART. *EBioMedicine* **11**: 68–72.

113. Williams, JP, Hurst, J, Stöhr, W, Robinson, N, Brown, H, Fisher, M, *et al.* (2014). HIV-1 DNA predicts disease progression and post-treatment virological control. *Elife* **3**: e03821.

114. Li, J, Etemad, B, Ahmed, H, Aga, E, Bosch, R, Mellors, J, *et al.* (2016). The size of the expressed HIV reservoir predicts timing of viral rebound after treatment interruption. *AIDS* **30**: 343–353.

115. Whitney, JB, Hill, AL, Sanisetty, S, Penaloza-MacMaster, P, Liu, J, Shetty, M, *et al.* (2014). Rapid seeding of the viral reservoir prior to SIV viraemia in rhesus monkeys. *Nature* **512**: 74–77.

116. Ramratnam, B, Ribeiro, R, He, T, Chung, C, Simon, V, Vanderhoeven, J, *et al.* (2004). Intensification of antiretroviral therapy accelerates the decay of the HIV-1 latent reservoir and decreases, but does not eliminate, ongoing virus replication. *J. Acquir. Immune Defic. Syndr.* **35**: 33–37.

117. Gandhi, RT, Bosch, RJ, Aga, E, Albrecht, M, Demeter, LM, Dykes, C, *et al.* (2010). No evidence for decay of the latent reservoir in HIV-1-infected patients receiving intensive enfuvirtide-containing antiretroviral therapy. *J. Infect. Dis.* **201**: 293–6.

118. Palmer, S, Maldarelli, F, Wiegand, A, Bernstein, B, Hanna, GJ, Brun, SC, *et al.* (2008). Low-level viremia persists for at least 7 years in patients on suppressive antiretroviral therapy. *Proc. Natl. Acad. Sci. U. S. A.* **105**: 3879–84.

119. Besson, GJ, Lalama, CM, Bosch, RJ, Gandhi, RT, Bedison, MA, Aga, E, *et al.* (2014). HIV-1 DNA decay dynamics in blood during more than a decade of suppressive antiretroviral therapy. *Clin. Infect. Dis.* **59**: 1312–1321.

120. Malatinkova, E, De Spiegelaere, W, Bonczkowski, P, Kiselinova, M, Vervisch, K, Trypsteen, W, *et al.* (2015). Impact of a decade of successful antiretroviral therapy initiated at HIV-1 seroconversion on blood and rectal reservoirs. *Elife* **4**: 1–17.

121. Archin, NM, Vaidya, NK, Kuruc, JD, Liberty, a. L, Wiegand, A, Kearney, MF, *et al.* (2012). Immediate antiviral therapy appears to restrict resting CD4+ cell HIV-1 infection without accelerating the decay of latent infection. *Proc. Natl. Acad. Sci.* **109**: 9523–9528.

122. Gandhi, RT, Zheng, L, Bosch, RJ, Chan, ES, Margolis, DM, Read, S, *et al.* (2010). The effect of raltegravir intensification on low-level residual viremia in HIV-infected patients on antiretroviral therapy: A randomized controlled trial. *PLoS Med.* **7**.

123. Lafeuillade, A, Assi, A, Poggi, C, Bresson-Cuquemelle, C, Jullian, E and Tamalet, C (2014). Failure of combined antiretroviral therapy intensification with maraviroc and raltegravir in chronically HIV-1 infected patients to reduce the viral reservoir: the IntensHIV randomized trial. *AIDS Res. Ther.* **11**: 33.

124. Dinoso, JB, Kim, SY, Wiegand, AM, Palmer, SE, Gange, SJ, Cranmer, L, *et al.* (2009). Treatment intensification does not reduce residual HIV-1 viremia in patients on highly active antiretroviral therapy. *Proc. Natl. Acad. Sci.* **106**: 9403–9408.

125. Brodin, J, Zanini, F, Thebo, L, Lanz, C, Bratt, G, Neher, RA, *et al.* (2016). Establishment and stability of the latent HIV-1 DNA reservoir. *Elife* **5**: 1–15.

126. Kearney, MF, Wiegand, A, Shao, W, McManus, WR, Bale, MJ, Luke, B, *et al.* (2017). Ongoing HIV Replication During ART Reconsidered. *Open Forum Infect. Dis.* **4**: 1–5.

127. Kieffer, TL, Finucane, MM, Nettles, RE, Quinn, TC, Broman, KW, Ray, SC, *et al.*

(2004). Genotypic Analysis of HIV-1 Drug Resistance at the Limit of Detection : Virus Production without Evolution in Treated Adults with Undetectable HIV Loads. *J. Infect. Dis.* **189**: 1452–65.

128. Laird, GM, Eisele, EE, Rabi, SA, Lai, J, Chioma, S, Blankson, JN, *et al.* (2013). Rapid quantification of the latent reservoir for HIV-1 using a viral outgrowth assay. *PLoS Pathog.* **9**: e1003398.

129. Donahue, DA, Wainberg, MA, Eisele, E, Siliciano, R, Lassen, K, Ramyar, K, *et al.* (2013). Cellular and molecular mechanisms involved in the establishment of HIV-1 latency. *Retrovirology* **10**: 11.

130. Dahabieh, MS, Battivelli, E and Verdin, E (2015). Understanding HIV latency: the road to an HIV cure. *Annu. Rev. Med.* **66**: 407–421.

131. Han, Y, Lin, YB, An, W, Xu, J, Yang, H, Connell, KO, *et al.* (2008). Orientation-dependent regulation of integrated HIV-1 expression by host gene transcriptional readthrough. *Cell Host Microbe* **4**: 134–146.

132. Callen, BP, Shearwin, KE and Egan, JB (2004). Transcriptional interference between convergent promoters caused by elongation over the promoter. *Mol. Cell* **14**: 647–656.

133. Kauder, SE, Bosque, A, Lindqvist, A, Planelles, V and Verdin, E (2009). Epigenetic regulation of HIV-1 latency by cytosine methylation. *PLoS Pathog.* **5**.

134. He, G and Margolis, DM (2002). Counterregulation of Chromatin Deacetylation and Histone Deacetylase Occupancy at the Integrated Promoter of Human Immunodeficiency Virus Type 1 (HIV-1) by the HIV-1 Repressor YY1 and HIV-1 Activator Tat. *Mol. Cell. Biol.* **22**: 2965–2973.

135. Lusic, M, Marcello, A, Cereseto, A and Giacca, M (2003). Regulation of HIV-1 gene expression by histone acetylation and factor recruitment at the LTR promoter.

EMBO J. **22**: 6550–6561.

136. Burstein, E, Hoberg, JE, Wilkinson, AS, Rumble, JM, Csomos, RA, Komarck, CM, *et al.* (2005). COMMD proteins, a novel family of structural and functional homologs of MURR1. *J. Biol. Chem.* **280**: 22222–22232.

137. Maine, GN, Mao, X, Komarck, CM and Burstein, E (2007). COMMD1 promotes the ubiquitination of NF-κB subunits through a cullin-containing ubiquitin ligase. *EMBO J.* **26**: 436–447.

138. Huang, J, Wang, F, Argyris, E, Chen, K, Liang, Z, Tian, H, *et al.* (2007). Cellular microRNAs contribute to HIV-1 latency in resting primary CD4+ T lymphocytes. *Nat. Med.* **13**: 1241–1247.

139. Imperial College London (2017). Research In Viral Eradication of HIV Reservoirs (RIVER). *Clin. Trials.gov*at <https://clinicaltrials.gov/ct2/show/NCT02336074>.

140. Gallo, RC (2016). Shock and kill with caution. *Science* **354**: 177–178.

141. Walker-Sperling, VEK, Cohen, VJ, Tarwater, PM and Blankson, JN (2015). Reactivation kinetics of HIV-1 and susceptibility of reactivated latently infected CD4+ T cells to HIV-1-specific CD8+ T cells. *J. Virol.* **21205**: JVI.01454-15.

142. Walker-Sperling, VE, Pohlmeyer, CW, Tarwater, PM and Blankson, JN (2016). The Effect of Latency Reversal Agents on Primary CD8+ T Cells: Implications for Shock and Kill Strategies for Human Immunodeficiency Virus Eradication. *EBioMedicine* **8**: 217–229.

143. Archin, NM, Liberty, AL, Kashuba, AD, Choudhary, SK, Kuruc, JD, Crooks, AM, *et al.* (2012). Administration of vorinostat disrupts HIV-1 latency in patients on antiretroviral therapy. *Nature* **487**: 482–485.

144. Darcis, G, Kula, A, Bouchat, S, Fujinaga, K, Corazza, F, Ait-Ammar, A, *et al.* (2015). An In-Depth Comparison of Latency-Reversing Agent Combinations in

Various In Vitro and Ex Vivo HIV-1 Latency Models Identified Bryostatin-1+JQ1 and Ingenol-B+JQ1 to Potently Reactivate Viral Gene Expression. *PLoS Pathog.* **11**: 1–36.

145. Darcis, G, Bouchat, S, Kula, A, Van Driessche, B, Delacourt, N, Vanhulle, C, *et al.* (2017). Reactivation capacity by latency-reversing agents ex vivo correlates with the size of the HIV-1 reservoir. *Aids* **31**: 181–189.

146. Tateishi, H, Monde, K, Anraku, K, Koga, R, Hayashi, Y, Ciftci, HI, *et al.* (2017). A clue to unprecedented strategy to HIV eradication: 'Lock-in and apoptosis'. *Sci. Rep.* **7**: 1–8.

147. Kessing, CF, Nixon, CC, Li, C, Tsai, P, Takata, H, Mousseau, G, *et al.* (2017). In Vivo Suppression of HIV Rebound by Didehydro-Cortistatin A, a 'Block-and-Lock' Strategy for HIV-1 Treatment. *Cell Rep.* **21**: 600–611.

148. Stacey, AR, Norris, PJ, Qin, L, Haygreen, EA, Taylor, E, Heitman, J, *et al.* (2009). Induction of a Striking Systemic Cytokine Cascade prior to Peak Viremia in Acute Human Immunodeficiency Virus Type 1 Infection, in Contrast to More Modest and Delayed Responses in Acute Hepatitis B and C Virus Infections. *J. Virol.* **83**: 3719–3733.

149. Lehmann, C, Lafferty, M, Garzino-Demo, A, Jung, N, Hartmann, P, Fätkenheuer, G, *et al.* (2010). Plasmacytoid dendritic cells accumulate and secrete interferon alpha in lymph nodes of HIV-1 patients. *PLoS One* **5**.

150. Donaghy, H, Gazzard, B, Gotch, F and Patterson, S (2003). Dysfunction and infection of freshly isolated blood myeloid and plasmacytoid dendritic cells in patients infected with HIV-1. *Reactions* **101**: 4505–4511.

151. Miller, EA, Spadaccia, MR, O'Brien, MP, Rolnitzky, L, Sabado, R, Manches, O, *et al.* (2012). Plasma factors during chronic HIV-1 infection impair IL-12 secretion

by myeloid dendritic cells via a virus-independent pathway. *J. Acquir. Immune Defic. Syndr.* **61**: 535–544.

152. Sabado, RL, Brien, MO, Subedi, A, Qin, L, Hu, N, Taylor, E, *et al.* (2010). Evidence of dysregulation of dendritic cells in primary HIV infection. *Blood* **116**: 3839–3852.

153. Malleret, B, Mane, B, Karlsson, I, Lebon, P, Nascimbeni, M, Perie, L, *et al.* (2008). Primary infection with simian immunodeficiency virus : plasmacytoid dendritic cell homing to lymph nodes , type I interferon , and immune suppression. *Blood* **112**: 4598–4608.

154. Ward, J, Bonaparte, M, Sacks, J, Guterman, J, Fogli, M, Mavilio, D, *et al.* (2007). HIV modulates the expression of ligands important in triggering natural killer cell cytotoxic responses on infected primary T-cell blasts. *Blood* **110**: 1207–1214.

155. Alter, G, Teigen, N, Ahern, R, Streeck, H, Meier, A, Rosenberg, ES, *et al.* (2007). Evolution of Innate and Adaptive Effector Cell Functions during Acute HIV-1 Infection. *J. Infect. Dis.* **195**: 1452–1460.

156. Alter, G, Heckerman, D, Schneidewind, A, Fadda, L, Kadie, CM, Carlson, JM, *et al.* (2011). HIV-1 adaptation to NK-cell-mediated immune pressure. *Nature* **476**: 96–100.

157. Goonetilleke, N, Liu, MKP, Salazar-Gonzalez, JF, Ferrari, G, Giorgi, E, Ganusov, V V, *et al.* (2009). The first T cell response to transmitted/founder virus contributes to the control of acute viremia in HIV-1 infection. *J. Exp. Med.* **206**: 1253–72.

158. Turnbull, EL, Wong, M, Wang, S, Wei, X, Jones, N a, Conrod, KE, *et al.* (2009). Kinetics of expansion of epitope-specific T cell responses during primary HIV-1 infection. *J. Immunol.* **182**: 7131–45.

159. Salazar-Gonzalez, JF, Salazar, MG, Keele, BF, Learn, GH, Giorgi, EE, Li, H, *et al.* (2009). Genetic identity, biological phenotype, and evolutionary pathways of transmitted/founder viruses in acute and early HIV-1 infection. *J. Exp. Med.* **206**: 1273–89.

160. Bernardin, F, Kong, D, Peddada, L, Baxter-lowe, A and Delwart, E (2005). Human Immunodeficiency Virus Mutations during the First Month of Infection Are Preferentially Found in Known Cytotoxic Human Immunodeficiency Virus Mutations during the First Month of Infection Are Preferentially Found in Known Cytotoxic T-Lymphocyte Epit. *J. Virol.* **79**: 11523–11528.

161. Wang, YE, Li, B, Carlson, JM, Streeck, H, Gladden, AD, Goodman, R, *et al.* (2009). Protective HLA class I alleles that restrict acute-phase CD8+ T-cell responses are associated with viral escape mutations located in highly conserved regions of human immunodeficiency virus type 1. *J. Virol.* **83**: 1845–55.

162. Roberts, HE, Hurst, J, Robinson, N, Brown, H, Flanagan, P, Vass, L, *et al.* (2015). Structured observations reveal slow HIV-1 CTL escape. *PLoS Genet.* **11**: e1004914.

163. Kaufmann, DE, Kaufmann, DE, Bailey, PM, Bailey, PM, Sidney, J, Sidney, J, *et al.* (2004). Comprehensive Analysis of Human Immunode ciency Virus Type 1-Speci c CD4 Responses Reveals Marked Immunodominance of. *J. Virol.* **78**: 4463–4477.

164. Oxenius, A, Fidler, S, Brady, M, Dawson, SJ, Ruth, K, Easterbrook, PJ, *et al.* (2001). Variable fate of virus-specific CD4(+) T cells during primary HIV-1 infection. *Eur J Immunol* **31**: 3782–8.

165. Pitcher, CJ, Quittner, C, Peterson, DM, Connors, M, Koup, R a, Maino, VC, *et al.* (1999). HIV-1-specific CD4+ T cells are detectable in most individuals with active

HIV-1 infection, but decline with prolonged viral suppression. *Nat. Med.* **5**: 518–525.

166. Younes, S-A, Yassine-Diab, B, Dumont, AR, Boulassel, M-R, Grossman, Z, Routy, J-P, *et al.* (2003). HIV-1 viremia prevents the establishment of interleukin 2-producing HIV-specific memory CD4+ T cells endowed with proliferative capacity. *J. Exp. Med.* **198**: 1909–22.

167. Douek, DC, Brenchley, JM, Betts, MR, Ambrozak, DR, Hill, BJ, Okamoto, Y, *et al.* (2002). HIV preferentially infects HIV-specific CD4+ T cells. *Nature* **417**: 95–98.

168. Tomaras, GD, Yates, NL, Liu, P, Qin, L, Fouda, GG, Chavez, LL, *et al.* (2008). Initial B-Cell Responses to Transmitted Human Immunodeficiency Virus Type 1: Virion-Binding Immunoglobulin M (IgM) and IgG Antibodies Followed by Plasma Anti-gp41 Antibodies with Ineffective Control of Initial Viremia. *J. Virol.* **82**: 12449–12463.

169. Gray, ES, Moore, PL, Choge, IA, Decker, JM, Bibollet-Ruche, F, Li, H, *et al.* (2007). Neutralizing Antibody Responses in Acute Human Immunodeficiency Virus Type 1 Subtype C Infection. *J. Virol.* **81**: 6187–6196.

170. Derdeyn, C a, Decker, JM, Bibollet-Ruche, F, Mokili, JL, Muldoon, M, Denham, S a, *et al.* (2004). Envelope-constrained neutralization-sensitive HIV-1 after heterosexual transmission. *Science* **303**: 2019–22.

171. Wei, X, Decker, JM, Wang, S, Hui, H, Kappes, JC, Wu, X, *et al.* (2003). Antibody neutralization and escape by HIV-1. *Nature* **422**: 307–312.

172. Richman, DD, Wrin, T, Little, SJ and Petropoulos, CJ (2003). Rapid evolution of the neutralizing antibody response to HIV type 1 infection. *Proc. Natl. Acad. Sci. U. S. A.* **100**: 4144–9.

173. Gray, ES, Madiga, MC, Moore, PL, Mlisana, K, Abdool Karim, SS, Binley, JM, *et al.* (2009). Broad Neutralization of Human Immunodeficiency Virus Type 1 Mediated by Plasma Antibodies against the gp41 Membrane Proximal External Region. *J. Virol.* **83**: 11265–11274.

174. Shen, X, Parks, RJ, Montefiori, DC, Kirchherr, JL, Keele, BF, Decker, JM, *et al.* (2009). In Vivo gp41 Antibodies Targeting the 2F5 Monoclonal Antibody Epitope Mediate Human Immunodeficiency Virus Type 1 Neutralization Breadth. *J. Virol.* **83**: 3617–3625.

175. Cubas, R a, Mudd, JC, Savoye, A-L, Perreau, M, van Grevenynghe, J, Metcalf, T, *et al.* (2013). Inadequate T follicular cell help impairs B cell immunity during HIV infection. *Nat. Med.* **19**: 494–9.

176. Alam, SM, Scearce, RM, Parks, RJ, Plonk, K, Plonk, SG, Sutherland, LL, *et al.* (2008). Human Immunodeficiency Virus Type 1 gp41 Antibodies That Mask Membrane Proximal Region Epitopes: Antibody Binding Kinetics, Induction, and Potential for Regulation in Acute Infection. *J. Virol.* **82**: 115–125.

177. Muro-Cacho, C, Pantaleo, G and Fauci, A (1995). Analysis of apoptosis in lymph nodes of HIV-infected persons. *J. Immunol.* **154**: 5555–5566.

178. Valdez, H, Connick, E, Smith, KY, Lederman, MM, Bosch, RJ, Kim, RS, *et al.* (2002). Limited immune restoration after 3 years' suppression of HIV-1 replication in patients with moderately advanced disease. *AIDS* **16**: 1859–66.

179. Kelley, CF, Kitchen, CMR, Hunt, PW, Rodriguez, B, Hecht, FM, Kitahata, M, *et al.* (2009). Incomplete Peripheral CD4+ Cell Count Restoration in HIV-Infected Patients Receiving Long-Term Antiretroviral Treatment. *Clin. Infect. Dis.* **48**: 787–794.

180. Klatt, NR, Chomont, N, Douek, DC and Deeks, SG (2013). Immune activation and

HIV persistence: implications for curative approaches to HIV infection. *Immunol. Rev.* **254**: 326–42.

181. Wallet, M, Rodriguez, C, Yin, L, Saporta, S, Chinratanapisit, S, Hou, W, *et al.* (2010). Microbial translocation induces persistent macrophage activation unrelated to HIV-1 levels or T cell activation following therapy. *AIDS* **24**: 1281–1290.

182. Estes, JD, Harris, LD, Klatt, NR, Tabb, B, Pittaluga, S, Paiardini, M, *et al.* (2010). Damaged intestinal epithelial integrity linked to microbial translocation in pathogenic simian immunodeficiency virus infections. *PLoS Pathog.* **6**: 49–50.

183. Canary, L, Vinton, C, Morcock, D, Pierce, J, Ester, J, Brenchley, J, *et al.* (2013). Rate of AIDS Progression is Associated with Gastrointestinal Dysfunction in SIV-infected Pigtail Macaques. *J Immunol.* **190**: 2959–2965.

184. Moir, S, Ho, J, Malaspina, A, Wang, W, DiPoto, AC, O'Shea, MA, *et al.* (2008). Evidence for HIV-associated B cell exhaustion in a dysfunctional memory B cell compartment in HIV-infected viremic individuals. *J. Exp. Med.* **205**: 1797–1805.

185. Moir, S, Malaspina, A, Ogwaro, KM, Donoghue, ET, Hallahan, CW, Ehler, LA, *et al.* (2001). HIV-1 induces phenotypic and functional perturbations of B cells in chronically infected individuals. *Proc. Natl. Acad. Sci. U. S. A.* **98**: 10362–7.

186. Moir, S, Ogwaro, KM, Malaspina, A, Vasquez, J, Donoghue, ET, Hallahan, CW, *et al.* (2003). Perturbations in B cell responsiveness to CD4+ T cell help in HIV-infected individuals. *Proc. Natl. Acad. Sci. U. S. A.* **100**: 6057–6062.

187. Hoffmann, M, Pantazis, N, Martin, GE, Hickling, S, Hurst, J, Meyerowitz, J, *et al.* (2016). Exhaustion of Activated CD8 T Cells Predicts Disease Progression in Primary HIV-1 Infection. *PLoS Pathog.* **12**: 1–19.

188. Deeks, SG, Kitchen, CMR, Liu, L, Guo, H, Gascon, R, Narváez, AB, *et al.* (2004). Immune activation set point during early HIV infection predicts subsequent CD4 +

T-cell changes independent of viral load. *Blood* **104**: 942–947.

189. Day, CL, Kaufmann, DE, Kiepiela, P, Brown, J a, Moodley, ES, Reddy, S, *et al.* (2006). PD-1 expression on HIV-specific T cells is associated with T-cell exhaustion and disease progression. *Nature* **443**: 350–354.

190. Petrovas, C, Casazza, JP, Brenchley, JM, Price, DA, Gostick, E, Adams, WC, *et al.* (2006). PD-1 is a regulator of virus-specific CD8(+) T cell survival in HIV infection. *J. Exp. Med.* **203**: 2281–2292.

191. D'Souza, M, Fontenot, AP, Mack, DG, Lozupone, C, Dillon, S, Meditz, A, *et al.* (2007). Programmed death 1 expression on HIV-specific CD4+ T cells is driven by viral replication and associated with T cell dysfunction. *J. Immunol.* **179**: 1979–1987.

192. Trautmann, L, Mbitikon-Kobo, Fl-M, Goulet, J, Peretz, Y, Shi, Y, Grevenynghe, V, *et al.* (2012). HIV-specific CD8 T cells in primary and chronic HIV infection Profound metabolic , functional , and cytolytic differences characterize HIV-specific CD8 T cells in primary and chronic HIV infection. *Blood* **120**: 3466–3477.

193. Zhang, JY, Zhang, Z, Wang, X, Fu, JL, Yao, J, Jiao, Y, *et al.* (2007). PD-1 up-regulation is correlated with HIV-specific memory CD8+ T-cell exhaustion in typical progressors but not in long-term nonprogressors. *Blood* **109**: 4671–4678.

194. Shankar, P, Russo, M, Harnisch, B, Patterson, M, Skolnik, P and Lieberman, J (2000). Impaired function of circulating HIV-specific CD8(+) T cells in chronic human immunodeficiency virus infection. *Blood* **96**: 3094–3101.

195. Wherry, EJ, Ha, SJ, Kaech, SM, Haining, WN, Sarkar, S, Kalia, V, *et al.* (2007). Molecular Signature of CD8+ T Cell Exhaustion during Chronic Viral Infection. *Immunity* **27**: 670–684.

196. Yang, H, Wu, H, Hancock, G, Clutton, G, Sande, N, Xu, X, *et al.* (2012). Antiviral

inhibitory capacity of CD8+ T cells predicts the rate of CD4+ T-cell decline in HIV-1 infection. *J. Infect. Dis.* **206**: 552–61.

197. Boswell, KL, Paris, R, Boritz, E, Ambrozak, D, Yamamoto, T, Darko, S, *et al.* (2014). Loss of Circulating CD4 T Cells with B Cell Helper Function during Chronic HIV Infection. *PLoS Pathog.* **10**: 1–14.

198. Betts, MR, Nason, MC, West, SM, Rosa, SC De, Migueles, SA, Abraham, J, *et al.* (2006). HIV nonprogressors preferentially maintain highly functional HIV-specific CD8+ T cells. *Immunobiology* **107**: 4781–4789.

199. Migueles, S a and Connors, M (2010). Long-term nonprogressive disease among untreated HIV-infected individuals: clinical implications of understanding immune control of HIV. *JAMA* **304**: 194–201.

200. Hatano, H, Scherzer, R, Wu, Y, Harvill, K, Maka, K, Hoh, R, *et al.* (2012). A Randomized, Controlled Trial Assessing the Effects of Raltegravir Intensification on Endothelial Function in Treated HIV Infection. *J Acquir Immune Defic Syndr* **61**: 317–325.

201. Hatano, H, Hayes, TL, Dahl, V, Sinclair, E, Lee, TH, Hoh, R, *et al.* (2011). A randomized, controlled trial of raltegravir intensification in antiretroviral-treated, HIV-infected patients with a suboptimal CD4+ T cell response. *J. Infect. Dis.* **203**: 960–968.

202. Massanella, M, Negredo, E, Puig, J, Puertas, MC, Buzón, MJ, Pérez-Álvarez, N, *et al.* (2012). Raltegravir intensification shows differing effects on CD8 and CD4 T cells in HIV-infected HAART-suppressed individuals with poor CD4 T-cell recovery. *Aids* **26**: 2285–2293.

203. Restifo, NP, Dudley, ME and Rosenberg, SA (2012). Adoptive immunotherapy for cancer: harnessing the T cell response. *Nat. Rev. Immunol.* **12**: 269–281.

204. Houot, R, Schultz, LM, Marabelle, A and Kohrt, H (2015). T-cell-based Immunotherapy: Adoptive Cell Transfer and Checkpoint Inhibition. *Cancer Immunol. Res.* **3**: 1115–1122.

205. Maus, M V., Fraietta, JA, Levine, BL, Kalos, M, Zhao, Y and June, CH (2014). Adoptive Immunotherapy for Cancer or Viruses. *Annu. Rev. Immunol.* **32**: 189–225.

206. Davis, T, Grillo-Lopez, A, White, C, McLaughlin, P, Czuczman, M, Link, B, *et al.* (2000). Rituximab Anti-CD20 Monoclonal Antibody Therapy in Non-Hodgkin's Lymphoma: Safety and Efficacy of Re-Treatment. *J. Clin. Oncol.* **18**: 3135–3143.

207. Klebanoff, CA, Acquavella, N, Yu, Z and Restifo, NP (2011). Therapeutic cancer vaccines: Are we there yet? *Immunol. Rev.* **239**: 27–44.

208. Lameris, R, de Bruin, RCG, Schneiders, FL, van Bergen en Henegouwen, PMP, Verheul, HMW, de Gruijl, TD, *et al.* (2014). Bispecific antibody platforms for cancer immunotherapy. *Crit. Rev. Oncol. Hematol.* **92**: 153–165.

209. Fan, G, Wang, Z, Hao, M and Li, J (2015). Bispecific antibodies and their applications. *J. Hematol. Oncol.* **8**.

210. Zeidler, R, Reisbach, G, Wollenberg, B, Lang, S, Chaubal, S, Schmitt, B, *et al.* (1999). Simultaneous activation of T cells and accessory cells by a new class of intact bispecific antibody results in efficient tumor cell killing. *J. Immunol.* **163**: 1246–52.

211. Sebastian, M, Passlick, B, Friccius-Quecke, H, Jäger, M, Lindhofer, H, Kanniess, F, *et al.* (2007). Treatment of non-small cell lung cancer patients with the trifunctional monoclonal antibody catumaxomab (anti-EpCAM x anti-CD3): A phase I study. *Cancer Immunol. Immunother.* **56**: 1637–1644.

212. Holliger, P and Hudson, PJ (2005). Engineered antibody fragments and the rise of

single domains. *Nat. Biotechnol.* **23**: 1126–1136.

213. Loffler, A, Kufer, P, Lutterbuse, R, Zettl, F, Daniel, PT, Schwenkenbecher, JM, *et al.* (2000). A recombinant bispecific single-chain antibody , CD19 x CD3 , induces rapid and high lymphoma-directed cytotoxicity by unstimulated T lymphocytes. *Blood* **95**: 2098–2104.

214. Haas, C, Krinner, E, Brischwein, K, Hoffmann, P, Lutterbüse, R, Schlereth, B, *et al.* (2009). Mode of cytotoxic action of T cell-engaging BiTE antibody MT110. *Immunobiology* **214**: 441–453.

215. Bargou, R, Leo, E, Zugmaier, G, Klinger, M, Goebeler, M, Knop, S, *et al.* (2008). Tumor Regression in Cancer Patients by Very Low Doses of a T Cell-Engaging Antibody. *Science* **321**: 974–977.

216. Johnson, S, Burke, S, Huang, L, Gorlatov, S, Li, H, Wang, W, *et al.* (2010). Effector cell recruitment with novel Fv-based dual-affinity re-targeting protein leads to potent tumor cytolysis and in vivo B-cell depletion. *J. Mol. Biol.* **399**: 436–449.

217. Moore, PA, Zhang, W, Rainey, GJ, Burke, S, Li, H, Huang, L, *et al.* (2011). Application of dual affinity retargeting molecules to achieve optimal redirected T-cell killing of B-cell lymphoma. *Blood* **117**: 4542–4551.

218. Müller, D and Kontermann, RE (2010). Bispecific Antibodies for Cancer Immunotherapy. *BioDrugs* **24**: 89–98.

219. Oates, J, Hassan, NJ and Jakobsen, BK (2015). ImmTACs for targeted cancer therapy: Why, what, how, and which. *Mol. Immunol.* **67**: 67–74.

220. Tranter, E, Peters, G, Boyce, M and Warrington, S (2013). Giving monoclonal antibodies to healthy volunteers in phase 1 trials: Is it safe? *Br. J. Clin. Pharmacol.* **76**: 164–172.

221. Teachey, DT, Rheingold, SR, Maude, SL, Zugmaier, G, Barrett, DM, Seif, AE, *et al.* (2013). Cytokine release syndrome after blinatumomab treatment related to abnormal macrophage activation and ameliorated with cytokine-directed therapy. *Blood* **121**: 5154–5157.

222. Kontermann, RE (2011). Strategies for extended serum half-life of protein therapeutics. *Curr. Opin. Biotechnol.* **22**: 868–876.

223. Stork, R, Campigna, E, Robert, B, Müller, D and Kontermann, RE (2009). Biodistribution of a bispecific single-chain diabody and its half-life extended derivatives. *J. Biol. Chem.* **284**: 25612–25619.

224. Jeong, KJ, Jang, SH and Velmurugan, N (2011). Recombinant antibodies: Engineering and production in yeast and bacterial hosts. *Biotechnol. J.* **6**: 16–27.

225. McCormack, E, Adams, KJ, Hassan, NJ, Kotian, A, Lissin, NM, Sami, M, *et al.* (2013). Bi-specific TCR-anti CD3 redirected T-cell targeting of NY-ESO-1- and LAGE-1-positive tumors. *Cancer Immunol. Immunother.* **62**: 773–785.

226. Liddy, N, Bossi, G, Adams, KJ, Lissina, A, Mahon, TM, Hassan, NJ, *et al.* (2012). Monoclonal TCR-redirected tumor cell killing. *Nat. Med.* **18**: 980–7.

227. Bossi, G, Buisson, S, Oates, J, Jakobsen, BK and Hassan, NJ (2014). ImmTAC-redirected tumour cell killing induces and potentiates antigen cross-presentation by dendritic cells. *Cancer Immunol. Immunother.* **63**: 437–448.

228. Middleton, MR, Steven, N, Evans, J, Indante, J, Sznol, M, Mulatero, C, *et al.* (2016). PD - Poster #338 - Safety, pharmacokinetics and efficacy of IMCgp100, a first-in-class soluble TCR-antiCD3 bispecific t cell redirector with solid tumour activity: Results from the FIH study in melanoma. *Am. Soc. Clin. Oncol.*: Abstract no.3016.

229. Coulie, PG, Van den Eynde, BJ, van der Bruggen, P and Boon, T (2014). Tumour

antigens recognized by T lymphocytes: at the core of cancer immunotherapy. *Nat. Rev. Cancer* **14**: 135–146.

230. Davies, H, Bignell, GR, Cox, C, Stephens, P, Edkins, S and S. Clegg, et al. (2002). Mutations of the BRAF gene in human cancer. *Nature* **417**: 949–954.

231. Kim, PS and Ahmed, R (2010). Features of Responding T cells in Cancer and Chronic Infection. *Curr Opin Immunol* **22**: 223–230.

232. Ahmadzadeh, M, Johnson, L a, Heemskerk, B, Wunderlich, JR, Dudley, ME, White, DE, *et al.* (2009). Tumor antigen − specific CD8 T cells infiltrating the tumor express high levels of PD-1 and are functionally impaired Tumor antigen – specific CD8 T cells infiltrating the tumor express high levels of PD-1 and are functionally impaired. *Blood* **114**: 1537–1544.

233. Mumprecht, S, Schu, C, Schwaller, J, Solenthaler, M, Ochsenbein, AF and Pd-l, P (2009). Programmed death 1 signaling on chronic myeloid leukemia – specific T cells results in T-cell exhaustion and disease progression. *Immunobiology* **114**: 1528–1536.

234. Yamamoto, K, Horikita, M, Tsuda, F, Itoh, K, Akahane, Y, Yotsumoto, S, *et al.* (1994). Naturally occuring escape mutants of hepatitis b virus with various mutations in the S gene in carriers seropositive for antibody to hepatitis B suraface antigen. *J Virol* **68**: 2671–2676.

235. Park, SS, Ryu, CJ, Kang, YJ, Kashmiri, S V and Hong, HJ (2000). Generation and characterization of a novel tetravalent bispecific antibody that binds to hepatitis B virus surface antigens. *Mol. Immunol.* **37**: 1123–30.

236. Duval, M, Posner, MR and Cavacini, LA (2008). A Bispecific Antibody Composed of a Nonneutralizing Antibody to the gp41 Immunodominant Region and an Anti-CD89 Antibody Directs Broad Human Immunodeficiency Virus

Destruction by Neutrophils. *J. Virol.* **82**: 4671–4674.

237. Koristka, S, Cartellieri, M, Theil, a, Feldmann, a, Arndt, C, Stamova, S, *et al.* (2012). Retargeting of human regulatory T cells by single-chain bispecific antibodies. *J Immunol* **188**: 1551–1558.

238. Sung, JAM, Pickeral, J, Liu, L, Stanfield-Oakley, SA, Kao Lam, CY, Garrido, C, *et al.* (2015). Dual-Affinity Re-Targeting proteins direct T cell-mediated cytolysis of latently HIV-infected cells. *J. Clin. Invest.* **125**: 4077–4090.

239. Pace, MJ, Graf, EH, Agosto, LM, Mexas, AM, Male, F, Brady, T, *et al.* (2012). Directly infected resting CD4+T cells can produce HIV Gag without spreading infection in a model of HIV latency. *PLoS Pathog.* **8**: e1002818.

240. Scheid, JF, Horwitz, JA, Bar-On, Y, Kreider, EF, Lu, C-L, Lorenzi, JCC, *et al.* (2016). HIV-1 antibody 3BNC117 suppresses viral rebound in humans during treatment interruption. *Nature* **535**: 556–560.

241. Sloan, DD, Lam, CYK, Irrinki, A, Liu, L, Tsai, A, Pace, CS, *et al.* (2015). Targeting HIV Reservoir in Infected CD4 T Cells by Dual-Affinity Re-targeting Molecules (DARTs) that Bind HIV Envelope and Recruit Cytotoxic T Cells. *PLoS Pathog.* **11**: 1–29.

242. Rudicell, RS, Kwon, YD, Ko, S-Y, Pegu, A, Louder, MK, Georgiev, IS, *et al.* (2014). Enhanced Potency of a Broadly Neutralizing HIV-1 Antibody In Vitro Improves Protection against Lentiviral Infection In Vivo. *J. Virol.* **88**: 12669–12682.

243. Petrovas, C, Ferrando-martinez, S, Gerner, MY, Casazza, JP, Pegu, A, Deleage, C, *et al.* (2017). Follicular CD8 T cells accumulate in HIV infection and can kill infected cells in vitro via bispecific antibodies. *Sci. Transl. Med.* **1**.

244. Varela-Rohena, A, Molloy, PE, Dunn, SM, Li, Y, Suhoski, MM, Carroll, RG, *et al.*

(2008). Control of HIV-1 immune escape by CD8 T cells expressing enhanced T-cell receptor. *Nat. Med.* **14**: 1390–5.

245. Yang, H, Buisson, S, Bossi, G, Wallace, Z, Hancock, G, So, C, *et al.* (2016). Elimination of Latently HIV-infected Cells from Antiretroviral Therapy-suppressed Subjects by Engineered Immune-mobilizing T-cell Receptors. *Mol. Ther.*doi:10.1038/mt.2016.114.

246. Dustin, ML, Chakraborty, AK and Shaw, AS (2010). Understanding the structure and function of the immunological synapse. *Cold Spring Harb. Perspect. Biol.* **2**: a002311.

247. Davis, DM and Dustin, ML (2004). What is the importance of the immunological synapse? *Trends Immunol.* **25**: 323–327.

248. Dustin, M (2014). The immunological synapse. *Cancer Immunol. Res.* **2**: 1023–1033.

249. Monks, CR, Freiberg, B a, Kupfer, H, Sciaky, N and Kupfer, A (1998). Three-dimensional segregation of supramolecular activation clusters in T cells. *Nature* **395**: 82–86.

250. Grakoui, A, Bromley, SK, Sumen, C, Davis, MM, Shaw, AS, Allen, PM, *et al.* (1999). The Immunological Synapse : A Molecular Machine Controlling T Cell Activation. *Science* **285**: 221–227.

251. Davis, DM, Chiu, I, Fassett, M, Cohen, GB, Mandelboim, O and Strominger, JL (1999). The human natural killer cell immune synapse. *Proc. Natl. Acad. Sci.* **96**: 15062–15067.

252. Jenkins, MR, Rudd-Schmidt, J a., Lopez, J a., Ramsbottom, KM, Mannering, SI, Andrews, DM, *et al.* (2015). Failed CTL/NK cell killing and cytokine hypersecretion are directly linked through prolonged synapse time. *J. Exp. Med.*

212: 307–317.

253. Tane, AH, Sakuma, M, Ike, H, Yokosuka, T, Kimura, Y, Ohara, O, *et al.* (2016). Micro – adhesion rings surrounding TCR microclusters are essential for T cell activation. *J. Exp. Med.*: 1–17doi:10.1084/jem.20151088.

254. Hioe, CE, Tuen, M, Vasiliver-Shamis, G, Alvarez, Y, Prins, KC, Banerjee, S, *et al.* (2011). HIV envelope gp120 activates LFA-1 on CD4 T-lymphocytes and increases cell susceptibility to LFA-1-targeting leukotoxin (LtxA). *PLoS One* **6**: 1–11.

255. McGavern, DB, Christen, U and Oldstone, MB a (2002). Molecular anatomy of antigen-specific CD8(+) T cell engagement and synapse formation in vivo. *Nat. Immunol.* **3**: 918–925.

256. Stinchcombe, JC, Bossi, G, Booth, S and Griffiths, GM (2001). The immunological synapse of CTL contains a secretory domain and membrane bridges. *Immunity* **15**: 751–761.

257. Dustin, ML, Olszowy, MW, Holdorf, AD, Li, J, Bromley, S, Desai, N, *et al.* (1998). A novel adaptor protein orchestrates receptor patterning and cytoskeletal polarity in T-cell contacts. *Cell* **94**: 667–677.

258. Lee, K, Holdorf, AD, Dustin, ML, Chan, AC, Allen, PM and Shaw, AS (2002). T Cell Receptor Signaling Precedes Immunological Synapse Formation. *Science* **295**: 1539–1543.

259. Mempel, TR, Henrickson, SE and Von Andrian, UH (2004). T-cell priming by dendritic cells in lymph nodes occurs in three distinct phases. *Nature* **427**: 154–9.

260. Henrickson, SE, Mempel, TR, Mazo, IB, Liu, B, Artyomov, MN, Zheng, H, *et al.* (2008). T cell sensing of antigen dose governs interactive behavior with dendritic cells and sets a threshold for T cell activation. *Nat. Immunol.* **9**: 282–91.

261. Scholer, A, Hugues, S, Boissonnas, A, Fetler, L and Amigorena, S (2008). Intercellular Adhesion Molecule-1-Dependent Stable Interactions between T Cells and Dendritic Cells Determine CD8+ T Cell Memory. *Immunity* **28**: 258–270.

262. Varma, R, Campi, G, Yokosuka, T, Saito, T and Dustin, M (2006). T Cell Receptor-Proximal Signals Are Sustained in Peripheral Microclusters and Terminated in the Central Supramolecular Activation Cluster. *Immunity* **25**: 117–127.

263. Springer, TA (1990). Adhesion receptors of the immune system. *Nature* **346**: 425–434.

264. Schmid, EM, Bakalar, MH, Choudhuri, K, Weichsel, J, Ann, HS, Geissler, PL, *et al.* (2016). Size-dependent protein segregation at membrane interfaces. *Nat. Phys.* **12**: 704–711.

265. Lee, K-H, Dinner, AR, Tu, C, Campi, G, Raychaudhuri, S, Varma, R, *et al.* (2003). The immunological synapse balances T cell receptor signaling and degradation. *Science* **302**: 1218–22.

266. Cemerski, S, Das, J, Giurisato, E, Markiewicz, M, Allen, P, Chakraborty, A, *et al.* (2008). Evidence for Signaling From the Center of the Immune Synapse. *Immunity* **29**: 414–422.

267. Williams, RL and Urbé, S (2007). The emerging shape of the ESCRT machinery. *Nat. Rev. Mol. Cell Biol.* **8**: 355–68.

268. Valitutti, BS, Müller, S, Salio, M and Lanzavecchia, A (1997). Degredation of T cell receptor (TCR) - CD3zeta complexes after antigenic stimulation. *J. Exp. Med* **185**: 1859–1864.

269. Guy, CS, Vignali, KM, Temirov, J, Bettini, ML, Overacre, AE, Smeltzer, M, *et al.* (2013). Distinct TCR signaling pathways drive proliferation and cytokine

production in T cells. *Nat. Immunol.* **14**: 262–270.

270. Lin, X, O'Mahony, A, Mu, Y, Geleziunas, R and Greene, WC (2000). Protein kinase C-theta participates in NF-kappaB activation induced by CD3-CD28 costimulation through selective activation of IkappaB kinase beta. *Mol. Cell. Biol.* **20**: 2933–40.

271. Sun, Z, Arendt, CW, Ellmeier, W, Schaeffer, EM, Sunshine, MJ, Gandhi, L, *et al.* (2000). PKC-theta is required for TCR-induced NF-kappaB activation in mature but not immature T lymphocytes. *Nature* **404**: 402–407.

272. Brezar, V, Tu, WJ and Seddiki, N (2015). PKC-theta in regulatory and effector T-cell functions. *Front. Immunol.* **6**: 1–10.

273. Feske, S (2007). Calcium signalling in lymphocyte activation and disease. *Nat. Rev. Immunol.* **7**: 690–702.

274. Lee, KM, Chuang, E, Griffin, M, Khattri, R, Hong, DK, Zhang, W, *et al.* (1998). Molecular basis of T cell inactivation by CTLA-4. *Science* **282**: 2263–2266.

275. Jacobelli, J, Chmura, S a, Buxton, DB, Davis, MM and Krummel, MF (2004). A single class II myosin modulates T cell motility and stopping, but not synapse formation. *Nat. Immunol.* **5**: 531–8.

276. Stinchcombe, JC, Majorovits, E, Bossi, G, Fuller, S and Griffiths, GM (2006). Centrosome polarization delivers secretory granules to the immunological synapse. *Nature* **443**: 462–5.

277. de la Roche, M, Asano, Y and Griffiths, GM (2016). Origins of the cytolytic synapse. *Nat. Rev. Immunol.* **16**: 421–432.

278. Jenkins, MR and Griffiths, GM (2010). The synapse and cytolytic machinery of cytotoxic T cells. *Curr. Opin. Immunol.* **22**: 308–13.

279. Dustin, ML and Choudhuri, K (2016). Signaling and Polarized Communication

Across the T Cell Immunological Synapse. *Annu. Rev. Cell Dev. Biol.* **32**: 303–325.

280. Dustin, M and Long, E (2010). Cytotoxic immunological synapses. *Immunol. Rev.* **235**: 24–34.

281. Stinchcombe, JC and Griffiths, GM (2007). Secretory mechanisms in cell-mediated cytotoxicity. *Annu. Rev. Cell Dev. Biol.* **23**: 495–517.

282. Purbhoo, M a, Irvine, DJ, Huppa, JB and Davis, MM (2004). T cell killing does not require the formation of a stable mature immunological synapse. *Nat. Immunol.* **5**: 524–30.

283. Beal, a. M, Anikeeva, N, Varma, R, Cameron, TO, Norris, PJ, Dustin, ML, *et al.* (2008). Protein Kinase C Regulates Stability of the Peripheral Adhesion Ring Junction and Contributes to the Sensitivity of Target Cell Lysis by CTL. *J. Immunol.* **181**: 4815–4824.

284. Beal, AM, Anikeeva, N, Varma, R, Cameron, TO, Vasiliver-Shamis, G, Norris, PJ, *et al.* (2009). Kinetics of early T cell receptor signaling regulate the pathway of lytic granule delivery to the secretory domain. *Immunity* **31**: 632–42.

285. Lettau, M, Qian, J, Linkermann, A, Latreille, M, Larose, L, Kabelitz, D, *et al.* (2006). The adaptor protein Nck interacts with Fas ligand: Guiding the death factor to the cytotoxic immunological synapse. *Proc Natl Acad Sci U S A* **103**: 5911–5916.

286. Poenie, M, Kuhn, J and Combs, J (2004). Real-time visualization of the cytoskeleton and effector functions in T cells. *Curr. Opin. Immunol.* **16**: 428–438.

287. Vyas, YM, Maniar, H and Dupont, B (2002). Cutting Edge: Differential Segregation of the Src Homology 2-Containing Protein Tyrosine Phosphatase-1 Within the Early NK Cell Immune Synapse Distinguishes Noncytolytic from

Cytolytic Interactions. *J. Immunol.* **168**: 3150–3154.

288. Vyas, YM, Maniar, H, Lyddane, CE, Sadelain, M and Dupont, B (2004). Ligand binding to inhibitory killer cell Ig-like receptors induce colocalization with Src homology domain 2-containing protein tyrosine phosphatase 1 and interruption of ongoing activation signals. *J. Immunol.* **173**: 1571–1578.

289. Wulfing, C, Purtic, B, Klem, J and Schatzle, JD (2003). Stepwise cytoskeletal polarization as a series of checkpoints in innate but not adaptive cytolytic killing. *Proc. Natl. Acad. Sci. U. S. A.* **100**: 7767–72.

290. Dorrell, L, Yang, H, Ondondo, B, Dong, T, Gleria, K, Suttill, A, *et al.* (2006). Expansion and Diversification of Virus-Specific T Cells following Immunization of Human Immunodeficiency Virus Type 1 (HIV-1) -Infected Individuals with a Recombinant Modified Vaccinia Virus Ankara / HIV-1 Gag Vaccine. *J. Virol.* **80**: 4705–4716.

291. Holloway, C, Ntusi, N, Suttie, J, Mahmod, M, Wainwright, E, Clutton, G, *et al.* (2013). Comprehensive cardiac magnetic resonance imaging and spectroscopy reveals a high burden of myocardial disease in HIV infection. *Circulation* **Epub**.

292. Hancock, G, Morón-López, S, Kopycinski, J, Puertas, MC, Giannoulatou, E, Rose, A, *et al.* (2017). Evaluation of the immunogenicity and impact on the latent HIV-1 reservoir of a conserved region vaccine, MVA.HIVconsv, in antiretroviral therapy-treated subjects. *J. Int. AIDS Soc.* **20**: 1–11.

293. Fidler, S, Porter, K, Ewings, F, Frater, J, Ramjee, G, Cooper, D, *et al.* (2013). Short-Course Antiretroviral Therapy in Primary HIV Infection. *N. Engl. J. Med.* **368**: 207–217.

294. Fun, A, Mok, HP, Wills, MR and Lever, AM (2017). A highly reproducible quantitative viral outgrowth assay for the measurement of the replication-

competent latent HIV-1 reservoir. *Sci. Rep.* **7**: 43231.

295. Yang, H, Yorke, E, Hancock, G, Clutton, G, Sande, N, Angus, B, *et al.* (2013). Improved quantification of HIV-1-infected CD4+ T cells using an optimised method of intracellular HIV-1 gag p24 antigen detection. *J. Immunol. Methods* **391**: 174–8.

296. Koup, R a, Ho, DD, Poli, G and Fauci, a S (2001). Isolation and quantitation of HIV in peripheral blood. *Curr. Protoc. Immunol.* **Chapter 12**: Unit 12.2.

297. Reed, LJ and Muench, H (1938). A Simple Method of Estimating Fifty Percent Endpoints. *J. Sociol.* **27**: 493–497.

298. ATCC (2016). Converting TCID50 to MOIat <https://www.lgcstandards-atcc.org/Global/FAQs/D/3/Converting TCID50 to MOI-410.aspx?geo_country=gb>.

299. Wallace, Z, Sanderson, S, Simon, AK and Dorrell, L (2016). Exposure to zidovudine adversely affects mitochondrial turnover in primary T cells. *Antiviral Res.* **133**: 178–182.

300. Melenhorst, JJ, Leen, AM, Bollard, CM, Quigley, MF, Price, DA, Rooney, CM, *et al.* (2010). Allogeneic virus-specific T cells with HLA alloreactivity do not produce GVHD in human subjects. *Blood* **116**: 4700–4702.

301. Baker, M (2016). Statisticians issue warning over misuse of P values. *Nature* **531**: 151–151.

302. Colquhoun, D (2014). An investigation of the false discovery rate and the misinterpretation of P values. *R. Soc. Open Sci.*: 1–15doi:10.1098/rsos.140216.

303. Ruelas, DS and Greene, WC (2013). An integrated overview of HIV-1 latency. *Cell* **155**: 519–29.

304. Pace, MJ, Agosto, L, Graf, EH and O'Doherty, U (2011). HIV reservoirs and

latency models. *Virology* **411**: 344–354.

305. Shan, L, Yang, H-C, Rabi, SA, Bravo, HC, Shroff, NS, Irizarry, RA, *et al.* (2011). Influence of host gene transcription level and orientation on HIV-1 latency in a primary-cell model. *J. Virol.* **85**: 5384–93.

306. Lassen, KG, Bailey, JR and Siliciano, RF (2004). Analysis of Human Immunodeficiency Virus Type 1 Transcriptional Elongation in Resting CD4 ∂ T Cells In Vivo. *J. Virol.* **78**: 9105–9114.

307. Zhang, Z, Schuler, T, Zupancic, M, Wietgrefe, S, Staskis, K, Reimann, K, *et al.* (1999). Sexual Transmission and Propagation of SIV and HIV in Resting and Activated CD4+ T Cells. *Science* **286**: 1353–1357.

308. Lassen, KG, Ramyar, KX, Bailey, JR, Zhou, Y and Siliciano, RF (2006). Nuclear retention of multiply spliced HIV-1 RNA in resting CD4+ T cells. *PLoS Pathog.* **2**: 0650–0661.

309. Zhang, Z-Q, Wietgrefe, SW, Li, Q, Shore, MD, Duan, L, Reilly, C, *et al.* (2004). Roles of substrate availability and infection of resting and activated CD4+ T cells in transmission and acute simian immunodeficiency virus infection. *Proc. Natl. Acad. Sci. U. S. A.* **101**: 5640–5645.

310. Graf, EH, Pace, MJ, Peterson, B a, Lynch, LJ, Chukwulebe, SB, Mexas, AM, *et al.* (2013). Gag-positive reservoir cells are susceptible to HIV-specific cytotoxic T lymphocyte mediated clearance. *PLoS One* **8**: e71879.

311. Churchill, MJ, Deeks, SG, Margolis, DM, Siliciano, RF and Swanstrom, R (2016). HIV reservoirs: what, where and how to target them. *Nat. Rev. Microbiol.* **14**: 1–6.

312. Colin, L and Van Lint, C (2009). Molecular control of HIV-1 postintegration latency: implications for the development of new therapeutic strategies. *Retrovirology* **6**: 111.

313. Xing, S and Siliciano, RF (2013). Targeting HIV latency: Pharmacologic strategies toward eradication. *Drug Discov. Today* **18**: 541–551.

314. Delagrèverie, HM, Delaugerre, C, Lewin, SR, Deeks, SG and Li, JZ (2016). Ongoing clinical trials of human immunodeficiency virus latency-reversing and immunomodulatory agents. *Open Forum Infect. Dis.* **3**.

315. Cillo, AR and Mellors, JW (2016). Which therapeutic strategy will achieve a cure for HIV-1? *Curr. Opin. Virol.* **18**: 14–19.

316. Laird, GM, Bullen, CK, Rosenbloom, DIS, Martin, AR, Hill, AL, Durand, CM, *et al.* (2015). Ex vivo analysis identifies effective HIV-1 latency – reversing drug combinations. *J. Clin. Invest.* **125**: 1901–1912.

317. Elliott, JH, Wightman, F, Solomon, A, Ghneim, K, Ahlers, J, Cameron, MJ, *et al.* (2014). Activation of HIV transcription with short-course vorinostat in HIV-infected patients on suppressive antiretroviral therapy. *PLoS Pathog.* **10**: e1004473.

318. Rasmussen, TA, Tolstrup, M, Brinkmann, CR, Olesen, R, Erikstrup, C, Solomon, A, *et al.* (2014). Panobinostat, a histone deacetylase inhibitor, for latent virus reactivation in HIV-infected patients on suppressive antiretroviral therapy: A phase 1/2, single group, clinical trial. *Lancet HIV* **1**: e13–e21.

319. Søgaard, OS, Graversen, ME, Leth, S, Olesen, R, Brinkmann, CR, Nissen, SK, *et al.* (2015). The Depsipeptide Romidepsin Reverses HIV-1 Latency In Vivo. *PLoS Pathog.* **11**: 1–22.

320. Descours, B, Avettand-Fenoel, V, Blanc, C, Samri, A, Mélard, A, Supervie, V, *et al.* (2012). Immune responses driven by protective human leukocyte antigen alleles from long-term nonprogressors are associated with low HIV reservoir in central memory CD4 T cells. *Clin. Infect. Dis.* **54**: 1495–1503.

321. Casazza, JP, Betts, MR, Picker, LJ and Koup, RA (2001). Decay Kinetics of Human Immunodeficiency Virus-Specific CD8+ T Cells in Peripheral Blood after Initiation of Highly Active Antiretroviral Therapy. *J. Virol.* **75**: 6508–6516.

322. Kalams, SA, Goulder, PJ, Shea, AK, Jones, NG, Trocha, AK, Ogg, GS, *et al.* (1999). Levels of Human Immunodeficiency Virus Type 1-Specific Cytotoxic T-Lymphocyte Effector and Memory Responses Decline after Suppression of Viremia with Highly Active Antiretroviral Therapy. *J Virol* **73**: 6721–6728.

323. Shan, L, Deng, K, Shroff, NS, Durand, CM, Rabi, SA, Yang, H-C, *et al.* (2012). Stimulation of HIV-1-specific cytolytic T lymphocytes facilitates elimination of latent viral reservoir after virus reactivation. *Immunity* **36**: 491–501.

324. Liu, MKP, Hawkins, N, Ritchie, AJ, Ganusov, V V., Whale, V, Brackenridge, S, *et al.* (2013). Vertical T cell immunodominance and epitope entropy determine HIV-1 escape. *J. Clin. Invest.* **123**: 380–393.

325. Casazza, JP, Bowman, KA, Adzaku, S, Smith, EC, Enama, ME, Bailer, RT, *et al.* (2013). Therapeutic vaccination expands and improves the function of the HIV-specific memory T-cell repertoire. *J. Infect. Dis.* **207**: 1829–1840.

326. Autran, B, Murphy, RL, Costagliola, D, Tubiana, R, Clotet, B, Gatell, J, *et al.* (2008). Greater viral rebound and reduced time to resume antiretroviral therapy after therapeutic immunization with the ALVAC-HIV vaccine (vCP1452). *AIDS* **22**: 1313–1322.

327. Pollard, RB, Rockstroh, JK, Pantaleo, G, Asmuth, DM, Peters, B, Lazzarin, A, *et al.* (2014). Safety and efficacy of the peptide-based therapeutic vaccine for HIV-1, Vacc-4x: A phase 2 randomised, double-blind, placebo-controlled trial. *Lancet Infect. Dis.* **14**: 291–300.

328. Schooley, RT, Spritzler, J, Wang, H, Lederman, MM, Havlir, D, Kuritzkes, DR, *et*

al. (2010). AIDS clinical trials group 5197: a placebo-controlled trial of immunization of HIV-1-infected persons with a replication-deficient adenovirus type 5 vaccine expressing the HIV-1 core protein. *J. Infect. Dis.* **202**: 705–16.

329. Andrés, C, Plana, M, Guardo, AC, Alvarez-Fernández, C, Climent, N, Gallart, T, *et al.* (2015). HIV-1 Reservoir Dynamics after Vaccination and Antiretroviral Therapy Interruption Are Associated with Dendritic Cell-Vaccine Induced T-Cell Responses. *J. Virol.* **89**: 9189–9199.

330. Persaud, D, Luzuriaga, K, Ziemniak, C, Muresan, P, Greenough, T, Fenton, T, *et al.* (2011). Effect of therapeutic HIV recombinant poxvirus vaccines on the size of the resting CD4+ T-cell latent HIV reservoir. *AIDS* **25**: 2227–2234.

331. IrsiCaixa (2016). Study to Evaluate the Safety and Effect of HIVconsv Vaccines in Combination With Histone Deacetylase Inhibitor Romidepsin on the Viral Rebound Kinetic After Treatment Interruption in Early Treated HIV-1 Infected Individuals. *ClinicalTrials.gov*at <https://clinicaltrials.gov/ct2/show/NCT02616874>.

332. Leth, S, Schleimann, MH, Nissen, SK, Hojen, JF, Olesen, R, Graversen, ME, *et al.* (2016). Combined effect of Vacc-4x, recombinant human granulocyte macrophage colony-stimulating factor vaccination, and romidepsin on the HIV-1 reservoir (REDUC): a single-arm, phase 1B/2A trial. *Lancet* **3**: e463–e472.

333. Hong, JJ, Amancha, PK, Rogers, K, Ansari, AA and Villinger, F (2013). Re-Evaluation of PD-1 Expression by T Cells as a Marker for Immune Exhaustion during SIV Infection. *PLoS One* **8**: 1–10.

334. Sauce, D, Almeida, JR, Larsen, M, Haro, L, Autran, B, Freeman, GJ, *et al.* (2007). PD-1 expression on human CD8 T cells depends on both state of differentiation and activation status. *Aids* **21**: 2005–2013.

335. Walker-Sperling, VEK, Cohen, VJ, Tarwater, PM and Blankson, JN (2015). Reactivation kinetics of HIV-1 and susceptibility of reactivated latently infected CD4+ T cells to HIV-1-specific CD8+ T cells. *J. Virol.* **89**: 9631–9638.

336. Gupta, PK, Godec, J, Wolski, D, Adland, E, Yates, K, Pauken, KE, *et al.* (2015). CD39 Expression Identifies Terminally Exhausted CD8+ T Cells. *PLoS Pathog.* **11**: 1–21.

337. Nikolova, M, Carriere, M, Jenabian, MA, Limou, S, Younas, M, Kök, A, *et al.* (2011). CD39/adenosine pathway is involved in AIDS progression. *PLoS Pathog.* **7**.

338. Saleh, S, Solomon, A, Wightman, F, Xhilagal, M, Cameron, P and Lewin, S (2007). The CCR7 ligands CCL19 and CCL21 increase permissiveness of resting CD4+ T cells to HIV infection. *Blood* **110**: 4161–4164.

339. Marini, A, Harper, JM and Romerio, F (2008). An in vitro system to model the establishment and reactivation of HIV-1 latency. *J. Immunol.* **181**: 7713–7720.

340. Bosque, A and Planelles, V (2011). Studies of HIV-1 latency in an ex vivo model that uses primary central memory T cells. *Methods* **53**: 54–61.

341. Sahu, GK, Lee, K, Ji, J, Braciale, V, Baron, S and Cloyd, MW (2006). A novel in vitro system to generate and study latently HIV-infected long-lived normal CD4+ T-lymphocytes. *Virology* **355**: 127–137.

342. Yang, H, Xing, S, Shan, L, Connell, KO, Dinoso, J, Shen, A, *et al.* (2009). Small-molecule screening using a human primary cell model of HIV latency identifies compounds that reverse latency without cellular activation. *J. Clin. Invest.* **119**: 3473-.

343. Tyagi, M, Pearson, RJ and Karn, J (2010). Establishment of HIV Latency in Primary CD4 Cells Is due to Epigenetic Transcriptional Silencing and P-TEFb

Restriction. *J. Virol.* **84**: 6425–6437.

344. Lassen, KG, Hebbeler, AM, Bhattacharyya, D, Lobritz, MA and Greene, WC (2012). A flexible model of HIV-1 latency permitting evaluation of many primary CD4 T-cell reservoirs. *PLoS One* **7**.

345. Chavez, L, Calvanese, V and Verdin, E (2015). HIV Latency Is Established Directly and Early in Both Resting and Activated Primary CD4 T Cells. *PLOS Pathog.* **11**: e1004955.

346. Burke, B, Brown, HJ, Marsden, MD, Bristol, G, Vatakis, DN and Zack, JA (2007). Primary cell model for activation-inducible human immunodeficiency virus. *J Virol* **81**: 7424–7434.

347. Denton, PW, Olesen, R, Choudhary, SK, Archin, NM, Wahl, A, Swanson, MD, *et al.* (2012). Generation of HIV latency in humanized BLT mice. *J. Virol.* **86**: 630–4.

348. Pegu, A, Asokan, M, Wu, L, Wang, K, Hataye, J, Casazza, JP, *et al.* (2015). Activation and lysis of human CD4 cells latently infected with HIV-1. *Nat. Commun.* **6**: 8447.

349. Dixon, JF, Law, JL and Favero, JJ (1989). Activation of human T lymphocytes by crosslinking of anti-CD3 monoclonal antibodies. *J. Leukoc. Biol.* **46**: 214–220.

350. Raman, MCC, Rizkallah, PJ, Simmons, R, Donnellan, Z, Dukes, J, Bossi, G, *et al.* (2016). Direct molecular mimicry enables off-target cardiovascular toxicity by an enhanced affinity TCR designed for cancer immunotherapy. *Sci. Rep.* **6**: 18851.

351. Li, P, Kaiser, P, Lampiris, HW, Kim, P, Yukl, SA, Diane, V, *et al.* (2016). Stimulating the RIG-I pathway to kill cells in the latent HIV reservoir following viral reactivation. *Nat. Med.* **22**: 807–811.

352. Clutton, G, Xu, Y, Baldoni, PL, Mollan, KR, Kirchherr, J, Newhard, W, *et al.* (2016). The differential short- and long-term effects of HIV-1 latency-reversing

agents on T cell function. *Sci. Rep.* **6**: 30749.

353. Spina, CA, Anderson, J, Archin, NM, Bosque, A, Chan, J, Famiglietti, M, *et al.* (2013). An In-Depth Comparison of Latent HIV-1 Reactivation in Multiple Cell Model Systems and Resting CD4+ T Cells from Aviremic Patients. *PLoS Pathog.* **9**: 1–15.

354. Wherry, EJ and Kurachi, M (2015). Molecular and cellular insights into T cell exhaustion. *Nat. Rev. Immunol.* **15**: 486–499.

355. Maldonado, RA and von Andrian, UH (2010). How Tolerogenic Dendritic Cells Induce Regulatory T Cells. *Adv. Immunol.* **108**: 111–165.

356. Duraiswamy, J, Ibegbu, CC, Masopust, D, Miller, JD, Araki, K, Doho, GH, *et al.* (2011). Phenotype, function, and gene expression profiles of programmed death-1(hi) CD8 T cells in healthy human adults. *J. Immunol.* **186**: 4200–12.

357. Agata, Y, Kawasaki, A, Nishimura, H, Ishida, Y, Tsubata, T, Yagita, H, *et al.* (1996). Expression of the PD-1 antigen on the surface of stimulated mouse T and B lymphocytes. *Int. Immunol.* **8**: 765–772.

358. Trautmann, L, Janbazian, L, Chomont, N, Said, EA, Gimmig, S, Bessette, B, *et al.* (2006). Upregulation of PD-1 expression on HIV-specific CD8 + T cells leads to reversible immune dysfunction. *Nat. Medi* **12**: 1198–1202.

359. Yamamoto, T, Price, D a, Casazza, JP, Ferrari, G, Nason, M, Pratip, K, *et al.* (2011). Surface expression patterns of negative regulatory molecules identify determinants of virus-specific CD8 + T-cell exhaustion in HIV infection. *Blood* **117**: 4805–4815.

360. Canale, FP, Ramello, MC, Núñez, N, Araujo Furlan, CL, Bossio, SN, Gorosito Serrán, M, *et al.* (2017). CD39 expression defines cell exhaustion in tumor-infiltrating CD8+ T cells. *Cancer Res.*: canres.2684.2016doi:10.1158/0008-

5472.CAN-16-2684.

361. Roederer, M, Quaye, L, Mangino, M, Beddall, MH, Chattopadhyay, P, Tosi, I, *et al.* (2015). The Genetic Architecture of the Human Immune System: A Bioresource for Autoimmunity and Disease Pathogenesis. *Cell* **161**: 387–403.

362. Buggert, M, Tauriainen, J, Yamamoto, T, Frederiksen, J, Ivarsson, MA, Michaëlsson, J, *et al.* (2014). T-bet and Eomes Are Differentially Linked to the Exhausted Phenotype of CD8+ T Cells in HIV Infection. *PLoS Pathog.* **10**.

363. Kaufmann, DE, Kavanagh, DG, Pereyra, F, Zaunders, JJ, Mackey, EW, Miura, T, *et al.* (2007). Upregulation of CTLA-4 by HIV-specific CD4+ T cells correlates with disease progression and defines a reversible immune dysfunction. *Nat. Immunol.* **8**: 1246–1254.

364. Blackburn, SD, Shin, H, Haining, WN, Zou, T, Workman, CJ, Polley, A, *et al.* (2009). Coregulation of CD8+ T cell exhaustion by multiple inhibitory receptors during chronic viral infection. *Nat. Immunol.* **10**: 29–37.

365. Hurst, J, Hoffmann, M, Pace, M, Williams, J, Thornhill, J, Hamlyn, E, *et al.* (2015). Immunological biomarkers predict HIV-1 viral rebound after treatment interruption. *Nat. Commun.* **6**: 8495.

366. Kamphorst, AO, Wieland, A, Nasti, T, Yang, S, Zhang, R, Barber, DL, *et al.* (2017). Rescue of exhausted CD8 T cells by PD-1 – targeted therapies is CD28-dependent. *Science* **3553**: 1423–1427.

367. Barber, DL, Wherry, EJ, Masopust, D, Zhu, B, Allison, JP, Sharpe, AH, *et al.* (2006). Restoring function in exhausted CD8 T cells during chronic viral infection. *Nature* **439**: 682–687.

368. Fenoglio, D, Dentone, C, Signori, A, Di Biagio, A, Parodi, A, Kalli, F, *et al.* (2017). CD8+CD28−CD127loCD39+ regulatory T-cell expansion: A new possible

pathogenic mechanism for HIV infection? *J. Allergy Clin. Immunol.*doi:https://doi.org/10.1016/j.jaci.2017.08.021.

369. Cardozo, EF, Andrade, A, Mellors, JW, Kuritzkes, DR, Perelson, AS and Ribeiro, RM (2017). Treatment with integrase inhibitor suggests a new interpretation of HIV RNA decay curves that reveals a subset of cells with slow integration. *PLOS Pathog.* **13**: e1006478.

370. Hell, SW, Sahl, SJ, Bates, M, Zhuang, X, Heintzmann, R, Booth, MJ, *et al.* (2015). The 2015 super-resolution microscopy roadmap. *J. Phys. D. Appl. Phys.* **48**: 443001.

371. Dustin, ML and Depoil, D (2011). New insights into the T cell synapse from single molecule techniques. *Nat. Rev. Immunol.* **11**: 672–684.

372. Sims, TN and Dustin, ML (2002). The immunological synapse: integrins take the stage. *Immunol. Rev.* **186**: 100–117.

373. Dustin, ML (2005). A dynamic view of the immunological synapse. *Semin. Immunol.* **17**: 400–410.

374. Dustin, ML and Davis, SJ (2014). TCR signaling: the barrier within. *Nat. Immunol.* **15**: 136–7.

375. Kaizuka, Y, Douglass, AD, Varma, R, Dustin, ML and Vale, RD (2007). Mechanisms for segregating T cell receptor and adhesion molecules during immunological synapse formation in Jurkat T cells. *Proc. Natl. Acad. Sci.* **104**: 20296–20301.

376. Brown, ACN, Oddos, S, Dobbie, IM, Alakoskela, JM, Parton, RM, Eissmann, P, *et al.* (2011). Remodelling of cortical actin where lytic granules dock at Natural Killer cell immune synapses revealed by super-resolution microscopy. *PLoS Biol.* **9**.

377. Rak, GD, Mace, EM, Banerjee, PP, Svitkina, T and Orange, JS (2011). Natural Killer cell lytic granule secretion occurs through a pervasive actin network at the immune synapse. *PLoS Biol.* **9**.

378. Friedl, P, den Boer, AT and Gunzer, M (2005). Tuning immune responses: diversity and adaptation of the immunological synapse. *Nat. Rev. Immunol.* **5**: 532–45.

379. Rossy, J, Pageon, S V, Davis, DM and Gaus, K (2013). Super-resolution microscopy of the immunological synapse. *Curr. Opin. Immunol.* **25**: 307–12.

380. Eggeling, C, Willig, KI and Barrantes, FJ (2013). STED microscopy of living cells--new frontiers in membrane and neurobiology. *J. Neurochem.* **126**: 203–12.

381. Fölling, J, Bossi, M, Bock, H, Medda, R, Wurm, CA, Hein, B, *et al.* (2008). Fluorescence nanoscopy by ground-state depletion and single-molecule return. *Nat. Methods* **5**: 943–945.

382. Hosseini, BH, Louban, I, Djandji, D, Wabnitz, GH, Deeg, J, Bulbuc, N, *et al.* (2009). Immune synapse formation determines interaction forces between T cells and antigen-presenting cells measured by atomic force microscopy. *Proc Natl Acad Sci U S A* **106**: 17852–17857.

383. Willig, KI, Rizzoli, SO, Westphal, V, Jahn, R and Hell, SW (2006). STED microscopy reveals that synaptotagmin remains clustered after synaptic vesicle exocytosis. *Nature* **440**: 935–939.

384. Petit, A-E, Demotte, N, Scheid, B, Wildmann, C, Bigirimana, R, Gordon-Alonso, M, *et al.* (2016). A major secretory defect of tumour-infiltrating T lymphocytes due to galectin impairing LFA-1-mediated synapse completion. *Nat. Commun.* **7**: 12242.

385. Jenkins, MR, Tsun, A, Stinchcombe, JC and Griffiths, GM (2009). The Strength of

T Cell Receptor Signal Controls the Polarization of Cytotoxic Machinery to the Immunological Synapse. *Immunity* **31**: 621–631.

386. Jenkins, MR, Stinchcombe, JC, Au-Yeung, BB, Asano, Y, Ritter, AT, Weiss, A, *et al.* (2014). Distinct structural and catalytic roles for Zap70 in formation of the immunological synapse in CTL. *Elife* **3**: e01310.

387. Felts, RL, Narayan, K, Estes, JD, Shi, D, Trubey, CM, Fu, J, *et al.* (2010). 3D visualization of HIV transfer at the virological synapse between dendritic cells and T cells. *Proc. Natl. Acad. Sci. U. S. A.* **107**: 13336–41.

388. Nyakeriga, AM, Fichtenbaum, CJ, Goebel, J, Nicolaou, S a, Conforti, L and Chougnet, C a (2009). Engagement of the CD4 receptor affects the redistribution of Lck to the immunological synapse in primary T cells: implications for T-cell activation during human immunodeficiency virus type 1 infection. *J. Virol.* **83**: 1193–1200.

389. Stephen, TL, Wilson, BS and Laufer, TM (2012). Subcellular distribution of Lck during CD4 T-cell maturation in the thymic medulla regulates the T-cell activation threshold. *Proc. Natl. Acad. Sci.* **109**: 7415–7420.

390. Nika, K, Soldani, C, Salek, M, Paster, W, Gray, A, Etzensperger, R, *et al.* (2010). Constitutively active lck kinase in T cells drives antigen receptor signal transduction. *Immunity* **32**: 766–777.

391. Davis, SJ and van der Merwe, PA (2011). Lck and the nature of the T cell receptor trigger. *Trends Immunol.* **32**: 1–5.

392. Holdorf, AD, Lee, K-H, Burack, WR, Allen, PM and Shaw, AS (2002). Regulation of Lck activity by CD4 and CD28 in the immunological synapse. *Nat. Immunol.* **3**: 259–264.

393. Reichardt, P, Dornbach, B and Gunzer, M (2007). The molecular makeup and

function of regulatory and effector synapses. *Immunol. Rev.* **218**: 165–177.

394. Jo, JH, Kwon, MS, Choi, HO, Oh, HM, Kim, HJ and Jun, CD (2010). Recycling and LFA-1-dependent trafficking of ICAM-1 to the immunological synapse. *J. Cell. Biochem.* **111**: 1125–1137.

395. Groppelli, E, Starling, S and Jolly, C (2015). Contact-Induced Mitochondrial Polarization Supports HIV-1 Virological Synapse Formation. *J. Virol.* **89**: 14–24.

396. Borg, C, Abdelali, J, Laderach, D, Maruyama, K, Wakasugi, H, Charrier, S, *et al.* (2004). NK Cell Activation by Dendritic Cells (DC) Require The Formation of a Synapse leading to IL-12 Polarization in DC. *Blood* **104**: 3267–3276.

397. Mace, EM and Orange, JS (2012). New views of the human NK cell immunological synapse: recent advances enabled by super- and high-resolution imaging techniques. *Front. Immunol.* **3**: 421.

398. Kopcow, HD, Allan, DSJ, Chen, X, Rybalov, B, Andzelm, MM, Ge, B, *et al.* (2005). Human decidual NK cells form immature activating synapses and are not cytotoxic. *Proc. Natl. Acad. Sci. U. S. A.* **102**: 15563–15568.

399. De Clercq, S, Zwaenepoel, O, Martens, E, Vandekerckhove, J, Guillabert, A and Gettemans, J (2012). Nanobody-induced perturbation of LFA-1/L-plastin phosphorylation impairs MTOC docking, immune synapse formation and T cell activation. *Cell. Mol. Life Sci.* **70**: 909–922.

400. Haller, C, Rauch, S, Michel, N, Hannemann, S, Lehmann, MJ, Keppler, OT, *et al.* (2006). The HIV-1 pathogenicity factor Nef interferes with maturation of stimulatory T-lymphocyte contacts by modulation of N-Wasp activity. *J. Biol. Chem.* **281**: 19618–19630.

401. Soares, H, Lasserre, R and Alcover, A (2013). Orchestrating cytoskeleton and intracellular vesicle traffic to build functional immunological synapses. *Immunol.*

Rev. **256**: 118–132.

402. Ilani, T, Khanna, C, Zhou, M, Veenstra, TD and Bretscher, A (2007). Immune synapse formation requires ZAP-70 recruitment by ezrin and CD43 removal by moesin. *J. Cell Biol.* **179**: 733–746.

403. Bertrand, F, Müller, S, Roh, K-H, Laurent, C, Dupré, L and Valitutti, S (2013). An initial and rapid step of lytic granule secretion precedes microtubule organizing center polarization at the cytotoxic T lymphocyte/target cell synapse. *Proc. Natl. Acad. Sci. U. S. A.* **110**: 6073–8.

404. Sol-Foulon, N, Sourisseau, M, Porrot, F, Thoulouze, M-I, Trouillet, C, Nobile, C, *et al.* (2007). ZAP-70 kinase regulates HIV cell-to-cell spread and virological synapse formation. *EMBO J.* **26**: 516–26.

405. Comrie, WA, Babich, A and Burkhardt, JK (2015). F-actin flow drives affinity maturation and spatial organization of LFA-1 at the immunological synapse. *J. Cell Biol.* **208**: 475–491.

406. Dustin, ML and Cooper, J a (2000). The immunological synapse and the actin cytoskeleton: molecular hardware for T cell signaling. *Nat. Immunol.* **1**: 23–29.

407. Khaznadar, Z, Henry, G, Setterblad, N, Agaugue, S, Raffoux, E, Boissel, N, *et al.* (2014). Acute myeloid leukemia impairs natural killer cells through the formation of a deficient cytotoxic immunological synapse. *Eur. J. Immunol.* **44**: 3068–3080.

408. Tsun, A, Qureshi, I, Stinchcombe, JC, Jenkins, MR, De La Roche, M, Kleczkowska, J, *et al.* (2011). Centrosome docking at the immunological synapse is controlled by Lck signaling. *J. Cell Biol.* **192**: 663–674.

409. Na, BR, Kim, HR, Piragyte, I, Oh, HM, Kwon, MS, Akber, U, *et al.* (2015). TAGLN2 regulates T cell activation by stabilizing the actin cytoskeleton at the immunological synapse. *J. Cell Biol.* **209**: 143–162.

410. Makedonas, G, Banerjee, PP, Pandey, R, Hersperger, AR, Sanborn, KB, Hardy, GAD, *et al.* (2009). Rapid Up-Regulation and Granule-Independent Transport of Perforin to the Immunological Synapse Define a Novel Mechanism of Antigen-Specific CD8+ T cell Cytotoxic Activity. *J. Immunol.* **182**: 5560–5569.

411. Orange, JS, Harris, KE, Andzelm, MM, Valter, MM, Geha, RS and Strominger, JL (2003). The mature activating natural killer cell immunologic synapse is formed in distinct stages. *Proc. Natl. Acad. Sci. U. S. A.* **100**: 14151–6.

412. Krzewski, K, Gil-krzewska, A, Nguyen, V, Peruzzi, G, Coligan, JE, Dc, W, *et al.* (2013). LAMP1 / CD107a is required for efficient perforin delivery to lytic granules LAMP1 / CD107a is required for ef fi cient perforin delivery to lytic granules and NK-cell cytotoxicity. *Immunobiology* **121**: 4672–4683.

413. Nyakeriga, AM, Fichtenbaum, CJ, Goebel, J, Nicolaou, S a, Conforti, L and Chougnet, C a (2009). Engagement of the CD4 receptor affects the redistribution of Lck to the immunological synapse in primary T cells: implications for T-cell activation during human immunodeficiency virus type 1 infection. *J. Virol.* **83**: 1193–200.

414. Li, Q-J, Dinner, AR, Qi, S, Irvine, DJ, Huppa, JB, Davis, MM, *et al.* (2004). CD4 enhances T cell sensitivity to antigen by coordinating Lck accumulation at the immunological synapse. *Nat. Immunol.* **5**: 791–799.

415. Tavano, R, Gri, G, Molon, B, Marinari, B, Rudd, CE, Tuosto, L, *et al.* (2004). CD28 and lipid rafts coordinate recruitment of Lck to the immunological synapse of human T lymphocytes. *J. Immunol.* **173**: 5392–5397.

416. Jamur, M and Oliver, C (2010). Permeabilization of Cell Membranes. *Methods Mol. Biol.* **588**: 63–66.

417. Kabanova, A, Sanseviero, F, Veronica, C, Gamberucci, A, Gozzetti, A,

Campoccia, G, *et al.* (2016). Human Cytotoxic T Lymphocytes Form Dysfunctional Immune Synapses with B Cells Characterized by Non-Polarized Lytic Granule Release. *Cell Rep.* **15**: 9–18.

418. Arhel, N, Lehmann, M, Clauß, K, Nienhaus, GU, Piguet, V and Kirchhoff, F (2009). The inability to disrupt the immunological synapse between infected human T cells and APCs distinguishes HIV-1 from most other primate lentiviruses. *J. Clin. Invest.* **119**: 2965–2975.

419. Ramsay, AG, Johnson, AJ, Lee, AM, Gorgün, G, Le Dieu, R, Blum, W, *et al.* (2008). Chronic lymphocytic leukemia T cells show impaired immunological synapse formation that can be reversed with an immunomodulating drug. *J. Clin. Invest.* **118**: 2427–37.

420. Kuhn, JR and Poenie, M (2002). Dynamic polarization of the microtubule cytoskeleton during CTL-mediated killing. *Immunity* **16**: 111–121.

421. Prasad, V, Semwogerere, D and Weeks, ER (2007). Confocal microscopy of colloids. *J. Phys. Condens. Matter* **19**: 113102.

422. (2017). Widefield Microscope. *Sci. Vol. Imaging*at <https://svi.nl/WideFieldMicroscope>.

423. Coker, A and Davidson, M. Comparison Between Confocal and Widefield Microscopy. *Educ. Microsc. Digit. Imaging*at <http://zeiss-campus.magnet.fsu.edu/tutorials/opticalsectioning/confocalwidefield/indexflash.html>.

424. Mace, EM and Orange, JS (2012). Dual channel STED nanoscopy of lytic granules on actin filaments in natural killer cells. *Commun. Integr. Biol.* **5**: 184–186.

425. Hashimoto-Tane, A, Yokosuka, T, Sakata-Sogawa, K, Sakuma, M, Ishihara, C, Tokunaga, M, *et al.* (2011). Dynein-Driven Transport of T Cell Receptor

Microclusters Regulates Immune Synapse Formation and T Cell Activation. *Immunity* **34**: 919–931.

426. Sanderson, NSR, Puntel, M, Kroeger, KM, Bondale, NS, Swerdlow, M, Iranmanesh, N, *et al.* (2012). Cytotoxic immunological synapses do not restrict the action of interferon-γ to antigenic target cells. *Proc. Natl. Acad. Sci. U. S. A.* **109**: 7835–40.

427. Campbell, EM and Hope, TJ (2008). Live cell imaging of the HIV-1 life cycle. *Trends Microbiol.* **16**: 580–7.

428. Foley, MH, Forcier, T, McAndrew, E, Gonzalez, M, Chen, H, Juelg, B, *et al.* (2014). High avidity CD8+ T cells efficiently eliminate motile HIV-infected targets and execute a locally focused program of anti-viral function. *PLoS One* **9**: e87873.

429. Halle, S, Halle, O and Förster, R (2017). Mechanisms and Dynamics of T Cell-Mediated Cytotoxicity In Vivo. *Trends Immunol.* **38**: 432–443.

430. Fackler, OT, Alcover, A and Schwartz, O (2007). Modulation of the immunological synapse: a key to HIV-1 pathogenesis? *Nat. Rev. Immunol.* **7**: 310–317.

431. Chorin, E, Gal-Garber, O, Yagel, Y, Turner, D, Avidor, B, Berke, G, *et al.* (2014). PBMC of HIV-infected patients contain CD8 T cells that form conjugates with and kill HIV- infected autologous CD4 T cells. *Immunology*doi:10.1111/imm.12385.

432. Sáez-Cirión, A, Lacabaratz, C, Lambotte, O, Versmisse, P, Urrutia, A, Boufassa, F, *et al.* (2007). HIV controllers exhibit potent CD8 T cell capacity to suppress HIV infection ex vivo and peculiar cytotoxic T lymphocyte activation phenotype. *Proc. Natl. Acad. Sci. U. S. A.* **104**: 6776–6781.

433. Piguet, V and Sattentau, Q (2004). Dangerous liaisons at the virological synapse. *J.*

Clin. Invest. **114**: 605–10.

434. Jolly, C (2010). T cell polarization at the virological synapse. *Viruses* **2**: 1261–1278.

435. Sowinski, S, Jolly, C, Berninghausen, O, Purbhoo, M a, Chauveau, A, Köhler, K, *et al.* (2008). Membrane nanotubes physically connect T cells over long distances presenting a novel route for HIV-1 transmission. *Nat. Cell Biol.* **10**: 211–9.

436. Dieckmann, NMG, Frazer, GL, Asano, Y, Stinchcombe, JC, Griffiths, GM, Azimzadeh, J, *et al.* (2016). The cytotoxic T lymphocyte immune synapse at a glance. *J. Cell Sci.* **129**: 2881–6.

437. Kabanova, A, Sanseviero, F, Veronica, C, Gamberucci, A, Gozzetti, A, Campoccia, G, *et al.* (2016). Human Cytotoxic T Lymphocytes Form Dysfunctional Immune Synapses with B Cells Characterized by Non-Polarized Lytic Granule Release - Supplementary. *Cell Rep.* **15**.

438. Clayton, KL, Haaland, MS, Douglas-Vail, MB, Mujib, S, Chew, GM, Ndhlovu, LC, *et al.* (2014). T cell Ig and mucin domain-containing protein 3 is recruited to the immune synapse, disrupts stable synapse formation, and associates with receptor phosphatases. *J. Immunol.* **192**: 782–91.

439. Vasiliver-Shamis, G, Dustin, ML and Hioe, CE (2010). HIV-1 Virological Synapse is not Simply a Copycat of the Immunological Synapse. *Viruses* **2**: 1239–60.

440. Banerjee, P and Orange, J (2010). Quantitative measurement of F-actin accumulation at the NK cell immunological synapse. *J Immunol Methods* **355**: 1–13.

441. Markey, KA, Gartlan, KH, Kuns, RD, MacDonald, KPA and Hill, GR (2015). Imaging the immunological synapse between dendritic cells and T cells. *J. Immunol. Methods* **423**: 40–44.

442. Volberding, P a and Deeks, SG (2010). Antiretroviral therapy and management of HIV infection. *Lancet* **376**: 49–62.

443. Barouch, DH and Deeks, SG (2014). Immunologic strategies for HIV-1 remission and eradication. *Science* **345**: 169–174.

444. Morgan, MM, Labno, CM, Van Seventer, G a, Denny, MF, Straus, DB and Burkhardt, JK (2001). Superantigen-induced T cell:B cell conjugation is mediated by LFA-1 and requires signaling through Lck, but not ZAP-70. *J. Immunol.* **167**: 5708–5718.

445. Vasconcelos, Z, Müller, S, Guipouy, D, Yu, W, Christophe, C, Gadat, S, *et al.* (2015). Individual Human Cytotoxic T Lymphocytes Exhibit Intraclonal Heterogeneity during Sustained Killing. *Cell Rep.* **11**: 1474–1485.

446. Ritter, AT, Asano, Y, Stinchcombe, JC, Dieckmann, NMG, Chen, BC, Gawden-Bone, C, *et al.* (2015). Actin Depletion Initiates Events Leading to Granule Secretion at the Immunological Synapse. *Immunity* **42**: 864–876.

447. Franciszkiewicz, K, Le Floc'H, A, Boutet, M, Vergnon, I, Schmitt, A and Mami-Chouaib, F (2013). CD103 or LFA-1 engagement at the immune synapse between cytotoxic T cells and tumor cells promotes maturation and regulates T-cell effector functions. *Cancer Res.* **73**: 617–628.

448. Blanchard, N, Di Bartolo, V and Hivroz, C (2002). In the immune synapse, ZAP-70 controls T cell polarization and recruitment of signaling proteins but not formation of the synaptic pattern. *Immunity* **17**: 389–399.

449. Fraser, JD (2011). Clarifying the mechanism of superantigen toxicity. *PLoS Biol.* **9**: 1–4.

450. Yokosuka, T, Sakata-Sogawa, K, Kobayashi, W, Hiroshima, M, Hashimoto-Tane, A, Tokunaga, M, *et al.* (2005). Newly generated T cell receptor microclusters

initiate and sustain T cell activation by recruitment of Zap70 and SLP-76. *Nat. Immunol.* **6**: 1253–62.

451. Penna, D, Müller, S, Martinon, F, Demotz, S, Iwashima, M and Valitutti, S (1999). Degradation of ZAP-70 following antigenic stimulation in human T lymphocytes: role of calpain proteolytic pathway. *J. Immunol.* **163**: 50–56.

452. Demers, KR, Makedonas, G, Buggert, M, Eller, MA, Ratcliffe, SJ, Goonetilleke, N, *et al.* (2016). Temporal Dynamics of CD8+ T Cell Effector Responses during Primary HIV Infection. *PLoS Pathog.* **12**: 1–24.

453. Singh, NJ and Schwartz, RH (2003). The Strength of Persistent Antigenic Stimulation Modulates Adaptive Tolerance in Peripheral CD4 $^{+}$ T Cells. *J. Exp. Med.* **198**: 1107–1117.

454. Poenie, M, Tsien, RY and Schmitt-Verhulst, A-M (1987). Sequential activation and lethal hit measured by [Ca2+]i in individual cytolytic T cells and targets. *EMBO J.* **6**: 2223–2232.

455. Halle, S, Keyser, KA, Stahl, FR, Busche, A, Marquardt, A, Zheng, X, *et al.* (2016). In Vivo Killing Capacity of Cytotoxic T Cells Is Limited and Involves Dynamic Interactions and T Cell Cooperativity. *Immunity* **44**: 233–245.

456. Guay, LA, Musoke, P, Fleming, T, Bagenda, D, Allen, M, Nakabiito, C, *et al.* (1999). Intrapartum and neonatal single-dose nevirapine compared with zidovudine for prevention of mother-to-child transmission of HIV-1 in Kampala, Uganda: 18-Month follow-up of the HIVNET 012 randomised trial. *Lancet* **354**: 795–802.

457. Hirsch, MS (1988). Aids commentary: Azidothymidine. *J. Infect. Dis.* **157**: 427–431.

458. Mitsuya, H, Yarchoan, R and Broder, S (1990). Molecular targets for AIDS Therapy. *Science* **249**: 1533–1543.

459. Bourdais, J, Biondi, R, Sarfati, S, Guerreiro, C, Lascu, I and Veron, M (1996). Cellular Phosphorylation of Anti-HIV Nucleosides. *J. Biol. Chem.*: 7887–7891.

460. Hachiya, A, Kodama, EN, Schuckmann, MM, Kirby, KA, Michailidis, E, Sakagami, Y, *et al.* (2011). K70Q adds high-level tenofovir resistance to 'Q151M complex' HIV reverse transcriptase through the enhanced discrimination mechanism. *PLoS One* **6**.

461. Apostolova, N, Blas-García, A and Esplugues, J V (2011). Mitochondrial interference by anti-HIV drugs: mechanisms beyond Pol-γ inhibition. *Trends Pharmacol. Sci.* **32**: 715–25.

462. Brinkman, K, Hofstede, HJM, Burger, DM, Smeitink, JAM and Koopmans, PP (1998). Adverse effects of reverse transcriptase inhibitors : mitochondrial toxicity as common pathway. *AIDS* **12**.

463. Scruggs, ER and Dirks Naylor, AJ (2008). Mechanisms of zidovudine-induced mitochondrial toxicity and myopathy. *Pharmacology* **82**: 83–88.

464. Lynx, MD and McKee, EE (2006). 3'-Azido-3'-deoxythymidine (AZT) is a competitive inhibitor of thymidine phosphorylation in isolated rat heart and liver mitochondria. *Biochem. Pharmacol.* **72**: 239–243.

465. Furman, PA, Fyfe, JA, St Clair, MH, Weinhold, K, Rideout, JL, Freeman, GA, *et al.* (1986). Phosphorylation of 3'-azido-3'-deoxythymidine and selective interaction of the 5'-triphosphate with human immunodeficiency virus reverse transcriptase. *Proc. Natl. Acad. Sci. U. S. A.* **83**: 8333–8337.

466. Maagaard, A and Kvale, D (2009). Long term adverse effects related to nucleoside reverse transcriptase inhibitors: clinical impact of mitochondrial toxicity. *Scand. J. Infect. Dis.* **41**: 808–17.

467. Côté, HCF, Brumme, ZL, Craib, KJP, Alexander, CS, Wynhoven, B, Ting, L, *et al.*

(2002). Changes in Mitochondrial DNA as a Marker of Nucleoside Toxicity in HIV-Infected Patients. *N. Engl. J. Med.* **346**: 811–820.

468. Benbrik, E, Chariot, P, Bonavaud, S, Ammi-Saïd, M, Frisdal, E, Rey, C, *et al.* (1997). Cellular and mitochondrial toxicity of zidovudine (AZT), didanosine (ddI) and zalcitabine (ddC) on cultured human muscle cells. *J. Neurol. Sci.* **149**: 19–25.

469. Gardner, K, Hall, P a, Chinnery, PF and Payne, B a I (2013). HIV Treatment and Associated Mitochondrial Pathology: Review of 25 Years of in Vitro, Animal, and Human Studies. *Toxicol. Pathol.* **42**: 811–822.

470. Johnson, A, Ray, a S, Hanes, J, Suo, Z, Colacino, JM, Anderson, KS, *et al.* (2001). Toxicity of antiviral nucleoside analogs and the human mitochondrial DNA polymerase. *J. Biol. Chem.* **276**: 40847–57.

471. Stankov, M V, Panayotova-Dimitrova, D, Leverkus, M, Schmidt, RE and Behrens, GMN (2013). Thymidine analogues suppress autophagy and adipogenesis in cultured adipocytes. *Antimicrob. Agents Chemother.* **57**: 543–51.

472. Stankov, M V, Panayotova-Dimitrova, D, Leverkus, M, Vondran, FWR, Bauerfeind, R, Binz, A, *et al.* (2012). Autophagy inhibition due to thymidine analogues as novel mechanism leading to hepatocyte dysfunction and lipid accumulation. *AIDS* **26**: 1995–2006.

473. Phadwal, K, Alegre-abarrategui, J, Watson, AS, Pike, L, Anbalagan, S, Hammond, EM, *et al.* (2012). A novel method for autophagy detection in primary cells. *Autophagy* **8**: 677–689.

474. Deretic, V, Saitoh, T and Akira, S (2013). Autophagy in infection, inflammation and immunity. *Nat. Rev. Immunol.* **13**: 722–37.

475. Dinkins, C et al. (2010). Autophagy and HIV. *Semin Cell Dev Bio* **21**: 712–718.

476. Wandeler, G, Gsponer, T, Mulenga, L, Garone, D, Wood, R, Maskew, M, *et al.*

(2013). Zidovudine impairs immunological recovery on first-line antiretroviral therapy: collaborative analysis of cohort studies in southern Africa. *AIDS* **27**: 2225–32.

477. Autran, B and Autran Li, T., Blanc, C., Mathez, D., Tubiana, R., Katlama, C., Debré, P. Leibowitch, J., B (1997). Positive Effects of Combined Antiretroviral Therapy on CD4+ T Cell Homeostasis and Function in Advanced HIV Disease. *Science* **277**: 112–116.

478. Petrovas, C, Mueller, YM, Dimitriou, ID, Altork, SR, Banerjee, A, Sklar, P, *et al.* (2007). Increased mitochondrial mass characterizes the survival defect of HIV-specific CD8(+) T cells. *Blood* **109**: 2505–13.

479. Simon, AK. Autophagy detection techniques in primary mammalian cells. *Cold Spring Harb. Protoc.*

480. Pua, HH, Guo, J, Komatsu, M and He, Y-W (2009). Autophagy is essential for mitochondrial clearance in mature T lymphocytes. *J. Immunol.* **182**: 4046–55.

481. Watanabe, R, Fujii, H, Shirai, T, Saito, S, Ishii, T and Harigae, H (2014). Autophagy plays a protective role as an anti-oxidant system in human T cells and represents a novel strategy for induction of T-cell apoptosis. *Eur. J. Immunol.* **44**: 2508–2520.

482. Yan, J, Sabbaj, S, Bansal, A, Amatya, N, Shacka, JJ, Goepfert, P a, *et al.* (2013). HIV-specific CD8+ T cells from elite controllers are primed for survival. *J. Virol.* **87**: 5170–81.

483. Migueles, S a, Weeks, K a, Nou, E, Berkley, AM, Rood, JE, Osborne, CM, *et al.* (2009). Defective human immunodeficiency virus-specific CD8+ T-cell polyfunctionality, proliferation, and cytotoxicity are not restored by antiretroviral therapy. *J. Virol.* **83**: 11876–89.

484. Yamaguchi, T, Katoh, I and Kurata, SI (2002). Azidothymidine causes functional and structural destruction of mitochondria, glutathione deficiency and HIV-1 promoter sensitization. *Eur. J. Biochem.* **269**: 2782–2788.

485. Pua, HH, Dzhagalov, I, Chuck, M, Mizushima, N and He, Y-W (2007). A critical role for the autophagy gene Atg5 in T cell survival and proliferation. *J. Exp. Med.* **204**: 25–31.

486. Gottlieb, R and Raquel, C (2010). Autophagy in health and disease. 5. Mitophagy as a way of life. *Am J Physiol Cell Physiol* **299**: C203–C210.

487. Dalakas, M, Ila, I, Pezeshkpour, GH, Laukaitis, J, Cohen, B and Griffin, J (1990). Mitochondrial myopathy caused by long-term Zidovudine therapy. *N. Engl. J. Med.* **322**.

488. Caron-Debarle, M, Lagathu, C, Boccara, F, Vigouroux, C and Capeau, J (2010). HIV-associated lipodystrophy: from fat injury to premature aging. *Trends Mol. Med.* **16**: 218–29.

489. Xu, X, Araki, K, Li, S, Han, J-H, Ye, L, Tan, WG, *et al.* (2014). Autophagy is essential for effector CD8+ T cell survival and memory formation. *Nat. Immunol.* **15**.

490. Mizushima, N, Yoshimori, T and Levine, B (2010). Methods in mammalian autophagy research. *Cell* **140**: 313–26.

491. Puleston, D, Phadwal, K, Watson, AS, Soilleux, EJ, Chittaranjan, S, Bortnik, S, *et al.* (2015). Techniques for the detection of autophagy in primary mammalian cells. *Cold Spring Harb. Protoc.* **2015**: 789–792.

492. Sagnier, S, Daussy, CF, Borel, S, Robert-Hebmann, V, Faure, M, Blanchet, FP, *et al.* (2015). Autophagy Restricts HIV-1 Infection by Selectively Degrading Tat in CD4 + T Lymphocytes. *J. Virol.* **89**: 615–625.

493. Maiuri, MC, Zalckvar, E, Kimchi, A and Kroemer, G (2007). Self-eating and self-killing: crosstalk between autophagy and apoptosis. *Nat. Rev. Mol. Cell Biol.* **8**: 741–52.

494. Tripathi, P and Hildeman, D (2004). Sensitization of T cells to apoptosis--a role for ROS? *Apoptosis* **9**: 515–23.

495. Tait, SW and Green, DR (2010). Mitochondria and cell death: outer membrane permeabilization and beyond. *Nat. Rev. cell Biol.* **11**: 621–632.

496. He, C and Klionsky, DJ (2009). Regulation Mechanisms and Signalling Pathways of Autophagy. *Annu. Rev. Genet.* **43**: 67.

497. Elmore, S (2007). Apoptosis: A Review of Programmed Cell Death. *Toxicol Pathol* **35**: 495–516.

498. Saelens, X, Festjens, N, Vande Walle, L, van Gurp, M, van Loo, G and Vandenabeele, P (2004). Toxic proteins released from mitochondria in cell death. *Oncogene* **23**: 2861–2874.

499. Watanabe, T, Bertoletti, A and Tanoto, TA (2010). PD-1/PD-L1 pathway and T-cell exhaustion in chronic hepatitis virus infection. *J. Viral Hepat.* **17**: 453–458.

500. Enomoto, L, Anderson, PL, Li, S, Edelstein, CL and Weinberg, A (2011). Effect of nucleoside and nucleotide analog reverse transcriptase inhibitors on cell-mediated immune functions. *AIDS Res. Hum. Retroviruses* **27**: 47–55.

501. Gao, W-Y, Shirasaka, T, Johns, D, Broder, S and Mitsuya, H (1993). Differential phosphorylation of azidothymidine, dideoxycytidine, and dideoxyinosine in resting and activated periperhal blood mononuclear cells. *J. Clin. Invest.* **91**: 2326–2333.

502. Hunt, PW, Martin, JN, Sinclair, E, Bredt, B, Hagos, E, Lampiris, H, *et al.* (2003). T Cell Activation Is Associated with Lower CD4+ T Cell Gains in Human Immunodeficiency Virus – Infected Patients with Sustained Viral Suppression

during Antiretroviral Therapy. *J. Infect. Dis.* **187**: 1534–1543.

503. Connor, E, Sperling, R, Gelber, R, Kiselev, P, Scott, G, O'Sullivan, M, *et al.* (1994). Reduction of maternal-infant transmission of human immunodeficiency virus type 1 with zidovudine treatment. *N. Engl. J. Med.* **331**.

504. Little, K, Thorne, C, Luo, C, Bunders, M, Ngongo, N, McDermott, P, *et al.* (2007). Disease progression in children with vertically-acquired HIV infection in sub-Saharan Africa: reviewing the need for HIV treatment. *Curr. HIV Res.* **5**: 139–153.

505. Blanche, S, Tardieu, M, Benhammou, V, Warszawski, J and Rustin, P (2006). Mitochondrial dysfunction following perinatal exposure to nucleoside analogues. *Aids* **20**: 1685–1690.

506. Blanche, S, Tardieu, M, Rustin, P, Slama, A, Barret, B and Firtion, G (1999). Persistent mitochondrial dysfunction and perinatal exposure to antiretroviral nucleoside analogues. *Lancet* **354**: 1084–1089.

507. Khaitan, A and Unutmaz, D (2011). Revisiting immune exhaustion during HIV infection. *Curr. HIV/AIDS Rep.* **8**: 4–11.

508. Jaafoura, S, de Goër de Herve, MG, Hernandez-Vargas, E a, Hendel-Chavez, H, Abdoh, M, Mateo, MC, *et al.* (2014). Progressive contraction of the latent HIV reservoir around a core of less-differentiated $CD4^+$ memory T Cells. *Nat. Commun.* **5**: 5407.

509. Chun, T-W, Justement, JS, Moir, S, Hallahan, CW, Maenza, J, Mullins, JI, *et al.* (2007). Decay of the HIV reservoir in patients receiving antiretroviral therapy for extended periods: implications for eradication of virus. *J. Infect. Dis.* **195**: 1762–4.

510. Chun, TW, Nickle, DC, Justement, JS, Large, D, Semerjian, A, Curlin, ME, *et al.* (2005). HIV-infected individuals receiving effective antiviral therapy for extended periods of time continually replenish their viral reservoir. *J. Clin. Invest.* **115**:

3250–3255.

511. Kulpa, DA, Brehm, JH, Fromentin, R, Cooper, A, Cooper, C, Ahlers, J, *et al.* (2013). The immunological synapse: the gateway to the HIV reservoir. *Immunol. Rev.* **254**: 305–25.

512. Evans, VA, Kumar, N, Filali, A, Procopio, FA, Yegorov, O, Goulet, JP, *et al.* (2013). Myeloid Dendritic Cells Induce HIV-1 Latency in Non-proliferating CD4+ T Cells. *PLoS Pathog.* **9**: 1–14.

513. Shen, A, Baker, JJ, Scott, GL, Davis, YP, Ho, Y-Y and Siliciano, RF (2013). Endothelial Cell Stimulation Overcomes Restriction and Promotes Productive and Latent HIV-1 Infection of Resting CD4+ T Cells. *J. Virol.* **87**: 9768–9779.

514. Choi, J, Walker, J, Talbert-Slagle, K, Wright, P, Pober, JS and Alexander, L (2005). Endothelial cells promote human immunodeficiency virus replication in nondividing memory T cells via Nef-, Vpr-, and T-cell receptor-dependent activation of NFAT. *J. Virol.* **79**: 11194–204.

515. Choi, J, Walker, J and Boichuk, S (2005). Human endothelial cells enhance human immunodeficiency virus type 1 replication in CD4+ T cells in a Nef-dependent manner in vitro and in vivo. *J. ...* **79**: 264–276.

516. Parry, R V, Chemnitz, JM, Frauwirth, K a, Lanfranco, AR, Braunstein, I, Sumire, V, *et al.* (2005). CTLA-4 and PD-1 Receptors Inhibit T-Cell Activation by Distinct Mechanisms. *Mol. Cell. Biol.* **25**: 9543–9553.

517. Lian, I, Kim, J, Okazawa, H, Zhao, J, Zhao, B, Yu, J, *et al.* (2010). The role of YAP transcription coactivator in regulating stem cell self-renewal and differentiation. *Genes Dev.* **24**: 1106–1118.

518. DaFonseca, S, Chomont, N, El Far, M, Boulassel, R, Routy, J and Sékaly, R (2010). Purging the HIV-1 reservoir through the disruption of the PD-1 pathway. *J.*

Int. AIDS Soc. **13**: O15.

519. Siewe, B, Wallace, J, Rygielski, S, Stapleton, JT, Martin, J, Deeks, SG, *et al.* (2014). Regulatory B cells inhibit cytotoxic T lymphocyte (CTL) activity and elimination of infected CD4 T cells after in vitro reactivation of HIV latent reservoirs. *PLoS One* **9**: 1–9.

520. Harriman, GR, Esser, AF, Podack, ER, Wunderlich, AC, Braude, AI, Lint, TF, *et al.* (1981). The role of C9 in complement-mediated killing of Neisseria. *J. Immunol.* **127**: 2386–2390.

521. Descours, B, Petitjean, G, López-Zaragoza, J-L, Bruel, T, Raffel, R, Psomas, C, *et al.* (2017). CD32a is a marker of a CD4 T-cell HIV reservoir harbouring replication-competent proviruses. *Nature* **543**: 564–567.

522. Tolomeo, M, Mancuso, S, Todaro, M, Stassi, G, Catalano, M, Arista, S, *et al.* (2003). Mitochondrial disruption and apoptosis in lymphocytes of an HIV infected patient affected by lactic acidosis after treatment with highly active antiretroviral therapy. *J. Clin. Pathol.* **56**: 147–151.

523. Arnaudo, E, Shanske, S, DiMauro, S, Schon, EA, Moraes, CT, Schon, EA, *et al.* (1991). Depletion of muscle mitochondrial DNA in AIDS patients with zidovudine-induced myopathy. *Lancet* **337**: 508–510.

524. Rathmell, JC, Heiden, MG Vander, Harris, MH, Frauwirth, KA and Thompson, CB (2000). In the absence of extrinsic signals, nutrient utilization by lymphocytes is insufficient to maintain either cell size or viability. *Mol. Cell* **6**: 683–692.

525. Bettonville, M, D'Aria, S and Braun, MY (2016). Metabolic programming in chronically stimulated T cells: Lessons from cancer and viral infections. *Eur. J. Immunol.* **46**: 1574–1582.

526. Vander Heiden, M, Cantley, L and Thompson, C (2009). Understanding the

Warburg effect: The metabolic requirements of cell proliferation. *Science* **324**: 1029–1033.

527. Frauwirth, K, Riley, J, Harris, M, Parry, R, Rathmell, J, Plas, D, *et al.* (2002). The CD28 signaling pathway regulates glucose metabolism. *Immunity* **16**: 769–777.

528. Finlay, DK, Rosenzweig, E, Sinclair, L V., Feijoo-Carnero, C, Hukelmann, JL, Rolf, J, *et al.* (2012). PDK1 regulation of mTOR and hypoxia-inducible factor 1 integrate metabolism and migration of CD8 $^{+}$ T cells. *J. Exp. Med.* **209**: 2441–2453.

529. van der Windt, GJW, O'Sullivan, D, Everts, B, Huang, SC-C, Buck, MD, Curtis, JD, *et al.* (2013). CD8 memory T cells have a bioenergetic advantage that underlies their rapid recall ability. *Proc. Natl. Acad. Sci.* **110**: 14336–14341.

530. Araki, K, Turner, AP, Shaffer, VO, Gangappa, S, Keller, SA, Bachmann, MF, *et al.* (2009). mTOR regulates memory CD8 T cell differentiation. *Nature* **460**: 108–112.

531. Bengsch, B, Johnson, AL, Kurachi, M, Odorizzi, PM, Pauken, KE, Attanasio, J, *et al.* (2016). Bioenergetic Insufficiencies Due to Metabolic Alterations Regulated by the Inhibitory Receptor PD-1 Are an Early Driver of CD8+ T Cell Exhaustion. *Immunity* **45**: 358–373.

532. Schurich, A, Pallett, LJ, Jajbhay, D, Wijngaarden, J, Otano, I, Gill, US, *et al.* (2016). Distinct Metabolic Requirements of Exhausted and Functional Virus-Specific CD8 T Cells in the Same Host. *Cell Rep.* **16**: 1243–1252.

533. Staron, MM, Gray, SM, Marshall, HD, Parish, IA, Chen, JH, Perry, CJ, *et al.* (2014). The Transcription Factor FoxO1 Sustains Expression of the Inhibitory Receptor PD-1 and Survival of Antiviral CD8 + T Cells during Chronic Infection. *Immunity* **41**: 802–814.

534. Mollan, KR, Smurzynski, M, Eron, JJ, Daar, ES, Campbell, TB, Sax, PE, *et al.* (2014). Association between efavirenz as initial therapy for HIV-1 infection and increased risk for suicidal ideation or attempted or completed suicide: An analysis of trial data. *Ann. Intern. Med.* **161**: 1–10.

535. Levi, J, Raymond, A, Pozniak, A, Vernazza, P, Kohler, P and Hill, A (2016). Can the UNAIDS 90-90-90 target be achieved? A systematic analysis of national HIV treatment cascades. *BMJ Glob. Heal.* **1**: e000010.

536. Nakagawa, F, Miners, A, Smith, CJ, Simmons, R, Lodwick, RK, Cambiano, V, *et al.* (2015). Projected lifetime healthcare costs associated with HIV infection. *PLoS One* **10**: 1–12.

APPENDIX

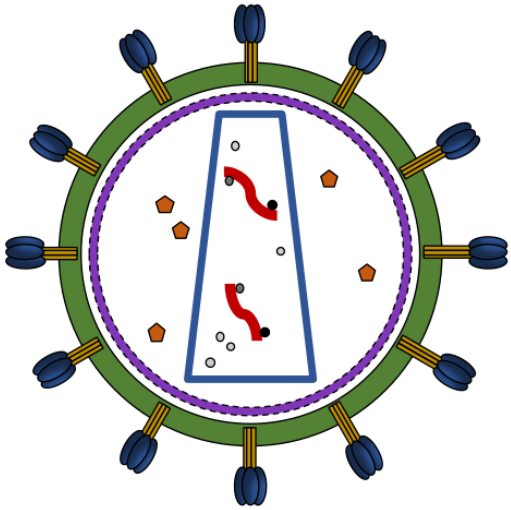

Appendix: Chapter One

Appendix 1.1: Structure of HIV-1 modelled in cake.

Appendix: Chapter Two

Appendix 2.1:

Equations A:

$$\mathbf{PD} = [\frac{(\%\ \mathbf{next\ above\ 50\%}) - \mathbf{50}}{(\%\ \mathbf{next\ above\ 50\%}) - (\%\ \mathbf{next\ below\ 50\%})}] * \mathbf{1}$$

***10-fold dilution = corrective factor of 1*

$$\mathbf{logTCID_{50}} = \mathbf{10}^{(\mathbf{exponential\ dilution > 50\%}) + \mathbf{PD}}$$

***Dilution of virus giving the next percentage of infected culture > 50% (ex: 10^{-1} → -1)*

$$\mathbf{PFU} = \mathbf{TCID_{50}} * \mathbf{0.69}$$

Equations B:

$$\mathbf{Infectious\ particles\ needed} = \#\ \mathbf{cells\ to\ infect} * \mathbf{MOI}$$

$$\mathbf{Volume\ virus\ needed} = \mathbf{infectious\ particles\ needed} / (\frac{\mathbf{PFU}}{\mathbf{ml}})$$

Appendix 2.2: HIV-1 consensus B Gag peptides (15-mer with 11 amino acid overlaps) for intracellular cytokine staining for IFNγ

Final pool 'A'
Peptides: 1, 2, 3, 4, 5, 6, 7, 11, 15, 16, 17, 18, 19, 20, 21, 23, 29, 30, 31, 32, 34, 38, 39, 42, 47, 48, 49, 50, 51, 53, 54, 61, 63, 64, 65, 66, 67, 69, 72, 78, 81, 82, 88, 89, 91, 96, 99, 102, 104, 112, 120, 121, 123

Final pool 'B'
Peptides: 8, 9, 10, 12, 13, 14, 22, 24, 25, 26, 27, 28, 33, 35, 36, 37, 40, 41, 43, 44, 45, 46, 52, 55, 56, 57, 58, 59, 60, 62, 68, 70, 71, 73, 74, 75, 76, 77, 79, 80, 83, 84, 85, 86, 87, 90, 92, 93, 94, 95, 97, 98, 100, 101, 103, 105, 106, 107, 108, 109, 110, 111, 113, 114, 115, 116, 117, 118, 119, 122

Peptide Number	Sequence	Peptide Number	Sequence
1	MGARASVLSGGELDR	**23**	HQRIEVKDTKEALEK
2	ASVLSGGELDRWEKI	**24**	EVKDTKEALEKIEEE
3	SGGELDRWEKIRLRP	**25**	TKEALEKIEEEQNKS
4	LDRWEKIRLRPGGKK	**26**	LEKIEEEQNKSKKKA
5	EKIRLRPGGKKKYKL	**27**	EEEQNKSKKKAQQAA
6	LRPGGKKKYKLKHIV	**28**	NKSKKKAQQAAADG
7	GKKKYKLKHIVWASR	**29**	KKAQQAAADTGNSSQ
8	YKLKHIVWASRELER	**30**	QAAADTGNSSQVSQN
9	HIVWASRELERFAVN	**31**	DTGNSSQVSQNYPIV
10	ASRELERFAVNPGLL	**32**	SSQVSQNYPIVQNLQ
11	LERFAVNPGLLETSE	**33**	SQNYPIVQNLQGQMV
12	AVNPGLLETSEGCRQ	**34**	PIVQNLQGQMVHQAI
13	GLLETSEGCRQILGQ	**35**	NLQGQMVHQAISPRT
14	TSEGCRQILGQLQPS	**36**	QMVHQAISPRTLNAW
15	CRQILGQLQPSLQTG	**37**	QAISPRTLNAWVKVV
16	LGQLQPSLQTGSEEL	**38**	PRTLNAWVKVVEEKA
17	QPSLQTGSEELRSLY	**39**	NAWVKVVEEKAFSPE
18	QTGSEELRSLYNTVA	**40**	KVVEEKAFSPEVIPM
19	EELRSLYNTVATLYC	**41**	EKAFSPEVIPMFSAL
20	SLYNTVATLYCVHQR	**42**	SPEVIPMFSALSEGA
21	TVATLYCVHQRIEVK	**43**	IPMFSALSEGATPQD
22	LYCVHQRIEVKDTKE	**44**	SALSEGATPQDLNTM

45	EGATPQDLNTMLNTV	**79**	VKNWMTETLLVQNAN
46	PQDLNTMLNTVGGHQ	**80**	MTETLLVQNANPDCK
47	NTMLNTVGGHQAAQ	**81**	LLVQNANPDCKTILK
48	NTVGGHQAAMQMLE	**82**	NANPDCKTILKALGP
49	GHQAAMQMLKETINE	**83**	DCKTILKALGPAATL
50	AMQMLKETINEEAAE	**84**	ILKALGPAATLEEMM
51	LKETINEEAAEWDRL	**85**	LGPAATLEEMMTACQ
52	INEEAAEWDRLHPVH	**86**	ATLEEMMTACQGVGG
53	AAEWDRLHPVHAGPI	**87**	EMMTACQGVGGPGHK
54	DRLHPVHAGPIAPGQ	**88**	ACQGVGGPGHKARVL
55	PVHAGPIAPGQMREP	**89**	VGGPGHKARVLAEAM
56	GPIAPGQMREPRGSD	**90**	GHKARVLAEAMSQVT
57	PGQMREPRGSDIAGT	**91**	RVLAEAMSQVTNSAT
58	REPRGSDIAGTTSTL	**92**	EAMSQVTNSATIMMQ
59	GSDIAGTTSTLQEQI	**93**	QVTNSATIMMQRGNF
60	AGTTSTLQEQIGWMT	**94**	SATIMMQRGNFRNQR
61	STLQEQIGWMTNNPP	**95**	MMQRGNFRNQRKTVK
62	EQIGWMTNNPPIPVG	**96**	GNFRNQRKTVKCFNC
63	WMTNNPPIPVGEIYK	**97**	NQRKTVKCFNCGKEG
64	NPPIPVGEIYKRWII	**98**	TVKCFNCGKEGHIAK
65	PVGEIYKRWIILGLN	**99**	FNCGKEGHIAKNCRA
66	IYKRWIILGLNKIVR	**100**	KEGHIAKNCRAPRKK
67	WIILGLNKIVRMYSP	**101**	IAKNCRAPRKKGCWK
68	GLNKIVRMYSPTSIL	**102**	CRAPRKKGCWKCGKE
69	IVRMYSPTSILDIRQ	**103**	RKKGCWKCGKEGHQM
70	YSPTSILDIRQGPKE	**104**	CWKCGKEGHQMKDCT
71	SILDIRQGPKEPFRD	**105**	GKEGHQMKDCTERQA
72	IRQGPKEPFRDYVDR	**106**	HQMKDCTERQANFLG
73	PKEPFRDYVDRFYKT	**107**	DCTERQANFLGKIWP
74	FRDYVDRFYKTLRAE	**108**	RQANFLGKIWPSHKG
75	VDRFYKTLRAEQASQ	**109**	FLGKIWPSHKGRPGN
76	YKTLRAEQASQEVKN	**110**	IWPSHKGRPGNFLQS
77	RAEQASQEVKNWMTE	**111**	HKGRPGNFLQSRPEP
78	ASQEVKNWMTETLLV	**112**	PGNFLQSRPEPTAPP

113	LQSRPEPTAPPEESF	**119**	SQKQEPIDKELYPLA
114	PEPTAPPEESFRFGE	**120**	EPIDKELYPLASLRS
115	APPEESFRFGEETTT	**121**	KELYPLASLRSLFGN
116	ESFRFGEETTTPSQK	**122**	PLASLRSLFGNDPSS
117	FGEETTTPSQKQEPI	**123**	LRSLFGNDPSSQ
118	TTTPSQKQEPIDKEL		

Appendix: Chapter Three

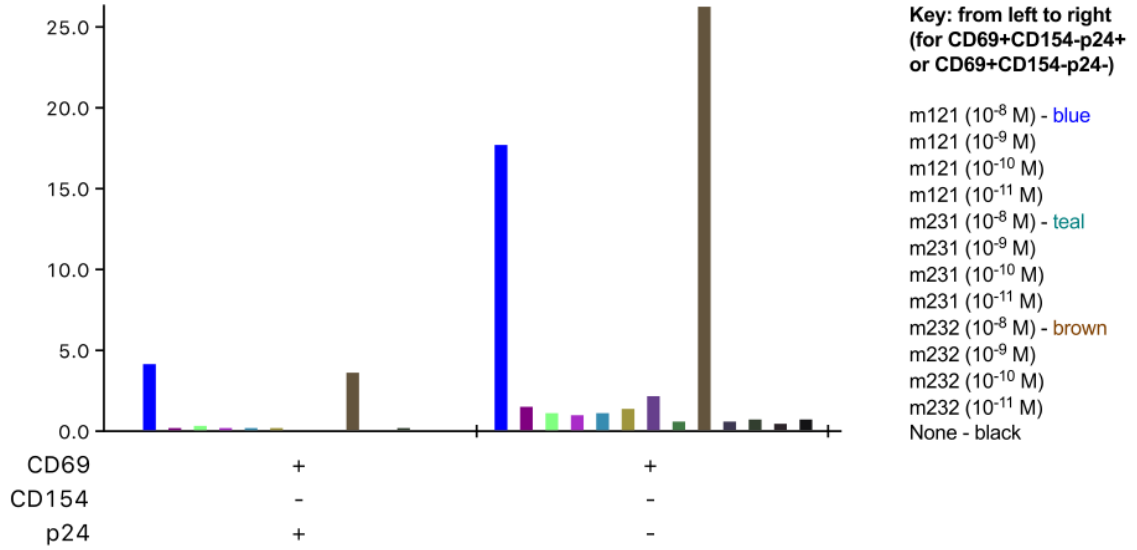

Appendix 3.1: SPICE plot of ImmTAV-induced reactivation of resting infected cells. Resting infected CD4+ T cells were cultured with m121, m231 or m232 ImmTAV at varying concentrations (10^{-11} – 10^{-8} M) for 48 hours before assessment of p24, CD69 and CD154 expression.

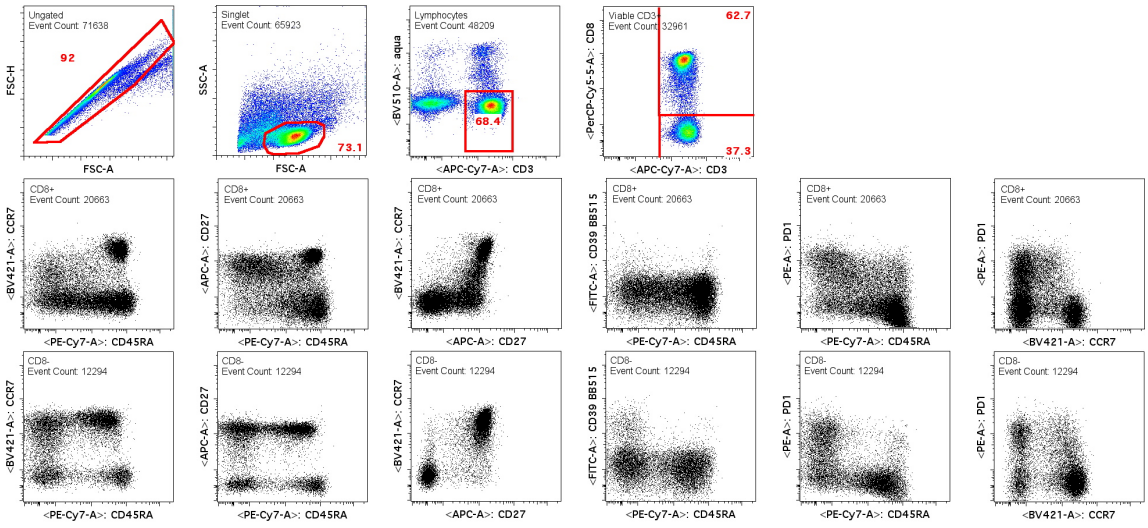

Appendix 3.2: FACS gating for exhaustion markers. Top row shows gating for single, lymphocyte, alive CD3+ and CD8+ or $CD8^{neg.}$ (CD4+) T cells. Middle (CD8+ T cells) and bottom ($CD8^{neg.}$ T cells) rows show expression of CD45RA, CCR7, CD27, PD-1 and CD39.

Appendix: Chapter Four

a

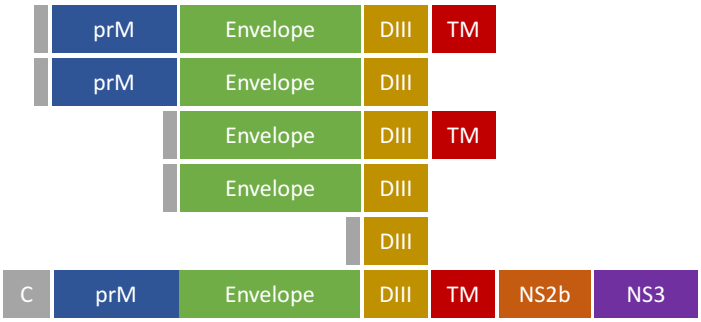

b

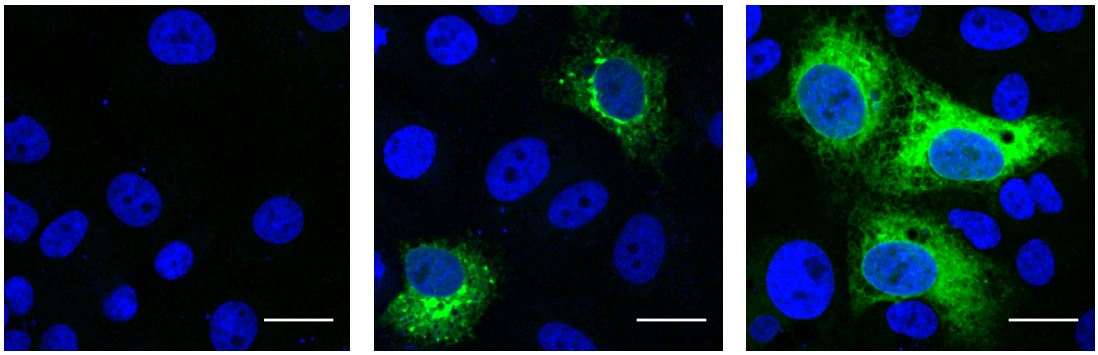

Appendix 4.1: Application of staining optimisation process to ZIKV vaccine candidate investigation. (a) Six DNA constructs for ZIKV vaccine candidates were designed incorporating the pre-membrane (prM), envelope, envelope C-terminus transmembrane domain (TM), domain III (DIII), non-structural 2b (NS2b) and/or non-structural (NS3) proteins. (b) Vero cells were used to optimise staining for Zika envelope antigens using an anti-flavivirus group antigen antibody. Optimised method was used to stain Vero cells transfected with the different DNA constructs (three examples of staining patterns shown for negative control, prM Env DIII, and prM Env DIII TM constructs). Green = flavivirus group antigen, blue = DAPI (nucleus). Scale bar = 20 μM.

Appendix: Chapter Five

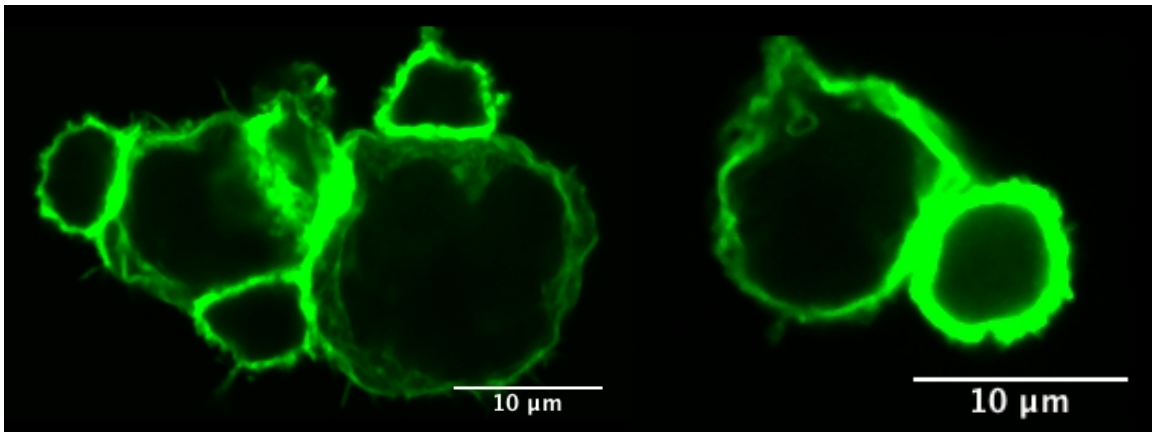

Appendix 5.1: F-actin expression in T2-T cell synapses. F-actin staining of T2-T cell synapses produced bright, oversaturated images that were difficult to use for quantification of F-actin expression.

a

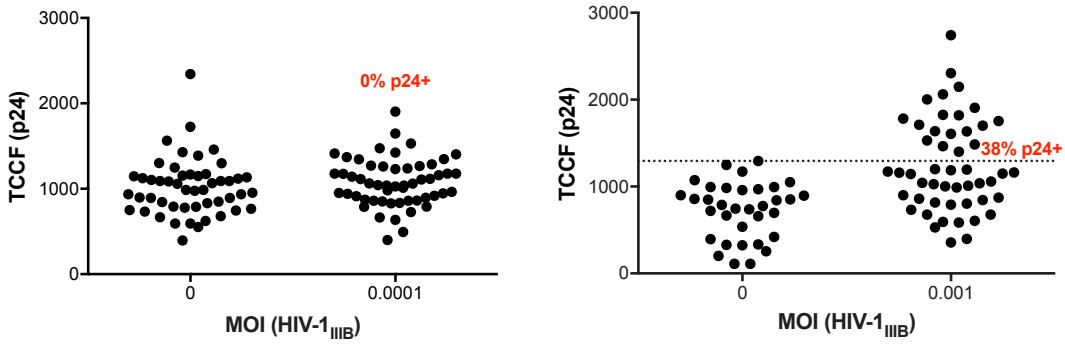

b

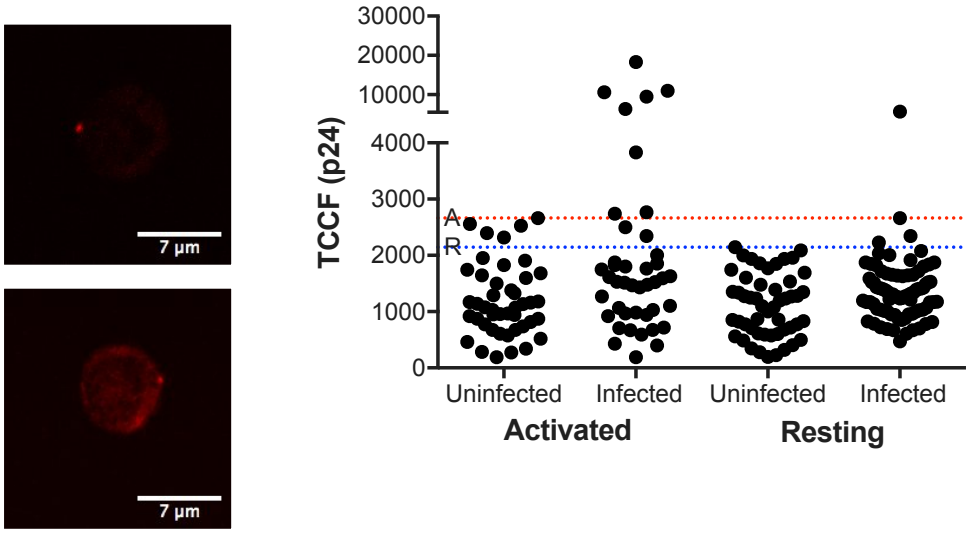

Appendix 5.2: TCCF(p24) measurements. Immunofluorescence images of the p24 stain were used to calculate the total corrected cellular fluorescence (TCCF(p24)) for all groups and the uninfected sample was used to set a cut-off for p24-positivity for the infected sample. (a) p24 infection in a sample can be detected by this method at an MOI of 0.001 but not 0.0001. (b) Uninfected controls must match the activation status of the infected cells (activated = red line/bottom infected cell, resting = blue line/top infected cell); each dot represents a cell. Red = p24.

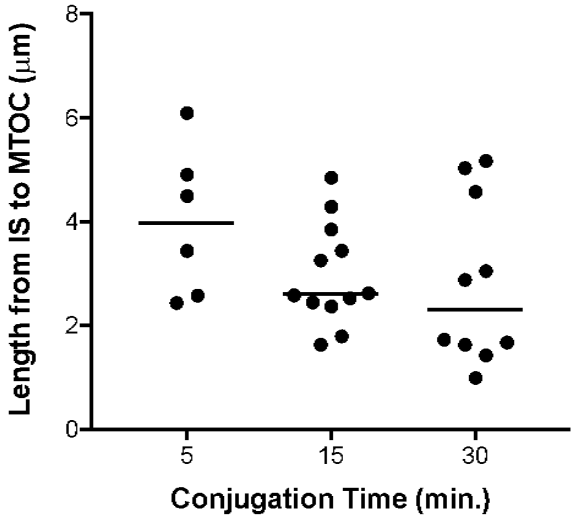

Appendix 5.3: Time course of MTOC localisation in T cell-T cell synapses. Progression of synapse formation can be seen in T cell-T cell synapses by measuring the length from the MTOC to the synapse (μm) over time; each dot represents a conjugate imaged by microscopy (n > 5/condition). Horizontal lines represent the mean.

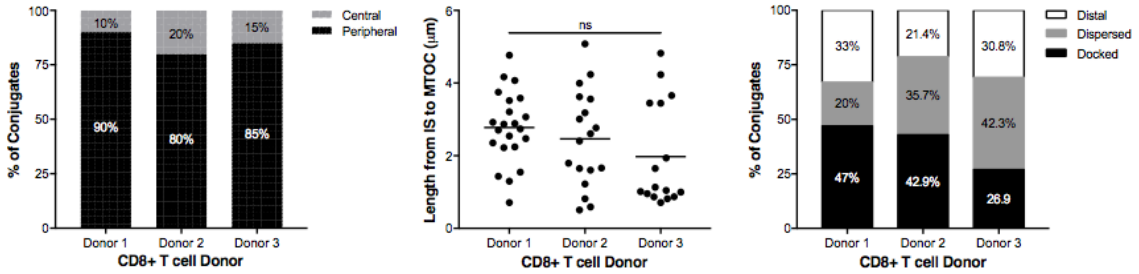

Appendix 5.4: Comparison of synapse formation amongst healthy donor CD8+ T cells. Breakdown of Zap70 expression (left; binned analysis), length from immunological synapse to MTOC (middle; μm) and perforin expression (right; binned analysis) for each of three healthy donors used for T2-T cell analysis; each dot represents a conjugate imaged by microscopy (n > 10/donor). Horizontal lines represent the mean. Groups were analysed by one-way ANOVA.

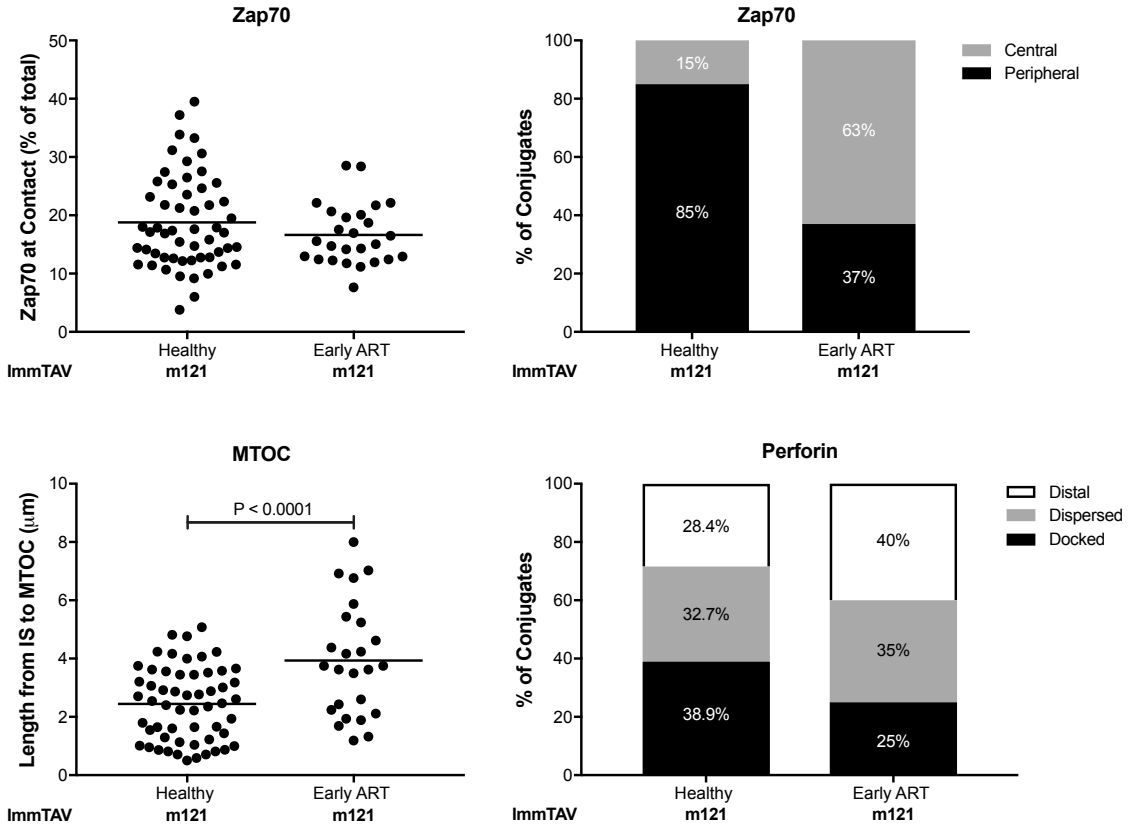

Appendix 5.5: T2-T cell synapses with CD8+ T cells from an early ART donor. SL9-pulsed T2 cells were cultured with m121 ImmTAV-redirected CD8+ T cells from one donor who began ART during PHI (early ART). Immunofluorescence images (n > 10 conjugates/stain) were used to measure Zap70 (%, binning), MTOC (length, μm) and perforin (binning) expression. Data for healthy donors from figures 5.16 – 18 is shown for comparison. Horizontal lines represent the mean. Groups were analysed by unpaired t test.

Appendix 5.6: Live cell imaging of the formation of primary CD8+ T cell immunological synapses (VIDEO). QR code for access to live-cell imaging video from figure 5.20 or follow this link: https://youtu.be/GIqBUpbmsPg

THE END